Analysis of Steady-State and Transient Chemical Rates in Molecular Interconversion

A DISSERTATION
SUBMITTED TO THE FACULTY OF THE
UNIVERSITY OF MINNESOTA
BY

Brandon R. Foley

IN PARTIAL FULFILLMENT OF THE REQUIREMENTS
FOR THE DEGREE OF
DOCTOR OF PHILOSOPHY

Advised by Professor Aditya Bhan

July 2020

Acknowledgments

I thank my partner, Faith, for her support, open ears, and affection that have kept me afloat and on course throughout my graduate career. Finally, I thank my family and friends, especially my sisters, Mikayla and Madison, my grandparents, and Ireland for giving me reasons to take much-needed breaks from research over the last five years.

Dedication

To my daughter, who I hope grows up to be just like her mother.

Table of Contents

List of Tables

List of Figures

Chapter 1

An introduction to the relationship between microscopic chemical phenomena and macroscopic observations

With a few notable exceptions,[2,3] the formation and scission of chemical bonds as a reaction progresses is not directly observed. Instead, chemists rely on making macroscopic measurements of reacting ensembles to elucidate the unseen events occurring at the molecular scale. The subject of chemical kinetics is the pursuit of the derivation of a rate function, which describes the rate of a reaction as a function of the chemical activities (or concentrations) and temperature, with the aim to develop predictive models that aid in the development of large-scale industrial processes or to obtain knowledge of the fundamental microscopic (or perhaps more appropriately, given the size of reacting molecules, "nanoscopic") phenomena that comprise what is referred to as the *mechanism* of a chemical reaction.[4,5] The mechanism includes the molecular motion, collisions, conformations, electron transfers, energies, etc., of molecules that define the chemical transformation of reacting species to products.[4,5]

The relationship between the dependence of the rate function of a reaction and the microscopic phenomena is determined by the Law of Mass Action,[4,6,7] which states that for an elementary step reaction of the form (eq. (1.1)):

$$-\nu_A A - \nu_B B \rightarrow \nu_C C + \nu_D D \tag{1.1}$$

the rate function is a product of the rate constant, k, and the chemical activities of *reacting* species, a_A and a_B, to the powers of negative their stoichiometric coefficients, ν_A and ν_B, which are negative for reactants and positive for products (eq. (1.2)):

$$r = k a_A^{-\nu_A} a_B^{-\nu_B} \tag{1.2}$$

where the stoichiometric coefficients describe the number of molecules consumed (for reactants) or formed (for products) in each reaction event. For example, if one measures the rate of an elementary step and determines that the powers, called reaction orders, of the activities of A and B are both one, this implies the elementary step reaction occurs via a collision between one A and one B to form the products C and D. This deceivingly trivial result is taken for granted by modern kineticists who aim to relate their determination of the rate function to the chemical events that occur during a reactive process. As such, the Law of Mass Action is at the crux of what distinguishes chemical kinetics as a fundamental science from an empirical endeavor.

Many theories have been dedicated to understanding the value of the rate constant, k, the most successful of which being transition state theory (TST).[4,8,9] In TST, all possible states (position and momentum) of reactant molecules and the states in which these molecules form an *activated complex*, or transition state, are enumerated using statistical mechanics.[10] These states are assumed to be in thermal equilibrium such that the population of these states is described by a Boltzmann distribution.[10] The transformation of the transition states to products of the elementary step reaction is then described by translation of atoms along a bond-breaking or bond-forming coordinate.[10] From a thermodynamic perspective, transition state theory describes an equilibrium between the transition state of an elementary step and the reactants of the elementary step, such that the rate constant is given by eq. (1.3):

$$k = \frac{k_B T}{h} \exp\left(\frac{G_{TS}^o + \sum_r \nu_r G_r^o}{k_B T}\right)$$

$$= \frac{k_B T}{h} \exp\left(\frac{S_{TS}^o + \sum_r \nu_r S_r^o}{k_B}\right) \exp\left(\frac{H_{TS}^o + \sum_r \nu_r H_r^o}{k_B T}\right) \tag{1.3}$$

where k_B is the Boltzmann constant, h is the Planck constant, T is the absolute temperature, and G_j^o, S_j^o, and H_j^o are the molecular standard-state free energies, entropies, and enthalpies of the transition state (TS) or reactants (r), respectively.[4,10] From eq. (1.3) we see that the rate constant is solely a function of the transition state, the reactants, and the absolute temperature. Thus by measuring the rate function (eq. (1.2)), one obtains information about the number and identity of reacting molecules that combine to form the transition state and the difference in entropy and enthalpy between the transition and the reactants, which informs about the mechanism of the elementary step reaction. This is the goal of the kineticist.

Rarely is a chemical reaction of interest a single elementary step, but instead is often a complex network of elementary steps that describes an overall composite reaction. The simplest composite reaction is given in eq. ((1.4)):

$$A \rightarrow B \rightarrow C \tag{1.4}$$

where B is an *intermediate* formed and consumed en route from reactant A to product C. For a composite system, the rate function is determined by solving the system of algebraic and differential equations that describe the formation and consumption of each species in the system, which are in turn related to the elementary step rate functions.[4,5] The overall rate functions thus do not necessarily take on the form given in eq. (1.2), which is for elementary steps. Nevertheless, kineticists understand there is a relationship

between the rate function of a composite reaction and the elementary steps reactions, and they use this knowledge as a means to eliminate postulated reaction mechanisms that are incoherent with the observed rate function. However, the rules that dictate the relationship between the properties of the composite rate function and the elementary steps that comprise the composite reaction network have not yet been described. In this dissertation, I disseminate this relationship and prove that eqs. (1.2) and (1.3) apply to composite reactions as so-called TST-form rate functions, and that these functions change with reaction conditions, creating a direct relationship between the reaction orders and temperature dependencies of the composite rate to those of the elementary steps that comprise the reaction. This work leverages the concept of rate-controlling steps, which is typically used to describe the extent to which the rate of a composite reaction is limited or throttled by a particular elementary step. I instead show that rate-controlling steps not only limit the rate of reaction, but also endow the composite rate function with their properties (reaction orders and temperature dependencies), such that the composite rate function is a weighted-average of the rate functions of all elementary steps that comprise the composite reaction network.

This dissertation focuses on relating macroscopic observable quantities to the fundamental elementary step reactions that mediate the chemical transformation of reactants to products in composite reactions. Chapter 2 describes the proofs that relate the elementary step rate functions to the overall rate function and derives relationships between the reaction orders, energies and entropies of activation, fractional coverages of surface intermediates in catalytic reactions, and the thermodynamic driving forces, which are leveraged to develop methods for investigating the mechanisms of composite

reactions. Chapter 3 applies these methods to overall reversible composite reactions to derive proofs regarding the implications of the principles of microscopic reversibility and detailed balance in composite reactions. Microscopic reversibility states that the forward and reverse rates of elementary step reactions must be equal at equilibrium, and detailed balance states that because the forward and reverse rate functions of elementary steps are described by the Law of Mass Action, the values of rate constants and reaction orders are constrained by relations that describe the overall equilibrium. Chapter 4 extends the concept of rate control to non-pseudo-steady-state transient reactions. Chapter 5 applies the concepts derived in Chapters 2 and 4 to the elucidation of the reaction mechanism for the formation of diphenylmethane from formaldehyde and benzene on HZSM-5 catalysts.

The reaction between formaldehyde and benzene is relevant to the study of deactivation during the dehydrative conversion of methanol to hydrocarbons on aluminosilicate zeolite or aluminosilicophosphate zeotype solid-acid catalysts. The study of deactivation in heterogeneous catalysts often utilizes empirical models to describe and study the rate of deactivation as a function of temperature and chemical activities. However, deactivation is simply caused by chemical reactions that consume active sites, rendering them inactive. The product of these reactions cannot be observed directly by monitoring the effluent of a reactor in the same way that the products of non-deactivating reactions are observed. Despite this, the rate of these reactions can be assessed indirectly, as described in Chapter 6, and thus can be measured as a function of temperature and chemical activities to elucidate the elementary step reactions that cause deactivation, as is demonstrated in Chapter 7 for methanol-to-hydrocarbons catalysis on HZSM-5.

Chapter 2

Degree of rate control and De Donder relations – An interpretation based on transition state theory

2.1 Conspectus

We describe sensitivities of elementary steps as salient parameters in determining the rate determining character of elementary steps within a reaction network and develop a formalism wherein the overall composite reaction is described by an apparent rate-determining step that is a sensitivity-weighted average of the elementary steps that comprise the reaction. Reaction parameters—apparent reaction orders, apparent enthalpy and entropy of activation—of the composite reaction network are determined within the framework we develop by application of transition state theory to the apparent rate-determining step. From this formalism we develop methods for determination of surface coverages by measuring only reaction orders, novel methods for discrimination between proposed mechanisms, a proof that the kinetic degrees of rate control sum to unity, and a proof for the relationship between fractional coverages and thermodynamic degrees of rate control. Two complementary formalisms for identifying rate-limiting transition states are broadly employed in chemical kinetics—De Donder relations based on measuring the thermodynamic driving forces of elementary steps during reaction and degrees of rate control based on knowledge of the kinetics of elementary reaction steps. The formalism developed herein unifies these two strategies to elucidate in the most general case a

relationship between the thermodynamic driving forces of elementary steps captured by the reversibilities and the kinetic and thermodynamic degrees of rate control.

2.2 Introduction

The degree of rate control is a mathematical formalism for identifying the rate-determining transition states and reaction intermediates in composite reaction networks.[11–13] Degrees of rate control quantify the extent to which changing the standard free energy of a transition state or an intermediate changes the overall *net* steady-state reaction rate. Degrees of rate control for *forward* or *reverse* rates or at non(pseudo)steady-state conditions are discussed in Chapters 3 and 4, respectively.[14,15] It is understood that reaction orders, reversibilities of elementary reaction steps, and, for catalytic reactions, surface coverages of intermediates, are dependent on the identity of rate-limiting steps in a reaction network as these concepts are used in the search of the rate-limiting transition states and for elucidating the mechanism of a reaction.[5] Here we describe a rate-control theory that rationalizes apparent reaction orders, surface coverages, and elementary-step reversibilities by application of transition state theory to apparent initial and transition states of composite reaction networks. To lay the groundwork for understanding the framework that we present, we first discuss kinetic and thermodynamic degrees of rate control, reversibilities, and sensitivities; we then identify sensitivity as the salient parameter for quantifying the rate-control of an elementary step on the overall reaction rate.

The kinetic degree of rate control of transition state i ($X_{RC,i}$) is defined as the relative change in the reaction rate from a set of reactants to a set of products per relative

change in the forward rate constant of step i (k_i), while keeping all other rate constants ($k_{j\neq i}$) and the equilibrium constant for step i (K_i) constant (eq. (2.1)).[11-13] Keeping K_i constant requires the reverse rate constant for step i (k_{-i}) to change as well, and thus the definition for the kinetic degree of rate control is equivalent to the relative change in the reaction rate per $k_B T$ decrease in the standard-state molecular free energy of transition state i ($G^o_{TS,i}$).[11]

$$X_{RC,i} = \left(\frac{\partial \ln r}{\partial \ln k_i}\right)_{k_{j\neq i},K_i} = \left(\frac{\partial \ln r}{\partial(-G^o_{TS,i}/k_B T)}\right)_{G^o_{j\neq TS,i}} \tag{2.1}$$

The kinetic degree of rate control is nonzero for transition states that control the rate of the reaction. When $X_{RC,i} > 0$, lowering the energy of transition state i will increase the reaction rate and when $X_{RC,i} < 0$, lowering the energy of transition state i will decrease the reaction rate.[12] For all reaction systems studied, it appears that $\sum_i X_{RC,i} = 1$.[12] This has been demonstrated for reaction networks leading to a single overall reaction.[16,17] When there is a single rate-determining transition state, the kinetic degree of rate control of that transition state will necessarily equal unity while all other kinetic degrees of rate control equal zero.[11,12]

Analogous to the definition of the kinetic degree of rate control is the thermodynamic degree of rate control ($X_{TRC,i}$), defined as the relative change in the reaction rate per $k_B T$ decrease in the standard-state molecular free energy of a stable species (G^o_i) while keeping all other free energies constant (eq. (2.2)) [11,18]:

$$X_{TRC,i} = \left(\frac{\partial \ln r}{\partial(-G^o_i/k_B T)}\right)_{G^o_{j\neq i}} \tag{2.2}$$

A mathematical relationship between coverage and the thermodynamic degree of control for surface species has been postulated (eq. (2.3))[11]:

$$X_{TRC,j^*} = -\sigma_* \theta_{j^*} \tag{2.3}$$

where θ_{j^*} is the fractional coverage of species j*, and σ_* is defined as "the average number of sites required in the rate-limiting steps,"[11] typically taking on a value between one and two depending on whether the rate-limiting step requires one or two active sites. The relationship described in eq. (2.3) has not been proven.[11,12] In this work, we prove that eq. (2.3) is true only in ideal cases, but is not true when the enthalpies of activation are functions of surface coverages, and we prove that the proportionality factor σ_* in ideal cases is the average number of surface species reacting in rate-limiting steps. Similar to the degree of rate control is sensitivity (s_i), defined in eq. (2.4)[19]:

$$s_i = \left(\frac{\partial \ln r}{\partial \ln k_i} \right)_{k_{j \neq i}} \tag{2.4}$$

which is related to the kinetic degree of rate control by eq. (2.5)[19]:

$$X_{RC,i} = s_i + s_{-i} \tag{2.5}$$

A complementary method for identifying rate-limiting transition states in composite reaction networks is De Donder's formalism, which analyzes reaction rates in terms of the free energy change of elementary reaction steps (ΔG_i), defined as (eq. (2.6))[20]:

$$\Delta G_i = \Delta G_i^o + k_B T \ln \prod_{j=species} a_j^{\nu_{ij}} \tag{2.6}$$

where ΔG_i^o is the *standard-state* molecular free energy change of reaction i, a_j is the activity of species j, and ν_{ij} is the stoichiometric coefficient in reaction i for species j, which is negative for reactants and positive for products. Dumesic[20] defines the reversibility, Z_i, as eq. (2.7):

$$Z_i = e^{\Delta G_i / k_B T} = \frac{\prod_{j=species} a_j^{\nu_{ij}}}{K_i} \tag{2.7}$$

where K_i is the equilibrium constant for reaction i, given by $K_i = e^{-\Delta G_i^o / k_B T}$. Reversibilities can be used to identify a sole rate-determining transition state in a reaction network when all steps without rate-determining transition states have $Z_i \approx 1$ and the step with the rate-determining transition state has $Z_i < 1$.[19–21] However, when there are multiple steps with $Z_i < 1$, identifying which transition states are rate-controlling is not immediately obvious.[19,21] For three first-order reactions in series with stoichiometric numbers all equal to one, it has been shown that the reversibilities are related to the kinetic degrees of rate control by equations of the form given in eq. (2.8)[19,22,23]:

$$X_{RC,i} = \frac{(1 - Z_i) \prod_{j<i} Z_j}{1 - \prod_{j=rxn} Z_j} \tag{2.8}$$

Reversibilities are calculated using thermodynamic data and pseudo-steady-state activities of reactants, intermediates, and products and do not require measurement of kinetic parameters, making eq. (2.8) a very powerful tool for assessing kinetic degrees of rate control. Equation (2.8) can also be utilized to estimate the kinetic degrees of rate control of composite series reaction networks using maximum rates—the rate of an elementary reaction step assuming all other steps are quasi-equilibrated.[22] Motagamwala et al.[22] applies eq. (2.8) to series reaction networks where the stoichiometric numbers of

reactions are not all equal to unity, but points out that in doing so they are assuming that eq. (2.8) approximates the true relationship between $X_{RC,i}$ and Z_i. There is currently no method for determining the functional form of the relationship between $X_{RC,i}$ and Z_i if one does exist for other types of composite reaction networks.

The key insights in this work are revealed in part by applying transition state theory, which is used for estimating the rate of elementary steps, to composite reaction networks. Conventional transition state theory (TST) assumes a Boltzmann distribution of occupied states of the reaction coordinate relevant to the reaction rate.[10] This is equivalent to assuming that the reactants, or initial state (IS), of an elementary step are in equilibrium with the transition state (TS) of the elementary step, such that the overall reaction from the IS to the final state (FS) can be written as (eqs. (2.9) and (2.10)):

$$\sum_{r=reactants} -v_r S_r \overset{K^{\ddagger}}{\rightleftharpoons} TS \tag{2.9}$$

$$TS \overset{v}{\rightarrow} \sum_{p=products} v_p S_p \tag{2.10}$$

where v_i are stoichiometric coefficients for species S_i, $K^{\ddagger}$ is the equilibrium constant between the transition state and the initial state, and v is the rate the transition state is converted to the final state of the elementary step, given by a frequency of motion over the transition state. There exist several derivations of the transition-state-theory rate function, but all arrive at the same result (eq. (2.11))[10]:

$$r = \frac{k_B T}{h} e^{-(G_{TS}^o - G_{IS}^o)/k_B T} \prod_{r=reactants} (a_r)^{-v_r} = k \prod_{r=reactants} (a_r)^{-v_r} \tag{2.11}$$

11

where k_B is the Boltzmann constant, h is the Planck constant, and G_{IS}^o and G_{TS}^o are molecular standard-state free energies of the initial and transition state, respectively, k is the elementary step rate constant, and a_r are activities of reactants. Statistical factors that arise from degeneracy of states are omitted here for simplicity. The molecular standard-state free energy of the initial state is negative the sum of the reactant free energies weighted by their stoichiometric coefficients, $G_{IS}^o = -\sum_r v_r G_r^o$, and the reaction orders of the activities are also negative the stoichiometric coefficients.

The potential energy surface (PES) coupled with the transition-state-theory rate function can describe the apparent reaction orders and the standard-state molecular free energy of activation $\left(\Delta G^{o\ddagger} = G_{TS}^o - G_{IS}^o\right)$. Figure 2.1 shows the PES for a hypothetical catalytic reaction where the adsorption of the reactant, A, is equilibrated and the irreversible transformation of A* to the product, B, is rate-limiting (see Table 2.1). The rate function for this composite reaction network is given by eq. (2.12):

$$\frac{r}{L} = \frac{k_2 K_1 a_A}{1 + K_1 a_A} \tag{2.12}$$

where L is the number of catalyst active sites. At high activities of A where $K_1 a_A \gg 1$ and the fractional surface coverage of A*, θ_{A^*}, is near unity, the rate function in eq. (2.12) simplifies to $r/L = k_2$. The apparent free energy of activation at this condition is given by the difference between the energy of the transition state for step 2 ($[A^*]^\ddagger$) and A^*, as depicted in Figure 2.1, and the reaction order in a_A is zero because A is not in the initial state for the elementary step reaction that forms $[A^*]^\ddagger$. At low activities where $K_1 a_A \ll 1$ and $\theta_{A^*} \approx 0$, the rate function simplifies to $r/L = k_2 K_1 a_A = k_{app} a_A$ where the apparent rate constant, k_{app}, equals $k_2 K_1$. At this condition, the apparent free energy of activation

12

is the energy difference between $[A^*]^\ddagger$ and $A + *$ (see Figure 2.1), and the reaction is first order in a_A because A is in the apparent initial state of the reaction. At this condition, $A + *$ is the *apparent* initial state of the overall reaction—it is not the initial state for the elementary step that forms the final product. We demonstrate that this method of estimating apparent standard free energies of activation and reaction orders from the PES is not restricted to limiting cases, but can be applied at any arbitrary reaction condition for any composite reaction network. For example, when $K_1 a_A = 1$, then $\theta_{A^*} = 0.5$ and the apparent initial state is $0.5A + 0.5 * + 0.5A^*$. We represent the energy of this apparent initial state on the PES as the red dotted line in Figure 2.1, and subsequently, we will prove that the rate of the reaction at this condition is equal to $r/L = K_1^{0.5} k_2 a_A^{0.5} \theta_*^{0.5} \theta_{A^*}^{0.5}$, where the apparent free energy of activation is the difference in energy between $[A^*]^\ddagger$ and $0.5A + 0.5 * + 0.5A^*$ with $k_{app} = K_1^{0.5} k_2$.

Table 2.1: Two-step catalytic reaction network for the conversion of A to B

Step	Reaction	Rate/Equilibrium Constant
1	$A + * \rightleftharpoons A^*$	K_1
2	$A^* \rightarrow B + *$	k_2
Overall	$A \rightarrow B$	

We posit and subsequently demonstrate that there exists an equilibrium between an apparent initial state ($\mathrm{IS_{app}}$) and an apparent transition state ($\mathrm{TS_{app}}$) for composite reaction networks to which TST can be applied. These apparent states are sensitivity-weighted averages of the initial and transition states of elementary steps and are functions of the kinetic and thermodynamic degrees of rate control. We rigorously prove relationships between energies of activation, reaction orders, and steady-state fractional coverages and
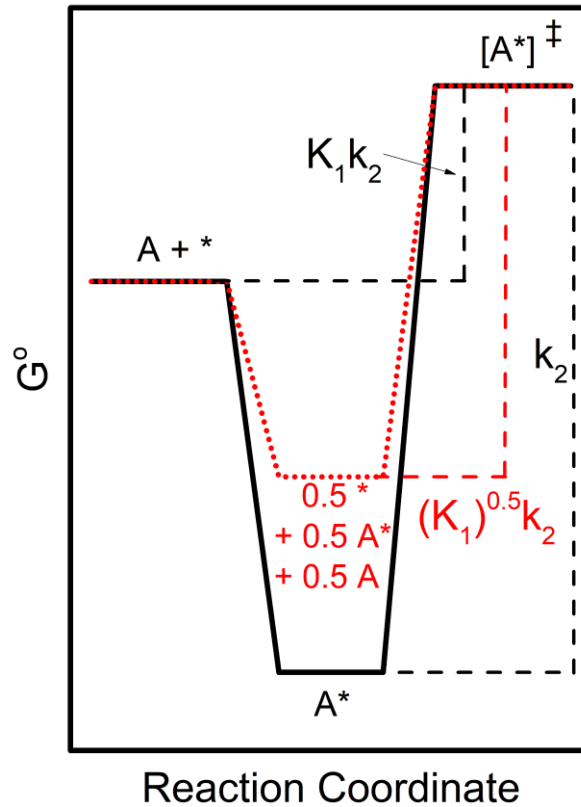
Figure 2.1: Potential energy surface for the catalytic conversion of A to B summarized in Table 2.1. Dashed lines indicate the apparent standard free energy of activation observed at different activities of A.

demonstrate how the derived relationships are applied to verify postulated mechanisms for ideal and non-ideal uncatalyzed and catalyzed composite reaction networks. These findings leads to key fundamental and practical insights regarding the degrees of rate control, sensitivities, and De Donder relations including the following:

1. The apparent rate-limiting elementary step is a sensitivity-weighted average of the elementary steps $(\sum_i s_i\,(IS_i \rightleftharpoons TS_i) = IS_{app} \rightleftharpoons TS_{app})$. In this way, the apparent standard-state free energy of activation of an overall/composite reaction rate is a sensitivity-weighted sum of the standard-state free energies of activation of elementary steps $\left(\Delta G_{app}^{o\ddagger} = \sum_i s_i \Delta G_i^{o\ddagger}\right)$.

2. The thermodynamic degree of rate control of a surface species is proportional to the fractional coverage of that species $(X_{TRC,j^*} = -\sigma_* \theta_{j*})$ in ideal cases. Otherwise, the thermodynamic degree of rate control is only a function of sensitivities and not proportional to fractional coverages. The steady-state fractional coverages are related to sensitivities by:

$$\theta_{N^*} = \sum_i s_i (\partial \ln r_i / \partial \ln \theta_{N^*})_{\theta_{m \neq N^*}} \bigg/ \sum_i \sum_{j^*} s_i (\partial \ln r_i / \partial \ln \theta_{j^*})_{\theta_{m \neq j^*}}$$

3. The kinetic and thermodynamic degrees of rate control can be determined by measuring the reversibilities of every reaction in systems where the pseudo-steady-state approximation is valid. Thus, for these systems, rate-controlling transition states can be identified simply by assessing the thermodynamic driving forces of elementary reaction steps. The functional form of the relationship between degrees of rate control and reversibilities depends on the connectivity of the composite reaction network.

In the following discussion, equations are derived for both uncatalyzed and catalyzed composition reactions. Sections 2.3.1-2.3.4 apply equally to uncatalyzed and catalyzed reactions, but examples provided are explicitly for non-catalyzed systems. Additional proofs, consequences, and examples of this work for catalyzed reaction systems are discussed in Sections 2.3.5-2.3.8. A summary of the symbols used in this work is given in Table 2.2 for reference.

Table 2.2: Summary of symbols and definitions for Chapter 2.

Symbol	Definition
a_j	Thermodynamic activity of species j
C', C	Arbitrary constant of integration
$E_{a,i}, (E_{a,app})$	(Apparent) activation energy of elementary step i (composite reaction)
FS	Final state
k_i	Rate constant for elementary step i
K_i	Equilibrium constant for elementary step i
$K^{\ddagger}$	Equilibrium constant between the transition state and initial state
k_B	Boltzmann constant
L	Number of catalyst active sites
$G_i^o\left(G_{TS,i}^o\right)\left[G_{IS,i}^o\right]$	Molecular standard-state free energy of species (transition state) [initial state] i
$G_{IS,app}^o\left(G_{TS,app}^o\right)$	Molecular standard-state free energy of the apparent initial state (transition state)
ΔG_i	Molecular free energy change of reaction i
ΔG_i^o	Molecular standard-state free energy change of reaction i
$\Delta G_i^{o\ddagger}\left(\Delta \tilde{G}_i^{o\ddagger}\right)$	Molecular (molar) standard-state free energy of activation for elementary reaction i
$\Delta G_{app}^{o\ddagger}\left(\Delta \tilde{G}_{app}^{o\ddagger}\right)$	Apparent molecular (molar) standard-state free energy of activation
$\Delta H_i^{o\ddagger}\left(\Delta \tilde{H}_i^{o\ddagger}\right)$	Molecular (molar) standard-state enthalpy of activation for elementary reaction i
$\Delta H_{app}^{o\ddagger}\left(\Delta \tilde{H}_{app}^{o\ddagger}\right)$	Apparent molecular (molar) standard-state enthalpy of activation
IS	Initial state
r	Rate function of steady-state net reaction rate
r_i	Rate function of elementary reaction i
r_{TST}	Transition-state-theory-form rate function of a composite reaction
s_i	Sensitivity of elementary step i
S_j	Species j
$\Delta S_i^{o\ddagger}\left(\Delta \tilde{S}_i^{o\ddagger}\right)$	Molecular (molar) standard-state entropy of activation for elementary reaction i
$\Delta S_{app}^{o\ddagger}\left(\Delta \tilde{S}_{app}^{o\ddagger}\right)$	Apparent molecular (molar) standard-state entropy of activation
T	Absolute temperature
TS	Transition state
$X_{RC,i}$	Kinetic degree of rate control for transition state i
$X_{TRC,i}$	Thermodynamic degree of rate control of species i
Z_i	Reversibility of reaction i
z	Coordination number of active sites
δ_{ij}	Krönecker delta
γ	An energy that describes the relative change in the rate per change in $1/k_B$
Γ_i	Parameter relating change in activation enthalpy for elementary step i with a change in fractional coverage
ψ_{ij}	Reaction order of species j in elementary reaction i
$\psi_{j,app}$	Apparent reaction order of species j for a composite reaction
$\psi_{\theta j^*,app}$	Apparent reaction order of θ_{j^*} in a composite reaction
$\sigma_*, \sigma_{*,app}$	Sensitivity-weighted average number of surface species in rate-limiting steps
θ_{j^*}	Fractional coverage of surface species j^*
v	Frequency of motion over transition state
v_{ij}	Stoichiometric coefficient for species j in reaction step i
$\rightarrow$	Irreversible reaction arrow
$\rightleftarrows$	Reversible reaction arrows
$\rightleftharpoons$	Equilibrium arrows

2.3 Results and Discussion

2.3.1 *Apparent rate-controlling steps of composite reaction networks*

For the rate of any elementary or composite reaction, we define an energy, γ, (γ_i for an elementary step, γ_{app} for composite reactions), defined in eqs. (2.13) and (2.14):

$$\gamma_i = T\left(\frac{\partial \ln r_i}{\partial(-1/k_B)}\right)_{a_j} = T\left(\frac{\partial \ln r_i}{\partial \ln k_i}\right)_{a_j}\left(\frac{\partial \ln k_i}{\partial(-1/k_B)}\right)_{a_j}$$

$$= T\left(\frac{\partial \ln k_i}{\partial(-1/k_B)}\right)_{a_j}$$

(2.13)

$$\gamma_{app} = T\left(\frac{\partial \ln r}{\partial(-1/k_B)}\right)_{a_j}$$

(2.14)

The γ_i for an elementary step is simplified to the partial derivative of $\ln k_i$ instead of $\ln r_i$ using the chain rule and noting that for TST-form rate functions of elementary steps, $\left(\frac{\partial \ln r_i}{\partial \ln k_i}\right)_{a_j} = 1$ (see eq. (2.11)). The apparent energy γ_{app} is related to the γ_i of each elementary step in a composite reaction sequence by the multivariable chain rule (eq. (2.15)):

$$\gamma_{app} = T\left(\frac{\partial \ln r}{\partial(-1/k_B)}\right)_{a_j} = \sum_{i=rxn}\left(\frac{\partial \ln r}{\partial \ln k_i}\right)_{k_{j\neq i}} T\left(\frac{\partial \ln k_i}{\partial(-1/k_B)}\right)_{a_j}$$

$$= \sum_{i=rxn} s_i \gamma_i$$

(2.15)

where the apparent energy γ_{app} is a sum of γ_i of elementary steps weighted by the sensitivities, s_i, and $i = rxn$ refers to the summation of both the forward $(i > 0)$ and reverse $(i < 0)$ elementary steps. This nomenclature will be followed throughout this article. The relationship between the energy γ_i and the standard-state free energy of

17

activation ($\Delta G_i^{o\ddagger} = G_{TS,i}^o - G_{IS,i}^o$) of an elementary step is found by calculating γ_i corresponding to the transition-state-theory rate function shown in eq. (2.11) (eq. (2.16)):

$$\gamma_i = T\left(\frac{\partial}{\partial(-1/k_B)}\ln\left(\frac{T}{\left(\frac{1}{k_B}\right)h}e^{\frac{-\Delta G_i^{o\ddagger}\left(\frac{1}{k_B}\right)}{T}}\prod_{r=reactants}a_r^{-\nu_r}\right)\right)_{a_j} \quad (2.16)$$

$$= \Delta G_i^{o\ddagger} + k_B T$$

By transposing the functional relationship between $\Delta G_i^{o\ddagger}$ and γ_i of an elementary step (eq. (2.16)), we propose to define the apparent standard-state molecular free energy of activation of the rate of a composite reaction as eq. (2.17):

$$\Delta G_{app}^{o\ddagger} = -k_B T + \gamma_{app} \quad (2.17)$$

Combining eqs. (2.13)-(2.17) and noting that $\sum_i s_i = 1$ (see section 2.3.3 below), we determine that $\Delta G_{app}^{o\ddagger}$ of the overall reaction is a sensitivity-weighted sum of $\Delta G_i^{o\ddagger}$ of the elementary steps (eq. (2.18)):

$$\Delta G_{app}^{o\ddagger} = -k_B T + \sum_{i=rxn} s_i\gamma_i = \sum_{i=rxn} s_i(-k_B T + \gamma_i) = \sum_{i=rxn} s_i \Delta G_i^{o\ddagger} \quad (2.18)$$

The relationship between $\Delta G_i^{o\ddagger}$ and $\Delta G_{app}^{o\ddagger}$ (eq. (2.18)) is proven in Section 2.3.2. In Section 2.3.9, we assess the apparent standard-state molecular free energy, enthalpy, and entropy of activation of a composite reaction and demonstrate that they are sensitivity-weighted averages of the free energies, enthalpies, and entropies of activation of elementary steps, as predicted by eq. (2.18). Equation (2.18) can be rewritten in terms of the transition state and initial state energies of the individual reaction steps (eq. (2.19)):

$$\Delta G_{app}^{o\ddagger} = \sum_{i=rxn} s_i \Delta G_i^{o\ddagger}$$

$$= \sum_{i=rxn} s_i \left(G_{TS,|i|}^o - G_{IS,i}^o \right) = \sum_{i=rxn} s_i G_{TS,|i|}^o - \sum_{i=rxn} s_i G_{IS,i}^o \qquad (2.19)$$

where the absolute value of i ($|i|$) is introduced in the subscript for transition state energies because reverse reactions (with negative i) have the same transition states as forward reactions (positive i). Based on eq. (2.19), the apparent transition state energy ($G_{TS,app}^o$) and the apparent initial state energy ($G_{IS,app}^o$) are defined as (eqs. (2.20) and (2.21)):

$$G_{TS,app}^o = \sum_{i=rxn} s_i G_{TS,|i|}^o = \sum_{i>0} (s_i + s_{-i}) G_{TS,i}^o \qquad (2.20)$$

$$G_{IS,app}^o = \sum_{i=rxn} s_i G_{IS,i}^o = \sum_{j=species} \sum_{i=rxn} -s_i \nu_{ij} G_j^o [\nu_{ij} < 0] \qquad (2.21)$$

where ν_{ij} is the stoichiometric coefficient of species j in reaction i and G_j^o is the molecular standard-state free energy of the fluid-phase or surface species j. The brackets in eq. (2.21) are per Iverson Bracket notation where $[\nu_{ij} < 0]$ is equal to unity if true and zero if false. In eq. (2.21), $G_{IS,i}^o$ is the sum of the energies of the individual reactant species multiplied by the stoichiometric coefficient of each reactant in reaction i. It has been proven previously that $X_{RC,i}$ is equal to the sum of the forward and reverse sensitivity of step i (eq. (2.22))[20]:

$$X_{RC,i} = \left(\frac{\partial \ln r}{\partial \ln k_i}\right)_{k_{m\neq i},K_i} = \sum_{j=rxn} \left(\frac{\partial \ln r}{\partial \ln k_j}\right)_{k_{n\neq j}} \left(\frac{\partial \ln k_j}{\partial \ln k_i}\right)_{k_{m\neq i},K_i}$$

$$= \left(\frac{\partial \ln r}{\partial \ln k_i}\right)_{k_{n\neq i}} + \left(\frac{\partial \ln r}{\partial \ln k_{-i}}\right)_{k_{n\neq -i}} = s_i + s_{-i}$$

(2.22)

and following an analogous procedure the thermodynamic degree of rate control of species j as a function of sensitivities is found in eq. (2.23):

$$X_{TRC,j} = \left(\frac{\partial \ln r}{\partial(-G_j^o/k_B T)}\right)_{G_{m\neq j}^o} = \sum_{i=rxn} \left(\frac{\partial \ln r}{\partial \ln k_i}\right)_{k_{n\neq i}} \left(\frac{\partial \ln k_i}{\partial(-G_j^o/k_B T)}\right)_{G_{m\neq j}^o}$$

$$= \sum_{i=rxn} s_i \nu_{ij} [\nu_{ij} < 0]$$

(2.23)

By combining eqs. (2.19)-(2.23), $\Delta G_{app}^{o\ddagger}$ defined in eq. (2.19) is equal to (eq. (2.24)):

$$\Delta G_{app}^{o\ddagger} = \sum_{i=TS} X_{RC,i} G_{TS,i}^o + \sum_{j=species} X_{TRC,j} G_j^o = G_{TS,app}^o - G_{IS,app}^o$$

(2.24)

and new definitions for $X_{RC,i}$ and $X_{TRC,j}$ arise (eqs. (2.25) and (2.26)):

$$X_{RC,i} = \left(\frac{\partial \Delta G_{app}^{o\ddagger}}{\partial G_{TS,i}^o}\right)_{G_{j\neq TS,i}^o} = \left(\frac{\partial G_{TS,app}^o}{\partial G_{TS,i}^o}\right)_{G_{j\neq TS,i}^o}$$

(2.25)

$$X_{TRC,j} = \left(\frac{\partial \Delta G_{app}^{o\ddagger}}{\partial G_j^o}\right)_{G_{i\neq j}^o} = -\left(\frac{\partial G_{IS,app}^o}{\partial G_j^o}\right)_{G_{i\neq j}^o}$$

(2.26)

where $X_{RC,i}$ and $X_{TRC,j}$ are equal to the change in $\Delta G_{app}^{o\ddagger}$ per change in $G_{TS,i}^o$ or G_j^o, respectively. The kinetic degree of rate control of transition state i is the change in $G_{TS,app}^o$ per change in $G_{TS,i}^o$. The thermodynamic degree of rate control of species j is negative the change in $G_{IS,app}^o$ per change in G_j^o.

In this section, we proposed that $\Delta G_{app}^{o\ddagger}$ of the overall/composite reaction is a sensitivity-weighted average of $\Delta G_i^{o\ddagger}$ of elementary steps (eq. (2.18)) and that $\Delta G_{app}^{o\ddagger}$ is related to $G_{TS,i}^o$ of transition states and G_j^o of species via the kinetic and thermodynamic degrees of rate control (eqs. (2.25)-(2.26)). In the following section, we discuss the implications of these results and prove them by deriving a broader definition for sensitivity as a derivative with respect to the elementary step rate functions instead of the elementary step rate constants (eq. (2.4)), which enables the derivation of the TST-form rate function of a composite reaction.

2.3.2 Deriving transition-state-theory-form rate functions of composite reaction networks

The assignment of $\Delta G_{app}^{o\ddagger}$ to an overall/composite reaction implies the presence of a $e^{-\Delta G_{app}^{o\ddagger}/k_B T}$ term in the overall rate function of the composite reaction. Expressions with Boltzmann factors have assumptions of equilibrium in their derivations.[10] In the case of $\Delta G_{app}^{o\ddagger}$, this assumption is the equilibrium between IS_{app} and TS_{app} (see eq. (2.24)) illustrated in eq. (2.27), which is related to the degrees of rate control by eq. (2.24) and to sensitivities by eqs. (2.20) and (2.21):

$$IS_{app} \rightleftharpoons TS_{app}$$

$$\Rightarrow -\sum_{j=species} X_{TRC,j}S_j \rightleftharpoons \sum_{i=TS} X_{RC,i}TS_i,$$

$$\Rightarrow -\sum_{i=rxn}\sum_{j=species} s_i v_{ij}[v_{ij} < 0]S_j \rightleftharpoons \sum_{i=rxn} s_i TS_{|i|} \qquad (2.27)$$

$$\Rightarrow \sum_{i=rxn} s_i \left(\sum_{j=species} -v_{ij}[v_{ij} < 0]S_j \rightleftharpoons TS_{|i|} \right)$$

$$\Rightarrow \sum_{i=rxn} s_i \left(IS_i \rightleftharpoons TS_{|i|} \right)$$

where S_j represent fluid-phase or surface species j. Equation (2.27) shows that if there exists an apparent initial and transition state, it is a sensitivity-weighted average of the IS and TS of elementary steps. This is equivalent to identifying that the thermodynamic and kinetic degrees of rate control are the stoichiometric coefficients in an equilibrium between an apparent transition state and apparent initial state of an apparent rate-determining step (eq. (2.27)). In transition state theory, the transition state then proceeds to products via a first-order reaction, which is depicted for the apparent transition state of the overall/composite reaction in eq. (2.28):

$$TS_{app} \xrightarrow{v} \sum_{j=species} v_j S_j \, [v_j > 0] \qquad (2.28)$$
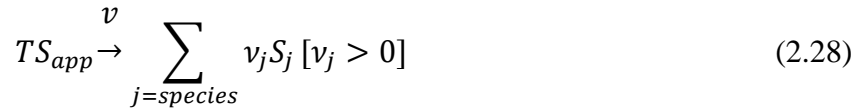
where v_j is the stoichiometric coefficient of species j of the overall reaction. In this section, we derive the TST-form rate function and we demonstrate that an apparent rate-determining step described by eqs. (2.27) and (2.28) captures the apparent reaction

orders, temperature dependencies, energies of activation, and every other parameter of the overall/composite reaction.

The rate function for the overall reaction, r, is a function of the elementary step rate functions, r_i (eq. (2.29)):

$$r = r(r_1, r_{-1}, r_2, r_{-2}, \dots, r_N, r_{-N}) \tag{2.29}$$

where N is the number of reactions in the overall/composite reaction network (see Section A2.1 of the Appendix for an example of how to write the overall rate function in terms of the elementary step rate functions). We emphasize here that r_i are functions that describe the rate of elementary step reactions in terms of the activities of reactants and elementary step rate constants and *not* the steady-state rates of elementary steps, which are the scalar outputs of the rate functions evaluated at the steady-state conditions. The rate function for each elementary step, r_i, is in the form of a transition-state-theory rate function (eq. (2.11)). The elementary step rate functions depend on the rate constants of the elementary steps (each elementary step r_i is associated with only one rate constant, k_i) and activities of reactants (eq. (2.30)):

$$r_i = r_i\big(k_i\big(G^o_{TS,i}, G^o_j, T, \dots\big), a_j\big) \tag{2.30}$$

where a_j are the activities of the reactant species in the elementary steps (including surface species). Notice that the overall rate r is a function of the rate constants k_i only because the rate functions of the elementary steps r_i are functions of the rate constants. From eqs. (2.29) and (2.30), it is possible to redefine sensitivities (originally defined in eq. (2.4)), as eq. (2.31) using the chain rule:

$$s_i = \left(\frac{\partial \ln r}{\partial \ln k_i}\right)_{k_{m \neq i}} = \sum_{j=rxn} \left(\frac{\partial \ln r}{\partial \ln r_j}\right)_{r_{n \neq j}} \left(\frac{\partial \ln r_j}{\partial \ln k_i}\right)_{k_{m \neq i}}$$

$$= \sum_{j=rxn} \left(\frac{\partial \ln r}{\partial \ln r_j}\right)_{r_{n \neq j}} \delta_{ij} \tag{2.31}$$

$$= \left(\frac{\partial \ln r}{\partial \ln r_i}\right)_{r_{n \neq i}}$$

where δ_{ij} is the Kronecker delta, which takes the value of unity if $i = j$ and is zero otherwise. We derive a different function, r_{TST}, that has the same sensitivities as the rate function, r, at a steady-state reaction condition denoted by the vector X, which contains the steady-state activities of fluid-phase and surface species, the reaction temperature, etc., by treating the sensitivities as constant and integrating eq. (2.31) with respect to each r_i to obtain eq. (2.32):

$$\ln r_{TST} = C' + \sum_i s_i \ln r_i \tag{2.32}$$

where C' is the constant of integration that is not a function of any of the elementary step rate functions. The function obtained after integration is denoted r_{TST} because it takes on the form of a TST rate function of an elementary step. The r_{TST} function does not have the same sensitivities as r everywhere, but it does at the reaction condition X and it behaves identically to differential changes in any variable about the point X, as is subsequently shown in eqs. (2.33)-(2.37) and in Section A2.2 of the Appendix. Equation (2.32) is a linearization of $\ln r_{TST}$ about X with respect to $\ln r_i$ via a first-order Taylor series expansion. Exponentiation of eq. (2.32) gives (eq. (2.33)):

$$r_{TST} = C \prod_i r_i^{s_i} \tag{2.33}$$

where $C = e^{C'}$. The sensitivities were calculated at a given reaction condition, $\mathbf{X}$. At this reaction condition, we specify that $r_{TST}|_X = r|_X$, and thus C is found by eq. (2.34):

$$C = \frac{r|_X}{\prod_i r_i^{s_i}|_X} \tag{2.34}$$

The new definition of sensitivity (eq. (2.31)) allows for the relation of derivatives of $\ln r$ to derivatives of $\ln r_i$ by the chain rule (eq. (2.35)):

$$\frac{d \ln r}{dx} = \sum_{i=rxn} \left(\frac{\partial \ln r}{\partial \ln r_i}\right)_{r_{n \neq i}} \left(\frac{d \ln r_i}{dx}\right) = \sum_{i=rxn} s_i \left(\frac{d \ln r_i}{dx}\right) \tag{2.35}$$

From eq. (2.35) we conclude that every relative change in the overall reaction rate caused by the change in a variable, x, is simply a sensitivity-weighted average of the relative change in the rates of elementary steps caused by a change in the variable x. Equation (2.35) is written as a total derivative but an analogous equation for partial derivatives can also be derived (see discussion in Section A2.1 of the Appendix). Equation (2.35) is used here to demonstrate that the apparent reaction order of species j ($\psi_{j,app}$) of the overall net rate is a sensitivity-weighted average of the reaction orders of species j in the elementary steps (ψ_{ij}) (eq. (2.36)):

$$\psi_{j,app} = \frac{d \ln r}{d \ln a_j} = \sum_{i=rxn} \left(\frac{\partial \ln r}{\partial \ln r_i}\right)_{r_{n \neq i}} \left(\frac{d \ln r_i}{d \ln a_j}\right) = \sum_{i=rxn} s_i \left(\frac{d \ln r_i}{d \ln a_j}\right)$$

$$= \sum_{i=rxn} s_i \psi_{ij} = - \sum_{i=rxn} s_i v_{ij}[v_{ij} < 0] = -X_{TRC,j} \tag{2.36}$$

The reaction order of a species in an elementary step is equal to negative the stoichiometric coefficient of that species if it is a reactant. From this, eq. (2.36) shows that the apparent reaction order of a species is equal to negative its thermodynamic degrees of rate control (see eq. (2.23)).

In Section A2.3 of the Appendix, the formal definition of a derivative as a limit is used to show that the derivative of $\ln r$ with respect to $\ln k_i$ is equivalent to the derivative of $\ln r$ with respect to $\ln r_i$ (eq. (2.31)). Using limits, we also illustrate that apparent reaction orders are sensitivity-weighted averages of the reaction orders of the elementary reactions (eq. (2.36)).

The right-hand side of eq. (2.35) is equal to the derivative of the r_{TST} function (eq. (2.37)):

$$\frac{d \ln r_{TST}}{dx} = \frac{1}{r_{TST}} \frac{d r_{TST}}{dx} = \frac{1}{C \prod_i r_i^{s_i}} \frac{d}{dx} C \prod_i r_i^{s_i}$$

$$= \frac{C \sum_i s_i \left(\frac{dr_i}{dx}\right) r_i^{s_i-1} \prod_{j \neq i} r_j^{s_j}}{C \prod_i r_i^{s_i}} = \frac{C \sum_i s_i \left(\frac{d \ln r_i}{dx}\right) r_i^{s_i} \prod_{j \neq i} r_j^{s_j}}{C \prod_i r_i^{s_i}} \qquad (2.37)$$

$$= \sum_i s_i \left(\frac{d \ln r_i}{dx}\right) = \frac{d \ln r}{dx}$$

Equation (2.37) shows that the relative change in the overall rate, r, is equal to the relative change in the function r_{TST} with respect to any variable. This is true with or without the arbitrary constant C. The inclusion of the arbitrary constant C renders $r = r_{TST}$ at reaction condition $\boldsymbol{X}$, and thus at this point, the function r_{TST} is tangent to the function r with respect to every variable (eq. (2.38)):

26

$$\left.\frac{dr}{dx}\right|_X = \left.\frac{dr_{TST}}{dx}\right|_X \tag{2.38}$$

as illustrated in Figures A2.1-A2.4 in Section A2.2 in the Appendix. Thus at the reaction condition X, $r \approx r_{TST}$ for differential changes in any variable. The function r_{TST} can be expanded to an equation that resembles a TST rate function of an elementary step (eq. (2.39)):

$$
\begin{aligned}
r_{TST} &= C \prod_i r_i^{s_i} \\
&= C \prod_i \left(\frac{k_B T}{h}\right)^{s_i} e^{-s_i\left(G_{TS,i}^o + \sum_j v_{ij}[v_{ij}<0]G_j^o\right)/k_B T} \prod_j a_j^{-v_{ij}[v_{ij}<0]s_i} \\
&= C \left(\frac{k_B T}{h}\right)^{\sum_i s_i} e^{-\sum_i\left(s_i G_{TS,|i|}^o + \sum_j s_i v_{ij}[v_{ij}<0]G_j^o\right)/k_B T} \prod_j a_j^{-\sum_i s_i v_{ij}[v_{ij}<0]} \\
&= C \frac{k_B T}{h} e^{-\left(\sum_i X_{RC,i}G_{TS,i}^o + \sum_j X_{TRC,j}G_j^o\right)/k_B T} \prod_j a_j^{-X_{TRC,j}}
\end{aligned}
\tag{2.39}
$$

where substitutions of sensitivities for degrees of rate control used eqs. (2.22) and (2.23) and the sum of sensitivities was assumed to equal unity (see Section 2.3.3). In eq. (2.39), $\Delta G_{app}^{o\ddagger}$ of the function r_{TST} is in agreement with the $\Delta G_{app}^{o\ddagger}$ equations derived in Section 2.3.1 (eqs. (2.19)-(2.24)), demonstrating that $\Delta G_{app}^{o\ddagger}$ for the composite rate function r is the same as the $\Delta G_{app}^{o\ddagger}$ for the TST-form composite rate function, r_{TST}. Notice that the reaction order of stable species (both fluid-phase and surface species) is related to the contribution of that species' G_j^o in the exponential, just like the transition-state-theory rate function for an elementary step (eq. 1.11). Application of transition state theory to the apparent rate-determining step described by eqs. (2.27) and (2.28) is equal to the

27

function r_{TST} (eq. (2.39)) within a multiplicative factor C. Multiplicative factors appear in TST-rate functions of elementary steps in the form of transmission coefficients κ or conversion coefficients ξ, and thus by analogy the factor C can be envisioned as such a corrective factor. We draw analogy between C and the conversion coefficient ξ in Section A2.4 of the Appendix. From this, we conclude that the conceptualization of an apparent rate-determining step for an overall/composite reaction network is a useful concept for rationalizing apparent reaction orders and apparent energies and entropies (see Section 2.3.9) of activation of the overall reaction rate.

From eq. (2.39), the apparent reaction orders of the activities are equal to the thermodynamic degrees of rate control of both fluid-phase and surface species. It may seem strange to the reader that a surface species has an apparent reaction order, but this is indeed the case. The difference between the reaction orders of surface species and the reaction orders of fluid-phase species is that fluid-phase species can be varied to measure their reaction orders. We utilize the concept of apparent reaction orders of surface species to prove the relationship between thermodynamic degrees of rate control and steady-state surface coverages (eq. (2.3)) in Section 2.3.5, and we illustrate in Section 2.3.9 that the apparent entropy of activation can be assessed for composite reactions only if the fractional coverages of surface species taken to their apparent reaction orders are included in the TST-form rate function of the composite reaction.

Thus far, we have intentionally avoided the term "rate-determining step" because, as pointed out previously by Kozuch and Martin,[24] this term is typically inaccurately attributed to the step with the rate-determining *transition state*. A "step" has three components: an initial state, a transition state, and a final state. Two of these states, the

28

initial state and the transition state, are kinetically relevant to the rate of the reaction. Considering only the transition state in the definition of the rate-determining step concept neglects the contribution of the initial state to the rate of the reaction. Kozuch and Martin[24] argued that the rate-determining step concept should be replaced with the concept of rate-determining states, determined by the kinetic and thermodynamic degrees of rate control. In the analysis presented here, there is a hypothetical equilibrium between stable species and transition states with stoichiometric coefficients equal to the thermodynamic and kinetic degrees of rate control (eq. (2.27)). The rate of the overall reaction depends both on the apparent initial state and the apparent transition state—in agreement with conclusions made by Kozuch and Martin.[24] We infer that the metric apposite to determine the rate control of a *step* is the sensitivity, s_i, which is a metric that incorporates contributions of both the initial state and the transition state of an elementary step to the apparent initial and apparent transition state of the composite/overall reaction.

In eq. (2.39) we assumed that the sum of sensitivities is equal to one such that the term $k_B T/h$ was taken to the power of one. The term $k_B T/h$ has units of s^{-1} and is the only term in eq. (2.39) to endow units of rate to the function r_{TST}, and thus, if the sum of sensitivities (which is equal to the sum of the kinetic degrees of rate control by eq. (2.22)) summed to any value other than unity, the function r_{TST} would not have units of rate. In the following section, we use this observation to prove that the sensitivities (and the kinetic degrees of rate control) sum to unity for any composite reaction network.

2.3.3 Proof that the sum of the sensitivities and kinetic degrees of rate control equal unity

The long-standing postulate in the field that the sum of the sensitivities and the degrees of rate control equals unity for all reaction networks has been proven for specific reaction schemes and appears to be true for all reactions studied.[12,13,25] Redefining sensitivities based on the rate functions of elementary steps (eq. (2.31)) provides a simple means for proving that the sum of the sensitivities equals unity. It requires the reader to accept the precept that the only quantity that endows units of s^{-1} for rates, whether they are rates of elementary steps or rates of composite reaction networks, is the term $\chi = k_B T/h$. Thus, the rate of an overall reaction must be of the form in eq. (2.40):

$$r = \chi f(\boldsymbol{X}) \tag{2.40}$$

where f is a function with unitless outputs and $\boldsymbol{X}$ is a vector of activities, energies, etc. Despite χ being composed of fundamental constants, mathematically the derivative of the log of the rate with respect to the log of χ is a defined quantity (eq. (2.41)):

$$\frac{d \ln r}{d \ln \chi} = \frac{\chi}{r}\left(\frac{dr}{d\chi}\right) = 1 \tag{2.41}$$

From eq. 2.2.9, this derivative is equal to the sum of the sensitivities (eq. (2.42)):

$$\frac{d \ln r}{d \ln \chi} = \sum_{i=rxn} s_i \left(\frac{d \ln r_i}{d \ln \chi}\right) = \sum_{i=rxn} s_i \tag{2.42}$$

Thus, from eqs. (2.41) and (2.42), it follows that $\sum_i s_i = \sum_i X_{RC,i} = 1$ (see eq. (2.22)). An equivalent argument could be made by instead replacing χ with s^{-1} in both eq. (2.41) and eq. (2.42). This more general proof can be found in Section A2.5 of the Appendix.

We demonstrated above that the only constraint for the sum of sensitivities and the kinetic degrees of rate control is imposed by the units—the rates of the elementary steps have the same units as the rate of the overall reaction, and thus the sensitivities must sum to unity. In this way, there is nothing inherently special about a reaction system that causes the sum of the sensitivities and kinetic degrees of rate control to sum to unity, but it is convenient, as the sensitivity thus becomes a measure of the relative contribution of an elementary step rate function to the TST-form rate function (eq. (2.39)). Because there is nothing inherently unique about composite reaction systems, the concept of sensitivities can be applied to other systems as we demonstrate by example for an external mass-transfer limited catalytic reaction system in Section A2.6 of the Appendix.

2.3.4 De Donder Relations and Degrees of Rate Control

As discussed in the Section 2.3.2, De Donder relations and degrees of rate control are complementary methods for assessing rate control in a reaction network.[19] The degrees of rate control require kinetic information about the rate constants for elementary steps, while the De Donder formalism examines reaction networks from the vantage point of thermodynamic driving forces. Reversibilities, Z_i, as defined within the De Donder formalism (eq. (2.7)), can be related to the kinetic degrees of rate control in systems of first-order reactions in series with stoichiometric numbers for all reactions being one by eq. (2.8) as discussed by Cortright and Dumesic.[23] The relationship between $X_{RC,i}$ and Z_i for other types of composite reaction networks (i.e. when reaction orders and stoichiometric numbers are not all one and/or reactions are not in series) is unclear, however, eq. (2.8) has been suggested as an approximation applicable for all reaction

networks in series, but equations for other types of reaction networks have not been proposed.[22] We demonstrate here a method for deriving $X_{RC,i}$ as functions of Z_i and show that the functional relationships between these quantities depend on the connectivity of the composite reaction network.

The method for relating $X_{RC,i}$ and Z_i for a reaction network with specified connectivity relies on the derived relationships between sensitivities and degrees of rate control and the TST-form rate function (eq. (2.39)). The key for finding the relationship between the kinetic degree of rate control and the reversibilities is recognizing that the reaction order (and $X_{TRC,i}$) of reactive intermediates is equal to zero (see eq. (2.39)). This gives eq. (2.43) for each reactive intermediate:

$$X_{TRC,j} = \sum_{i=rxn} v_{ij} s_i [v_{ij} < 0] = 0, \qquad j = \text{reactive intermediate} \qquad (2.43)$$

We stress here that a species is only considered reactive if $X_{TRC,j} \approx 0$. We distinguish *reactive* intermediate from a *reaction* intermediate. Reactive intermediates are unstable species that are rapidly consumed and thus have thermodynamic activities that approach zero at (pseudo) steady-state reaction conditions. Reaction intermediates are any species formed and consumed during reaction but are not always unstable, highly reactive species and thus do not necessarily have thermodynamic activities that approach zero at (pseudo) steady-state reaction conditions. For surface species in catalyzed reactions, this requires that the coverage of that species is nearly zero to be considered a reactive intermediate—otherwise it is only a reaction intermediate if it has a nonzero steady-state surface coverage (see eq. (2.3)).[11] The additional consequences of this work that are unique to catalytic reactions are discussed in Sections 2.3.5-2.3.8.

32

It has been proven previously for some reaction systems that the ratio of the forward and reverse sensitivities of a reaction is equal to negative the reversibility of that reaction (eq. (2.44))[19,23]:

$$\frac{s_{-i}}{s_i} = -Z_i \tag{2.44}$$

This is proven more generally by analyzing the total derivative of $\ln k_i$ with $\ln k_{-i}$ and $\ln r$ as the independent variables (eqs. (2.45)-(2.47)):

$$d \ln k_i = \left(\frac{\partial \ln k_i}{\partial \ln k_{-i}}\right)_r d \ln k_{-i} + \left(\frac{\partial \ln k_i}{\partial \ln r}\right)_{k_{-i}} d \ln r \tag{2.45}$$

$$\left(\frac{\partial \ln k_i}{\partial \ln k_{-i}}\right)_{k_i} = \left(\frac{\partial \ln k_i}{\partial \ln k_{-i}}\right)_r \left(\frac{\partial \ln k_{-i}}{\partial \ln k_{-i}}\right)_{k_i} + \left(\frac{\partial \ln k_i}{\partial \ln r}\right)_{k_{-i}} \left(\frac{\partial \ln r}{\partial \ln k_{-i}}\right)_{k_i} \tag{2.46}$$

$$0 = \left(\frac{\partial \ln k_i}{\partial \ln k_{-i}}\right)_r + s_{-i}/s_i \tag{2.47}$$

Next, we evaluate the first term in eq. (2.47) by writing the overall rate as the forward minus the reverse rate of a step i (eq. (2.48)):

$$r = 1/\sigma_i \left(k_i \prod_{j=species} a_j^{-v_{ij}[v_{ij}<0]} - k_{-i} \prod_{j=species} a_j^{v_{ij}[v_{ij}>0]} \right) \tag{2.48}$$

where σ_i is equal to the stoichiometric number for the steps that comprise the overall closed reaction scheme. Solving for k_i gives eq. (2.49):

$$k_i = r\sigma_i \prod_{j=species} a_j^{v_{ij}[v_{ij}<0]} + k_{-i} \prod_{j=species} a_j^{v_{ij}} \tag{2.49}$$

and then taking the partial derivative of k_i with respect to k_{-i} while keeping the rate constant (eq. (2.50)):

$$\left(\frac{\partial \ln k_i}{\partial \ln k_{-i}}\right)_r = \frac{k_{-i}}{k_i}\left(\frac{\partial k_i}{\partial k_{-i}}\right)_r = \frac{\prod_j a_j^{v_{ij}}}{k_i/k_{-i}} = \frac{\prod_j a_j^{v_{ij}}}{K_i^{eq}} = Z_i \qquad (2.50)$$

Combining eq. (2.50) with eq. (2.47), it is clear that $s_{-i}/s_i = -Z_i$. With this identity, the kinetic degree of rate control is written as eq. (2.51) as in reference [23]:

$$X_{RC,i} = s_i + s_{-i} = s_i(1 - Z_i) \qquad (2.51)$$

Now eq. (2.43), eq. (2.44), eq. (2.51), and $\sum_i X_{RC,i} = 1$ provide a system of algebraic equations that can be solved to eliminate all sensitivities to arrive at equations for $X_{RC,i}$ that depend only on Z_i. These methods are demonstrated for two different reaction networks presented in Table 2.3 that sum to the same overall reaction. In both reaction networks, B and C are reactive intermediates for which the pseudo-steady-state approximation is valid.

Table 2.3: Two reaction networks that sum to the same overall reaction and consider B and C as reactive intermediates.

| | **Reaction Network 1** | | **Reaction Network 2** | |
Step	Reaction	σ_i	Reaction	σ_i
1	$A \rightleftarrows B$	2	$A \rightleftarrows B$	1
2	$B \rightleftarrows C$	1	$A \rightleftarrows C$	1
3	$B + C \rightleftarrows D$	1	$B + C \rightleftarrows D$	1
Overall	$2A \rightleftarrows D$		$2A \rightleftarrows D$	

From eq. (2.43), the $X_{TRC,j}$ (or reaction orders) of a_B and a_C for Reaction Network 1 are given by eq. (2.52) and eq. (2.53), respectively:

$$s_{-1} + s_2 + s_3 = 0 \qquad (2.52)$$

$$s_{-2} + s_3 = 0 \tag{2.53}$$

Knowing that $s_{-i} = -Z_i s_i$, eqs. 2.4.10 and 2.4.11 can be solved for s_2 and s_3 (eqs. (2.54) and (2.55)):

$$s_2 = \frac{Z_1}{1 + Z_2} s_1 \tag{2.54}$$

$$s_3 = \frac{Z_1 Z_2}{1 + Z_2} s_1 \tag{2.55}$$

The kinetic degrees of rate control (see eq. (2.51) above) are thus (eqs. (2.56)-(2.58)):

$$X_{RC,1} = (1 - Z_1) s_1 \tag{2.56}$$

$$X_{RC,2} = s_2 (1 - Z_2) = \frac{Z_1 (1 - Z_2)}{1 + Z_2} s_1 \tag{2.57}$$

$$X_{RC,3} = s_3 (1 - Z_3) = \frac{Z_1 Z_2 (1 - Z_3)}{1 + Z_2} s_1 \tag{2.58}$$

Since $\sum_i X_{RC,i} = 1$ as discussed in Section 2.3.3, we can write $X_{RC,i}$ as shown in eq. (2.59):

$$X_{RC,i} = \frac{X_{RC,i}}{\sum_i X_{RC,i}} \tag{2.59}$$

and thus the kinetic degrees of rate control as a function of the reversibilities for Reaction Network 1 in Table 2.3 are (eq. (2.60)-(2.62)):

$$X_{RC,1} = \frac{(1 - Z_1)(1 + Z_2)}{(1 - Z_1)(1 + Z_2) + Z_1(1 - Z_2) + Z_1 Z_2(1 - Z_3)} \tag{2.60}$$

$$X_{RC,2} = \frac{Z_1(1 - Z_2)}{(1 - Z_1)(1 + Z_2) + Z_1(1 - Z_2) + Z_1 Z_2(1 - Z_3)} \tag{2.61}$$

$$X_{RC,3} = \frac{Z_1 Z_2 (1 - Z_3)}{(1 - Z_1)(1 + Z_2) + Z_1(1 - Z_2) + Z_1 Z_2 (1 - Z_3)} \qquad (2.62)$$

and all sensitivities are easily found from eqs. (2.60)-(2.62) and eq. (2.44). Thus, by assessing only the reversibilities, all sensitivities and degrees of rate control are obtained. Following the same procedure, the kinetic degrees of rate control for Reaction Network 2 in Table 2.3 are (eq. (2.63)-(2.65)):

$$X_{RC,1} = \frac{Z_2 (1 - Z_1)}{(1 - Z_1)Z_2 + Z_1(1 - Z_2) + Z_1 Z_2 (1 - Z_3)} \qquad (2.63)$$

$$X_{RC,2} = \frac{Z_1 (1 - Z_2)}{(1 - Z_1)Z_2 + Z_1(1 - Z_2) + Z_1 Z_2 (1 - Z_3)} \qquad (2.64)$$

$$X_{RC,3} = \frac{Z_1 Z_2 (1 - Z_3)}{(1 - Z_1)Z_2 + Z_1(1 - Z_2) + Z_1 Z_2 (1 - Z_3)} \qquad (2.65)$$

The differences between eqs. (2.60)-(2.62) and eqs. (2.63)-(2.65) reveal that the equations relating $X_{RC,i}$ to Z_i vary with the connectivity of the reaction network. For example, when $Z_1 = 0.3, Z_2 = 0.01$, and $Z_3 = 0.1$, the value for $X_{RC,1} = 0.7$ for Reaction Network 1 (eq. (2.60)) and $X_{RC,1} = 0.02$ for Reaction Network 2 (eq. (2.63)).

In a recent publication, Bhan and coworkers[26] employed the method described above to derive a relationship between kinetic degrees of rate control and reversibilities during methane dehydroaromatization to benzene on Mo/HZSM-5 catalysts. Those equations were used to assess the kinetic degrees of rate control by measurements of pseudo-steady-state activities of reaction intermediates in the effluent gas stream to identify transition states involving acetylene formation and consumption as kinetically-relevant in the overall $6CH_4 \rightarrow C_6H_6 + 9H_2$ reaction.[26]

If sensitivities can be determined as a function of reversibilities, the reaction orders with respect to activities, which depend only on sensitivities and stoichiometric coefficients (eq. (2.36)), are also determined as functions of the reversibilities.[*] The functional relationship between the reaction orders and the reversibilities via the sensitivities can be leveraged to discriminate between competing mechanistic postulates when the pseudo-steady-state approximation is valid, as is demonstrated in the following example.

Consider two possible reaction mechanisms for the conversion of E to P shown in Table 2.4 where the thermodynamic activities of all species are ideal. Both reaction mechanisms can have reaction orders in E that vary from one to three depending on which transition states are rate-limiting, thus discerning between these two reaction mechanisms is challenging. However, the relationship between the reaction order and the reversibilities changes with connectivity of the reaction network, and thus, this relationship can be used as a means for determining which mechanism is consistent with experimental observations.

Table 2.4: Two possible mechanisms for the overall reaction $3E \rightleftarrows P$

Step	Mechanism 1		Mechanism 2	
	Reaction	σ_i	Reaction	σ_i
1	$E \rightleftarrows I_1$	*1*	$E \rightleftarrows I_1$	*3*
2	$E + I_1 \rightleftarrows I_2$	*1*	$2I_1 \rightleftarrows I_2$	*1*
3	$E + I_2 \rightleftarrows P$	*1*	$I_1 + I_2 \rightleftarrows P$	*1*
Overall	$3E \rightleftarrows P$		$3E \rightleftarrows P$	

---

[*]Here we are referring to the exponent on the activity as the reaction order, which may differ from the reaction order with respect to concentration if the fluid-phase is non-ideal.

Negative the sum of the sensitivities of each elementary step multiplied by the stoichiometric coefficient of E (eq. (2.36)) gives the apparent reaction order of E in Mechanism 1 (eq. (2.66)) and Mechanism 2 (eq. (2.67)):

$$\psi_{E,app,1} = s_1 + s_2 + s_3 \tag{2.66}$$

$$\psi_{E,app,2} = s_1 \tag{2.67}$$

Assuming that the pseudo-steady-state approximation is valid on reactive intermediates I_1 and I_2, then the sum of the sensitivities multiplied by the stoichiometric coefficients for these species equals zero (see eq. (2.43)). For Mechanism 1, these equations are (eq. (2.68) and eq. (2.69)):

$$s_{-1} + s_2 = 0 \tag{2.68}$$

$$s_{-2} + s_3 = 0 \tag{2.69}$$

and for Mechanism 2, these equation are (eq. (2.70) and eq. (2.71)):

$$s_{-1} + 2s_2 + s_3 = 0 \tag{2.70}$$

$$s_{-2} + s_3 = 0 \tag{2.71}$$

Noting that $\sum_i s_i = 1$ and $s_{-i} = -Z_i s_i$, the reaction order of E as a function of reversibilities is determined by solving the system of algebraic equations. For Mechanism 1, the reaction order of E is (eq. (2.72)):

$$\psi_{E,app,1} = \frac{1 + Z_1 + Z_1 Z_2}{1 - Z_1 Z_2 Z_3} \tag{2.72}$$

For Mechanism 2, the reaction order of E is (eq. (2.73)):

$$\psi_{E,app,2} = \frac{2 + Z_2}{2 + Z_2 - Z_1 - Z_1 Z_2 - Z_1 Z_2 Z_3} \tag{2.73}$$

The difference in the reaction order for Mechanism 1 (eq. (2.72)) and Mechanism 2 (eq. (2.73)) can be used to identify the mechanism for the reaction under study. As a demonstration, consider the case where the reaction order of E is measured when $Z_2 = Z_3 = 0$. The reaction order as a function of Z_1 is shown in Figure 2.2 where the points represent the reaction order obtained by simulating the reaction rate of Mechanisms 1 and 2 and the lines are the reaction orders predicted by eqs. (2.72) and (2.73). By measuring the reaction order of E and the reversibility of the reaction $E \rightleftarrows I_1$, the prevalent reaction mechanism can be ascertained.
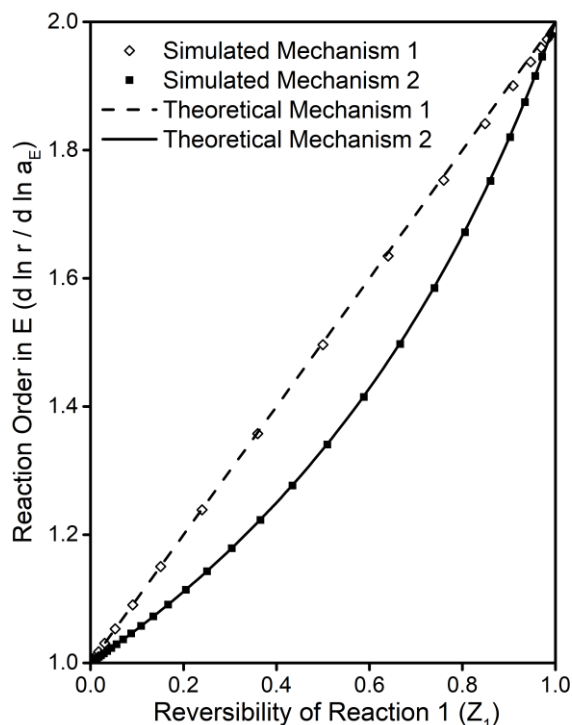
Figure 2.2: Reaction orders as a function of the reversibility of reaction 1 in Mechanism 1 and 2 in Table 2.4 with $Z_2 = Z_3 = 0$. The points are reaction orders for the simulated reaction rates in Matlab and the lines are the reaction orders predicted by eqs. (2.72) and (2.73).

Thus far we have only considered the implications of application of transition state theory to composite/overall reaction networks that apply to both uncatalyzed and

catalyzed reactions and have only considered examples for uncatalyzed reactions. Site balances in catalyzed reactions introduce additional algebraic constraints, and these constraints, in turn, lead to additional conclusions regarding the relationship between steady-state fractional coverages, sensitivities, and degrees of rate control. In the following sections, we rigorously derive these relationships and demonstrate by example how these are applied to catalyzed composite reactions.

2.3.5 Application of transition state theory to a composite network of catalytic reactions

Catalytic reactions are a special case of composite reactions, and all the equations derived in the preceding sections apply to composite catalytic reaction networks. The difference between composite catalytic reactions and composite fluid-phase reactions is that there is a constraint on the surface reaction intermediates in the catalytic reaction—the sum of the fractional coverages of surface species is equal to unity (eq. (2.74)):

$$\sum_{\substack{j^*=surface \\ species}} \theta_{j^*} = 1 \tag{2.74}$$

This constraint introduces features that are only true for catalytic systems. One of these was observed by Stegelmann et al.,[11] who reported that the thermodynamic degrees of rate control are proportional to surface coverages by $X_{TRC,j^*} = -\sigma_* \theta_{j^*}$, where σ_* was referred to as the average number of sites in the rate-determining steps, but neither an equation for σ_* nor a proof for this relationship were reported. We provide a proof for this and show that the proportional relationship between surface coverage and thermodynamic degrees of rate control is only true when surface species behave ideally, i.e., each site is

independent and the free energies of transition states and surface species are not functions of surface coverage.

Before presenting this proof, we discuss the logic behind the proof by envisioning the potential energy surface of a closed catalytic cycle (Figure 2.3); the reaction sequence simply represents a series of steps that induce reactants into the sequence and steps that emit products that are formed. During steady-state catalysis, surface sites traverse the catalytic cycle at a constant rate—each trip around the cycle denoting a *turnover*.[27] The number of turnovers each site completes per unit time is referred to as the *turnover frequency* or *turnover rate*.[27] Each site traverses the same catalytic cycle and therefore experiences the same rate-limiting transition states, but at steady state, each site is in a different trough of the potential energy surface. The fraction of sites in each trough is given by the fractional coverage. With this in mind, we write the equilibrium between IS_{app} and TS_{app} of the apparent rate-determining step as (eq. (2.75)):

$$\sum_{r=reactants} -\nu_{r,app}S_r + \sum_{\substack{j^*=surface \\ species}} -\nu_{j^*,app}S_{j^*} \rightleftharpoons TS_{app} \tag{2.75}$$
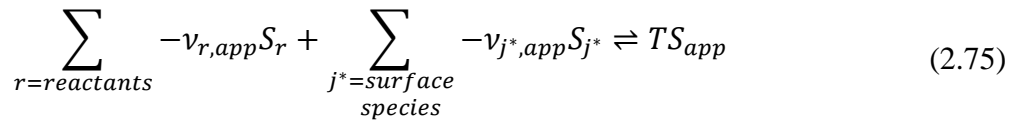
Consider the scenario in which we form one TS_{app}. Because each site traverses the catalytic cycle at the same rate, it is necessary that the surface species in eq. (2.75) are consumed in ratios correspondent to their steady-state coverages. Therefore, we speculate that the apparent stoichiometric coefficients are related to the steady-state surface coverages by eq. (2.76):

$$\frac{\nu_{m^*,app}}{\sum_{j^*}\nu_{j^*,app}} = \theta_{m^*} \tag{2.76}$$

We prove this relationship in the subsequent discussion.
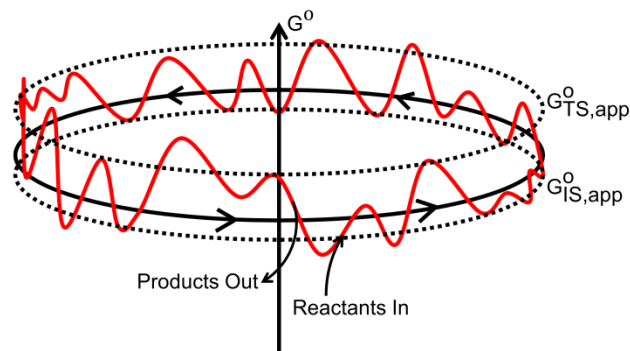
Figure 2.3: Hypothetical potential energy surface for a closed catalytic cycle. The dotted lines represent the apparent initial state and transition state energies.

For elementary reactions, the reaction order is equal to the stoichiometric coefficient of the reactant species. We thus define the apparent stoichiometric coefficient of a surface species as the apparent reaction order with respect to the fractional coverage of a species in the composite reaction $(\psi_{\theta j^*, app})$. We digress to mention a subtle distinction between $\psi_{\theta j^*, app}$ here and $\psi_{j^*, app}$ (from eq. (2.36)). The former is the apparent reaction order with respect to the fractional coverage θ_{j^*}, while the latter is the apparent reaction order with respect to the activity of the surface species j^*. These are equal in cases where the system is ideal, i.e., when free energies of activation are not functions of surface coverages. The apparent reaction order with respect to the fractional coverage of a surface species is the relative change in the rate per relative change in the fractional coverage of the surface species while keeping all other fractional coverages constant (eq. (2.77)):

$$-v_{\theta j^*,app} = \psi_{\theta j^*,app} = \left(\frac{\partial \ln r}{\partial \ln \theta_{j^*}}\right)_{\theta_{n \neq j^*}} = \sum_{i=rxn} \left(\frac{\partial \ln r}{\partial \ln r_i}\right)_{r_{m \neq i}} \left(\frac{\partial \ln r_i}{\partial \ln \theta_{j^*}}\right)_{\theta_{n \neq j^*}}$$

(2.77)

$$= \sum_{i=rxn} s_i \left(\frac{\partial \ln r_i}{\partial \ln \theta_{j^*}}\right)_{\theta_{n \neq j^*}}$$

Consider a reaction with N unique surface species, where each surface species is arbitrarily assigned a value between 1 and N. We can relate the reaction orders of two different surface species starting with the n-tuple product rule (an expanded form of the more well-known triple product rule) (eq. (2.78)):

$$\left(\frac{\partial r}{\partial \theta_{1^*}}\right)_{\theta_{m \neq 1^*}} \left(\prod_{n=1}^{N-1} \left(\frac{\partial \theta_{n^*}}{\partial \theta_{(n+1)^*}}\right)_{r, \theta_{m \neq \{n^*,(n+1)^*\}}}\right) \left(\frac{\partial \theta_{N^*}}{\partial r}\right)_{\theta_{m \neq N^*}} = (-1)^{N+1}$$

(2.78)

Because the sum of the fractional coverages must equal unity, changing the fractional coverage of one species $((n+1)^*)$ requires an equal and opposite change in another species (n^*) when keeping all other fractional coverages constant. Using eq. (2.74), we can evaluate the partial derivatives of the fractional coverage of one surface species with respect to another surface species as (eq. (2.79)):

$$\left(\frac{\partial \theta_{n^*}}{\partial \theta_{(n+1)^*}}\right)_{r, \theta_{m \neq (n^*,(n+1)^*)}} = -1$$

(2.79)

Substitution of eq. (2.79) into eq. (2.78) and simplification obtains eq. (2.80):

$$\left(\frac{\partial r}{\partial \theta_{1^*}}\right)_{\theta_{m \neq 1^*}} (-1)^{N-1} \left(\frac{\partial \theta_{N^*}}{\partial r}\right)_{\theta_{m \neq N^*}} = (-1)^{N+1}$$

(2.80)

Both sides of eq. (2.80) are divided by $(-1)^{N-1}$ and multiplied by $(r/r)(\theta_{1^*}/\theta_{N^*})$ to obtain eq. (2.81):

$$\frac{\theta_{1^*}}{r}\left(\frac{\partial r}{\partial \theta_{1^*}}\right)_{\theta_{m\neq 1^*}} \frac{r}{\theta_{N^*}}\left(\frac{\partial \theta_{N^*}}{\partial r}\right)_{\theta_{m\neq N^*}} = \left(\frac{\partial \ln r}{\partial \ln \theta_{1^*}}\right)_{\theta_{m\neq 1^*}} \left(\frac{\partial \ln \theta_{N^*}}{\partial \ln r}\right)_{\theta_{m\neq N^*}}$$

$$= \frac{\psi_{\theta 1^*,app}}{\psi_{\theta N^*,app}} = \frac{\theta_{1^*}}{\theta_{N^*}}$$

(2.81)

The values 1 and N were arbitrary assigned to surface species, thus (eq. (2.82)):

$$\frac{\psi_{\theta N^*,app}}{\sum_{j^*}\psi_{\theta j^*,app}} = \left(\sum_{j^*}\frac{\psi_{\theta j^*,app}}{\psi_{\theta N^*,app}}\right)^{-1} = \left(\sum_{j^*}\frac{\theta_{j^*}}{\theta_{N^*}}\right)^{-1} = \left(\frac{1}{\theta_{N^*}}\right)^{-1} = \theta_{N^*}$$

(2.82)

which is identical to the equation derived from the thought experiment (eq. (2.76)). The apparent reaction order of each surface species, $\psi_{\theta j^*,app}$, is related to sensitivities by eq. (2.77), and thus eq. (2.82) can be written in terms of sensitivities (eq. (2.83)):

$$\frac{\psi_{\theta N^*,app}}{\sum_{j^*}\psi_{\theta j^*,app}} = \frac{\sum_i s_i \left(\frac{\partial \ln r_i}{\partial \ln \theta_{N^*}}\right)_{\theta_{m\neq N^*}}}{\sum_{j^*}\sum_i s_i \left(\frac{\partial \ln r_i}{\partial \ln \theta_{j^*}}\right)_{\theta_{m\neq j^*}}} = \theta_{N^*}$$

(2.83)

Equation (2.83) describes a relationship between the sensitivities and the fractional coverages of surface intermediates. In the special case where surface species behave ideally and $\Delta G_i^{o\ddagger}$ are not functions of surface coverages, the apparent reaction order of a surface species is equal to negative the stoichiometric coefficient of the surface species for that elementary step when it is a reactant and zero otherwise (eq. (2.84)):

$$\left(\frac{\partial \ln r_i}{\partial \ln \theta_{j^*}}\right)_{\theta_{n\neq j^*}} = -\nu_{ij^*}[\nu_{ij^*} < 0]$$

(2.84)

and in this case, we find that the apparent reaction order of a surface species is equal to negative its thermodynamic degree of rate control (eq. (2.85)):

$$\psi_{\theta j^*,app} = \sum_{i=rxn} s_i \left(\frac{\partial \ln r_i}{\partial \ln \theta_{j^*}} \right)_{\theta_{n \neq j^*}} = \sum_{i=rxn} -s_i v_{ij^*} [v_{ij^*} < 0] = -X_{TRC,j^*} \qquad (2.85)$$

Equation (2.85) can then be rewritten as a function of thermodynamic degrees of rate control in this limiting case as (eq. (2.86)):

$$\frac{\psi_{\theta N^*,app}}{\sum_{j^*} \psi_{\theta j^*,app}} = \frac{\sum_i s_i v_{iN^*} [v_{iN^*} < 0]}{\sum_{j^*} \sum_i s_i v_{ij^*} [v_{ij^*} < 0]} = \frac{X_{TRC,N^*}}{\sum_{j^*} X_{TRC,j^*}} = \theta_{N^*} \qquad (2.86)$$

The denominator is related to the average number of surface species reacting in rate-limiting steps by eq. (2.87) (see eq. (2.23)):

$$\sum_{j^*} X_{TRC,j^*} = \sum_{i=rxn} s_i \sum_{j^*} v_{ij^*} = -\sum_{i=rxn} s_i \sigma_{*,i} = -\sigma_{*,app} \qquad (2.87)$$

where $\sigma_{*,i} = -\sum_{j^*} v_{ij^*}$ is the number of surface species reacting in step i and $\sigma_{*,app}$ is the number of reacting surface species in the apparent initial state, which is the sensitivity-weighted average of the number of reacting surface species in each initial state, or the sum of the X_{TRC,j^*}. This is in contrast to the proportionality factor definition proposed by Stegelmann et al.[11], who defined it as the average number of *sites* in rate-determining steps. The distinction arises, for example, in reactions involving surface species bound to multiple sites, such as $A^{**} \rightarrow B + 2 *$, where there are two sites in the reaction, but only one surface species reacting ($v_{A^{**}} = -1$). Combining and rearranging eqs. (2.86) and (2.87) we obtain eq. (2.3), which is the relationship reported by Stegelmann et al.[11] (eq. (2.88)):

$$\sum_{i=rxn} s_i v_{iN^*} [v_{iN}^* < 0] = X_{TRC,N^*} = \sum_{\substack{j^*=surface \\ species}} X_{TRC,j^*} \theta_{N^*} = -\sigma_{*,app} \theta_{N^*} \qquad (2.88)$$

45

We stress that eq. (2.88) is only true when surface species are ideal. Equation (2.83) describes the relationship between sensitivities and the fractional coverages of surface species for non-ideal or ideal surface species. When the surface species behave ideally, then the fractional coverages are given as an explicit function of the sensitivities (eq. (2.86)). When a surface species is a *reactive* intermediate (i.e. an unstable intermediate that at steady-state has $\theta_{j^*} \approx 0$) eq. (2.88) simplifies to eq. (2.43) which was key for relating the kinetic degrees of rate control to the reversibilities in Section 2.3.4. The same procedure in Section 2.3.4 can now be followed to calculate the kinetic degrees of rate control using eq. (2.86) for catalytic reactions (or eq. (2.83) if surface species are non-ideal) instead of eq. (2.43). Rather than reiterating an example of this calculation, we instead show how eq. (2.86) is leveraged to calculate fractional coverages of surface species by measuring the reaction orders of fluid-phase species in the following section.

2.3.6 Determining surface coverages from measured reaction orders

A method for relating reaction orders and surface coverages has been previously illustrated by Harris et al.,[28] however, the provenance of this relationship has not been established. We demonstrate this relationship is a consequence of the relationship between surface coverages and sensitivities (eq. (2.83)) and the relationship between reaction orders and sensitivities (eq. (2.36)). We illustrate this for the reaction system depicted in Table 2.5, where every reaction is quasi-equilibrated except for the surface reaction between A^* and B^* which contains the sole rate-determining transition state. The rate of the reaction (shown in Table 2.5) is (eq. (2.89)):

46

$$\frac{r}{L} = \frac{k_3 K_1 K_2 a_A a_B z}{(1 + K_1 a_A + K_2 a_B + K_4 a_C)^2} \tag{2.89}$$

where z is the coordination number. The apparent reaction order of A is found by taking the derivative of the log of the rate with respect to the log of the activity of A (eq. (2.90)):

$$\frac{d \ln r/L}{d \ln a_A} = 1 - 2\frac{K_1 a_A}{1 + K_1 a_A + K_2 a_B + K_4 a_C} = 1 - 2\theta_{A^*} \tag{2.90}$$

where $K_1 a_A/(1 + K_1 a_A + K_2 a_B + K_4 a_C)$ is the fractional coverage of A given by the Langmuir isotherm. Equation (2.90) thus describes the relationship between the reaction order of A and the surface coverage of A for the reaction network depicted in Table 2.5. A similar relationship for B and C is found by following the same procedure (eqs. (2.91) and (2.92)):

$$\frac{d \ln r}{d \ln a_B} = 1 - 2\frac{K_2 a_B}{1 + K_1 a_A + K_2 a_B + K_4 a_C} = 1 - 2\theta_{B^*} \tag{2.91}$$

$$\frac{d \ln r}{d \ln a_C} = -2\frac{K_4 a_C}{1 + K_1 a_A + K_2 a_B + K_4 a_C} = -2\theta_{C^*} \tag{2.92}$$

Finding a relationship between reaction orders and the surface coverages has been demonstrated previously,[28] but here we rationalize why this relationship exists and demonstrate a purely algebraic method for deriving this relationship using sensitivities. In Table 2.5, it is assumed that the reversibilities of elementary steps are $Z_1 = Z_2 = Z_4 = 1$ and $Z_3 = 0$ and that $X_{RC,3} = s_3 + s_{-3} = 1$. From eq. (2.44), because $Z_3 = 0$ it follows that $s_{-3} = 0$ and thus $s_3 = 1$. These assumptions were necessary for the derivation of the closed-form steady-state rate function (eq. (2.89)). With this information, it requires only algebraic manipulation of the equations presented in this work to demonstrate the

relationship between reaction orders and surface coverages. From eq. (2.86), we can write

an equation for the surface coverage of A as a function of sensitivities (eq. (2.93)):

$$\theta_{A^*} = \frac{s_{-1} + s_3}{s_1 + s_{-1} + s_2 + s_{-2} + 2s_3 + 2s_{-3} + s_4 + s_{-4}} = \frac{s_{-1} + 1}{2} \tag{2.93}$$

The denominator in eq. (2.93) was simplified to 2 because $\sum_i s_i = 1$, $s_3 = 1$, and $s_{-3} = 0$. Recall from eq. (2.44) that $s_{-1} = -Z_1 s_1 = -s_1$. From eq. (2.36), the apparent reaction

order of A is given by (eq. (2.94)):

$$\psi_{A,app} = \frac{d\ln r}{d\ln a_A} = -\sum_{i=rxn} s_i \nu_{iA} [\nu_{i,A} < 0] = s_1 \tag{2.94}$$

Substitution of eq. (2.94) and $s_{-1} = -s_1 = -\psi_{A,app}$ into eq. (2.93) gives an equation

relating surface coverage of A to the reaction order of A (eq. (2.95)):

$$\theta_{A^*} = \frac{-\psi_{A,app} + 1}{2} \tag{2.95}$$

Rearrangement of eq. (2.95) reveals that the algebraic approach demonstrated here

arrives at the same equation derived in eq. (2.90) (eq. (2.96)):

$$\psi_{A,app} = \frac{d\ln r}{d\ln a_A} = 1 - 2\theta_{A^*} \tag{2.96}$$

showing that the relationship between the reaction order and the surface coverage can be

derived algebraically using sensitivities. This approach can similarly be applied to the

fractional coverages of B and C to arrive at equations identical to eqs. (2.91) and (2.92).

The ability to relate surface coverages to reaction orders solely by solving a system of

algebraic equations is useful for estimation of surface coverages for complex reaction

networks and can be used for determining whether a proposed reaction mechanism is

falsifiable because of differences in the surface coverages predicted by the reaction orders and the measured surface coverages.

Table 2.5: A hypothetical catalytic reaction network with quasi-equilibrated surface species

Step	Reaction	σ_i	Rate/Equilibrium Constant
1	$A + * \rightleftharpoons A^*$	1	K_1, Quasi-Equilibrated
2	$B + * \rightleftharpoons B^*$	1	K_2, Quasi-Equilibrated
3	$A^* + B^* \rightarrow 2C^*$	1	k_3, Rate-determining TS, irreversible
4	$C^* \rightleftharpoons C + *$	2	K_4, Quasi-Equilibrated
Overall	$A + B \rightarrow 2C$		

2.3.7 Demonstrating the relationship between sensitivities and macroscopic properties of composite reactions—A case study for water-gas shift on Cu(111)

In the preceding sections, we derived relationships between the properties of the overall/composite net rate (e.g., apparent reaction orders, apparent free energy of activation, and steady-state surface coverages). Traditionally, the degrees of rate control are calculated using eq. (2.1), which requires numerically calculating the derivative in eq. (2.1) by perturbing the energy of each transition state and surface species individually and measuring the change in the overall reaction rate. Likewise, calculation of reaction orders requires repeat simulations with varying activities of each fluid-phase species, and determination of the apparent activation energy requires simulation of the steady-state rate at multiple temperatures. We show in this section that the degrees of rate control, reaction orders, and the apparent activation energy can be determined from a single microkinetic model simulation by leveraging the relationships these quantities have with sensitivities that were derived in the preceding sections.

We consider a case study on the redox mechanism for water-gas shift (WGS) on Cu(111) for the reaction sequence depicted in Table 2.6. Motagamwala et al.[22] used

microkinetic models with previously reported DFT derived enthalpies and entropies from Gokhale et al.[29] to calculate steady-state surface coverages of surface intermediates (CO*, H$_2$O*, H*, OH*, O*, CO*, CO$_2$*), reaction orders of gas-phase species (CO, CO$_2$, H$_2$, H$_2$O), and apparent activation energies of the overall reaction at 523 K with $P_{CO}, P_{H_2O}, P_{H_2}$, and P_{CO_2} equal to 0.07 atm, 0.21 atm, 0.38 atm, and 0.085 atm, respectively. Table 2.6 reports the forward rate constant and equilibrium constant for each step, reproduced from Motagamwala et al.[22], and the forward $\left(\Delta H_f^{o\ddagger}\right)$ and reverse $\left(\Delta H_r^{o\ddagger}\right)$ enthalpies of activation of each elementary step in the reaction sequence, which are reproduced from Gokhale et al.[29] The enthalpy values in Table 2.6 are zero-point energy (ZPE) corrected. The ZPE corrected enthalpies of activation are only reported in one direction by Gokhale et al.,[29] but all the necessary data to calculate the ZPE energy corrected enthalpies in both directions is reported. The steady-state surface coverages reported by Motagamwala et al.[22] as determined by the microkinetic model are shown in Table 2.7. We demonstrate here that the steady-state coverages and the equilibrium constant for each elementary step provides sufficient information for calculating the kinetic and thermodynamic degrees of rate control and the reaction order of every species for the net overall reaction. Further, with the inclusion of the activation enthalpies (or energies) of the elementary steps, the activation enthalpy (or energy) of the overall reaction can be calculated.

The reversibilities in Table 2.6 were calculated using the definition in eq. 2.7 and the steady-state surface coverages presented in Table 2.7. For the microkinetic modeling calculations reported by Motagamwala et al.[22], surface species were assumed to be ideal,

Table 2.6: Kinetic and thermodynamic parameters of elementary steps of the water gas shift redox mechanism and steady-state reversibilities

#	Reaction	$k_{f,i}$ / s^{-1}	K_i	$\Delta H_f^{o\ddagger}$ / eV[a]	$\Delta H_r^{o\ddagger}$ / eV[a]	Z_i^{b}
1	CO+*$\rightleftarrows$CO*	1.33 x 10^8	2.15 x 10^2	0.00	0.51	1.00
2	H$_2$O+*$\rightleftarrows$H$_2$O*	2.01 x 10^{11}	5.93 x 10^{-5}	0.00	0.18	0.93^c
3	H$_2$O*+*$\rightleftarrows$H*+OH*	2.64 x 10^6	6.28 x 10^{-2}	1.10	0.98	1.19^d
4	OH*+*$\rightleftarrows$H*+O*	5.24 x 10^1	1.18 x 10^{-5}	1.77	1.19	0.13
5	CO*+O*$\rightleftarrows$CO$_2$*+*	2.05 x 10^5	1.03 x 10^3	0.79	1.75	0.13
6	CO$_2$*$\rightleftarrows$CO$_2$+*	1.48 x 10^{12}	1.92 x 10^5	0.09	0.00	1.31^d
7	2H*$\rightleftarrows$H$_2$+2*	5.32 x 10^2	4.50 x 10^1	1.07	0.50	1.09

[a]Enthalpies of activation are zero-point energy corrected.
[b]Reversibilities calculated at steady state at T = 523 K with P_{CO}, P_{H_2O}, P_{H_2}, and P_{CO_2} equal to 0.07 atm, 0.21 atm, 0.38 atm, and 0.085 atm, respectively.
[c]H$_2$O adsorption is barrierless and has the largest forward and reverse rate constants in the entire system, thus it is necessarily equilibrated with the surface. The Z_i was increased to 1 in calculations to reflect this.
[d]$Z_i > 1$ were reduced to 1 in calculations because super-equilibrium concentrations are not possible.

Table 2.7: Steady-state fractional surface coverages of species at T = 523 K with P_{CO}, P_{H_2O}, P_{H_2}, and P_{CO_2} equal to 0.07 atm, 0.21 atm, 0.38 atm, and 0.085 atm, respectively, as reported by Motagamwala et al.[22]

Surface Species	Coverage
CO*	9.32 x 10^{-1}
H$_2$O*	7.21 x 10^{-7}
H*	5.46 x 10^{-3}
OH*	6.14 x 10^{-7}
O*	1.05 x 10^{-11}
CO$_2$*	2.10 x 10^{-8}
* (Vacant Sites)	6.20 x 10^{-2}

and therefore the relationship between the fractional coverage and the sensitivities is simplified to eq. (2.88) (see entries 1-6 in Table 2.8) where $\sigma_{*,app} = -\sum_{j*}\sum_i \nu_{ij*}s_i = \sum_i s_i\sigma_{*,i}$ (eq. (2.87)) (see entry 7 in Table 2.8). Equation (2.44) relates sensitivities to reversibilities of elementary steps at steady state, which are calculated by the microkinetic model, providing an additional equation for each elementary step in the reaction sequence (entries 8-15 in Table 2.8). Finally, the sensitivities must all sum to unity (entry 16 in Table 2.8). This gives 15 unknowns (14 sensitivities, one forward and

one reverse for each elementary reaction shown in Table 2.6, and $\sigma_{*,app}$) and 16

equations (see Table 2.8), implying that the system is over specified. The system is over

specified because the sum of equations 1-6 in Table 2.8 gives entry 7 in Table 2.8, since

the fractional coverages sum to one. The system of equations is solved by varying the

sensitivities and minimizing the sum of the squares; the solution to this system of

equations gives the sensitivities and $\sigma_{*,app}$ shown in Table 2.9. The kinetic degrees of

rate control ($X_{RC,i}$) in Table 2.9 were calculated using eq. (2.22). These $X_{RC,i}$ are in good

agreement with the $X_{RC,i}$ determined from the microkinetic model reported in reference

[22], which determined each $X_{RC,i}$ by numerically calculating the derivative in eq. (2.1)

using multiple microkinetic model simulations. Thus, with only knowledge of the

thermodynamic driving forces of elementary steps via reversibilities, the kinetic degrees

of rate control are accurately determined. With the sensitivities of each elementary step

defined, it is also possible to calculate the thermodynamic degrees of rate control of each

surface species using eq. (2.88) (Table 2.10). The sensitivities also define the reaction

orders of the activities and temperature dependencies of the overall reaction, as we

demonstrate next.

The reaction orders of gas-phase species are functions of the sensitivities and

stoichiometric coefficients of elementary reaction steps (eq. (2.36)). The reaction orders

of fluid-phase species as a function of sensitivities are shown in Table 2.11 and are

evaluated using the sensitivities reported in Table 2.9. The reaction orders calculated here

using data from a single microkinetic model calculation are in good agreement with the

reaction orders determined by numerically estimating the derivative of $\ln r$ with respect

Table 2.8: System of equations that relate sensitivities to fractional coverages and reversibilities

#	Equations
1	$CO^*: s_{-1} + s_5 = \sigma_{*,app}\theta_{CO^*}$
2	$H_2O^*: s_{-1} + s_5 = \sigma_{*,app}\theta_{H_2O^*}$
3	$H^*: s_{-3} + s_{-4} + 2s_7 = \sigma_{*,app}\theta_{H^*}$
4	$OH^*: s_{-3} + s_4 = \sigma_{*,app}\theta_{OH^*}$
5	$O^*: s_{-4} + s_5 = \sigma_{*,app}\theta_{O^*}$
6	$CO_2^*: s_{-5} + s_6 = \sigma_{*,app}\theta_{CO_2^*}$
7	$\sigma_{*,app} = \sum_i s_i \sigma_{*,i}$
8-15	$s_{-i} = -Z_i s_i$
16	$1 = \sum_i s_i$

Table 2.9: Solution to the systems of algebraic equations shown in Table 2.8 using reversibilities calculated in Table 2.6 at T = 523 K with $P_{CO}, P_{H_2O}, P_{H_2}$, and P_{CO_2} equal to 0.07 atm, 0.21 atm, 0.38 atm, and 0.085 atm, respectively.

Reaction #	s_i	s_{-i}	$X_{RC,i}$	$X_{RC,i}$ Microkinetic Model[a]
1	-1.738	1.736	0.00	0.00
2	1.019	-1.019	0.00	0.00
3	1.019	-1.019	0.00	0.00
4	1.019	-0.130	0.89	0.89
5	0.130	-0.017	0.11	0.14
6	0.017	-0.017	0.00	0.00
7	0.580	-0.580	0.00	0.00
$\sigma_{*,app}$	2.00			

[a]From Motagamwala et al. [22]

53

Table 2.10: Thermodynamic degrees of rate control of surface species at T = 523 K with $P_{CO}, P_{H_2O}, P_{H_2}$, and P_{CO_2} equal to 0.07 atm, 0.21 atm, 0.38 atm, and 0.085 atm, respectively.

Surface Species, j^*	$X_{TRC,j^*} = -\sigma_{*,app}\theta_{j^*}$
CO*	-1.86 x 10^0
H_2O*	-1.44 x 10^{-6}
H*	-1.09 x 10^{-2}
OH*	-1.23 x 10^{-6}
O*	-2.10 x 10^{-11}
CO_2*	-4.20 x 10^{-8}
* (Vacant Sites)	-1.24 x 10^{-1}

to $\ln a_j$ using multiple microkinetic model calculations for each fluid-phase species in reference [22]. From eq. (2.35), the apparent activation energy is related to the activation energy of the elementary steps by $E_{a,app} = \sum_i s_i E_{a,i}$.[30] The activation *energy* of an elementary step is related to the activation *enthalpy* by $E_{a,i} = \Delta H_i^{o\ddagger} - P\Delta V^{o\ddagger} + RT$.[4] In the microkinetic model the standard change in volume of activation, $\Delta V^{o\ddagger}$, was treated as zero, simplifying to $E_{a,i} = \Delta H_i^{o\ddagger} + RT$. The activation energy calculated via sensitivities using the data provided by a single microkinetic model simulation is in agreement with the activation energy calculated by simulating the microkinetic model at multiple temperatures from reference [22]. This case study demonstrates that the steady-state thermodynamic driving forces of elementary steps are related to the sensitivities, degrees of rate control, reaction orders, and activation energies of the overall reaction rate, which enables us to calculate each of these quantities from a single microkinetic model simulation.

In catalysis, the most abundant surface intermediate (MASI) concept is used to simplify rate functions for overall reactions and can be a useful tool for simplifying complex potential energy surfaces. During the WGS reaction described above, the MASI

Table 2.11: Reaction orders and activation energy equations as a function of sensitivities and the calculated reaction orders and activation energy compared to values calculated from the microkinetic model.

Reaction Order / Activation Energy	Equation	Calculated from Sensitivities	Microkinetic Model[a]
H_2O	$\psi_{H_2O} = s_2$	1.02	1.07
CO	$\psi_{CO} = s_1$	-1.74	-1.84
H_2	$\psi_{H_2} = s_{-7}$	-0.58	-0.59
CO_2	$\psi_{CO_2} = s_{-6}$	-0.02	-0.04
Activation Energy / kJ $(mol)^{-1}$	$E_{a,app} = \sum_i s_i E_{a,i}$	282	282

[a]From Motagamwala et al. [22]

is CO*, and the most rate-controlling transition state is O-H bond scission of OH* (reaction 4 in Table 2.10). By the MASI approximation, the forward reaction requires a completely CO* covered catalyst surface to form the transition state for OH* splitting, as shown by the simplified potential energy surface depicted in Figure 2.4a. In the initial state, it is necessary to add or subtract gas-phase reactants/product species to balance atoms with the transition state. Equivalently, the reactants/products could be added/subtracted from the transition state to achieve atom balance. From Figure 2.4a, the free energy of activation is approximately the difference in energy of the transition state for OH* bond scission and the initial state, which includes 2 CO* and 1 H_2O (g), but also requires the subtraction of ½ H_2 (g) and 2 CO (g). From the MASI approximation, one would expect reaction orders equal to the coefficients in the initial state, and thus the reaction order for H_2O, H_2, CO, and CO_2 would be 1, -1/2, -2, and 0, respectively, in moderate agreement with those reported in Table 2.11. However, the MASI approximation only works for irreversible overall reactions where there is a single MASI that has a surface coverage near unity and there is a sole rate-determining transition state.

The concept of apparent initial and transition states converges to the MASI approximation in these limiting cases, but also allows for non-integer coefficients for species and transition states, as shown in Figure 2.4b.
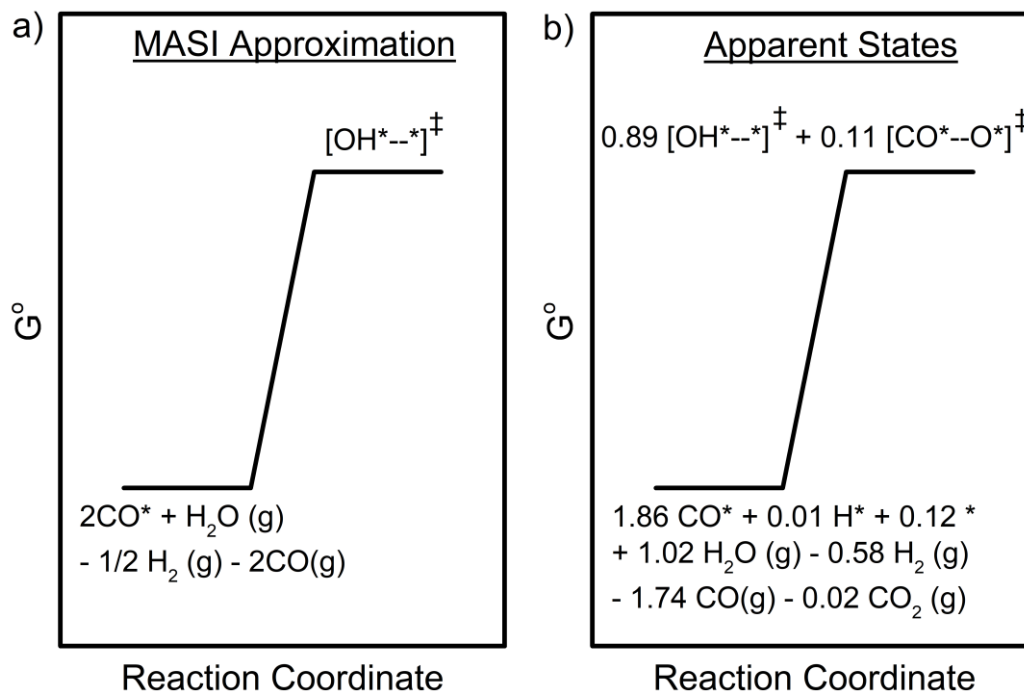
Figure 2.4: a) A simplified potential energy surface using the MASI approximation and assuming one, sole-rate determining transition state. b) The simplified potential energy surface containing the apparent initial and apparent transition states as determined by the degrees of rate control reported in Tables 2.9 and 2.10. Only surface species with $|X_{TRC,j^*}| > 0.01$ are reported.

In the preceding example, surface species were assumed to behave ideally in order to simplify the microkinetic modeling.[22] The binding energy of CO, however, is a quadratic function of the fractional coverage of CO during WGS on Cu(111),[29] and thus in this system where surface species are not treated as ideal, entries 1-6 in Table 2.8 do not describe the relationship between fractional coverages and sensitivities. Instead, eq. (2.83), which relates fractional coverages to sensitivities without making the ideal surface

species simplification, is required. These methods are demonstrated in the following section on a simple two-step catalytic reaction with non-ideal surface species where the enthalpies of activation are linear functions of the fractional coverage.

2.3.8 *Relating fractional coverages to sensitivities for ideal and non-ideal surface species*

In this section, we demonstrate by example the relationship between sensitivities and fractional coverages for systems with ideal and non-ideal surface species. In each case, we consider the reaction network shown in Table 2.12. To simulate non-idealities, the enthalpy of activation of each of the elementary steps is assumed to have a BEP-like linear relationship with the fractional coverage θ_{A^*}, given by the form (eq. (2.97)):

$$\Delta H_i^{o\ddagger} = \Delta H_{i,0}^{o\ddagger} - k_B T \Gamma_i \theta_{A^*} \tag{2.97}$$

where $\Delta H_{i,0}^{o\ddagger}$ is the enthalpy of activation of step i when the fractional coverage of A* is zero and Γ_i is defined as (eq. (2.98)):

$$\Gamma_i = \frac{\Delta H_i^{o\ddagger}(\theta_{A^*} = 0) - \Delta H_i^{o\ddagger}(\theta_{A^*} = 1)}{k_B T} \tag{2.98}$$

such that Γ_i is the difference between the enthalpies of activation of step i at $\theta_{A^*} = 0$ and $\theta_{A^*} = 1$ divided by $k_B T$ so that Γ_i are unitless.

Table 2.12: Two-step bimolecular catalytic reaction with reversible adsorption

#	Reaction	Rate Constants
1.	$A + * \rightarrow A^*$	k_1
-1.	$A^* \rightarrow A + *$	k_{-1}
2.	$2A^* \rightarrow B + *$	k_2

The rate of each elementary step in Table 2.12 is given by eqs. (2.99)-(2.101):

$$r_1 = \frac{k_B T}{h} e^{\left(\Delta S_1^{o\ddagger}/k_B\right)} e^{\left(-\Delta H_1^{o\ddagger}/k_B T\right)} a_A \theta_*$$

$$= \frac{k_B T}{h} e^{\left(\Delta S_1^{o\ddagger}/k_B\right)} e^{\left(-\Delta H_{1,0}^{o\ddagger}/k_B T\right)} e^{\Gamma_1 \theta_{A^*}} a_A \theta_* = k_{1,0} e^{\Gamma_1 \theta_{A^*}} a_A \theta_* \tag{2.99}$$

$$r_{-1} = \frac{k_B T}{h} e^{\left(\Delta S_{-1}^{o\ddagger}/k_B\right)} e^{\left(-\Delta H_{-1}^{o\ddagger}/k_B T\right)} \theta_{A^*}$$

$$= \frac{k_B T}{h} e^{\left(\Delta S_{-1}^{o\ddagger}/k_B\right)} e^{\left(-\Delta H_{-1,0}^{o\ddagger}/k_B T\right)} e^{\Gamma_{-1} \theta_{A^*}} \theta_{A^*} \tag{2.100}$$

$$= k_{-1,0} e^{\Gamma_{-1} \theta_{A^*}} \theta_{A^*}$$

$$r_2 = \frac{k_B T}{h} e^{\left(\Delta S_2^{o\ddagger}/k_B\right)} e^{\left(-\Delta H_2^{o\ddagger}/k_B T\right)} \theta_{A^*}^2 \left(\frac{Z}{2}\right)$$

$$= \frac{k_B T}{h} e^{\left(\Delta S_2^{o\ddagger}/k_B\right)} e^{\left(-\Delta H_{2,0}^{o\ddagger}/k_B T\right)} e^{\Gamma_2 \theta_{A^*}} \theta_{A^*}^2 \left(\frac{Z}{2}\right) \tag{2.101}$$

$$= k_{2,0} e^{\Gamma_2 \theta_{A^*}} \theta_{A^*}^2 \left(\frac{Z}{2}\right)$$

where the enthalpies of activation have been substituted for in terms of $\Delta H_{i,0}^{o\ddagger}$ and Γ_i. The rate constants $k_{i,0}$ correspond to the rate constants of the elementary steps when $\theta_{A^*} = 0$. The steady-state reaction rate is found by solving the algebraic equation, eq. (2.102), for the steady-state surface coverage $\theta_{A^*,SS}$:

$$\frac{d\theta_{A^*}}{dt} = 0 = r_1(\theta_{*,SS}, \theta_{A^*,SS}) - r_{-1}(\theta_{A^*,SS}) - 2r_2(\theta_{A^*,SS}) \tag{2.102}$$

with the constraint that the sum of the fractional coverages equals one $\left(\theta_{A^*,SS} + \theta_{*,SS} = 1\right)$. The steady-state rate is then found by evaluating r_2 (eq. (2.101)) at the steady-state surface coverage, $\theta_{A^*,SS}$. For each case study below, the values of $k_{i,0}$ are taken as $k_{1,0} = k_{-1,0} = k_{2,0} \left(\frac{Z}{2}\right) = 1 \ s^{-1}$ and the activity of A (a_A) is varied. The rate is solved by

forward integrating from a clean surface using Matlab ($\theta_*(t = 0) = 1, \theta_{A^*}(t = 0) = 0$) until the surface coverages are invariant in time (steady state). In each of the following cases, the Γ_i are altered to produce differently behaving reaction systems.

Case 1: Ideal surface species

When surface species behave ideally, the enthalpies of activation are not functions of the fractional coverages of surface species, and thus $\Gamma_1 = \Gamma_{-1} = \Gamma_2 = 0$. From eq. (2.86), the fractional coverage of A* as a function of the sensitivities for ideal surface species is given by (eq. (2.103)):

$$\theta_{A^*} = \frac{\sum_i s_i \nu_{iA^*}[\nu_{iA^*} < 0]}{\sum_{j^*} \sum_i s_i \nu_{ij^*}[\nu_{ij^*} < 0]} = \frac{-s_{-1} - 2s_2}{-s_1 - s_{-1} - 2s_2} = \frac{s_{-1} + 2s_2}{1 + s_2} \tag{2.103}$$

where the denominator is simplified by noting that $s_1 + s_{-1} + s_2 = 1$. For the ideal system, the rate of the composite reaction and the fractional coverage of A* are shown as a function of the activity of A, a_A, in Figures 2.5a and 2.5b. The right-hand side of eq. (2.103) is plotted as points in Figure 2.5b and falls on the same curve as the fractional coverage of A*, demonstrating that eq. (2.103) describes the relationship between the fractional surface coverage of A* and sensitivities for the ideal case. From eq. (2.88), the thermodynamic degrees of rate control are all proportional to their surface coverages and share the same proportionality factor $(\sigma_{*,app})$, as illustrated in eq. (2.104):

$$-\frac{X_{TRC,*}}{\theta_*} = -\frac{X_{TRC,A^*}}{\theta_{A^*}} = \sigma_{*,app} \tag{2.104}$$

The $\sigma_{*,app}$ of the overall reaction and the thermodynamic degree of rate control of each surface species (vacant sites are treated as surface species) divided by its fractional coverage is plotted as a function of the activity of A in Figure 2.5c. The X_{TRC,j^*}
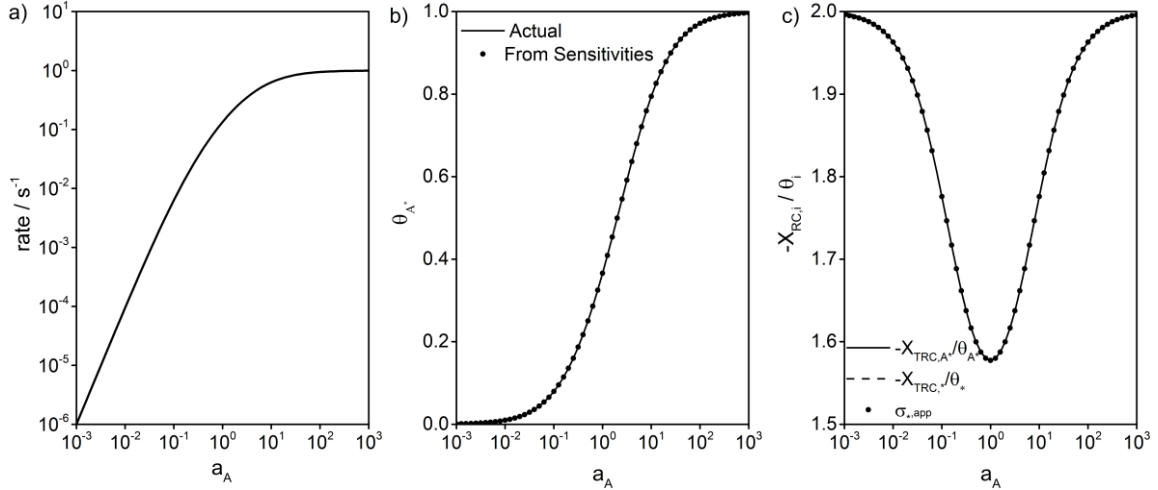
Figure 2.5: Simulation results for Case 1 (ideal surface species) for the catalytic reaction shown in Table 2.12, with $k_{1,0}=k_{-1,0}=k_{2,0}\left(\frac{z}{2}\right)=1$ s^{-1}. a) Rate as a function of the activity of A, b) Steady-state fractional coverage of A* as a function of the activity of A. The solid line is the actual coverage from the simulation and the points are predicted from sensitivities using eq. (2.103). c) Thermodynamic degrees of rate control normalized by surface coverage and $\sigma_{*,app}$ as a function of the activity of A.

normalized by fractional coverage for each surface species overlay, demonstrating that X_{TRC,j^*} of each species is indeed proportional to their respective fractional surface coverages and share the same proportionality factor. These curves overlay with $\sigma_{*,app}$, showing that $\sigma_{*,app}$ is the proportionality factor for relating surface coverage to X_{TRC,j^*} in the ideal system. We next demonstrate that the X_{TRC,j^*} are not proportional to the fractional coverages of surface species in non-ideal systems.

<u>Case 2: Simple non-ideal system: Demonstration of the relationship between sensitivities and fractional coverages for non-ideal surface species</u>

For Case 2, the enthalpies of activation are functions of the fractional surface coverage of A*. We consider here the most general case where each activation enthalpy changes differently as a function of θ_{A^*} with $\Gamma_1 = 2, \Gamma_{-1} = 3$ and $\Gamma_2 = -2$. The fractional coverage of A* is related to the sensitivities by eq. (2.83) (eq. (2.105)):

60

$$\theta_{A^*} = \frac{\sum_i s_i \left(\frac{\partial \ln r_i}{\partial \ln \theta_{A^*}}\right)_{\theta_{m \neq A^*}}}{\sum_{j^*} \sum_i s_i \left(\frac{\partial \ln r_i}{\partial \ln \theta_{j^*}}\right)_{\theta_{m \neq j^*}}} =$$

$$\frac{s_1 \psi_{1,\theta_{A^*}} + s_{-1} \psi_{-1,\theta_{A^*}} + s_2 \psi_{2,\theta_{A^*}}}{s_1 (\psi_{1,\theta_{A^*}} + \psi_{1,\theta_*}) + s_{-1}(\psi_{-1,\theta_{A^*}} + \psi_{-1,\theta_*}) + s_2 (\psi_{2,\theta_{A^*}} + \psi_{2,\theta_*})} \quad (2.105)$$

$$= \frac{s_1(\Gamma_1 \theta_{A^*}) + s_{-1}(\Gamma_{-1}\theta_{A^*} + 1) + s_2(\Gamma_2 \theta_{A^*} + 2)}{s_1(\Gamma_1 \theta_{A^*} + 1) + s_{-1}(\Gamma_{-1}\theta_{A^*} + 1) + s_2(\Gamma_2 \theta_{A^*} + 2)}$$

$$= \frac{s_1(\Gamma_1 \theta_{A^*}) + s_{-1}(\Gamma_{-1}\theta_{A^*}) + s_2(\Gamma_2 \theta_{A^*}) - X_{TRC,A^*}}{s_1(\Gamma_1 \theta_{A^*}) + s_{-1}(\Gamma_{-1}\theta_{A^*}) + s_2(\Gamma_2 \theta_{A^*}) + \sigma_{*,app}}$$

Notice when surface species are not ideal, the fractional coverage is no longer a one-to-one function of sensitivities, i.e. each set of sensitivities no longer corresponds to one unique surface coverage. In addition, the denominator of eq. (2.105) is not $\sigma_{*,app}$ and the numerator is not X_{TRC,A^*}, suggesting that there is not a proportional relationship between the fractional coverage of a species and its thermodynamic degree of rate control. The net rate of the overall reaction and the fractional coverage of A* are shown as a function of the activity of A in Figures 2.6a and 2.6b. The right-hand side of eq. (2.105) is plotted as points in Figure 2.6b. These points fall on the curve for coverage as a function of the activity of A, demonstrating that eq. (2.105) is the correct equation for relating sensitivities to the fractional coverage of A*. In Figure 2.6c, X_{TRC,j^*} divided by the fractional coverage for each species is plotted with $\sigma_{*,app}$ as a function of the activity of A. The X_{TRC,j^*} divided by their respective fractional coverages do not overlay, demonstrating that the X_{TRC,j^*} of surface species are no longer proportional to their fractional coverages. The X_{TRC,j^*} divided by the surface coverage appears to converge to $\sigma_{*,app}$ at the limit of low (for vacant sites) and high (for A*) activities of A, but neither

follows $\sigma_{*,app}$ over the entire domain, and thus $\sigma_{*,app}$ does not generally relate X_{TRC,j^*} and the fractional coverage of a surface species when surface species are non-ideal.
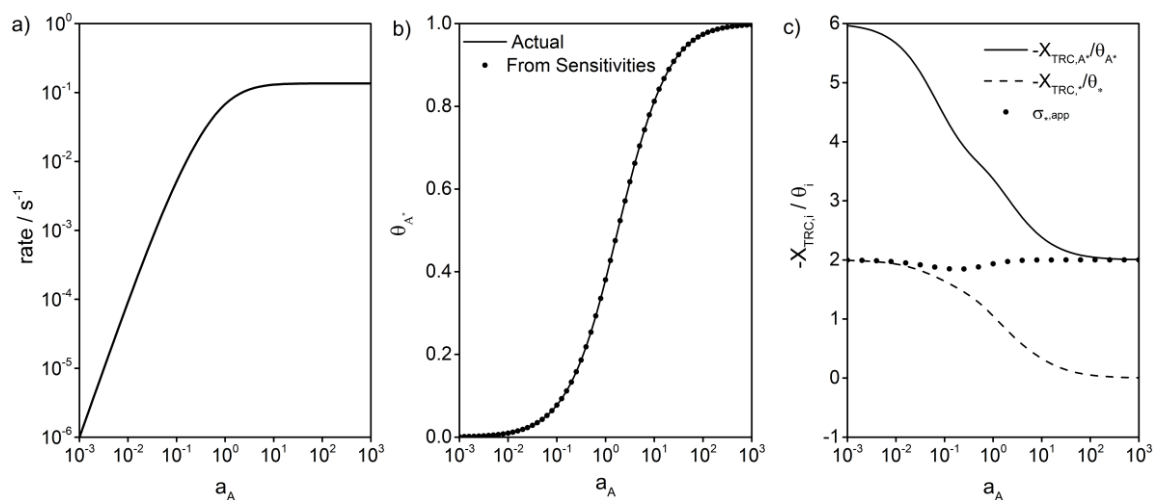
Figure 2.6: Simulation results for Case 2 (non-ideal surface species) for the catalytic reaction shown in Table 2.12, with $k_{1,0}=k_{-1,0}=k_{2,0}\left(\frac{z}{2}\right)=1$ s^{-1} and $\Gamma_1 = 2, \Gamma_{-1} = 3$ and $\Gamma_2 = -2$ (see eqs. (2.99)-(2.101)). a) Rate as a function of the activity of A, b) Steady-state fractional coverage of A* as a function of the activity of A. The solid line is the actual coverage from the simulation and the points are predicted from sensitivities using eq. (2.105). c) Thermodynamic degrees of rate control normalized by surface coverage and $\sigma_{*,app}$ as a function of the activity of A.

<u>Case 3: Non-ideal system with a kinetic phase-transition</u>

In Case 3, the enthalpies of activation are functions of the fractional coverage of A* such that increasing coverages of A* promotes further adsorption of A* and slows the reaction of A* to product species, creating a positive feedback loop for the adsorption of A*. This results in a *kinetic phase-transition* at a critical activity of A. For Case 3, $\Gamma_1 = 20, \Gamma_{-1} = 0,$ and $\Gamma_2 = -10$. At the critical activity of A ($\sim 10^{-1.7}$), the fractional coverage of A* and the overall reaction rate change discontinuously as shown in Figures 2.7a and 2.7b. At the kinetic phase-transition, the surface changes discontinuously from a mostly clean surface ($\theta_{A^*} < 0.1$) to a surface covered in A* ($\theta_{A^*} \approx 1$). The right-hand

side of eq. (2.105) still describes the relationship between fractional coverages and sensitivities, as demonstrated in Figure 2.7b. The thermodynamic degrees of rate control are not proportional to the surface coverage in Case 3, as shown in Figure 2.7c, where the thermodynamic degrees of rate control normalized by the fractional coverages do not overlay and are not equal to $\sigma_{*,app}$.
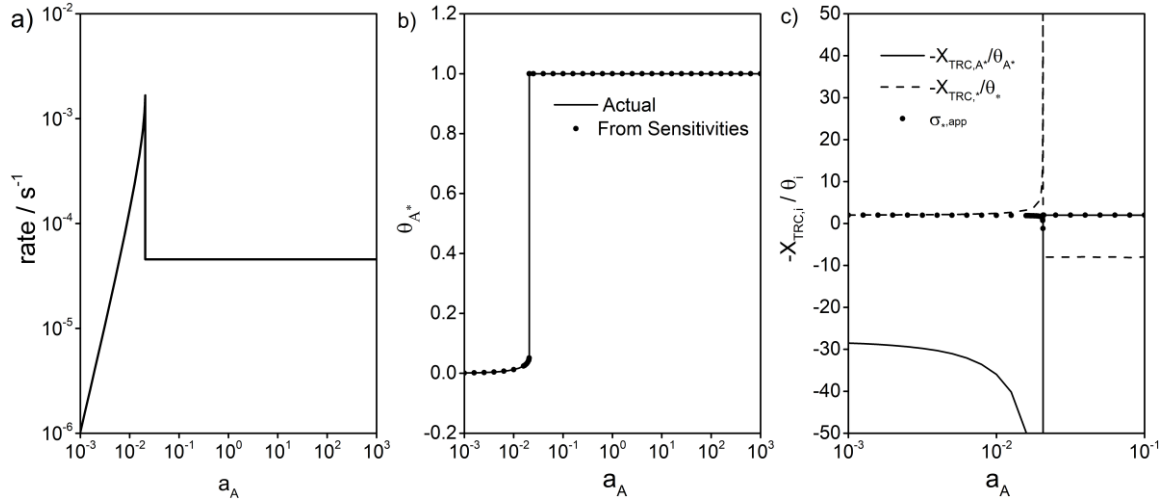
Figure 2.7: Simulation results for Case 3 (kinetic phase transition) for the catalytic reaction shown in Table 2.12, with $k_{1,0}=k_{-1,0}=k_{2,0}\left(\frac{z}{2}\right)=1$ s^{-1} and $\Gamma_1 = 20, \Gamma_{-1} = 0$ and $\Gamma_2 = -10$ (see eqs. (2.99)-(2.101)). a) Rate as a function of the activity of A, b) Steady-state fractional coverage of A* as a function of the activity of A. The solid line is the actual coverage from the simulation and the points are predicted from sensitivities using eq. (2.105). c) Thermodynamic degrees of rate control normalized by surface coverage and $\sigma_{*,app}$ as a function of the activity of A.

In each of the case studies, eq. (2.105) correctly relates the fractional coverages of surface species to the sensitivities of the reaction, and only in the ideal case is the fractional coverage proportional to the thermodynamic degree of rate control. From eq. (2.36), the reaction order of the activity of A, $\psi_{A,app}$, is related to the sensitivities by eq. (2.106):

63

$$\psi_{A,app} = -\sum_i s_i \nu_{ij} [\nu_{ij} < 0] = s_1 \qquad (2.106)$$

Equation (2.106) holds even when the surface species are not ideal, as illustrated for Case 3 in Figure 2.8, where the reaction order of A and the sensitivity s_1 overlay and both diverge to infinity as the activity of A approaches the kinetic phase-transition. The functional form of the relationships between reaction orders and sensitivities depend on whether surface species behave ideally, implying that it is necessary to include non-idealities in the microkinetic model to accurately estimate the apparent reaction orders. A microkinetic model where energies are approximated as constants will not have the correct reaction orders of fluid-phase species.
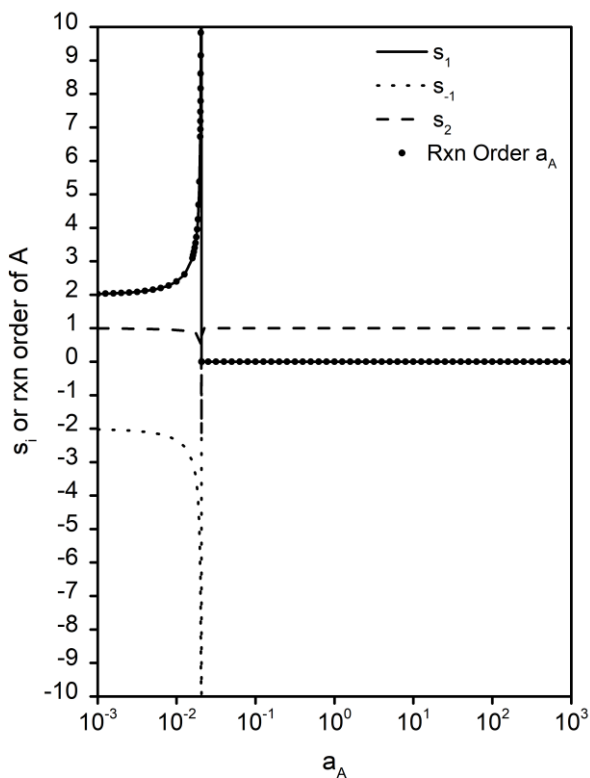
Figure 2.8: Sensitivities and reaction order of a_A as a function of a_A for the reaction scheme shown in Table 2.12, with $k_{1,0} = k_{-1,0} = k_{2,0} \left(\frac{z}{2}\right) = 1 \text{ s}^{-1}$ and $\Gamma_1 = 20, \Gamma_{-1} = 0$ and $\Gamma_2 = -10$ (see eqs. (2.99)-(2.101)), corresponding to Case 3 (kinetic phase-transition).

64

2.3.9 Using sensitivities and the TST-form rate function, r_{TST}, to assess apparent entropies of activation

In Section 2.3.1, we postulated that the apparent free energy of activation of the overall net rate is a sensitivity-weighted average of the free energies of activation of the elementary steps (eq. (2.18)), and in Section 2.3.2 we derived the TST-form rate function (eq. (2.39)) proving this relationship. Using the thermodynamic relationship $G = H - TS$, it follows that $\Delta G_{app}^{o\ddagger}$ is related to $\Delta H_{app}^{o\ddagger}$ and $\Delta S_{app}^{o\ddagger}$ by eq. (2.107):

$$\Delta G_{app}^{o\ddagger} = \Delta H_{app}^{o\ddagger} - T\Delta S_{app}^{o\ddagger} \tag{2.107}$$

Substitution of the thermodynamic relationship between free energy, enthalpy, and entropy into eq. (2.18) and comparing to eq. (2.107) gives (eq. (2.108))

$$\Delta G_{app}^{o\ddagger} = \sum_{i=rxn} s_i \Delta G_i^{o\ddagger} = \sum_{i=rxn} s_i \Delta H_i^{o\ddagger} - T \sum_{i=rxn} s_i \Delta S_i^{o\ddagger} = \Delta H_{app}^{o\ddagger} - T\Delta S_{app}^{o\ddagger} \tag{2.108}$$

which reveals that $\Delta S_{app}^{o\ddagger}$ and $\Delta H_{app}^{o\ddagger}$ of the composite reaction are sensitivity-weighted averages of $\Delta S_i^{o\ddagger}$ and $\Delta H_i^{o\ddagger}$ of elementary steps (eqs. (2.109)-(2.110)):

$$\Delta S_{app}^{o\ddagger} = \sum_{i=rxn} s_i \Delta S_i^{o\ddagger} \tag{2.109}$$

$$\Delta H_{app}^{o\ddagger} = \sum_{i=rxn} s_i \Delta H_i^{o\ddagger} \tag{2.110}$$

In this section, we demonstrate how to assess $\Delta S_{app}^{o\ddagger}$ using eq. (2.109) and the TST-form rate function (eq. (2.39)).

Consider the two-step catalytic reaction sequence in Table 2.13. The closed-form rate function is (eq. (2.111)):

$$\frac{r}{L} = \frac{k_1 a_A k_2 a_B}{k_1 a_A + k_{-1} + k_2 a_B} \tag{2.111}$$

where the rate constants are of the TST-form given in eq. (2.112):

$$k_i = \frac{k_B T}{h} e^{\frac{\Delta \tilde{S}_i^{o\ddagger}}{R}} e^{\frac{-\Delta \tilde{H}_i^{o\ddagger}}{RT}} \tag{2.112}$$

where the tildes ($\sim$) indicate molar quantities. Typically, when approximating the overall rate about a given reaction condition, it is assumed to be of the power-law form (r_p) given in eq. (2.113):

$$r_p/L = k_{app,p} \prod_{\substack{j=fluid-phase \\ species}} a_j^{\psi_{j,p}} = \frac{k_B T}{h} e^{\frac{\Delta \tilde{S}_p^{o\ddagger}}{R}} e^{\frac{-\Delta \tilde{H}_p^{o\ddagger}}{RT}} a_A^{\psi_{A,p}} a_B^{\psi_{B,p}} \tag{2.113}$$

where only the activities of the fluid-phase species are considered. However, from eq. (2.39), the TST-form rate function, r_{TST}, is given by eq. (2.114):

$$r_{TST} = C \prod_i r_i^{s_i}$$

$$= C \frac{k_B T}{h} e^{\frac{\Delta \tilde{S}_{TST}^{o\ddagger}}{R}} e^{\frac{-\Delta \tilde{H}_{TST}^{o\ddagger}}{RT}} a_A^{\psi_{A,TST}} a_B^{\psi_{B,TST}} (\theta_* L)^{\psi_{*,TST}} (\theta_{A^*} L)^{\psi_{A^*,TST}} \tag{2.114}$$

where the activities of the surface species and the arbitrary constant of integration, C, are considered. The quantities $\Delta \tilde{S}_x^{o\ddagger}$ and $\Delta \tilde{H}_x^{o\ddagger}$ where $x=p$ or TST are the apparent activation entropy and enthalpy of the composite reaction as assessed by the power-law form or TST-form rate functions. We demonstrate here that $\Delta \tilde{S}_{TST}^{o\ddagger}$ in eq. (2.114) is the apparent entropy of activation while $\Delta \tilde{S}_p^{o\ddagger}$ in eq. (2.113) cannot be assigned a single value because

the power-law rate function does not approximate the overall rate function with respect to every variable.

Table 2.13: A hypothetical catalytic reaction sequence with one reversible step

#	Reaction
1	$A + * \rightleftarrows A^*, k_1, k_{-1}$
2	$A^* + B \rightarrow C + *, k_2$

Consider the reaction scheme in Table 2.13 with the elementary step entropies and enthalpies of activation given in Table 2.14. We aim to determine $\Delta S_{app}^{o\ddagger}$ of the overall reaction at the point $a_A = a_B = 1$ and $T = 300\ K$. At this point r_{TST} and r_p are functional approximations of the rate r such that $r \approx r_{TST}$ and $r \approx r_p$ about the point $a_A = 1, a_B = 1$, and $T = 300\ K$. The apparent entropy of activation is assessed by linearizing eqs. (2.113) and (2.114) such that $\ln r = m(1/T) + b$ where the y-intercept, b, is a known function of the apparent entropy of activation. The linearized forms of eqs. (2.113) and (2.114) are given by eqs. (2.115) and (2.116) respectively:

$$\ln r_p/L = \left(-\frac{\Delta \widetilde{H}_p^{o\ddagger}}{R} - T\right)\left(\frac{1}{T}\right) + \ln\left(\frac{k_B}{h}\right) - \ln\left(\frac{1}{T}\right) + 1 + \frac{\Delta \widetilde{S}_p^{o\ddagger}}{R} + \psi_{A,p} \ln a_A$$

$$+ \psi_{B,p} \ln a_B$$

(2.115)

$$\ln r_{TST}/L = \left(-\frac{\Delta \widetilde{H}_{TST}^{o\ddagger}}{R} - T\right)\left(\frac{1}{T}\right) + \ln C + \ln\left(\frac{k_B}{h}\right) - \ln\left(\frac{1}{T}\right) + 1 + \frac{\Delta \widetilde{S}_{TST}^{o\ddagger}}{R}$$

$$+ \psi_{A,TST} \ln a_A + \psi_{B,TST} \ln a_B + \psi_{*,TST} \ln \theta_* + \psi_{A^*,TST} \ln \theta_{A^*}$$

(2.116)

The y-intercept of the linearized power-law form and the TST-form rate functions can be rearranged to equations for the apparent entropy of activation (eq. (2.117) and eq. (2.118)):

$$\Delta \tilde{S}_p^{o\ddagger} = R\left(b_p - \ln\left(\frac{k_B}{h}\right) + \ln\left(\frac{1}{T}\right) - 1 - \psi_{A,p}\ln a_A - \psi_{B,p}\ln a_B\right) \tag{2.117}$$

$$\Delta \tilde{S}_{TST}^{o\ddagger} = R\Big(b_{TST} - \ln C$$

$$- \ln\left(\frac{k_B}{h}\right) + \ln\left(\frac{1}{T}\right) - 1 - \psi_{A,TST}\ln a_A - \psi_{B,TST}\ln a_B \tag{2.118}$$

$$- \psi_{*,TST}\ln\theta_* - \psi_{A^*,TST}\ln\theta_{A^*}\Big)$$

Determining the entropy of activation for both the power-law rate and the TST-form rate functions requires assessment of the reaction orders of A and B, which can be found by the slope of $\ln r$ versus $\ln a_j$. The slopes of these lines give the reaction orders as $\psi_{A,TST} = \psi_{A,p} = 0.698$ and $\psi_{B,TST} = \psi_{B,p} = 0.753$, as shown in Figure 2.9.

Table 2.14: Enthalpies and entropies of activation for the reactions depicted in Table 2.13.

Reaction, i	$\Delta \tilde{S}_i^{o\ddagger}$ / J (mol K)$^{-1}$	$\Delta \tilde{H}_i^{o\ddagger}$ / kJ mol^{-1}
1	10	80
-1	30	85
2	75	100

From eq. (2.36), the sensitivities can be related to the measured apparent reaction orders of A and B (eqs. (2.119)-(2.121)):

$$\psi_{A,p} = \psi_{A,TST} = -\sum_i s_i \nu_{iA}[\nu_{iA} < 0] = s_1 = 0.698 \tag{2.119}$$

$$\psi_{B,p} = \psi_{B,TST} = -\sum_i s_i \nu_{iB}[\nu_{iB} < 0] = s_2 = 0.753 \tag{2.120}$$

$$s_{-1} = 1 - s_1 - s_2 = 1 - 0.698 - 0.753 = -0.451 \tag{2.121}$$
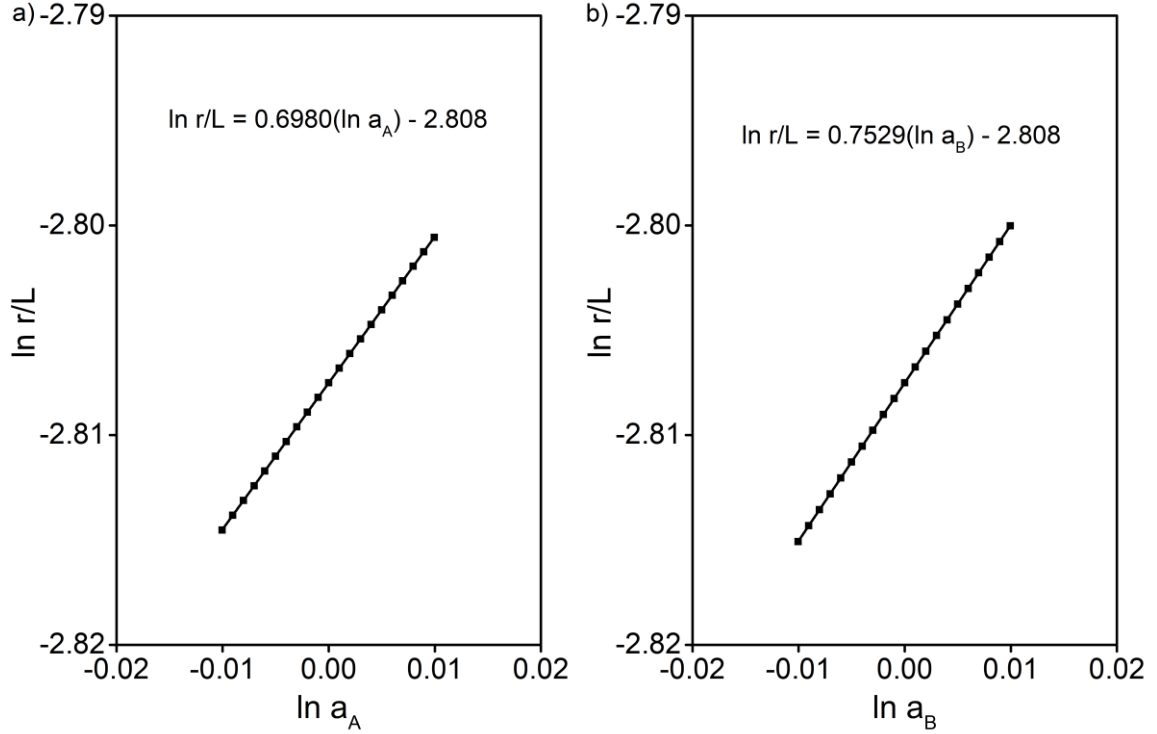
Figure 2.9: Log-log plot of rate versus activity of reactants for the reaction scheme depicted in Table 2.13 with the entropies and energies of activation given in Table 2.14 with T = 300 K. a) varying activity of A with the activity of B equal to unity and b) varying activity of B with the activity of A equal to unity. Solid curves are best-fit lines.

The reaction orders of the activities of the surface species also calculated using eq. (2.36) (which is equivalent to eq. (2.77) because the surface species are ideal in this example) are (eqs. (2.122) and (2.123)):

$$\psi_{*,p} = \psi_{*,TST} = -\sum_i s_i \nu_{i*}[\nu_{i*} < 0] = s_1 = 0.698 \tag{2.122}$$

$$\psi_{A^*,p} = \psi_{A^*,TST} = -\sum_i s_i \nu_{iA^*}[\nu_{iA^*} < 0] = s_{-1} + s_2 = -0.451 + 0.753 \tag{2.123}$$

$$= 0.302$$

The fractional coverages are calculated using eq. (2.86) because the surface species behave ideally (eqs. (2.124) and eq. (2.125)):

69

$$\theta_* = \frac{\sum_i s_i \nu_{i*}}{\sum_{j^*} \sum_i s_i \nu_{ij^*}} = \frac{s_1}{1} = 0.698 \tag{2.124}$$

$$\theta_{A^*} = \frac{\sum_i s_i \nu_{iA^*}}{\sum_{j^*} \sum_i s_i \nu_{ij^*}} = \frac{s_{-1} + s_2}{1} = 1 - s_1 = 0.302 \tag{2.125}$$

The arbitrary constant $C = 0.6353$, as determined using eq. (2.34). Determination of C requires knowing the rates of the elementary steps in the composite reaction network, which may not be experimentally feasible. The apparent entropy of activation is determined by measuring the y-intercept of the $\ln r$ versus $1/T$ linear fit. The best-fit line of these data is given by the equation $\ln r/L = \left(\frac{1}{T}\right) + b = -1.1462 * 10^4 \left(\frac{1}{T}\right) + 35.40$ and is shown in Figure 2.10. Using eqs. (2.117) and (2.118), the entropy of activation for the power-law function and the TST-form rate functions are (eqs. (2.126) and (2.127)):

$$\Delta \tilde{S}_p^{o\ddagger} = R\left(b - \ln\left(\frac{k_B}{h}\right) + \ln\left(\frac{1}{T}\right) - 1 - \psi_{A,p} \ln a_A - \psi_{B,p} \ln a_B\right)$$

$$= R\left(35.40 - \ln\left(\frac{k_B}{h}\right) + \ln\left(\frac{1}{300}\right) - 1 - 0.689 \ln 1\right) \tag{2.126}$$

$$- 0.753 \ln 1\right) = 41.05 \frac{J}{mol\ K}$$

$$\Delta \tilde{S}_{TST}^{o\ddagger} = R\left(b - \ln C - \ln\left(\frac{k_B}{h}\right) + \ln\left(\frac{1}{T}\right) - 1 - \psi_{A,TST} \ln a_A - \psi_{B,TST} \ln a_B \right.$$
$$- \psi_{*,TST} \ln \theta_* - \psi_{A^*,TST} \ln A^*\right)$$

$$= R\left(35.40 - \ln 0.6353 - \ln\left(\frac{k_B}{h}\right) + \ln\left(\frac{1}{300}\right) - 1 - 0.698 \ln 1\right.$$

$$\left. - 0.753 \ln 1 - 0.698 \ln 0.698 - 0.302 \ln 0.302\right) \tag{2.127}$$

$$= 49.92 \frac{J}{mol\ K}$$
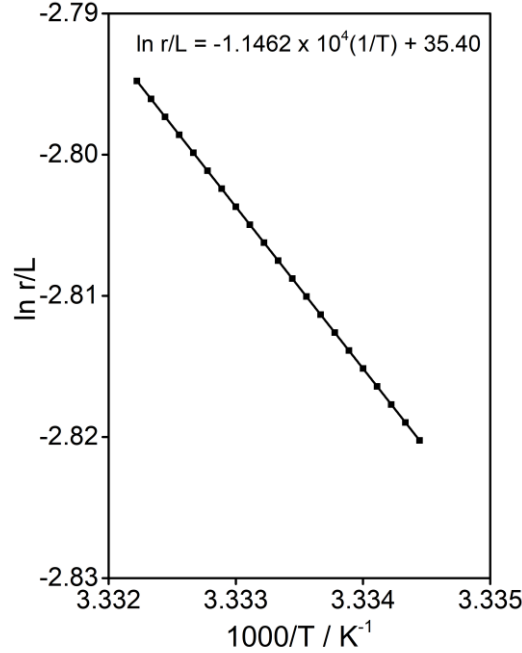
Figure 2.10: Natural log of rate versus 1000/T for the reaction scheme depicted in Table 2.13 with the entropies and energies of activation given in Table 2.14 and $a_A = a_B = 1$. The solid curve is a best-fit line.

and differ in this instance by nearly 20%. Even though the gas constant, R, is a universal constant, we can take the derivative with respect to $1/R$ to derive an equation for the apparent entropy of activation. For both the power-law form (eq. (2.113)) and the TST-form (eq. (2.114)) rate functions (eq. (2.128)):

$$\frac{d \ln r/L}{d(1/R)} = \Delta \tilde{S}_x^{o\ddagger} - \frac{\Delta \tilde{H}_x^{o\ddagger}}{T}, x = TST \ or \ p \tag{2.128}$$

and thus the apparent entropy of activation is given by eq. (2.129):

$$\Delta \tilde{S}_x^{o\ddagger} = \frac{d \ln r/L}{d(1/R)} + \frac{\Delta \tilde{H}_x^{o\ddagger}}{T}, x = TST \ or \ p \tag{2.129}$$

The quantity $\frac{d \ln r/L}{d(1/R)}$ is approximated by the slope of the line of $\ln r/L$ versus 1/R (Figure 2.11), and $\Delta \tilde{H}_x^{o\ddagger}$ is found by the slope of the line of ln r/L versus 1/T (Figure 2.10), which

71
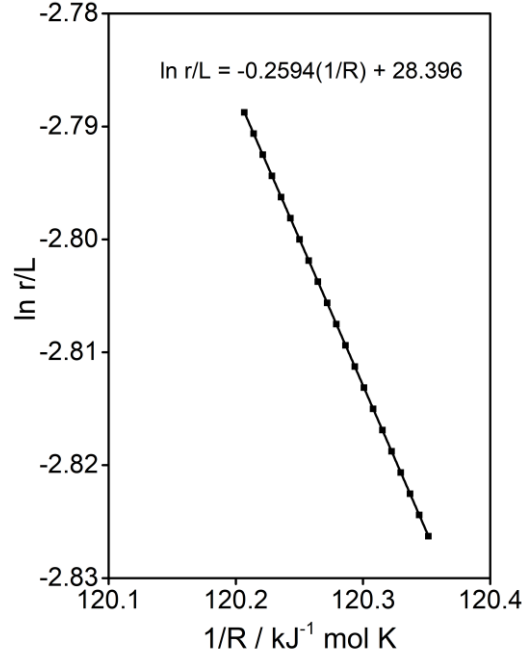
Figure 2.11: Natural log of rate versus 1/R for the reaction scheme depicted in Table 2.13 with the entropies and energies of activation given in Table 2.14 and $a_A = a_B = 1$, T=300 K. The solid curve is a best-fit line.

from eqs. (2.115) and (2.116) is given by eq. (2.130) for both the power-law and the TST-form rate function:

$$\Delta \widetilde{H}_p^{o\ddagger} = \Delta \widetilde{H}_{TST}^{o\ddagger} = -mR - RT = (1.1462 * 10^4) * R - R * 300K$$

$$= 92.80 \frac{kJ}{mol}$$

(2.130)

The slope of the best-fit line in Figure 2.11 is -0.2594, and thus the apparent entropy of activation found by this method is (eq. (2.131)):

$$\Delta \widetilde{S}_p^{o\ddagger} = \Delta \widetilde{S}_{TST}^{o\ddagger} = \frac{d \ln r/L}{d(1/R)} + \frac{\Delta \widetilde{H}_{app}^{o\ddagger}}{T} = -0.2594 \frac{kJ}{mol\,K} + \frac{92.80 \frac{kJ}{mol}}{300K}$$

$$= 0.04993 \frac{kJ}{mol\,K} = 49.93 \frac{J}{mol\,K}$$

(2.131)

72

which is in agreement with the entropy of activation found using the TST-form rate function (eq. (2.114)) but in disagreement with the power-law form rate function (eq. (2.113)). The discrepancy between the entropy of activation assessed by varying temperature and by varying R for the power-law form (eq. (2.113)) arises because the power-law form rate function is not an approximation of overall rate with respect to every variable because this form neglects the activities of surface species. In contrast, the TST-form rate function approximates the overall net rate with respect to every variable (see eq. (2.38) and Section A2.2 of the Appendix), and hence, the TST-form rate function (eq. (2.114)) is the correct form for approximating rate functions of composite reaction networks. The implication is that when a catalytic reaction is approximated by a rate constant multiplied by the activities of reactants taken to the power of their apparent reaction orders, it is important to note that this rate constant, k_p, is a function of both the arbitrary constant of integration, C, and the fractional coverages of surface species (eq. (2.132)):

$$k_p = C \frac{k_B T}{h} e^{\frac{\Delta \tilde{S}_{app}^{o\ddagger}}{R}} e^{\frac{-\Delta \tilde{H}_{app}^{o\ddagger}}{RT}} \prod_{\substack{j^*=surface \\ species}} \theta_{j^*}^{\psi_{j^*,app}} \tag{2.132}$$

which affects the experimental assessment of $\Delta \tilde{S}_{app}^{o\ddagger}$ (see eqs. (2.117) and (2.118)), but not $\Delta \tilde{H}_{app}^{o\ddagger}$ (see eq. (2.130)).

The purpose of this exercise is not to renounce the power-law form rate functions for composite reactions, but to demonstrate that rigorously the activities of surface species and an arbitrary constant of integration should also be included in the rate function. Further, we illustrate that when the rate function of the composite reaction is

written in TST-form (eq. (2.114)), the typical method for assessing the entropy of activation by analyzing the y-intercept of the best-fit line of $\ln r$ versus 1/T can be used to assess the apparent entropy of activation of composite reactions. Finally, we show here that the apparent entropy and enthalpy of activation are sensitivity-weighted averages of the activation entropies and enthalpies of elementary steps as predicted by eqs. (2.18), (2.109), and (2.110) (eq. (2.133)-(2.134)):

$$\Delta \widetilde{H}_{app}^{o\ddagger} = \sum_{i=rxn} s_i \, \Delta \widetilde{H}_i^{o\ddagger}$$

$$= 0.698(80 \; kJ \; mol^{-1}) - 0.451(85 \; kJ \; mol^{-1}) \qquad (2.133)$$

$$+ \, 0.753(100 \; kJ \; mol^{-1}) = 92.81 \; kJ \; mol^{-1}$$

$$\Delta \tilde{S}_{app}^{o\ddagger} = \sum_{i=rxn} s_i \, \Delta \tilde{S}_i^{o\ddagger}$$

$$= 0.698(10 \; J \; mol^{-1}K^{-1}) - 0.451(30 \; J \; mol^{-1}K^{-1}) \qquad (2.134)$$

$$+ \, 0.753(75 \; J \; mol^{-1}K^{-1}) = 49.93 \; J \; mol^{-1}K^{-1}$$

which are consistent with the values for the apparent enthalpy and entropy of activation given in eqs. (2.130) and (2.131), respectively. Thus, we conclude that (i) the TST-form rate function given in eq. (2.39) is the correct form for approximating the overall/composite rate about a point, and (ii) the apparent entropies and enthalpies of activation are sensitivity-weighted averages of the activation entropies and enthalpies of elementary steps.

2.4 Conclusion

We show that transition state theory can be applied to composite reaction networks where the equilibrium reaction between the initial state and transition state of an elementary step is replaced with a weighted-average of all initial state-transition state equilibrium reactions where the weights are the sensitivities, s_i. The resulting rate function is denoted the transition-state-theory-form rate function (r_{TST}). The application of transition state theory to composite reaction networks enabled calculation of the kinetic and thermodynamic degrees of rate control by measuring only reversibilities, Z_i, which are measures of thermodynamic driving forces of elementary step reactions used in De Donder relations. Further, the reaction order of a species is shown to equal negative the thermodynamic degree of rate control of that species, and thus a relationship between reversibilities and the reaction orders is established. The application of these concepts to catalytic systems facilitated the derivation of (i) a proof that the thermodynamic degree of rate control of a surface species is proportional to its fractional coverage when surface species are ideal, (ii) a relationship between fractional coverages and sensitivities for ideal and non-ideal surface species, and (iii) a method for determining the fractional surface coverages of intermediates by measuring only the reaction orders when the reaction mechanism is specified.

The derived relationships between sensitivities and the macroscopic properties of the overall/composite rate, such as apparent reaction orders, apparent energies of activation, and steady-state surface coverages, are utilized in multiple examples, including (i) the calculation of the reaction orders, activation energy, and degrees of rate control from a single microkinetic model simulation (i.e. without numerically calculating

any derivatives), (ii) relating steady-state fractional coverages of surface species to sensitivities when the enthalpies of activation of elementary steps are functions of the surface coverage, and (iii) the assessment of apparent entropies of activation of composite reactions using the TST-form rate function. Finally, by redefining sensitivities as a derivative with respect to elementary step rate functions, r_i, instead of the elementary step rate constants, k_i, the sum of the sensitivities and kinetic degrees of rate control is proven to equal unity for any reaction system, and it is determined that this constraint arises because the overall rate function r and the rate functions of elementary steps r_i both have units of s^{-1}.

Chapter 3

Thermodynamically consistent forward and reverse degrees of rate control in reversible reactions

3.1 Conspectus

The net rate of a composite reaction is the difference between the forward and reverse reaction rates, which are kinetically distinct despite sharing elementary reaction steps and therefore have different rate-controlling transition states and species. Thus, degrees of rate control defined to identify rate-controlling transition states and species for the net rate confound contributions from the forward and reverse reactions. Herein, the forward and reverse degrees of rate control are defined to independently quantify the extent that species and transition states control the forward and reverse rates in reversible reactions. These degrees of rate control are defined as the relative change in the forward and reverse reaction rates per $k_B T$ decrease in the standard-state molecular free energies of transition states and species, and they are related to experimentally measurable quantities such as steady-state fractional coverages, reaction orders, and energies and entropies of activation of the forward and reverse reaction rates. The forward/reverse degrees of rate control represent stoichiometric coefficients for species and transition states in an equilibrium between the apparent initial states and the apparent transition states of the apparent rate-controlling steps of forward and reverse overall reactions. At equilibrium, the apparent transition states for the forward reaction and reverse reaction converge, and thus the

forward and reverse rate-controlling steps combine to form a single apparent rate-controlling step at equilibrium. This apparent rate-controlling step is comprised of an apparent initial state, transition state, and final state, where the apparent final state of the forward reaction is the apparent initial state of the reverse reaction. The apparent rate-controlling step behaves identically to an elementary step reaction at equilibrium with a pseudo-mass-action rate function given by the transition-state-theory (TST) form rate function derived in Chapter 2 with a stoichiometric number equal to the affinity-averaged stoichiometric number, $\bar{\sigma}$. The ratio of the forward and reverse TST-form rate functions is identical to the overall thermodynamic equilibrium relation, consistent with the principles of microscopic reversibility and detailed balance at equilibrium.

3.2 Introduction

The study of reactions under near-equilibrium conditions is of fundamental and practical interest in CO_2 hydrogenation,[31–33] ammonia synthesis,[34–39] water-gas shift,[40–42] sulfur dioxide oxidation,[43–45] hydrocarbon hydrogenation/dehydrogenation,[46–48] and methane dehydroaromatization.[26,49–52] As reactions approach equilibrium, the reverse reaction rate non-negligibly contributes to the net reaction rate, which is the difference between the forward ($\vec{r}$) and reverse ($\overleftarrow{r}$) rate (eq. (3.1))[45,53,54]:

$$r = \vec{r} - \overleftarrow{r} \tag{3.1}$$

The forward and reverse reactions share the same elementary step reactions and potential energy surface, but in opposing directions. As a consequence, the forward and reverse reactions are kinetically distinct, as they have different rate-controlling transition states and reaction orders.[4,55] The rate-control of transition states and species in overall *net*

reactions are unambiguously quantified by the kinetic ($X_{RC,i}$) and thermodynamic ($X_{TRC,j}$) degrees of rate control, defined as (eqs. (3.2) and (3.3)) [11,56–59]:

$$X_{RC,i} = \left(\frac{\partial \ln r}{\partial \left(- G^o_{TS,i} / k_B T \right)} \right)_{G^o_{j \neq TS,i}}$$ (3.2)

$$X_{TRC,j} = \left(\frac{\partial \ln r}{\partial \left(- G^o_j / k_B T \right)} \right)_{G^o_{i \neq j}}$$ (3.3)

where $G^o_{TS,i}$ and G^o_j are molecular standard-state free energies of transition state i and species j, respectively. For reversible reactions however, the degrees of rate control for the net rate confound contributions of the kinetically distinct forward and reverse reactions. We argue that a more complete description of composite reactions is one that assesses the kinetically relevant transition states and species for the forward and reverse reactions independently via what we define herein as the forward and reverse degrees of rate control.

In Chapter 2, we developed a formalism that describes the apparent rate-controlling step for the net rate of a composite reaction, which consists of an equilibrium between an apparent initial state and an apparent transition state (eq. (3.4))[60]:

$$IS_{app} \overset{K^{\ddagger}_{app}}{\rightleftharpoons} TS_{app} \overset{\nu}{\rightarrow} Products$$ (3.4)

where $K^{\ddagger}_{app}$ is the apparent equilibrium constant between the apparent initial and transition state and ν is the frequency that TS_{app} transforms to products. Equation (3.4) is related to the degrees of rate control by eq. (3.5)[60]:

$$-\sum_{j=\text{species}} X_{\text{TRC},j} S_j \overset{K^{\ddagger}}{\rightleftharpoons} \sum_{i=\text{TS}} X_{\text{RC},i} TS_i \overset{\nu}{\rightarrow} \text{Products} \qquad (3.5)$$
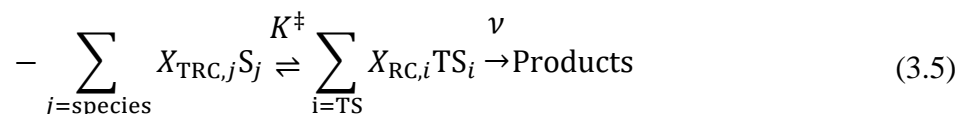
where the degrees of rate control represent stoichiometric coefficients in the equilibrium between species j (S_j) and transition states i (TS_i). Transition state theory (TST) is applied to eq. (3.5) to derive the TST-form rate function, r_{TST}, for the net rate of a composite reaction (eq. (3.6))[60]:

$$r_{\text{TST}} = C\frac{k_B T}{h} e^{-(\sum_i X_{\text{RC},i} G_{\text{TS},i}^o + \sum_j X_{\text{TRC},j} G_j^o)/k_B T} \prod_j a_j^{-X_{\text{TRC},j}} \qquad (3.6)$$

where C is a constant and a_j are activities of species j, including reactants, products, and intermediates. Within the framework of this formalism and these definitions, apparent rate-controlling steps and TST-form rate functions are derived for forward and reverse overall reactions. By defining forward and reverse degrees of rate control, apparent rate-controlling steps and TST-form rate functions for the forward and reverse reactions can be determined. We prove that the forward and reverse reactions share apparent transition states at chemical equilibrium, such that a single apparent rate-controlling step for the equilibrium reaction is defined with an apparent initial state, transition state, and final state where the apparent final state of the forward reaction is the apparent initial state of the reverse reaction. We demonstrate that this formalism is thermodynamically consistent, as the functional forms of the forward and reverse TST-form rate functions comply with the thermodynamic restrictions imposed by the principles of microscopic reversibility and detailed balance at equilibrium.[4,34,36,45,55,61]

The ratio of the reverse and forward reaction rate of a composite reaction is the effective reversibility (Z_{eff}),[26] the value of which is determined by the thermodynamic driving force of the overall reaction described by the molecular free energy change of the overall reaction, ΔG, as shown in eq. (3.7)[26,34,45,53,54]:

$$r = \vec{r} - \overleftarrow{r} = \vec{r}(1 - Z_{eff}) = \vec{r}(1 - \exp(\Delta G/\bar{\sigma}k_B T))$$
(3.7)

where the molecular free energy change of the overall reaction is a sum of the elementary step molecular free energy changes (ΔG_i) multiplied by the elementary step stoichiometric numbers, σ_i $(\Delta G = \sum_i \sigma_i \Delta G_i)$, and $\bar{\sigma}$ is the affinity-averaged stoichiometric number where the weights are the free energy changes of the elementary steps (the affinity is defined as $A_i \equiv -\Delta G_i$) of the composite reaction network (eq. (3.8))[34,36,37,45,53]:

$$\bar{\sigma} = \frac{\sum_i \sigma_i \Delta G_i}{\sum_i \Delta G_i} = \frac{\sum_i \sigma_i \ln(Z_i)}{\sum_i \ln(Z_i)}$$
(3.8)

where Z_i are the reversibilities of elementary steps, defined in eq. (3.9)[20]:

$$Z_i = \frac{r_{-i}}{r_i} = \exp(\Delta G_i/k_B T)$$
(3.9)

The effective reversibility of the overall reaction is related to the equilibrium constant of the overall reaction, K_{ov}, by eq. (3.10)[34,45]:

$$Z_{eff} = \frac{\overleftarrow{r}}{\vec{r}} = \left(\frac{\prod_j a_j^{v_j}}{K_{ov}} \right)^{\frac{1}{\bar{\sigma}}} = \left(\frac{\prod_j a_j^{v_j}}{\prod_i K_i^{\sigma_i}} \right)^{\frac{1}{\bar{\sigma}}}$$
(3.10)

where v_j are the stoichiometric coefficients of species j in the overall reaction and a_j are the thermodynamic activities of species j. Prior reports claim that that the ratio of the

forward and reverse rate constants is related to the overall equilibrium constant by eq. (3.11)[5,34,38,45,62]:

$$\frac{\vec{k}}{\overleftarrow{k}} = K_{\text{eff}} = K_{\text{ov}}^{1/\bar{\sigma}} \tag{3.11}$$

where K_{eff} is the effective equilibrium constant of the overall reaction by analogy to elementary steps, and K_{ov} is the equilibrium constant for the overall reaction. Eqs. (3.7)-(3.11) illustrate that thermodynamic constraints are superimposed on kinetic descriptions of the net rate in reversible reaction systems. To determine the kinetic hurdles for the forward and reverse reactions, i.e., for correlations of structure to function in composite catalytic reactions, it is necessary to dissociate the thermodynamic contributions to the net rate and identify instead the forward and reverse reaction rates. Quantification of the rate-control of transition states and species on both the forward and reverse rates is then achieved by means of forward and reverse degrees of rate control.

A number of proofs of the relationship described by eq. (3.11) involve a sole rate-determining step and such proofs are then extended to composite reactions with multiple rate-determining steps.[36,62] These proofs also differ in definitions for the forward and reverse rate constants and reaction orders, where the forward and reverse rate constants multiply irreducible polynomial factors that are functions of both elementary step rate constants and activities, while the reaction orders only consider the power of activities that do not appear within the irreducible factor.[34,45,62]

We argue that definitions for forward (or reverse) reaction orders must be consistent with definitions of reaction orders for net reactions: $d \ln \vec{r} / d \ln a_j$ for fluid-

phase species or $\left(\partial \ln \vec{r} / \partial \ln a_{j*}\right)_{a_{i \neq j*}}$ for surface species.[60] We also contend that the forward and reverse rate constants are the free-energy and temperature dependent factors that multiply the product of thermodynamic activities of species to their respective reaction orders to give the appropriate rate in a pseudo-mass-action rate function, in analogy to the rate constant definition for an elementary step. We claim that this vantage point is unambiguous and does not include irreducible polynomial factors. Such a formalism arises from descriptions of the rate of composite reactions by pseudo-elementary apparent rate-controlling steps of the forward and reverse reactions, with rate functions analogous to the TST-form rate function for the net reaction shown in eq. (3.6). Within this formalism, we will prove that eq. (3.11) must be true at equilibrium and only under special conditions away from equilibrium, as may be the case when there is a sole rate-controlling transition state.

3.3 Results and Discussion

3.3.1 Forward and reverse degrees of rate control and the apparent rate-controlling step for forward and reverse reactions

The derivation of the TST-form rate functions for forward and reverse reaction rates of composite reactions requires first the definition of their respective degrees of rate control. The equations regarding forward and reverse rates are identical, and therefore for brevity we will show only equations for forward rates and consider that the corresponding equations for reverse rates are implied. The forward degrees of rate control for transition states and species are defined in eqs. (3.12) and (3.13):

$$\vec{X}_{\text{RC},i} = \left(\frac{\partial \ln \vec{r}}{\partial \left(-G^o_{\text{TS},i}/k_B T \right)} \right)_{G^o_{j \neq \text{TS},i}} \tag{3.12}$$

$$\vec{X}_{\text{TRC},j} = \left(\frac{\partial \ln \vec{r}}{\partial \left(-G^o_j/k_B T \right)} \right)_{G^o_{i \neq j}} \tag{3.13}$$

Likewise, a concept related to the degrees of rate control, the sensitivity, s_i,[19,23] is also redefined for the forward rate as eq. (3.14):

$$\vec{s}_i = \left(\frac{\partial \ln \vec{r}}{\partial \ln r_i} \right)_{r_{j \neq i}} = \left(\frac{\partial \ln \vec{r}}{\partial \ln k_i} \right)_{k_{j \neq i}} \tag{3.14}$$

The forward sensitivities are related to the forward degrees of rate control by the same equations that relate degrees of rate control and sensitivities for net rates (eqs. (3.15) and (3.16))[23,60]:

$$\vec{X}_{\text{RC},i} = \vec{s}_i + \vec{s}_{-i} \tag{3.15}$$

$$\vec{X}_{\text{TRC},j} = \sum_j \vec{s}_i \nu_{ij} [\nu_{ij} < 0] \tag{3.16}$$

The proofs for eqs. (3.15) and (3.16) are analogous to those reported in Chapter 2.[19,23,60] We omit such proofs from the present chaper but report them in Section A3.1 of the Appendix.

In Chapter 2, we demonstrated that the rate of the net composite reaction is described by an apparent rate-controlling step where the degrees of rate control are stoichiometric coefficients in an equilibrium between apparent initial and transition states (eq. (3.5)),[60]. Application of transition state theory to this function gives the TST-form

rate function of the net reaction (eq. (3.6)).[60] Analogously, the apparent rate-controlling step for the forward reaction is given by eq. (3.17):

$$-\sum_{j=\text{species}} \vec{X}_{\text{TRC},j} S_j \overset{\vec{K}^{\ddagger}}{\rightleftharpoons} \sum_{i=\text{TS}} \vec{X}_{RC,i} TS_i \overset{\vec{v}}{\rightarrow} \text{Products} \tag{3.17}$$
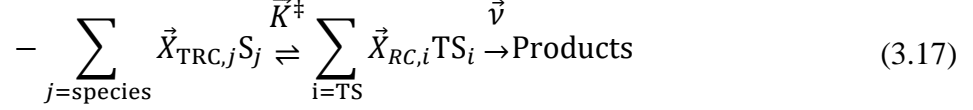
and the TST-form forward rate function is thus given by eq. (3.18):

$$\vec{r}_{\text{TST}} = \vec{C} \frac{k_B T}{h} e^{-(\sum_i \vec{X}_{\text{RC},i} G^o_{\text{TS},i} + \sum_j \vec{X}_{\text{TRC},j} G^o_j)/k_B T} \prod_j a_j^{-\vec{X}_{\text{TRC},j}}$$

$$= \vec{C} \prod_i k_i^{\vec{s}_i} \prod_j a_j^{-\vec{X}_{\text{TRC},j}} = \vec{k} \prod_j a_j^{\vec{\alpha}_j} \tag{3.18}$$

where $\vec{C} = \vec{r}|_X / \prod_i r_i^{\vec{s}_i}\big|_X$ is an arbitrary constant of integration found by evaluating the rate function at a reaction condition X, which is the same reaction condition that $\vec{s}_i$ were calculated.[60] The sensitivities and degrees of rate control that appear in eq. (3.18) are constants that were determined at a specified steady-state reaction condition.[60] Within this formalism, it is apparent why degrees of rate control are not the same for forward and reverse reactions. The thermodynamic activities that drive the forward/reverse reactions differ, as forward rates are primarily driven by reactants while reverse rates are primarily driven by products, and these reaction orders are equal to negative the thermodynamic degrees of rate control. Further, the dependence of forward and reverse rates on transition state energies can differ away from equilibrium,[4,55] and the dependence of these rates on transition state energies are determined by the forward/reverse kinetic degrees of rate control.

There is a different forward/reverse/net TST-form rate function (r_{TST}) for each steady-state reaction condition, and these r_{TST} functions are identical to the forward/reverse/net rates with respect to differential changes in any variable about the reaction condition X at which the degrees of rate control/sensitivities were determined.[60] Thus, the forward/reverse/net r_{TST} functions have the same reaction orders and apparent energies and entropies of activation as the forward/reverse/net rates and thus forward/reverse sensitivities and degrees of rate control are experimentally assessable quantities (see Section A3.2 of the Appendix).[60] The relationship between sensitivities/degrees of rate control and activation energies,[30,60,63] reaction orders,[60] and fractional coverages[60] for net rates still hold for forward/reverse degrees of rate control and their respective forward/reverse rates. For fluid-phase intermediates where the pseudo-steady-state assumption is valid, the reaction orders, which are equal to negative the thermodynamic degrees of rate control,[60] are zero for net, forward, and reverse reactions (eq. (3.19)):

$$X_{\text{TRC},j} = \vec{X}_{\text{TRC},j} = \overleftarrow{X}_{\text{TRC},j} = 0 \text{ for fluid-phase intermediates} \tag{3.19}$$

as is proven in Section A3.3 of the Appendix. When the pseudo-steady-state approximation is not valid, the definition for degrees of rate control differ from those reported in eqs. (3.12) and (3.13), as will be discussed in Chapter 4.[15]

We show that the forward, reverse, and net degrees of rate control are distinct by examples for both non-catalytic and catalytic reaction sequences and do so specifically in systems that do not have a sole rate-controlling transition state, and then we derive proofs for the various relationships that are observed in these illustrative reaction systems.

86

3.3.2 Forward and reverse degrees of rate control example for a non-catalytic reaction sequence

We first consider the non-catalytic reaction sequence shown in Scheme 3.1. The steady-state net rate was calculated at specified concentrations of A, C, and D while making the steady-state assumption on the concentration of B (eq. (3.20)):

$$\frac{d[B]}{dt} = 0 = k_1[A] + 2k_{-2}[D] - k_{-1}[B][C] - 2k_2[B]^2 \tag{3.20}$$

with rate constants $k_1 = 1$ au, $k_{-1} = 20$ au, $k_2 = 20$ au, $k_{-2} = 1$ au for a thermodynamically ideal system such that activities are replaced with concentrations. This was achieved by fixing the concentrations of A, C, and D and forward simulating until the concentration of B reached steady-state. The net rate of D formation was then defined as eq. (3.21):

$$r = k_2[B]^2 - k_{-2}[D] \tag{3.21}$$

The effective reversibility of the overall reaction, Z_{eff}, was calculated using eq. (3.22)[20,26,45]:

$$Z_{\text{eff}} = \prod_i Z_i \tag{3.22}$$

where Z_i are the reversibilities on the single-path from reactants to products. The forward and reverse rates of the overall reaction were calculated by eqs. (3.23) and (3.24):

$$\vec{r} = \frac{r}{1 - Z_{\text{eff}}} \tag{3.23}$$

$$\overleftarrow{r} = \frac{Z_{\text{eff}} r}{1 - Z_{\text{eff}}} \tag{3.24}$$

The forward, reverse, and net rate sensitivities were calculated numerically by perturbing the value of the rate constant of each elementary step and the kinetic and thermodynamic degrees of rate control were calculated using eqs. (3.15) and (3.16). Starting from [A] = 1.2 au, [C] = 0 au, [D] = 0 au, the concentration of reactants/products were varied systematically by varying the extent of reaction, ε, from 0 to 0.2 such that [A] = $1.2 - 2\varepsilon$ au, [C] = 2ε au, [D] = ε au, where $\varepsilon = 0$ and $\varepsilon = 0.2$ corresponds to $Z_{\text{eff}} = 0$ and $Z_{\text{eff}} = 1$, respectively. The Matlab code for these calculations is provided in Section A3.4 of the Appendix.

<div align="center">

Scheme 3.1: Sequence of fluid-phase reactions

</div>

$$
\begin{array}{ll}
\overset{k_1}{\underset{k_{-1}}{A \rightleftarrows B + C}} & \sigma_1 = 2 \\[2em]
\overset{k_2}{\underset{k_{-2}}{2B \rightleftarrows D}} & \sigma_2 = 1
\end{array}
$$

Overall: $2A \Rightarrow 2C + D$
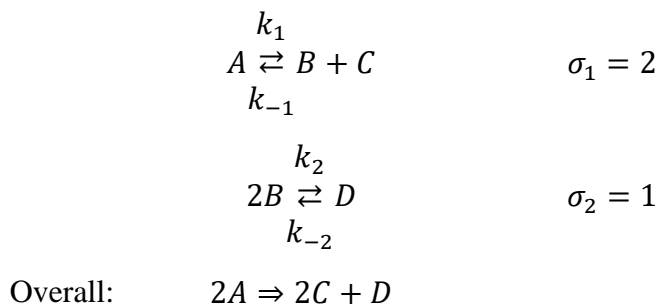
The kinetic degrees of rate control for the forward and reverse rates are reported as a function of Z_{eff} in Figure 3.1. In general, the $X_{\text{RC},i}$ of the net, forward, and reverse reactions all differ, demonstrating that the forward and reverse degrees of rate control provide distinct information from the traditional degrees of rate control for net rates. Considering that the net rate is zero at equilibrium, we propose that the forward and reverse degrees of rate control provide more information about the reaction systems at
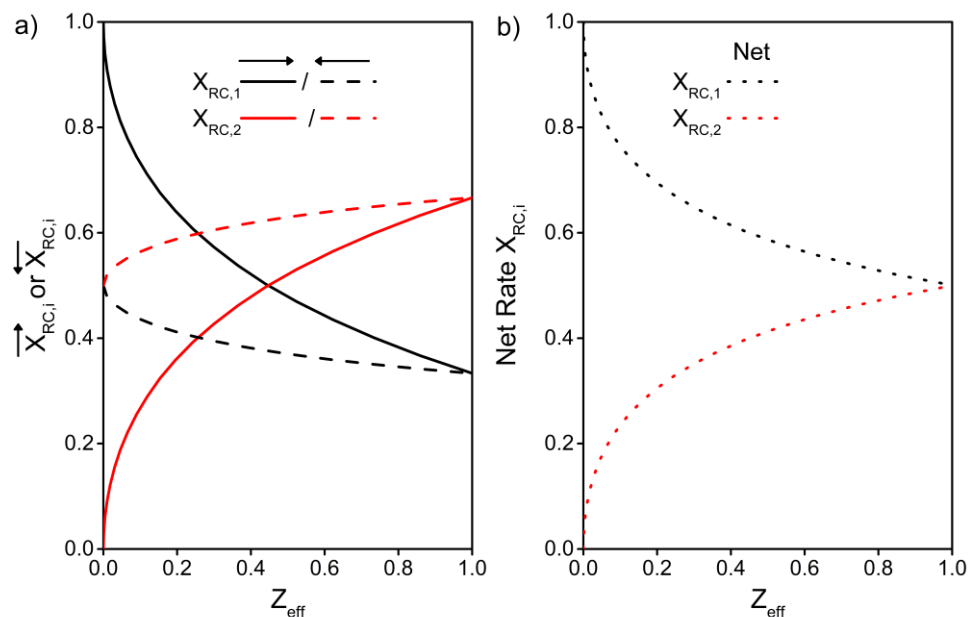
Figure 3.1: a) Forward (solid lines) and reverse (dashed lines) kinetic degrees of rate control and b) net (dotted lines) kinetic degrees of rate control as a function of Z_{eff} for the composite reaction shown in Scheme 3.1 with $[A]_0 = 1.2$ au. At $Z_{eff} = 0$ and $Z_{eff} = 1$, all $Z_i = 0$ or 1, respectively.

near-equilibrium conditions. Away from equilibrium, the forward and reverse kinetic degrees of rate control differ, and thus any enhancement of the forward rate by stabilization of a transition state will not necessarily enhance the rate of the reverse reaction since the rate-controlling transition states differ. The kinetic degrees of rate control for the forward and reverse reactions are equal at equilibrium ($Z_{eff} = 1$), as required by the principles of microscopic reversibility and detailed balance at equilibrium.[4,55] The forward/reverse reaction orders (or negative the forward/reverse thermodynamic degrees of rate control) are reported as a function of Z_{eff} in Figure 3.2. The thermodynamic degree of rate control of species B is always zero for both the forward and the reverse reactions because it is a fluid-phase intermediate (eq. (3.19)). In Figure 3.3, the forward/reverse sensitivities, s_i, are reported as functions of Z_{eff}. The

sensitivities are the apparent powers of the elementary step rate constants as they appear in the TST-form rate function (see eq. (3.18)), and since $\vec{k} = \vec{C} \prod_i k_i^{\vec{s_i}}$, the forward/reverse rate constants change as the concentration of reactants and products evolve with extent of reaction, as illustrated in Figure 3.4.
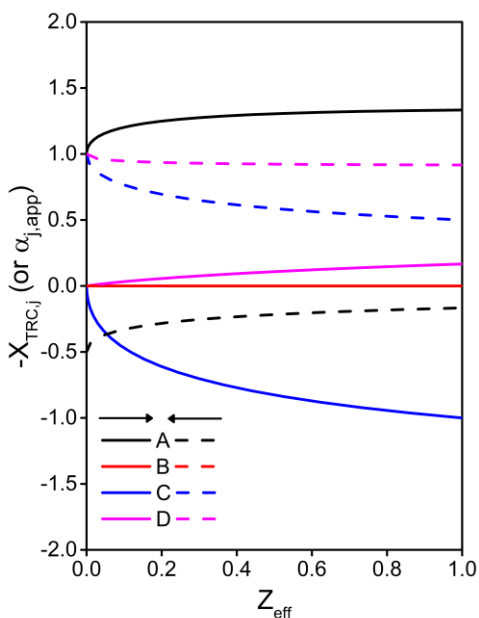
Figure 3.2: Forward (solid lines) and reverse (dashed lines) $-X_{TRC,j}$ (or apparent reaction orders) as a function of Z_{eff} for the composite reaction shown in Scheme 3.1 with $[A]_0 = 1.2$ au. At $Z_{eff} = 0$ and $Z_{eff} = 1$, all $Z_i = 0$ or 1, respectively. Forward and reverse $-X_{TRC,B} = 0$ for all Z_{eff}.

Let us now express the rate in the form of the apparent rate-controlling step at equilibrium $(Z_{eff} = 1)$. Recall from eq. (3.18) this involves expressing the forward/reverse rate constants as a product of the elementary step rate constants to the power of forward/reverse sensitivities (Figure 3.3) multiplied by the forward/reverse constants C (Figure A3.2). The forward/reverse rate constants multiply the product of species activities to negative the forward/reverse thermodynamic degrees of rate control (Figure 3.2), giving the forward and reverse TST-form rate functions at equilibrium (eqs. (3.25) and (3.26)):
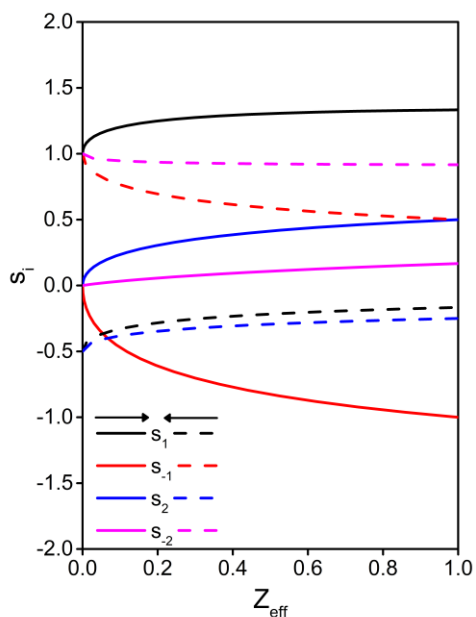
Figure 3.3: Forward (solid lines) and reverse (dashed lines) sensitivities as a function of Z_{eff} for the composite reaction shown in Scheme 3.1 with $[A]_0 = 1.2$ au.
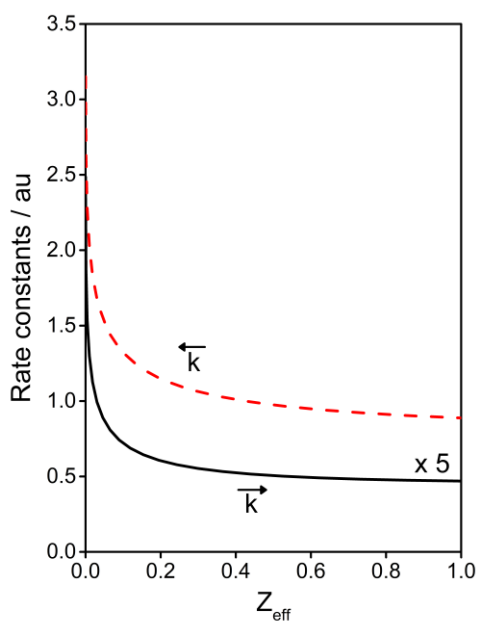
Figure 3.4. Forward (solid lines) and reverse (dashed lines) rate constants as a function of Z_{eff} for the reaction shown in Scheme 3.1 with $[A]_0 = 1.2$ au.

$$\vec{r} = \frac{2^{\frac{1}{3}}}{3}(k_1)^{\frac{4}{3}}(k_{-1})^{-1}(k_2)^{\frac{1}{2}}(k_{-2})^{\frac{1}{6}}[A]^{\frac{4}{3}}[B]^0[C]^{-1}[D]^{\frac{1}{6}}$$

$$= \frac{2^{\frac{1}{3}}}{3}\frac{k_B T}{h}\exp\left(-\frac{\left(\frac{1}{3}G^o_{TS,1} + \frac{2}{3}G^o_{TS,2} - \frac{4}{3}G^o_A + G^o_C - \frac{1}{6}G^o_D\right)}{k_B T}\right)[A]^{\frac{4}{3}}[C]^{-1}[D]^{\frac{1}{6}} \quad (3.25)$$

$$= \vec{k}[A]^{\frac{4}{3}}[C]^{-1}[D]^{\frac{1}{6}}$$

$$\overleftarrow{r} = \frac{2^{\frac{1}{3}}}{3}(k_1)^{-\frac{1}{6}}(k_{-1})^{\frac{1}{2}}(k_2)^{-\frac{1}{4}}(k_{-2})^{\frac{11}{12}}[A]^{-\frac{1}{6}}[B]^0[C]^{\frac{1}{2}}[D]^{\frac{11}{12}}$$

$$= \frac{2^{\frac{1}{3}}}{3}\frac{k_B T}{h}\exp\left(-\frac{\left(\frac{1}{3}G^o_{TS,1} + \frac{2}{3}G^o_{TS,2} + \frac{1}{6}G^o_A - \frac{1}{2}G^o_C - \frac{11}{12}G^o_D\right)}{k_B T}\right)[A]^{-\frac{1}{6}}[C]^{\frac{1}{2}}[D]^{\frac{11}{12}} \quad (3.26)$$

$$= \overleftarrow{k}[A]^{-\frac{1}{6}}[C]^{\frac{1}{2}}[D]^{\frac{11}{12}}$$

Recall from eqs. (3.15) and (3.16) that the degrees of rate control are related to the sensitivities, and after multiplying the rate constants in eqs. (3.25) and (3.26), the dependence of the rates on transition state and species standard-state free energies are determined by the degrees of rate control (Figure 3.1 and Figure 3.2). At equilibrium, $\overleftarrow{r}/\vec{r} = 1$, and thus by substitution and rearrangement of eqs. (3.25) and (3.26), we arrive at (eq. (3.27)):

$$1 = \frac{\overleftarrow{r}}{\vec{r}} = \frac{\overleftarrow{k}[A]^{-\frac{1}{6}}[B]^0[C]^{\frac{1}{2}}[D]^{\frac{11}{12}}}{\vec{k}[A]^{\frac{4}{3}}[B]^0[C]^{-1}[D]^{\frac{1}{6}}} = \frac{[A]^{-\frac{3}{2}}[C]^{\frac{3}{2}}[D]^{\frac{3}{4}}}{\vec{k}/\overleftarrow{k}} = \frac{[A]^{-\frac{3}{2}}[C]^{\frac{3}{2}}[D]^{\frac{3}{4}}}{K_{\text{eff}}} \quad (3.27)$$

where the ratio $\vec{k}/\overleftarrow{k}$ is the effective equilibrium constant (see eq. (3.11)) of the overall reaction. If we evaluate K_{eff} to find it in terms of the elementary step rate constants we find that is related to K_{ov} by eqs. (3.10) and (3.11) (eq. (3.28)):

$$K_{\text{eff}} = \frac{\vec{k}}{\overleftarrow{k}} = \frac{\frac{2^{\frac{1}{3}}}{3}(k_1)^{\frac{4}{3}}(k_{-1})^{-1}(k_2)^{\frac{1}{2}}(k_{-2})^{\frac{1}{6}}}{\frac{2^{\frac{1}{3}}}{3}(k_1)^{-\frac{1}{6}}(k_{-1})^{\frac{1}{2}}(k_2)^{-\frac{1}{4}}(k_{-2})^{\frac{11}{12}}} = k_1^{-\frac{3}{2}}k_{-1}^{-\frac{3}{2}}k_2^{\frac{3}{4}}k_{-2}^{\frac{3}{4}}$$

$$= (K_1^2 K_2)^{1/(4/3)} = (K_{\text{ov}})^{1/(4/3)}$$

(3.28)

where $\bar{\sigma} = 4/3$. By substitution of the reverse and forward TST-form rate functions into eq. (3.10), we arrive at eq. (3.29):

$$\frac{\overleftarrow{r}}{\vec{r}} = \frac{\overleftarrow{r}_{\text{TST}}}{\vec{r}_{\text{TST}}} = \frac{a_A^{\overleftarrow{\alpha}_A^{\text{eq}}-\vec{\alpha}_A^{\text{eq}}} a_B^{\overleftarrow{\alpha}_B^{\text{eq}}-\vec{\alpha}_B^{\text{eq}}} a_C^{\overleftarrow{\alpha}_C^{\text{eq}}-\vec{\alpha}_C^{\text{eq}}} a_D^{\overleftarrow{\alpha}_D^{\text{eq}}-\vec{\alpha}_D^{\text{eq}}}}{K_{\text{ov}}^{1/\bar{\sigma}}} = \left(\frac{\prod_j a_j^{\nu_j}}{K_{\text{ov}}}\right)^{\frac{1}{\bar{\sigma}}}$$

(3.29)

$$= \frac{[A]^{-\frac{3}{2}}[B]^0[C]^{-\frac{3}{2}}[D]^{\frac{3}{4}}}{K_{\text{ov}}^{1/(4/3)}} = \left(\frac{[A]^{-2}[B]^0[C]^2[D]^1}{K_{\text{ov}}}\right)^{\frac{1}{4/3}}$$

where the right-hand side of the equation is determined by thermodynamics and the left-hand side is determined by the ratio of the forward and reverse rate functions. By inspection of eq. (3.29), it follows that the exponents on concentrations on the left-hand of the equation are equal the exponents on the concentrations on the right-hand side of the equation, such that (eq. (3.30)):

$$0 = -\frac{\nu_j}{\bar{\sigma}} + \overleftarrow{\alpha_j} - \vec{\alpha_j}$$

(3.30)

93

as was originally proposed by Boudart.[34,45] We state that this relationship is only valid at equilibrium as illustrated in Figure 3.5, a point not explicitly noted previously.
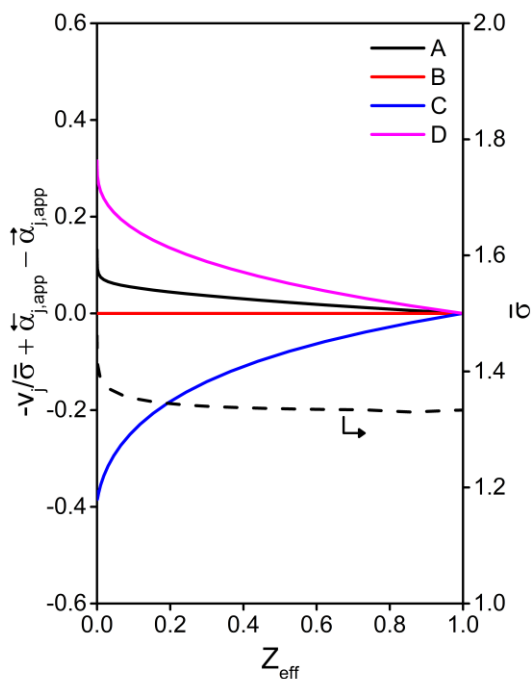
Figure 3.5: $\bar{\sigma}$ (dashed line, right axis) and $-v_j/\bar{\sigma} + \overset{\leftarrow}{\alpha}_{j,\mathrm{app}} - \overset{\rightarrow}{\alpha}_{j,\mathrm{app}}$ (left axis, see eq. (3.30)) for each species j as a function of Z_{eff} for the reaction shown in Scheme 3.1 with $[A]_0 = 1.2$.

We demonstrated in Chapter 2 that the apparent initial and transition states can be envisioned on an apparent potential energy surface for net overall reactions.[60] At equilibrium, the apparent transition state for the forward and reverse rates of the composite reaction presented in Scheme 3.1 are identical (see Figure 3.1). Thus, the hypothetical potential energy surface for the forward and reverse rates can be envisioned on a single potential energy surface where the apparent initial state of the reverse reaction is the apparent final state of the forward reaction, as shown in Figure 3.6. From Figure 3.6, the reaction at equilibrium behaves like an elementary step of the form (eq. (3.31)):

$$\frac{4}{3}A - C + \frac{1}{6}D \rightleftharpoons -\frac{1}{6}A + \frac{1}{2}C + \frac{11}{12}D \tag{3.31}$$
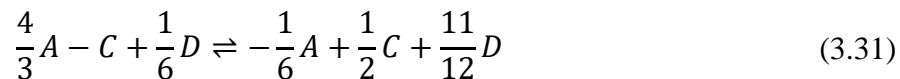
where the transition state is $1/3$ TS$_1$ + $2/3$ TS$_2$. In eq. (3.31) there is a net formation of $3/2$

C and $3/4$ D, hence the apparent stoichiometric number of the apparent rate-controlling

step is equal to $4/3$, since 2 C and 1 D are formed in the overall reaction in Scheme 3.1.

This is identical to the affinity-averaged stoichiometric number, $\bar{\sigma}$, at equilibrium, as

shown in Figure 3.5.
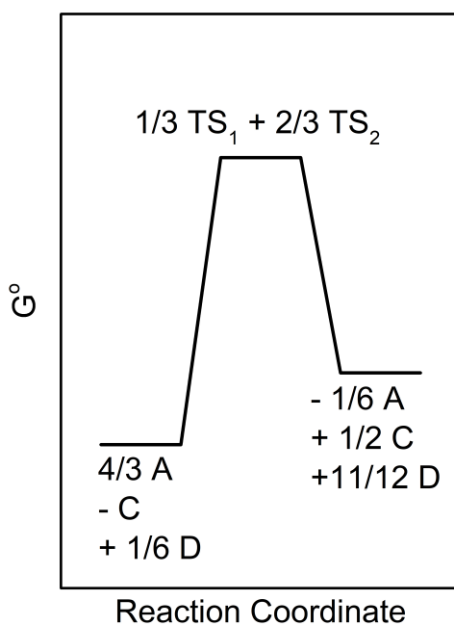
Figure 3.6: The potential energy surface for the apparent rate-controlling elementary step
for the forward and reverse reactions at equilibrium.

Thus far, we have demonstrated that the forward and reverse degrees of rate

control describe how the energies of transition states and species control the rate of the

forward and reverse reaction and how these degrees of rate control can be used to

develop the TST-form rate functions for the forward and reverse rates. The virtue of

formulating rates in the form given by the TST-form rate function is that the rate

constants (i) depend only on temperature and the free energies of transition states and species and (ii) multiply the product of activities of species to the appropriate apparent reaction orders, as they do in elementary step rate functions. Thus, the forward/reverse rate constants are unambiguously defined in the apparent rate-controlling step formalism. The TST-form rate function is derived by application of transition state theory to the apparent rate-controlling steps for the forward and reverse reaction. At equilibrium, the apparent forward and reverse rate-controlling steps share an apparent transition state, which enables the definition of an apparent rate-controlling elementary step where the apparent final state for the forward reaction is the apparent initial state of the reverse reaction, as depicted in Figure 3.6. This apparent rate-controlling elementary step is thermodynamically consistent and obeys the principles of microscopic reversibility and detailed balance at equilibrium, as illustrated by eq. (3.29). In the following section, we prove that the apparent rate-controlling step formalism is always thermodynamically consistent, such that at equilibrium the ratio of the forward and reverse rate constants are related to the overall equilibrium constant, K_{ov}, by eq. (3.11), regardless of the number of rate-controlling transition states, and that the forward and reverse reaction orders are related to the overall stoichiometric coefficients by eq. (3.30), as proposed by Boudart.[34,45]

3.3.3 Proof of microscopic reversibility and detailed balance for composite reactions described by apparent rate-controlling steps

We begin this section by first deriving relationships between the forward and reverse sensitivities and sensitivities for the net rate, as this will lead us to a proof that the kinetic degrees of rate control for the forward and reverse reactions are equal at

equilibrium, thus affirming that the composite overall forward and reverse reactions have identical apparent transition states at equilibrium. It is important to recognize that the rate of the net overall reaction as defined in eq. (3.7) is a function of the elementary step rate functions, r_i, such that we can write (eq. (3.32)):

$$r = r\left(\vec{r}(r_1, r_{-1}, \dots, r_N, r_{-N}), \overleftarrow{r}(r_1, r_{-1}, \dots, r_N, r_{-N})\right) \tag{3.32}$$

If we calculate the sensitivities for the net rate function of the form given by eq. (3.32), we derive eq. (3.33):

$$s_i = \left(\frac{\partial \ln r}{\partial \ln r_i}\right)_{r_{j\neq i}} = \left(\frac{\partial \ln r}{\partial \ln \vec{r}}\right)_{\overleftarrow{r}}\left(\frac{\partial \ln \vec{r}}{\partial \ln r_i}\right)_{r_{j\neq i}} + \left(\frac{\partial \ln r}{\partial \ln \overleftarrow{r}}\right)_{\vec{r}}\left(\frac{\partial \ln \overleftarrow{r}}{\partial \ln r_i}\right)_{r_{j\neq i}}$$

$$= \left(\frac{\partial \ln r}{\partial \ln \vec{r}}\right)_{\overleftarrow{r}}\vec{s}_i + \left(\frac{\partial \ln r}{\partial \ln \overleftarrow{r}}\right)_{\vec{r}}\overleftarrow{s}_i \tag{3.33}$$

Following an analogous proof presented in Chapter 2,[60] we can prove that the remaining partial derivatives in eq. (3.33) are related to Z_{eff} by eq. (3.34) (see Section A3.1 of the Appendix for the full derivation):

$$\left(\frac{\partial \ln r}{\partial \ln \overleftarrow{r}}\right)_{\vec{r}} \Big/ \left(\frac{\partial \ln r}{\partial \ln \vec{r}}\right)_{\overleftarrow{r}} = -Z_{\text{eff}} \tag{3.34}$$

By noting that $\left(\frac{\partial \ln r}{\partial \ln \overleftarrow{r}}\right)_{\vec{r}} + \left(\frac{\partial \ln r}{\partial \ln \vec{r}}\right)_{\overleftarrow{r}} = 1$ because these partial derivatives represent a complete set of sensitivities of the net rate, and these sensitivities must sum to unity (see Section A3.1 of the Appendix for a proof), we can substitute eq. (3.34) into eq. (3.33) to derive a function that relates sensitivities of net rates, s_i, to the forward and reverse sensitivities (eq. (3.35)):

$$s_i = \frac{\vec{s_i} - Z_{\text{eff}}\overleftarrow{s_i}}{1 - Z_{\text{eff}}} \tag{3.35}$$

Because all relative changes in the net reaction rate with respect to a perturbation in a quantity, x, are sensitivity-weighted averages of the relative changes of the elementary step rate functions to the quantity x,[60] eq. (3.35) relates the relative changes in the net rate to the relative changes in the forward and reverse rates by eq. (3.36):

$$\frac{d\ln r}{dx} = \sum_i s_i \frac{d\ln r_i}{dx} = \frac{\sum_i \vec{s_i}\dfrac{d\ln r_i}{dx} - Z_{\text{eff}}\sum_i \overleftarrow{s_i}\dfrac{d\ln r_i}{dx}}{1 - Z_{\text{eff}}} = \frac{\dfrac{d\ln \vec{r}}{dx} - Z_{\text{eff}}\dfrac{d\ln \overleftarrow{r}}{dx}}{1 - Z_{\text{eff}}} \tag{3.36}$$

where the relative changes in the forward and reverse rates with respect to a differential change in x are forward- or reverse-sensitivity weighted averages of the changes in the rates of the elementary steps. Equation (3.36) can also be used to relate partial derivatives. For example, the kinetic degree of rate control of transition state i for the net rate is related to forward and reverse kinetic degrees of rate control by eq. (3.37):

$$X_{\text{RC},i} = \left(\frac{\partial \ln r}{\partial\left(-G^o_{\text{TS},i}/k_B T\right)}\right)_{G^o_{j \neq \text{TS},i}}$$

$$= \frac{\left(\dfrac{\partial \ln \vec{r}}{\partial\left(-G^o_{\text{TS},i}/k_B T\right)}\right)_{G^o_{j \neq \text{TS},i}} - Z_{\text{eff}}\left(\dfrac{\partial \ln \overleftarrow{r}}{\partial\left(-G^o_{\text{TS},i}/k_B T\right)}\right)_{G^o_{j \neq \text{TS},i}}}{1 - Z_{\text{eff}}} \tag{3.37}$$

$$= \frac{\vec{X}_{\text{RC},i} - Z_{\text{eff}}\overleftarrow{X}_{\text{RC},i}}{1 - Z_{\text{eff}}}$$

The net rate sensitivities are related to the elementary step reversibilities by $s_{-i}/s_i = -Z_i$,[23] which are related to forward/reverse sensitivities using eq. (3.35) (eq. (3.38)):

98

$$-Z_i = \frac{s_{-i}}{s_i} = \frac{\vec{s}_{-i} - Z_{\text{eff}} \overleftarrow{s}_{-i}}{\vec{s}_i - Z_{\text{eff}} \overleftarrow{s}_i} \tag{3.38}$$

At equilibrium, $Z_i = Z_{\text{eff}} = 1$, and by rearrangement of eq. (3.38) at equilibrium, we find

(eqs. (3.39)-(3.41)):

$$-1 = \frac{\vec{s}_{-i} - \overleftarrow{s}_{-i}}{\vec{s}_i - \overleftarrow{s}_i} \tag{3.39}$$

$$\vec{s}_i + \vec{s}_{-i} = \overleftarrow{s}_i + \overleftarrow{s}_{-i} \tag{3.40}$$

$$\vec{X}_{\text{RC},i} = \overleftarrow{X}_{\text{RC},i} \tag{3.41}$$

and thus at equilibrium, the forward and reverse kinetic degrees of rate control are equal, and therefore, the apparent transition state for the forward and reverse reactions are identical at equilibrium. The forward and reverse rate functions share an apparent transition state at equilibrium, and thus the apparent initial, transition, and final state of the apparent rate-controlling step can be determined. It follows that the stoichiometric number of this step must be equal to $\bar{\sigma}_{\text{eq}}$, where the subscript "eq" is added to indicate that this is the stoichiometric number of the apparent rate-controlling step at equilibrium, and therefore is a constant. An alternative proof of eq. (3.41) is found by recognizing that at equilibrium, the ratio of the reverse rate to the forward rate is given by eq. (3.42):

$$\frac{\overleftarrow{r}}{\vec{r}} = \left(\frac{\prod_i a_j^{\nu_j}}{\exp(-\Delta G^o / k_B T)} \right)^{\frac{1}{\bar{\sigma}_{\text{eq}}}} \tag{3.42}$$

At equilibrium, eq. (3.42) is equal to unity. The standard-state free energy change of reaction, $\Delta G^o = \sum_j \nu_j G_j^o$, is a function only of the reactant and product standard-state

free energies. Thus, because the quantity inside of the fraction on the right-hand side is not a function of any $G^o_{TS,i}$ or G^o_j of intermediates and is equal to one at equilibrium, then the right-hand side is always unity at equilibrium. By substitution of the forward and reverse TST-form rate functions into eq. (3.42), we can examine the functional dependence of the ratio of the reverse and forward rates (eq. (3.43)):

$$
\frac{\overleftarrow{C}}{\overrightarrow{C}} \exp\left(-\frac{\left(\sum_i (\overleftarrow{X}_{RC,i} - \overrightarrow{X}_{RC,i}) G^o_{TS,i} + \sum_j (\overleftarrow{X}_{TRC,j} - \overrightarrow{X}_{TRC,j}) G^o_j \right)}{k_B T} \right) \prod_j a_j^{\overrightarrow{X}_{TRC,j} - \overleftarrow{X}_{TRC,j}}
$$

$$
= \left(\frac{\prod_j a_j^{\nu_j}}{\exp(-\Delta G^o / k_B T)} \right)^{\frac{1}{\overline{\sigma}_{eq}}}
\tag{3.43}
$$

and since the left-hand side cannot depend on the free-energy of transition states or reaction intermediates, it follows that the forward/reverse degrees of rate control for transition states (eq. (3.41)) and reaction intermediates with $\nu_j = 0$ (eq. (3.44)) must be equal at equilibrium:

$$
\overleftarrow{X}_{TRC,j} = \overrightarrow{X}_{TRC,j} \text{ at equilibrium } \forall \text{ intermediates j with } \nu_j = 0
\tag{3.44}
$$

From eq. (3.19), the forward/reverse thermodynamic degrees of rate control of fluid-phase intermediates are zero at or away from equilibrium (see Section A3.3 of the Appendix), so for these species, eq. (3.44) does not confer any additional constraints. However, catalytic intermediates have nonzero forward/reverse thermodynamic degrees of rate control,[11,57,60] and thus eq. (3.44) states that the forward and reverse thermodynamic degrees of rate control for catalytic species are equal at equilibrium. The TST-form rate functions represent the pseudo-mass-action functions for the forward and

reverse rates at a point, and there is a different TST-form rate function for each steady-state reaction condition (see Section 2.3.2). The sensitivities and degrees of rate control are not inputs to the r_{TST} functions, but instead constants within the function. Equation (3.43) can be written as functions f and g where (eqs. (3.45) and (3.46)):

$$f(G_j^o[v_j \neq 0], a_j, T)$$

$$= \frac{\overleftarrow{C}}{\overrightarrow{C}} \exp\left(-\frac{\left(\sum_i (\overleftarrow{X}_{RC,i} - \overrightarrow{X}_{RC,i}) G_{TS,i}^o + \sum_j (\overleftarrow{X}_{TRC,j} - \overrightarrow{X}_{TRC,j}) G_j^o \right)}{k_B T} \right) \prod_j a_j^{\overrightarrow{X}_{TRC,j} - \overleftarrow{X}_{TRC,j}} \quad (3.45)$$

$$g(G_j^o[v_j \neq 0], a_j, T) = \left(\frac{\prod_j a_j^{v_j}}{\exp(-\Delta G^o / k_B T)} \right)^{\frac{1}{\overline{\sigma}_{eq}}} \quad (3.46)$$

where $G_j^o[v_j \neq 0]$ implies that only standard-state free energies with nonzero stoichiometric coefficients in the overall reaction appear as independent variables in f and g. At equilibrium, we know that $\overleftarrow{X}_{RC,i} - \overrightarrow{X}_{RC,i} = 0$ and $\overleftarrow{X}_{TRC,j} - \overrightarrow{X}_{TRC,j}$ for $v_j = 0$, and thus at equilibrium the function f depends only on the standard-state free energies of reactants and products. Deducing that f and g map the same independent variables to the same outputs is the same as proving that f is identical to g at equilibrium (eq. (3.47)):

$$f \equiv g \quad (3.47)$$

which is critical for relating the forward/reverse reaction orders to stoichiometric coefficients of the overall reaction (eq. (3.30)) and for determining the relationship between that ratio of the forward and reverse rate constants and the overall equilibrium constant (eq. (3.11)) for a composite reaction with an arbitrary number of rate-controlling transition states. The ratio of the rates (function f) is always numerically equal to the

overall thermodynamic relation (function g) however, away from equilibrium f is a function of transition state energies (since $\vec{X}_{\text{RC},i} \neq \overleftarrow{X}_{\text{RC},i}$, see eq. (3.45)), and thus f and g have different inputs and are therefore different functions such that eq. (3.47) does not hold. At equilibrium, since eq. (3.47) is true, we can follow the rationale of Boudart,[34] where he notes that the powers on activities of species in function f $(\overleftarrow{\alpha}_j - \vec{\alpha}_j)$ must be equal to the powers on activities of species in function g $(\nu_j/\bar{\sigma})$, such that (eq. (3.48)):

$$0 = -\frac{\nu_j}{\bar{\sigma}} + \overleftarrow{\alpha}_j - \vec{\alpha}_j = -\frac{\nu_j}{\bar{\sigma}} - \overleftarrow{X}_{\text{TRC},j} + \vec{X}_{\text{TRC},j} \tag{3.48}$$

where we note that the forward/reverse reaction orders are equal to negative the forward/reverse thermodynamic degrees of rate control. Now, the ratio of the reverse and forward rates equated to the thermodynamic equilibrium function is given by eq. (3.49):

$$\frac{\prod_j a_j^{\overleftarrow{\alpha}_j - \vec{\alpha}_j}}{\vec{k}/\overleftarrow{k}} = \frac{\prod_j a_j^{\nu_j/\bar{\sigma}}}{K_{\text{ov}}^{1/\bar{\sigma}}} \tag{3.49}$$

The numerators in eq. (3.49) are identically equal by eq. (3.48), and it follows that the denominators are also identically equal (eq. (3.50)):

$$\vec{k}/\overleftarrow{k} \equiv K_{\text{ov}}^{1/\bar{\sigma}} \tag{3.50}$$

and since no multiplicative factor appears in K_{ov}, it follows that at equilibrium, the $\vec{C}$ and $\overleftarrow{C}$ that appear in the forward and reverse rate constants must be equal so that they cancel in the ratio (eq. (3.51)):

$$\vec{C} = \overleftarrow{C} \text{ at equilibrium} \tag{3.51}$$

as is observed for the reaction in Scheme 3.1 (Figure A3.2).

The ratio of the reverse and forward rate functions are always numerically equal to the overall thermodynamic relation as shown in eq. (3.43), but the relationship between the forward and reverse rate constants and the overall equilibrium constant (eq. (3.50)) is only guaranteed to be valid at equilibrium. Away from equilibrium, the forward and reverse rate constants depend differently on the standard-state free energies of transition states, such that their ratio is a function of transition state energies, which K_{ov} is not, and thus these are not identically equal.[4,55] However, for elementary steps, because the rate functions of the forward and reverse reactions are identical at and away from equilibrium, the relationship between the elementary step rate constants and the equilibrium constant is always true. Likewise, for composite reactions, if the rate functions of the forward and reverse reactions do not change when the reaction moves away from equilibrium, as may be the case when there is a sole rate-controlling transition state, then the relationship between the rate constants and the overall equilibrium constant will hold, even away from equilibrium.

From the potential energy surface for the apparent rate-controlling elementary step at equilibrium (Figure 3.6), we determined that at equilibrium $\bar{\sigma}$ can be rationalized as the stoichiometric number of the apparent rate-controlling step. The stoichiometric numbers σ_i represent how many crossings of TS_i in the forward direction are required to form the final products in the overall reaction, in this case, 2 C and 1 D, hence the stoichiometric number for crossing TS_1 is 2 and the stoichiometric number for crossing TS_2 is 1. The apparent transition state depicted in Figure 3.6 is $1/3\ TS_1 + 2/3\ TS_2$, and thus the apparent stoichiometric number of the reaction must be $1/3\ \sigma_1 + 2/3\ \sigma_2 = 1/3*2 +$

$2/3 * 1 = 4/3 = \bar{\sigma}$. In general, we posit that at equilibrium $\bar{\sigma}$ is related to the forward/reverse kinetic degrees of rate control by (eq. (3.52)):

$$\bar{\sigma}^{\mathrm{eq}} = \sum_i \sigma_i \vec{X}_{\mathrm{RC},i}^{\,\mathrm{eq}} = \sum_i \sigma_i \overset{\leftarrow}{X}_{\mathrm{RC},i}^{\,\mathrm{eq}}$$ (3.52)

and thus by comparison to the definition for $\bar{\sigma}$ (eq.(3.8)) at the limit as the reaction approaches equilibrium, the forward and reverse degrees of rate control are calculated at the equilibrium limit as eq. (3.53):

$$\vec{X}_{\mathrm{RC},i}^{\,\mathrm{eq}} = \overset{\leftarrow}{X}_{\mathrm{RC},i}^{\,\mathrm{eq}} = \frac{\ln(Z_i)}{\sum_j \ln(Z_j)} = X_{\mathrm{ZC},i} \text{ at near equilibrium}$$ (3.53)

where $X_{\mathrm{ZC},i}$ is the "degree of reversibility control," a concept recently introduced by Razdan et al.[26] The degree of reversibility control quantifies the extent each elementary step controls the value of $\bar{\sigma}$. Razdan et al.[26] determined that away from equilibrium, the degrees of reversibility control were insufficient to provide information about which steps were rate controlling, but that at the limit of equilibrium the conclusions were quantitatively similar. We posit that the concepts of degrees of reversibility control and forward/reverse kinetic degrees of rate control converge at equilibrium (eq. (3.53)). From the $X_{\mathrm{ZC},i}$ reported by Razdan et al.[26] for methane dehydroaromatization on Mo/HZSM-5 catalysts, the rate-controlling transition state for the forward and reverse reactions at equilibrium are $\vec{X}_{\mathrm{RC},i}^{\,\mathrm{eq}} = \overset{\leftarrow}{X}_{\mathrm{RC},i}^{\,\mathrm{eq}} \approx 1$ for the transition state between ethylene and acetylene.

The example shown in Scheme 3.1 involved a non-catalytic reaction sequence, and as such, at all steady-state reaction conditions the reaction orders (or negative the thermodynamic degree of rate control) of fluid-phase intermediates were zero, regardless

of whether the reaction was at equilibrium. This restriction does not exist for surface species (see Section A3.3 of the Appendix). In Chapter 2 we proved[60] a relationship posited by Stegelmann et al.[11] and demonstrated further by Mao and Campbell[64] for surface species either adsorbed on one site or adsorbed on two different types of sites that the thermodynamic degrees of rate control of surface species are proportional to their fractional coverages when standard-state free energies of activation of elementary steps are not functions of the surface coverage. Following an analogous proof (see Section A3.1 of the Appendix), it follows that the same relationship holds for forward and reverse thermodynamic degrees of rate control (eq. (3.54)):

$$\theta_{j^*} = -\frac{X_{\text{TRC},j^*}}{\sigma_{*,\text{app}}} = -\frac{\vec{X}_{\text{TRC},j^*}}{\vec{\sigma}_{*,\text{app}}} = -\frac{\overleftarrow{X}_{\text{TRC},j^*}}{\overleftarrow{\sigma}_{*,\text{app}}} \tag{3.54}$$

where $\sigma_{*,\text{app}}$, $\vec{\sigma}_{*,\text{app}}$, and $\overleftarrow{\sigma}_{*,\text{app}}$ are the number of surface species reacting in the apparent initial state of the net, forward, and reverse reactions, respectively, defined as $\sigma_{*,\text{app}} = \sum_i s_i \sigma_{*,i}$, $\vec{\sigma}_{*,\text{app}} = \sum_i \vec{s}_i \sigma_{*,i}$, and $\overleftarrow{\sigma}_{*,\text{app}} = \sum_i \overleftarrow{s}_i \sigma_{*,i}$.[60] In general, $\sigma_{*,\text{app}} \neq \vec{\sigma}_{*,\text{app}} \neq \overleftarrow{\sigma}_{*,\text{app}}$ because the apparent initial states for the net, forward, and reverse reactions may have different numbers of reacting surface species. However, at equilibrium, $\vec{X}_{\text{TRC},j^*} = \overleftarrow{X}_{\text{TRC},j^*}$ (eq. (3.48)) requiring that $\vec{\sigma}_{*,\text{app}} = \overleftarrow{\sigma}_{*,\text{app}}$ (eq. (3.54)).

We demonstrate these concepts for the catalytic reaction sequence shown in Scheme 3.2, with $k_1 = 1$ au, $k_{-1} = 20$ au, $k_2 z/2 = 20$ au, $k_{-2} z/2 = 1$ au, where z is the coordination number, and an initial concentration $[A]_0 = 1$ au. The forward/reverse sensitivities and degrees of rate control are numerically calculated as a function of Z_{eff} using Matlab by forward integration from a clean ($\theta_{*,0} = 1$) catalyst surface (see the code

in Section A3.4 of the Appendix). The hypothetical potential energy surface for the apparent rate-controlling elementary step at equilibrium as determined by these calculations is shown in Figure 3.7a. Notice that the initial states for the forward and reverse reactions are both 1.19 A* + 0.17 * at equilibrium, and again that the forward and reverse reactions share an apparent transition state at equilibrium. Figure 3.7b shows the $\sigma_{*,\text{app}}$ for the net, forward, and reverse reaction as a function of Z_{eff}. At equilibrium, because the forward and reverse reactions share the same catalytic initial state, the number of surface species reacting in each initial state is identical. Thus $\vec{\sigma}_{*,\text{app}} = \overleftarrow{\sigma}_{*,\text{app}}$ at equilibrium. Notice that these differ from the number of surface species reacting in the apparent initial state for the net rate, $\sigma_{*,\text{app}}$. When the reaction is nearly irreversible in the forward direction (low Z_{eff}), $\sigma_{*,\text{app}} \approx \vec{\sigma}_{*,\text{app}}$, and when the reaction proceeds in the reverse direction and is nearly irreversible (high Z_{eff}), $\sigma_{*,\text{app}} \approx \overleftarrow{\sigma}_{*,\text{app}}$. This again highlights that the forward and reverse sensitivities and degrees of rate control provide novel information about the reaction system that differs from traditional sensitivities and degrees of rate control for the net rate. The concepts converge when the reaction is irreversible in either direction, but as the reaction approaches equilibrium, the forward and reverse degrees of rate control differ from net degrees of rate control. At equilibrium the forward/reverse degrees of rate control converge to values appropriate for an apparent rate-controlling elementary step with an initial state, transition state, and final state that is thermodynamically consistent with detailed balance at equilibrium.

Scheme 3.2. Sequence of fluid-phase reactions

$$A + * \underset{k_{-1}}{\overset{k_1}{\rightleftarrows}} A^* \qquad\qquad \sigma_1 = 2$$

$$A \qquad 2A^* \underset{k_{-2}}{\overset{k_2}{\rightleftarrows}} B + 2* \qquad\qquad \sigma_2 = 1$$

Overall: $\qquad 2A \Rightarrow B$
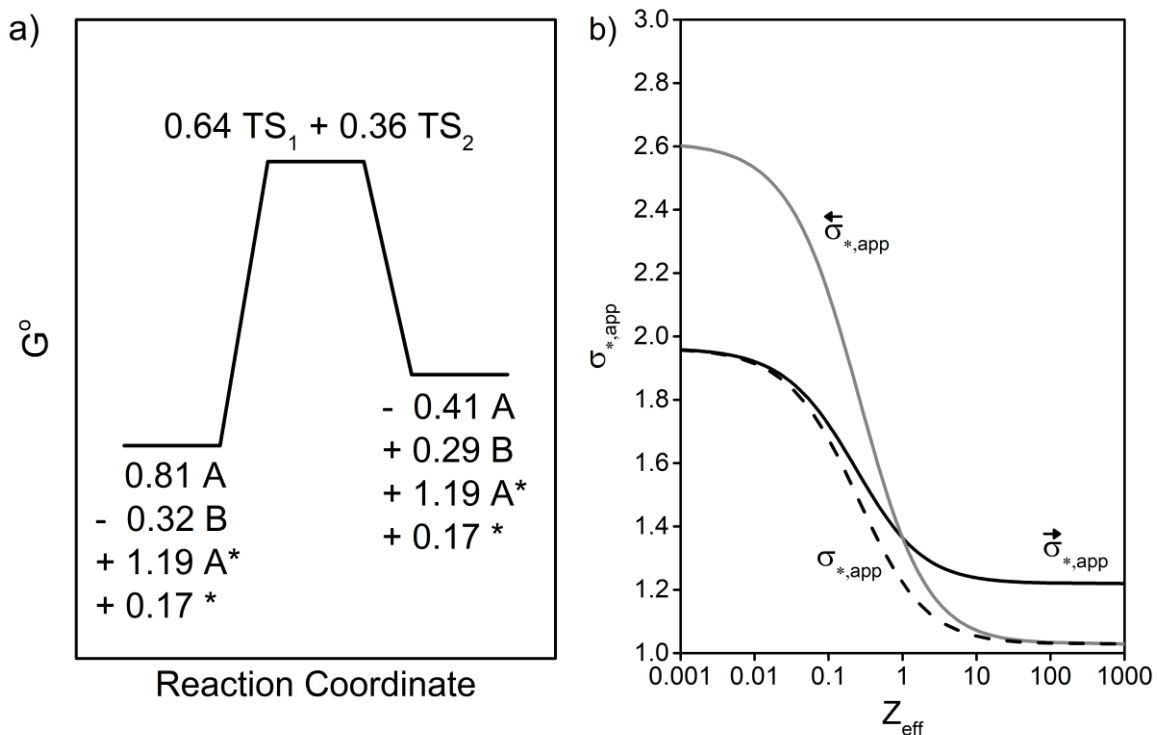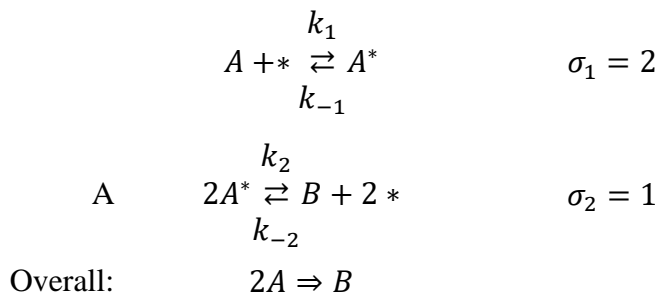
Figure 3.7: a) The potential energy surface for the apparent rate-controlling elementary step at equilibrium and b) $\sigma_{*,app}$ for the forward (solid black line), reverse (solid gray line), and net (dashed black line) reaction as a function of Z_{eff} for the reaction shown in Scheme 3.2 with $k_1 = 1$ au, $k_{-1} = 0.01$ au, $k_2 = 0.01$ au, $k_{-2} = 1$ au.

3.3.4 Forward and reverse degrees of rate control for ammonia synthesis and decomposition on Ru(0001) step sites

The preceding examples involved simple hypothetical reaction systems to illustrate the

consequences of forward/reverse degrees of rate control at and away from equilibrium for

non-catalytic and catalytic reaction networks. Herein, we analyze the oft-studied reversible synthesis of NH_3 from N_2 and H_2 on Ru(0001) step sites using kinetic parameters derived from density functional theory (DFT) calculations reported by Logadóttir and Nørskov.[1] The elementary-step reaction sequence for the catalytic ammonia synthesis/decomposition chemistry is reported in Scheme 3.3. We modeled the forward and reverse rates and calculated the forward/reverse degrees of rate control as a function of Z_{eff} for NH_3 synthesis/decomposition at 700 K with $P_{N_2} = 50 - \varepsilon$ bar, $P_{H_2} = 150 - 3\varepsilon$ bar, and $P_{NH_3} = 2\varepsilon$ bar where ε is an extent of reaction (see Section A3.5 of the Appendix for full details on the microkinetic model). The forward and reverse kinetic degrees of rate control are reported in Figure 3.8a and the thermodynamic degrees of rate control for surface and fluid-phase species are reported in Figure 3.9. In general, the kinetic degrees of rate control for the forward and reverse reactions differ, but at equilibrium they are equal as required by microscopic reversibility and detailed balance at equilibrium.

The kinetic degrees of rate control shown in Figure 3.8a demonstrate that the sole rate-controlling transition state for the forward rate (NH_3 synthesis) is the transition state for dissociative adsorption of N_2 (reaction 1 in Scheme 3.3) from $10^{-10} < Z_{eff} < 10^1$. Even when the net reaction is shifted toward NH_3 decomposition ($Z_{eff} > 1$), the rate-controlling transition state for the forward reaction is still N_2 dissociation. However, as NH_3 decomposition becomes more thermodynamically favored, the transition state for $NH^* + H^* \rightleftarrows NH_2^* + *$ also becomes rate controlling. From inspection of the thermodynamic degrees of rate control in Figure 3.9, when the kinetic degree of rate control for transition state 3 begins to increase (see Figure 3.8), there is a decrease in

Scheme 3.3: Reaction sequence for ammonia synthesis/decomposition on Ru(0001) step sites.

$$
\begin{array}{lll}
1. & N_2 + 2* \underset{k_{-1}}{\overset{k_1}{\rightleftarrows}} 2N^* & \sigma_1 = 1 \\[2em]
2. & N^* + H^* \underset{k_{-2}}{\overset{k_2}{\rightleftarrows}} NH^* + * & \sigma_2 = 2 \\[2em]
3. & NH^* + H^* \underset{k_{-3}}{\overset{k_3}{\rightleftarrows}} NH_2^* + * & \sigma_3 = 2 \\[2em]
4. & NH_2^* + H^* \underset{k_{-4}}{\overset{k_4}{\rightleftarrows}} NH_3^* + * & \sigma_4 = 2 \\[2em]
5. & NH_3^* \underset{k_{-5}}{\overset{k_5}{\rightleftarrows}} NH_3 + * & \sigma_5 = 2 \\[2em]
6. & H_2 + 2* \underset{k_{-6}}{\overset{k_6}{\rightleftarrows}} 2H^* & \sigma_6 = 3
\end{array}
$$

Overall: $\quad N_2 + 3H_2 \Rightarrow 2NH_3$
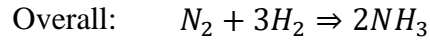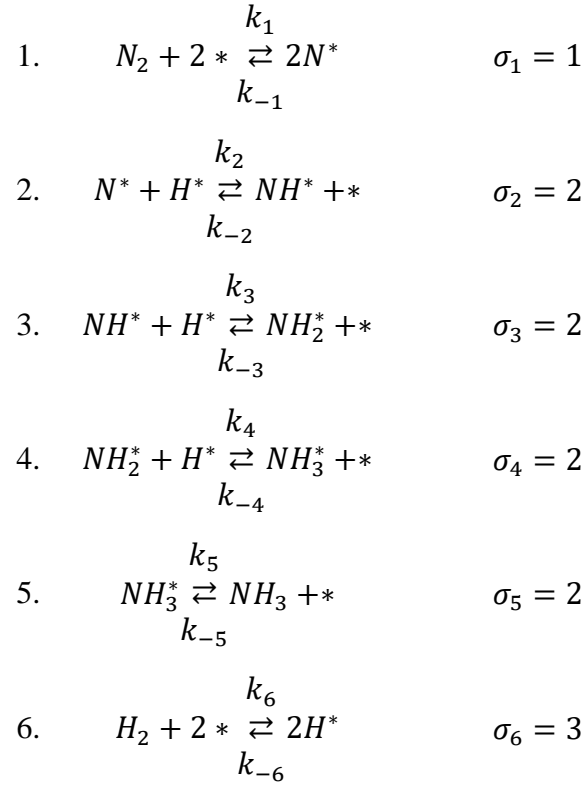
$-X_{TRC,H^*}$, indicative that the fractional coverage of H* is decreasing. This occurs at the same time as an increase in $-X_{TRC,H_2}$, suggesting that there is insufficient H* on the surface to hydrogenate NH_x^* species on the surface, allowing them to recombine to N_2 before hydrogenation to NH_3. The reason for the change in the kinetic degrees of rate control is not due explicitly to a change in the reversibility of the overall reaction, but
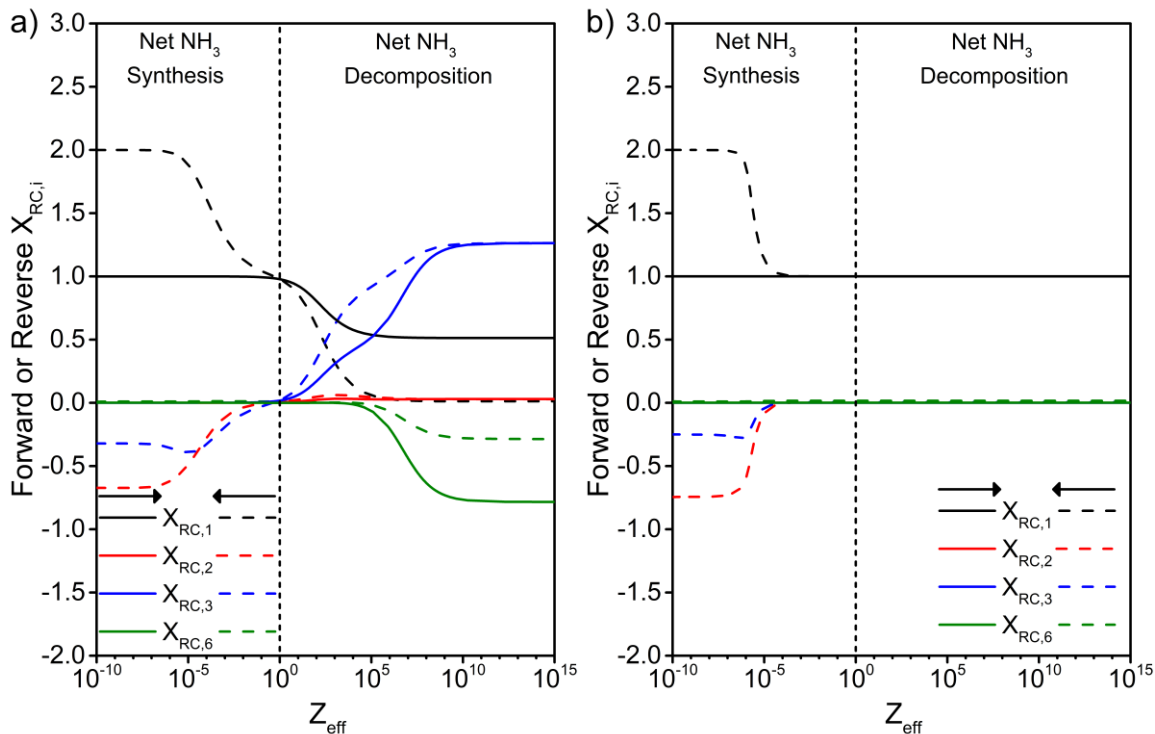
Figure 3.8: Forward and reverse kinetic degrees of rate control for transition states of NH_3 synthesis/decomposition reactions on Ru(0001) step sites using kinetic parameters derived from DFT calculations reported by Logadóttir and Nørskov[1] at 700 K with a) $P_{N_2} = 50 - \varepsilon$ bar, $P_{H_2} = 150 - 3\varepsilon$ bar, and $P_{NH_3} = 2\varepsilon$ bar and b) $P_{N_2} = 50 - \varepsilon$ bar, $P_{H_2} = 300 - 3\varepsilon$ bar, and $P_{NH_3} = 2\varepsilon$ bar. Numbers correspond to the transition states of the elementary step reactions reported in Scheme 3.3. Only the four transition states with the largest maximum magnitudes in the kinetic degrees of rate control are reported.

instead a result of the changing reaction conditions as N_2 and H_2 pressures decrease and NH_3 pressures increase. Many different reaction conditions exist for each Z_{eff}. For example, if the initial reaction mixture contained excess H_2, then the rate-controlling transition state for the forward rate may not change as a function of the reversibility, as shown in Figure 3.8b for $P_{N_2} = 50 - \varepsilon$ bar, $P_{H_2} = 300 - 3\varepsilon$ bar, and $P_{NH_3} = 2\varepsilon$ bar, where the initial H_2:N_2 ratio is excess of stoichiometric (6:1). With a higher initial H_2 pressure, as H_2 is consumed, a high enough H_2 pressure is maintained even as NH_3 decomposition is strongly thermodynamically favored, such that the transition state for

110
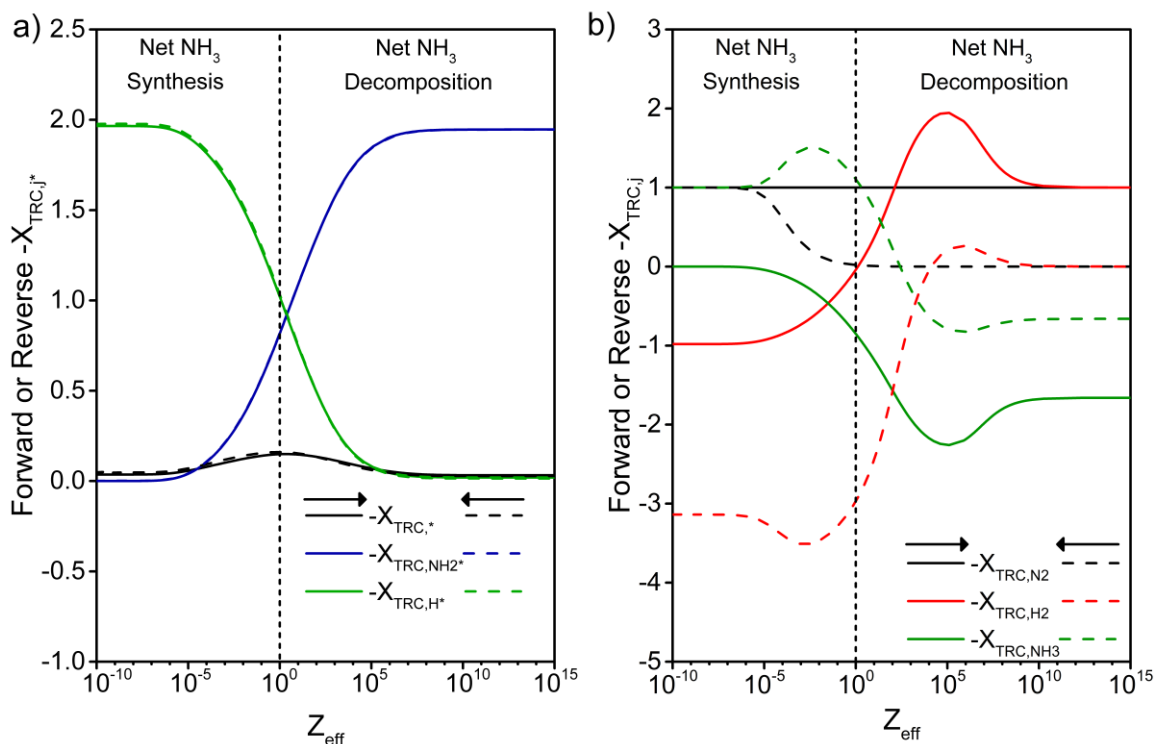
Figure 3.9: Negative the forward and reverse thermodynamic degrees of rate control for a) surface species and b) fluid-phase species for NH_3 synthesis/decomposition reactions on Ru(0001) step sites using kinetic parameters derived from DFT calculations reported by Logadóttir and Nørskov.[1] Only the three surface species with the largest maximum magnitudes in the thermodynamic degrees of rate control are reported.

dissociative N_2 adsorption is always rate controlling for the forward rate, in contrast to when the initial H_2:N_2 was stoichiometric (3:1).

In Figure 3.9a, the forward and reverse thermodynamic degrees of rate control of surface species are nearly identical because $\overrightarrow{\sigma_*} \approx \overleftarrow{\sigma_*}$ at all reaction conditions (see eq. (3.54)). All of the degrees of rate control for the forward reaction are nearly invariant from $10^{-10} < Z_{eff} < 10^{-4}$ when the initial N_2 and H_2 pressures are 50 and 150 bar, respectively. Thus at these conditions, the forward rate function is also invariant, and, based on this microkinetic model, is approximately given by eq. (3.55):

$$\vec{r}/L \approx \vec{k}\theta_{H^*}^2 P_{N_2} P_{H_2}^{-1} \tag{3.55}$$

where $\theta_{H^*} \approx 1$ and the forward apparent rate constant is given by eq. (3.56):

$$\vec{k} \approx k_1 K_6^{-1} \tag{3.56}$$

where the exponents on the rate constants are determined by the forward sensitivities and

$\vec{C} = 1$ (see eq. (3.18)). Thus, the forward rate is given by eq. (3.57):

$$\vec{r}/L \approx k_1 K_6^{-1} P_{N_2} P_{H_2}^{-1} \tag{3.57}$$

from $10^{-10} < Z_{eff} < 10^{-4}$. Thus, the degrees of a rate control offer a method to reduce the forward and reverse rate functions and to identify the valid ranges of the rate functions. For example, eq. (3.57) is an acceptable rate function for modeling the reaction rate for a reactor operating at 700 K with initial N_2 and H_2 pressures of 50 and 150 bar, respectively, as long as Z_{eff} does not exceed 10^{-4}.

It is worth noting that if one were to employ the methods eloquently described by Enomoto and Horiuti[37] to experimentally measure $\bar{\sigma}$ at equilibrium for the reaction conditions used in Figure 3.8a, one would find that $\bar{\sigma} = 1$, implying that the rate-controlling step has a stoichiometric number of one (see eq. (3.52)) which is consistent with the rate-controlling transition state being that for N_2 dissociation, which, as shown in Figure 3.8a, is the rate-controlling transition state for the forward reaction when NH_3 synthesis is nearly irreversible (low Z_{eff}). However, the rate-controlling transition state at equilibrium may be distinct from the rate-controlling transition state away from equilibrium. The conclusion that the rate-controlling step at NH_3 decomposition conditions (high Z_{eff}) has a stoichiometric number of one based on measurements at

equilibrium would be incorrect, since the NH_2^* decomposition transition state is more rate controlling under these conditions when reactants and products are in stoichiometric ratios, as shown in Figure 3.8a.

This difference in rate-controlling steps at and away from equilibrium in Figure 3.8a also offers an illustrative explanation for why a catalyst that is good for the forward reaction (i.e., NH_3 synthesis) is not necessarily a good catalyst for the reverse reaction (i.e., NH_3 decomposition).[65] It is counter-intuitive that this is not the case, considering that the catalyst stabilizes transition states that are part of both the forward and reverse reaction pathways. However, the extent to which each transition state controls the forward and reverse reactions are not equal. A good NH_3 synthesis catalyst will, for example, lower the free energies of rate-controlling transition state at low Z_{eff}, i.e., it will lower the free energy of the forward apparent transition state, $\vec{G}_{TS,app}^o = \sum_i \vec{X}_{RC,i} G_{TS,i}^o$, while a good catalyst for NH_3 decomposition will lower the free energy of the reverse apparent transition state, $\overleftarrow{G}_{TS,app}^o = \sum_i \overleftarrow{X}_{RC,i} G_{TS,i}^o$, at high Z_{eff}. These quantities are only related when $\vec{X}_{RC,i}\big|_{low\ Z_{eff}} \approx \overleftarrow{X}_{RC,i}\big|_{high\ Z_{eff}}$, which will only occur when there is a sole rate-controlling transition state. Thus, there is no reason to expect that a catalyst optimized for the forward reaction will also be proficient in catalyzing the reverse reaction.

3.4 Conclusion

A degree of rate control formalism for forward and reverse reactions is developed to identify rate-controlling transition states and species specific to the forward or reverse rates of reversible composite reactions. The degrees of rate control are distinct for the forward and reverse reactions. These can be thought of as representing stoichiometric coefficients in an equilibrium between an apparent initial and transition state, which differ for the forward and reverse reactions, and within such a formalism the apparent forward/reverse transition states converge at chemical equilibrium. The forward and reverse apparent rate-controlling steps combine to form a single apparent rate-controlling step at equilibrium, with an apparent initial, transition, and final state where the apparent final state of the forward reaction is the apparent initial state of the reverse reaction. The stoichiometric number of this apparent rate-controlling step is equal to the affinity-averaged stoichiometric number, $\bar{\sigma}$, and the ratio of the forward and reverse rate functions is proven to be identically equal to the overall equilibrium equation to the power of $1/\bar{\sigma}$, which is thermodynamically consistent with the principles of microscopic reversibility and detailed balance at equilibrium. The forward and reverse degrees of rate control are demonstrated by example in non-catalytic and catalytic reactions, including NH_3 synthesis and decomposition.

Chapter 4

Degrees of rate control at non(pseudo)steady-state conditions

4.1 Conspectus

The degrees of rate control enable identification of rate-controlling transition states and species during (pseudo-)steady-state reaction. We demonstrate a method for identifying rate-controlling transition states and species at non(pseudo)steady-state conditions through modification of the definitions for degrees of rate control and sensitivities by superimposing the condition that time constants of the analytical rate function are kept constant when taking the partial derivatives of rate with respect to the rate constants/free energies. The utility of transient degrees of rate control is demonstrated for catalytic reaction networks to rationalize features of the transient rate including extrema and discontinuities.

4.2 Introduction

The degrees of rate control unambiguously identify rate-controlling transition states and stable species in a composite reaction network.[12,21] The kinetic degree of rate control ($X_{RC,i}$) is defined as the relative change in the rate per RT decrease in the standard molar free energy of transition state i while keeping all other standard free energies constant, which is equivalent to the relative change in the rate per relative change in the

rate constant of step i while keeping all other rate constants (k_j) and the equilibrium constant for step i (K_i) constant (eq. (3.5))[11,13,56]:

$$X_{RC,i} = \left(\frac{\partial \ln r}{\partial(-G^o_{TS,i}/RT)}\right)_{G^o_{j\neq TS,i}} = \left(\frac{\partial \ln r}{\partial \ln k_i}\right)_{k_{j\neq i},K_i} \quad (4.1)$$

The thermodynamic degree of rate control ($X_{TRC,j}$) is analogously defined as (eq. (4.2))[11,57]:

$$X_{TRC,j} = \left(\frac{\partial \ln r}{\partial(-G^o_j/RT)}\right)_{G^o_{i\neq j}} \quad (4.2)$$

Quantities similar to the degrees of rate control are sensitivities, s_i (eq. (4.3))[19,23]:

$$s_i = \left(\frac{\partial \ln r}{\partial \ln k_i}\right)_{k_{j\neq i}} \quad (4.3)$$

which are related to the kinetic and thermodynamic degrees of rate control by eqs. (4.4)[19,23] and (4.5)[6060]:

$$X_{RC,i} = s_i + s_{-i} \quad (4.4)$$

$$X_{TRC,j} = \sum_{j=species} \nu_{ij} s_i [\nu_{ij} < 0] \quad (4.5)$$

where ν_{ij} is the stoichiometric coefficient of species j in reaction i and $[\nu_{ij} < 0]$ equals unity if true and zero if false.

A condition implicit in the calculation of the degrees of rate control is that the reaction is operating under (pseudo-)steady-state conditions.[21,56] The kinetic degrees of rate control can, however, be functions of the activities of fluid-phase reactant and product species, and thus, as reactant species are consumed and product species are

116

formed during reaction, the degrees of rate control can change in time.[21,56] Campbell reported a numerical method for assessing the kinetic degrees of rate control for transients that result due to changing activities of reactant and product species.[21,56] This method requires forward simulation to a time, t, at which point a transition state energy is perturbed a differential amount. The reaction is then forward simulated a differential time, dt, that is long enough to re-establish pseudo-steady-state activities and surface coverages of reaction intermediates.[21,56]

The method described above is for assessing degrees of rate control for transients under (pseudo-)steady-state conditions. We inquire instead how to identify rate-controlling steps and transition states during non(pseudo)steady-state transients, which are ubiquitous in catalysis, for example, transients that result from changing surface coverages in time.

In this work, we define degree-of-rate-control formulae specifically for transient systems where the (pseudo-)steady-state assumption is invalid, and activities of reactant and product species are constant, such that changing activities and surface coverages of reaction intermediates are the only causes of transients in the rate. We demonstrate the utility of this new definition by rationalizing observed features in the transient rate, such as discontinuities and extrema.

4.3 Discussion

When the reaction rate is changing in time because the activities of reactants and products of overall reactions are changing in time, such as in a batch reactor, the overall reaction rate can itself operate at pseudo-steady-state conditions—where the activities of

reaction intermediates are solved using the pseudo-steady-state approximation—despite the rate itself being transient. The focus of this work is on assessing degrees of rate control during non(pseudo)steady-state transients where the activities of reaction intermediates cannot be determined by making pseudo-steady-state assumptions. To understand how to calculate degrees of rate control at non(pseudo)steady conditions, we first discuss how to calculate degrees of rate control during pseudo-steady-state transients. The equations derived in the following section are explicitly derived for a batch reactor, where the pseudo-state state assumption is valid for all reaction intermediates, however we note that time-dependent rates in batch reactors when the pseudo-steady state assumption is valid are analogous to variations in rate with contact time in ideal plug flow reactors operating at steady state. Thus all equations derived in the following section also apply to plug-flow reactors operating at steady-state by changing time, t, in each equation to contact-time, τ.

Case Study 1: Degrees of rate control for pseudo-steady-state transients in batch reactors

Consider the catalytic reaction in Scheme 4.1 where the solution to the system of algebraic eqs. (4.6)-(4.8) gives the pseudo-steady-state reaction rate, r_C/L:

$$\frac{d\theta_{A^*}(t)}{dt} = 0 = r_1(t) - r_{-1}(t) - r_2(t)$$

$$= k_1 a_A(t)\theta_*(t)L - k_{-1}\theta_{A^*}(t)L - k_2 a_B(t)\theta_{A^*}(t)L \tag{4.6}$$

$$\theta_*(t) + \theta_{A^*}(t) = 1 \tag{4.7}$$

$$r_C(t)/L = k_2 a_B(t)\theta_{A^*}(t) \tag{4.8}$$

118

where a_i are thermodynamic activities and L is the number of active sites. The pseudo-steady-state approximation is made on the fractional coverage of A in eq. (4.6). The solution to this system of algebraic equations is given by eq. (4.9):

$$r_C(t)/L = \frac{k_1 a_A(t) k_2 a_B(t)}{k_1 a_A(t) + k_{-1} + k_2 a_B(t)} \tag{4.9}$$

Scheme 4.1: Hypothetical two-step catalytic reaction with a reversible first step

$$A + * \leftrightarrow A^* \qquad\qquad k_1, k_{-1}$$

$$A^* + B \rightarrow C + * \qquad\qquad k_2$$

In a batch reactor, the activities of reaction intermediates are changing in time and thus the rate of formation of the product, C, is changing in time. The transient rate in a batch reactor is found by solving the coupled differential equations and initial conditions in eqs. (4.10)-(4.13) to solve for $a_A(t)$ and $a_B(t)$ and substitution of these functions into eq. (4.9):

$$\frac{da_A}{dt} = -\frac{k_1 a_A(t) k_2 a_B(t)}{k_1 a_A(t) + k_{-1} + k_2 a_B(t)} \tag{4.10}$$

$$\frac{da_B}{dt} = -\frac{k_1 a_A(t) k_2 a_B(t)}{k_1 a_A(t) + k_{-1} + k_2 a_B(t)} \tag{4.11}$$

$$a_A(t = 0) = a_{A,0} \tag{4.12}$$

$$a_B(t = 0) = a_{B,0} \tag{4.13}$$

The solution to this system of equations gives the rate, r_C, as a function of the rate constants and the activities of the reactants A and B, which are themselves functions of the rate constants, the initial activities, and time (eq. (4.14)):

$$r_C = r_C\left(k_1, k_{-1}, k_2, a_A(a_{A,0}, a_{B,0}, k_1, k_{-1}, k_2, t), a_B(a_{A,0}, a_{B,0}, k_1, k_{-1}, k_2, t)\right) \quad (4.14)$$

With the rate in the functional form given in eq. (4.14), the degrees of rate control can be calculated as a function of time. However, we will demonstrate that eqs. (4.3) and (4.4) in their present form will give erroneous results. This is because the rate during a transient does not depend solely on rate constants and activities of reactants and products, but also on time, t. Because the rate is also a function of time, the sum of the degrees of rate control will not equal unity because there is an additional sensitivity, $s_{1/t}$, that is in the sum to unity, such that $\sum_i X_{RC,i} = 1 - s_{1/t}$. We demonstrate this by applying the degree of rate control formulae (eqs. (4.3) and (4.4)) to eq. (4.14) for transition state 2 (TS2) to show that calculating the degree of rate control in this way has terms for the dependence of activity on the rate constants and the apparent reaction orders (eq. (4.15)):

$$X_{RC,2} = s_2 + s_{-2} = s_2 = \left(\frac{\partial \ln r_C}{\partial \ln k_2}\right)_{k_1, k_{-1}}$$

$$= \left(\frac{\partial \ln r_C}{\partial \ln k_2}\right)_{k_1, k_{-1}, a_A, a_B} \left(\frac{\partial \ln k_2}{\partial \ln k_2}\right)_{k_1, k_{-1}}$$

$$+ \left(\frac{\partial \ln r_C}{\partial \ln a_A}\right)_{k_1, k_{-1}, k_2, a_B} \left(\frac{\partial \ln a_A}{\partial \ln k_2}\right)_{k_1, k_{-1}}$$

$$+ \left(\frac{\partial \ln r_C}{\partial \ln a_B}\right)_{k_1, k_{-1}, k_2, a_A} \left(\frac{\partial \ln a_B}{\partial \ln k_2}\right)_{k_1, k_{-1}}$$

$$= \left(\frac{\partial \ln r_C}{\partial \ln k_2}\right)_{k_1, k_{-1}, a_A, a_B} + \alpha_A \left(\frac{\partial \ln a_A}{\partial \ln k_2}\right)_{k_1, k_{-1}}$$

$$+ \alpha_B \left(\frac{\partial \ln a_B}{\partial \ln k_2}\right)_{k_1, k_{-1}}$$

(4.15)

where the partial derivative for sensitivity defined in eq. (4.3) is related to the apparent reaction orders, α_j, and derivatives of activity with respect to k_2 by the chain rule. When the degrees of rate control are assessed at initial time in a batch reactor (or at differential conversion conditions in a flow reactor), the activities of A and B are constants and their derivatives are zero, and thus the degree of rate control of TS2 simplifies to the first term in the final equation of eq. (4.15). However, at longer times, activities of reactants are functions of the rate constants, and thus their derivatives are nonzero in eq. (4.15). The consequence of this is that the degrees of rate control calculated by eq. (4.15) will give different results depending on whether it is at the initial time or at non-initial times even at identical reactor compositions.

The numerical approach discussed by Campbell for calculating the transient degrees of rate control in a pseudo-steady-state batch reactor circumvents this issue by

121

treating a transient batch reactor at time t as a batch reactor that has the same composition but at $t = 0$. Campbell then assesses the degrees of rate control for the initial rates in this hypothetical batch reactor. The numerical method Campbell employs is equivalent to an analytical approach where the definitions for degrees of rate control and sensitivities are modified to keep constant the activities of reactants and products that are changing in time (eqs. (4.16)-(4.18)):

$$X_{RC,i}(\text{t}) = \left(\frac{\partial \ln r}{\partial(-G_{TS,i}^o/RT)}\right)_{G_{j\neq TS,i}^o, a_R, a_P} = \left(\frac{\partial \ln r}{\partial \ln k_i}\right)_{k_{j\neq i}, K_i, a_R, a_P} \tag{4.16}$$

$$X_{TRC,j}(\text{t}) = \left(\frac{\partial \ln r}{\partial(-G_j^o/RT)}\right)_{G_{i\neq j}^o, a_R, a_P} \tag{4.17}$$

$$s_i(t) = \left(\frac{\partial \ln r}{\partial \ln k_i}\right)_{k_{j\neq i}, a_R, a_P} \tag{4.18}$$

With these equations, the degree of rate control for TS2 for the rate of the form given in eq. (4.14) does not contain terms for the dependence of activities on rate constants (eq. (4.19)). Calculation of the degree of rate control for TS2 for the rate given in eq. (4.9) gives a function that depends only on the activities of A and B at time t (eq. (4.19)):

$$X_{RC,2}(t) = s_2(t) + s_{-2}(t) = s_2(t) = \left(\frac{\partial \ln r_C}{\partial \ln k_2}\right)_{k_1, k_{-1}, a_A, a_B}$$

$$= \frac{k_1 a_A(t) + k_{-1}}{k_1 a_A(t) + k_{-1} + k_2 a_B(t)} \tag{4.19}$$

In this first case-study we demonstrate that the numerical approach for calculating degrees of rate control as a function of time at pseudo-steady-state conditions implicitly

alters the original definitions given in eqs. (4.3)-(4.5) by keeping constant the activities of reactant and product species when taking the partial derivative of rate with respect to the free energy or rate constant, and thus there is a precedent for altering the degree-of-rate control definitions for transient conditions. This method used in Case 1 is only appropriate for calculating degrees of rate control during pseudo-steady-state transients, but non(pseudo)steady-state transients where surface coverages or activities of reaction intermediates evolve in time, as opposed to activities of reactants and products, occur frequently in catalysis. Assessing the degrees of rate control during these non(pseudo)steady-state transients require different modifications to the degree-of-rate-control formulae than those for pseudo-steady-state transients. We illustrate that degrees of rate control and sensitivities can be assessed during non(pseudo)steady-state transients by identifying the time constants, τ_j, that describe the transient time-scales and including a condition that these τ_j are not differentiated when calculating the degrees of rate control.

Case Study 2: Calculating degrees of rate control during non(pseudo)steady-state transients at differential conversion for systems with a single time constant, τ

In this second case study, we consider a transient where the fractional coverages of reaction intermediates are changing in time, instead of activities of reactants and products. In this system, differential conversion in a flow reactor is assumed such that activities of reactants and products are constant, and the pseudo-steady-state assumption is not valid for reaction intermediates, allowing the fractional coverages to change in time.

Reaction orders provide mechanistic insights about the rate-controlling species and transition states at steady state.[60] We proved[60] in Chapter 2 that the reaction orders of

123

composite reactions are sensitivity-weighted averages of the elementary step reaction

orders, as shown by eq. (4.20) (see Section A4.1 of the Appendix for derivation):

$$\alpha_j = \sum_i s_i \alpha_{ij} \qquad (4.20)$$

where α_j is the reaction order of species j for the overall steady-state reaction rate, α_{ij} is

the reaction order of species j for elementary reaction i, and s_i is the sensitivity for

elementary step i. Thus, the measured reaction orders for the steady-state rate are related

to the sensitivities by eq. (4.20) which in turn are related to the degrees of rate control by

eqs. (4.4) and (4.5). A sole, rate-determining, irreversible elementary step will have $s_i = 1$

while all other sensitivities equal zero, and thus the measured reaction order for the

overall reaction is the same as the reaction order for that elementary step. Here, we

identify reaction orders during non(pseudo)steady-state transients to demonstrate that the

rate-limiting step during a non(pseudo)steady-state transient is not necessarily the same

as the rate-limiting step at steady-state conditions by considering a transient reaction in a

flow reactor. Consider the case where this flow reactor begins by operating at steady state

at differential conversion conditions such that the activities of A and B are constant

throughout the reactor. Heterogeneous catalytic reactions offer the unique ability to

rapidly change the activities of reactant species inside the reactor by changing the inlet

composition, while the activities of reaction intermediates, which are confined to the

surface of the solid catalyst, change to new steady-state values on relatively longer time-

scales that are dictated by the reaction kinetics. Step-changing the activity of the reactant

species in the fluid phase induces a transient in the rate as the activities of surface species

approach new steady-state values. The transient reaction rate for a flow reactor operating

124

at differential conversion for the reaction in Scheme 4.1 when a reactant species is step-changed is given by eq. (4.21) (see Section A4.2 of the Appendix for derivation):

$$\frac{r(t)}{L} = \frac{k_1 a_A k_2 a_B}{k_1 a_A + k_{-1} + k_2 a_B}\left(1 - e^{-(k_1 a_A + k_{-1} + k_2 a_B)t}\right)$$
$$+ k_2 a_B \theta_{A^*,0} e^{-(k_1 a_A + k_{-1} + k_2 a_B)t}$$

(4.21)

where $\theta_{A^*,0}$ is the fractional coverage of species A at the time of the step-change and t is the time after the step-change. At a time immediately after the step-change, $t = 0^+$, the rate is given by eq. (4.22):

$$r(t = 0^+)/L = k_2 a_B \theta_{A^*,0}$$

(4.22)

At time $t = 0^+$, only the rate constant for the second step appears in the rate function with the initial coverage of the reaction intermediate, and thus the sensitivities found by applying eq. (4.3) to eq. (4.22) gives $s_1 = 0$ and $s_2 = 1$. At longer times on stream, the coverage of the intermediate changes as the reaction approaches steady-state, and from eq. (4.21), both k_1 and k_{-1} will appear in the equation that describes the rate at time t. To determine how sensitivities, and, in turn, the kinetic and thermodynamic degrees of rate control change during the transient, we consider the reaction presented in Scheme 4.1 with $k_1 = 10^{-5}\ a.u., k_{-1} = 0\ a.u., k_2 = 1\ a.u.,\ a_A = 1,\ a_B(t < 0) = 1$ and $a_B(t \geq 0) = 3$. Since $k_{-1} = 0$ and $k_1 \ll k_2$, the transient rate given in eq. (4.21) is approximately (eq. (4.23)):

$$r(t)/L = k_1 a_A\left(1 - e^{-(k_2 a_B)t}\right) + k_2 a_B \theta_{A^*,0} e^{-(k_2 a_B)t}$$

(4.23)

Notice that the steady-state rate $r(t \to \infty)/L = k_1 a_A$ depends only on the activity of A and the rate constant k_1, while the initial rate $r(t = 0^+)/L = k_2 a_B \theta_{A^*,0}$ depends on the activity of B, the rate constant k_2, and the initial coverage of A. The rate as a function of time is shown in Figure 4.1, where the contribution of each term in eq. (4.23) is indicated by the shading, with the first term corresponding to the contribution of the steady-state rate to the overall rate (orange) and the second term in eq. (4.23) corresponding to the contribution of the initial rate to the overall rate (purple). The sensitivities were calculated above at steady-state and at the time of a step-change using eq. (4.3), and here we calculate the sensitivities/degrees of rate control by applying eqs. (4.3) and (4.4) to the transient rate function (eq. (4.23)) at all times during the transient, as shown in Figure 4.2. The sensitivities at the time of the step-change are $s_1 = X_{RC,1} = 0$ and $s_2 = X_{RC,2} = 1$ and at steady state are $s_1 = X_{RC,1} = 1$ and $s_2 = X_{RC,2} = 0$, as expected. However, at intermediate times between the step-change and steady state, the sensitivity $s_2 = X_{RC,2} < 0$ at some times t and the sum of the sensitivities $s_1 + s_2$ (or kinetic degrees of rate control, $X_{RC,1} + X_{RC,2}$) do not equal unity. We proved[60] in Chapter 2 that the constraint that kinetic degrees of rate control and sensitivities sum to unity exists because the sensitivities of rate with respect to quantities that have units of inverse time need to sum to unity. During a non(pseudo)steady-state transient reaction, the quantity $1/t$ (see eq. (4.23)), which also has units of inverse time, appears in the rate function ($r = r(k_i, a_j, t)$). Thus, there exists a sensitivity for each of the rate constants and another sensitivity for transient reactions, $s_{1/t}$, which is the sensitivity of the rate to the quantity $1/t$. The sum $s_1 + s_2 + s_{1/t} = 1$ for all t, as shown in Figure 4.2. The kinetic degrees of

126
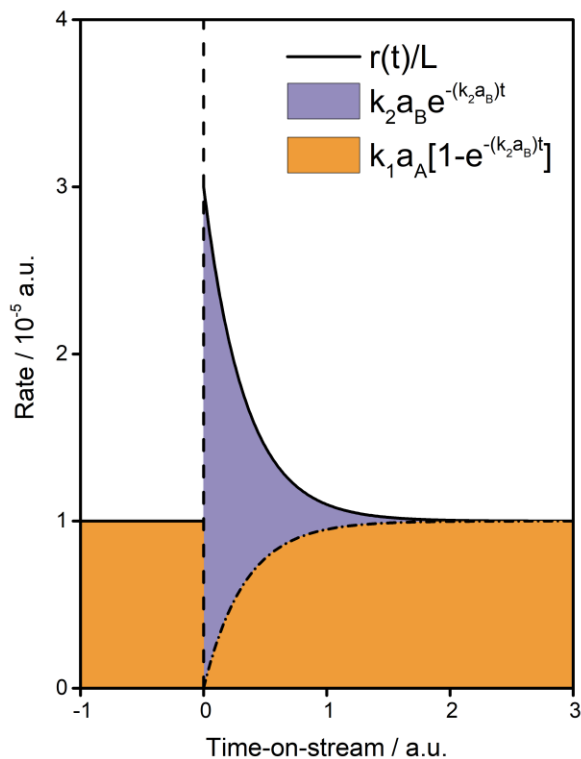
Figure 4.1: Transient after a step-change at time t = 0 au for the reaction in Scheme 4.1. Shaded regions indicate the contribution of the initial rate (purple) and steady-state rate (orange) to the transient rate as a function of time.

rate control summing to unity is one of the appealing features of these mathematical formalisms for describing rate-control under (pseudo-)steady-state conditions, and the loss of this characteristic renders uncertain the application of established formalisms of degrees of rate-control to non(pseudo)steady-conditions. In addition, from eq. (4.20) we note that the reaction order of B, α_B, is equal to the sensitivity s_2. The initial transient rate is first-order in B and the steady-state rate is zero-order in B, and, as depicted by the shading in Figure 4.1, the rate during the transient is a weighted sum of these two states, where the weighting factors for the initial and steady-state rates are $e^{-(k_2 a_B)t}$ and $1 - e^{-(k_2 a_B)t}$, respectively (see eq. (4.23)). With this in mind, we argue that the sensitivity s_2 should never be negative during the transient, and instead propose modified

definitions for sensitivity and the kinetic and thermodynamic degrees of rate control to assess rate-control during non(pseudo)steady-state conditions.
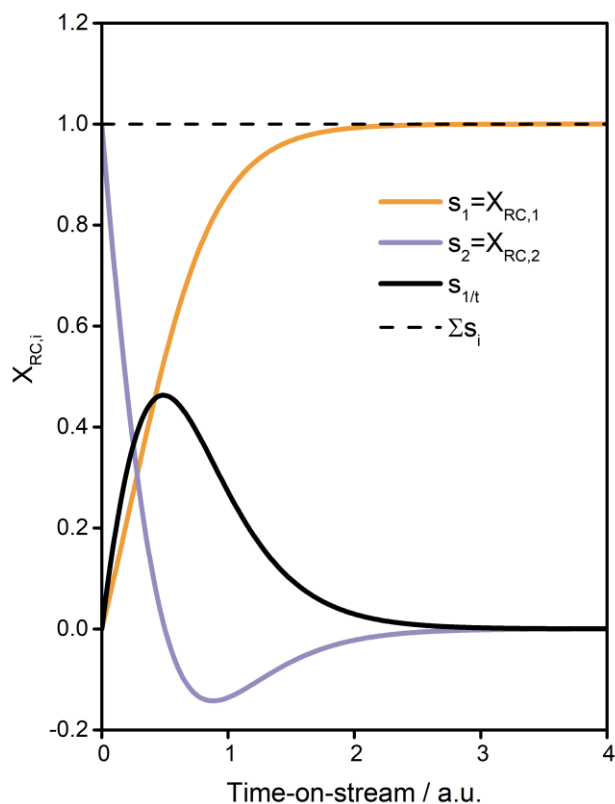
Figure 4.2: Sensitivities as a function of time calculated by applying the unmodified sensitivity formula (eq. (4.3)) to the analytical function for the transient rate for the reaction in Scheme 4.1 (eq. (4.23)). We note that this formalism does not conserve the sum of sensitivities or kinetic degrees of rate control equaling one because now rates depend not only on activities of chemical species and rate constants but also on time. We propose a modified definition where time-constants τ_j are kept constant when taking the partial derivatives of rate (eqs. (4.26)-(4.28)), which conserves the sums to unity (see Figure 4.4).

During a non(pseudo)steady-state transient, the reaction rate is a function that depends on the elementary step rate constants k_i and time t, such that $r = f(k_i, t)$. With the (pseudo-)steady-state definitions, the sensitivities and kinetic degrees of rate control do not sum to unity during a transient because there is another independent variable, $1/t$,

that has units of inverse time. Because the sensitivities of all independent variables with units of inverse time need to sum to unity, it is necessary to find a means of eliminating the dependence of the rate on time, t. This is achieved by transforming the rate function, $r = f(k_i, t)$, to a different function, $r = g(k_i, t_j')$, where the time dependence is transformed to dimensionless time quantities, t_j', such that the only independent variables for the transient rate with units of inverse time are the rate constants, k_i. If the rate can be transformed to a function $r = g(k_i, t_j')$, then the sums of the sensitivities of elementary steps and the kinetic degrees of rate control will again be constrained to unity.

In an effort to assess how to modify the definitions of sensitivity and degrees of rate control, we first identify why the sensitivity s_2 becomes negative during the transient. When applying the definition for sensitivity (eq. (4.3)), the derivative is a measure of the change in the rate with a perturbation to a rate constant at a particular time, as illustrated by eq. (4.24):

$$s_i = \frac{k_i}{r(t, k_i)} \frac{\left(r(t, k_i + \Delta k_i) - r(t, k_i)\right)}{\Delta k_i} \tag{4.24}$$

where Δk_i is a differential perturbation in the rate constant k_i. Perturbation of a rate constant, however, changes how quickly the reaction approaches steady-state, as illustrated in Figure 4.3a for an increase in k_2 from 1 to 2, though this same effect would be observed on a smaller scale for differential changes in k_2. Thus, at some times during the transient, increasing k_2 will decrease the rate, causing s_2 as calculated by eq. (4.3) to be negative at these times. We argue that a more appropriate comparison of perturbed and
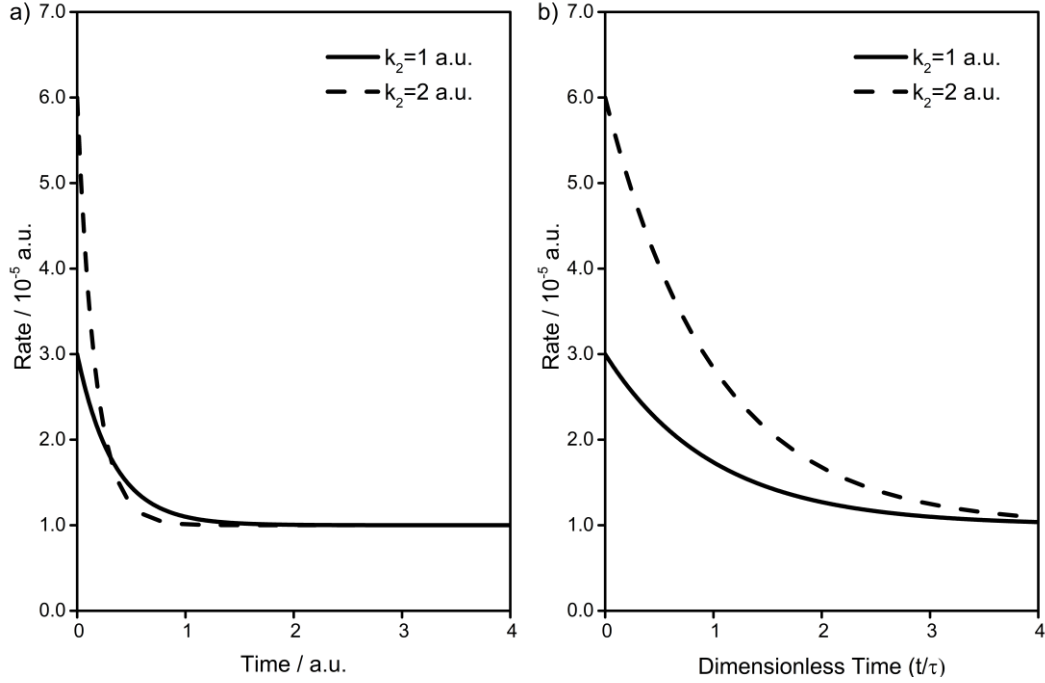
Figure 4.3: Comparison of transient rates with different values for k_2 after a step-change in a_B from 1 to 3 at $t = 0$. $k_{-1} = 0$, $k_1 = 10^{-5}$, $\theta_{A,0} = 10^{-5}$ for the reaction in Scheme 4.1. a) rate versus time (t) b) rate versus dimensionless time (t/τ).

unperturbed rates during a transient is on a dimensionless time scale, such that the sensitivity is given by (eq. (4.25)):

$$s_i = \frac{k_i}{r(t', k_i)} \frac{\left(r(t', k_i + \Delta k_i) - r(t', k_i)\right)}{\Delta k_i} \tag{4.25}$$

where $t' = t/\tau$ is the dimensionless time scale and τ is a function of rate constants. In general, the time-constant τ is the function of rate constants and activities that multiply t in the analytical rate function. Comparing transient rates with perturbed and unperturbed rate constants on a dimensionless time-scale resolves the issue of the perturbed rate approaching steady state faster or slower than the unperturbed rate. Writing eq. (4.25) in differential form, the definition for sensitivity becomes (eq. (4.26)):

130

$$s_i(t) = \left(\frac{\partial \ln r\,(t)}{\partial \ln k_i} \right)_{k_{j \neq i}, \tau_j} \tag{4.26}$$

where τ_j are the time constants of the transient rate, of which there can be more than one as will be illustrated in an example below. With the modified definition for transient sensitivities, we analogously define the kinetic and thermodynamic degrees of rate control during a transient at non(pseudo)steady-state conditions as (eqs. (4.27) and (4.28)):

$$X_{RC,i}(t) = \left(\frac{\partial \ln r\,(t)}{\partial \ln k_i} \right)_{k_{j \neq i}, K_i, \tau_j} = \left(\frac{\partial \ln r\,(t)}{\partial(-G^o_{TS,i}/RT)} \right)_{G^o_{j \neq TS,i}, \tau_j} \tag{4.27}$$

$$X_{TRC,i}(t) = \left(\frac{\partial \ln r\,(t)}{\partial(-G^o_i/RT)} \right)_{G^o_{j \neq i}, \tau_j} \tag{4.28}$$

The relations between sensitivities and the degrees of rate control shown in eqs. (4.4) and (4.5) still hold as shown in eqs. (4.29) and (4.30) (see Section A4.3 of the Appendix for a step-wise derivation):

$$
\begin{aligned}
X_{RC,i}(t) &= \left(\frac{\partial \ln r(t)}{\partial \ln k_i} \right)_{k_{j \neq i}, K_i, \tau_j} \\
&= \sum_n \left(\frac{\partial \ln r(t)}{\partial \ln k_n} \right)_{k_{j \neq n}, \tau_j} \left(\frac{\partial \ln k_n}{\partial \ln k_i} \right)_{k_{j \neq i}, K_i, \tau_j} \\
&\quad + \sum_n \left(\frac{\partial \ln r(t)}{\partial \ln \tau_n} \right)_{k_j, \tau_{j \neq i}} \left(\frac{\partial \ln \tau_n}{\partial \ln k_i} \right)_{k_{j \neq i}, K_i, \tau_j} \\
&= \left(\frac{\partial \ln r(t)}{\partial \ln k_i} \right)_{k_{j \neq i}, \tau_j} + \left(\frac{\partial \ln r(t)}{\partial \ln k_{-i}} \right)_{k_{j \neq -i}, \tau_j} = s_i(t) + s_{-i}(t)
\end{aligned}
\tag{4.29}
$$

131

$$X_{TRC,j}(t) = \left(\frac{\partial \ln r(t)}{\partial (-G_j^o/k_B T)} \right)_{G_{n \neq j}^o, \tau_n}$$

$$= \sum_i \left(\frac{\partial \ln r(t)}{\partial \ln k_i} \right)_{k_{n \neq i}, \tau_n} \left(\frac{\partial \ln k_i}{\partial (-G_j^o/k_B T)} \right)_{G_{n \neq j}^o, \tau_n} \tag{4.30}$$

$$+ \sum_i \left(\frac{\partial \ln r(t)}{\partial \ln \tau_i} \right)_{k_n, \tau_{n \neq i}} \left(\frac{\partial \ln \tau_i}{\partial (-G_j^o/k_B T)} \right)_{G_{n \neq j}^o, \tau_n} = \sum_i \nu_{ij} s_i(t) [\nu_{ij} < 0]$$

The transient rate function for the reaction depicted in Scheme 4.1 (eq. (4.23)) can be rewritten as eq. (4.31):

$$r(t)/L = k_1 a_A \left(1 - e^{-t/\tau} \right) + k_2 a_B \theta_{A,0} e^{-t/\tau} \tag{4.31}$$

where $\tau = (k_2 a_B)^{-1}$ is identified as the time-constant for the reaction. Perturbation of a rate constant in eq. (4.31) now does not change how quickly the reaction approaches steady state on a dimensionless time scale t/τ, as shown in Figure 4.3b. Applying eq. (4.26) to the transient rate given by eq. (4.31) gives the sensitivities (and kinetic degrees of rate control) shown in eqs. (4.32) and (4.33):

$$X_{RC,1} = s_1 + s_{-1} = s_1 = \left(\frac{\partial \ln r}{\partial \ln k_1} \right)_{k_2, \tau} = \frac{k_1}{r} \left(\frac{\partial r}{\partial k_1} \right)_{k_2, \tau}$$

$$= \frac{k_1 a_A \left(1 - e^{-t/\tau} \right)}{k_1 a_A (1 - e^{-t/\tau}) + k_2 a_B \theta_{A,0} e^{-t/\tau}} \tag{4.32}$$

$$X_{RC,2} = s_2 + s_{-2} = s_2 = \left(\frac{\partial \ln r}{\partial \ln k_2} \right)_{k_1, \tau} = \frac{k_2}{r} \left(\frac{\partial r}{\partial k_2} \right)_{k_1, \tau}$$

$$= \frac{k_2 a_B \theta_{A,0} e^{-t/\tau}}{k_1 a_A (1 - e^{-t/\tau}) + k_2 a_B \theta_{A,0} e^{-t/\tau}} \tag{4.33}$$

Notice that that as $t \to \infty, X_{RC,1} \to 1$ and $X_{RC,2} \to 0$, converging to the steady-state solutions for the degrees of rate control. The degrees of rate control are reported as a function of time in Figure 4.4. With the new definition for sensitivity, s_2 is never less than zero for this reaction system and the sum of the sensitivities of the elementary steps equals unity at all t.

In the example above, we considered the limiting case where $k_{-1} = 0$ and $k_2 \gg k_1$ for the reaction network presented in Scheme 4.1. We show the transient kinetic and thermodynamic degrees of rate control for the reaction in Scheme 4.1 where the first step is reversible in Figure 4.5, with $k_1 = k_{-1} = k_2 = 1 \, a.u.$ and $a_A = 1$, $a_B(t < 0) = 3$, $a_B(t \geq 0) = 1$. At the time of the step-change, only transition state 2 and A^* have nonzero degrees of rate control for transition states and surface species, respectively. This is in agreement with only k_2 appearing in the rate equation at the time of the perturbation (eq. (4.22)), which depends only on the energies of A^*, B, and the transition state for step 2.

At steady-state, the reversibility of a step, $Z_i = \prod_j a_j^{\nu_{ij}} / K_i$, is related to the sensitivities by $Z_i = -s_{-i}/s_i$.[19,23,60] This relationship is used in De Donder relations for identifying the rate-controlling transition states during (pseudo-)steady-state reaction. The reversibility of Reaction 1, $Z_1(t)$, and $-s_{-1}(t)/s_1(t)$ during the transient are shown in Figure 4.6, where it is clear that $Z_i(t) \neq -s_{-i}(t)/s_i(t)$, suggesting that reversibilities of elementary steps during a transient do not provide information about rate-controlling transition states during non(pseudo)steady-state conditions.
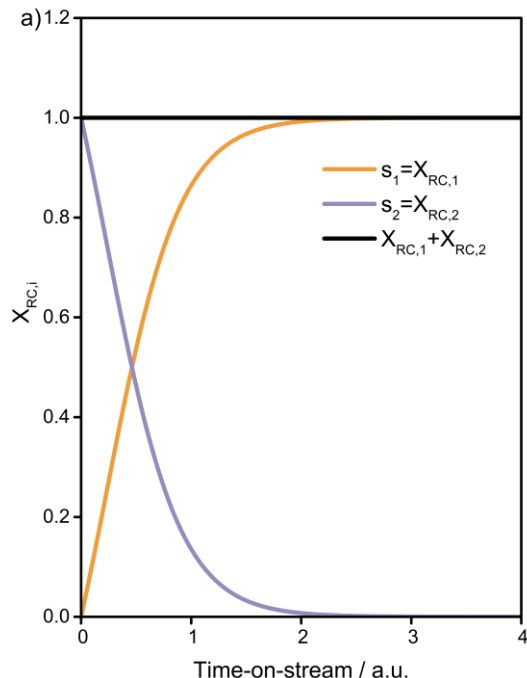
Figure 4.4: Transient sensitivities (and kinetic degrees of rate control) for the reaction in Scheme 4.1 calculated by applying eq. (4.26) to eq. (4.31). $k_1 = 10^{-5}$ au, $k_{-1} = 0$ au, $k_2 = 1$ au, $a_A = 1$, $a_B(t < 0) = 1$, $a_B(t \geq 0) = 3$.

In this second case study, we discussed how to assess sensitivities and degrees of rate control for a non(pseudo)steady-state transient for a reaction scheme where there is only one time constant, τ, that appears in the transient rate function. In what follows, we demonstrate that the same methods can be applied to reactions with multiple time constants by considering the non-pseudo-steady transient rate for a sequence of four irreversible catalytic reactions.

Case Study 3: Calculating degrees of rate control during non(pseudo)steady-state transients at differential conversion for systems with a multiple time constants, τ_j

Consider the overall reaction consisting of the sequence of four irreversible elementary reactions shown in Scheme 4.2. The fractional coverages as a function of time

134
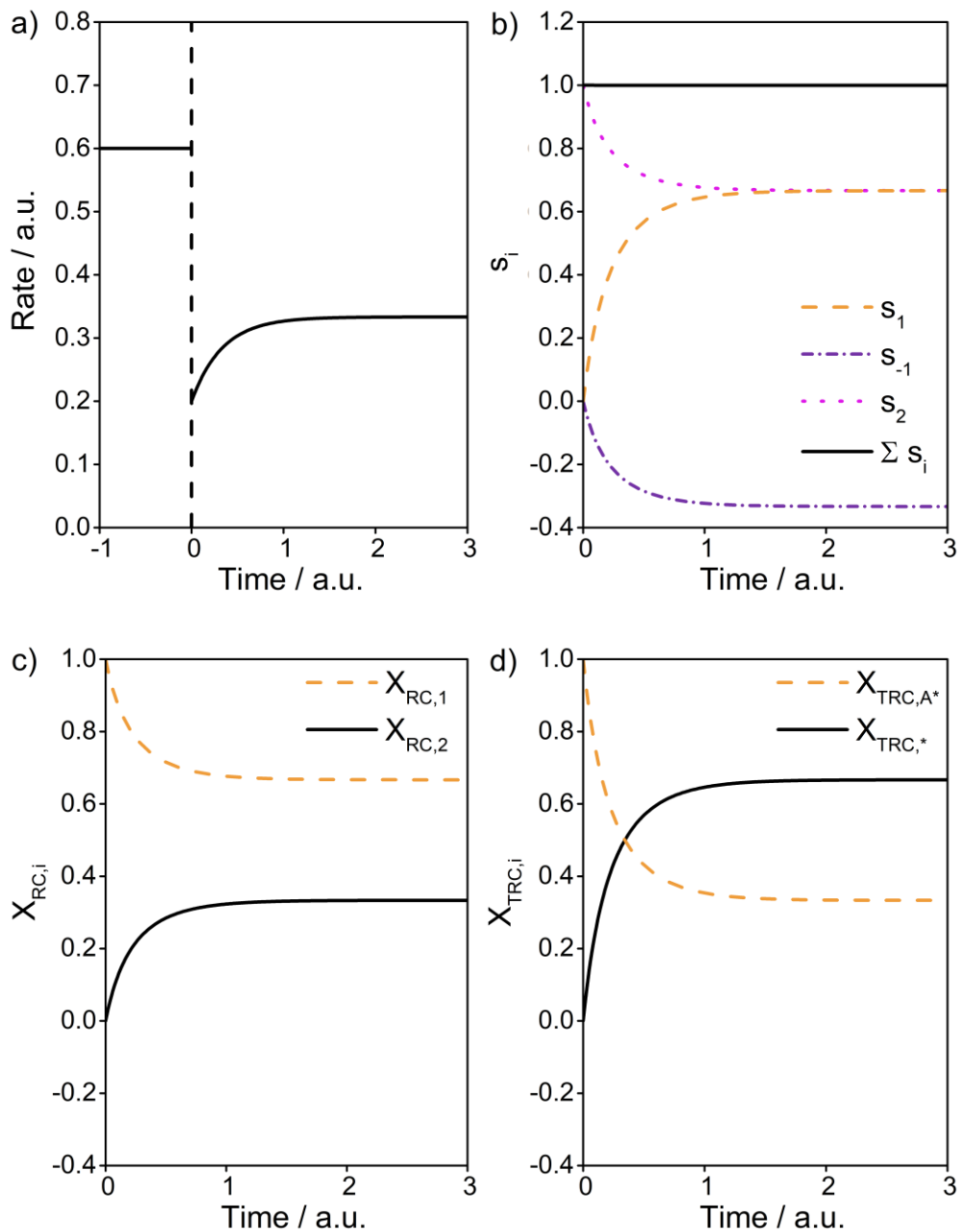
Figure 4.5: Analysis of the transient rate using degrees of rate control for the composite reaction in Scheme 4.1 with $k_1=k_{-1}=k_2=1$ au and $a_A = 1$ and $a_B = 3$. at $t < 0$ and $a_B = 1$ for $t \geq 0$ a) Transient rate. b) Transient sensitivities. c) Transient kinetic degrees of rate control. d) Transient thermodynamic degrees of rate control of surface species.
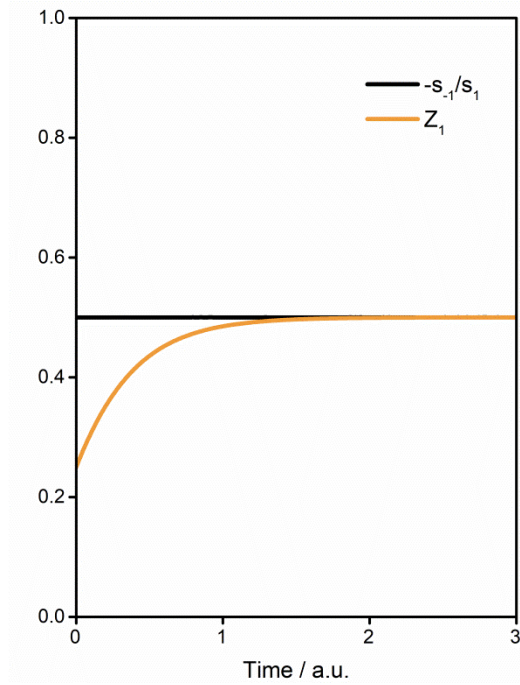
Figure 4.6: Reversibility of step 1 in Scheme 4.1 and $-s_{-1}/s_1$ during the transient with $k_1=k_{-1}=k_2=1$ au and $a_A = 1$ and $a_B = 3$. at t<0 and $a_B = 1$ at t≥0.

for the surface species in Scheme 4.2 are described by a system of differential equations (eq. (4.34)):

$$\frac{d\boldsymbol{\theta}}{dt} = \boldsymbol{A\theta} + \boldsymbol{b}, \qquad \boldsymbol{\theta}(t = 0) = \boldsymbol{\theta_0} \tag{4.34}$$

where $\boldsymbol{\theta}$ is a vector of fractional coverages, $\boldsymbol{\theta_0}$ is a vector of the fractional coverages at the time of a step-change, $\boldsymbol{A}$ is a matrix of rate constants and stoichiometric coefficients, and $\boldsymbol{b}$ is a vector containing rate constants and stoichiometric coefficients. The solution to this system of differential equations is of the form (eq. (4.35)):

$$\boldsymbol{\theta} = \boldsymbol{\theta_p} + \sum_i c_i \boldsymbol{v}_i e^{\lambda_i t} \tag{4.35}$$

136

where $\boldsymbol{\theta_p}$ is the particular solution to the inhomogeneous differential equation, $\boldsymbol{v_i}$ are eigenvectors of matrix $\boldsymbol{A}$, λ_i are eigenvalues of matrix $\boldsymbol{A}$, and c_i are constants of integration whose values are found by substitution of the initial condition into eq. (4.35). For the reaction in Scheme 4.2, the rate is given by eq. (4.36):

$$r(t)/L = k_4 a_F \theta_C(t) = k_4 a_F \left(\theta_{p,C} + \sum_i c_i v_{i,C} e^{\lambda_i t} \right) \tag{4.36}$$

where $\theta_C(t)$ is the fractional coverage of C as a function of time, $\theta_{p,C}$ and $v_{i,C}$ are the elements of the particular solution and the eigenvectors corresponding to the fractional coverage of C from the solution in eq. (4.35). The eigenvalues, eigenvectors, and constants of integration for the reaction in Scheme 4.2 were calculated in Matlab (see Section A4.4 in the Appendix) for the transient induced by step-changing the activity of species D while at steady-state conversion. The transient reaction rate of P formation is shown in Figure 4.7a after increasing the activity of D at time $t = 0$ au from 1 to 3. The fractional surface coverage for each of these intermediates is shown in Figure 4.7b as a function of time. The kinetic degrees of rate control are calculated by applying eq. (4.26) to eq. (4.36) and recognizing that because time is always multiplied by an eigenvalue in this system, these eigenvalues are equal to inverse the time constants ($\lambda_j = 1/\tau_j$) that need to be kept constant when calculating the transient kinetic degrees of rate control (eq. (4.37)):

$$X_{RC,i}(t) = \frac{k_i}{k_4 P_F\left(\theta_{p,C} + \sum_j c_i \nu_{i,C} e^{t/\tau_j}\right)} \left(\frac{\partial}{\partial k_i} k_4 P_F\left(\theta_{p,C}\right.\right.$$

$$\left.\left.\left. + \sum_j c_i \nu_{i,C} e^{t/\tau_j}\right)\right)\right|_{k_{j\neq i}, K_i, \tau_j}$$

(4.37)

The kinetic degrees of rate control during the transient were calculated using Matlab (see code in Section A4.4 of the Appendix).

Scheme 4.2: Hypothetical reaction network for case study 2 with four irreversible Eley-Rideal elementary surface reactions in series to produce product P.

$$Rxn\ 1: A + * \rightarrow A^* \qquad\qquad k_1$$

$$Rxn\ 2: A^* + D \rightarrow B^* \qquad\qquad k_2$$

$$Rxn\ 3: B^* + E \rightarrow C^* \qquad\qquad k_3$$

$$Rxn\ 4: C^* + F \rightarrow P + * \qquad\qquad k_4$$

Overall: $A + D + E + F \rightarrow P$
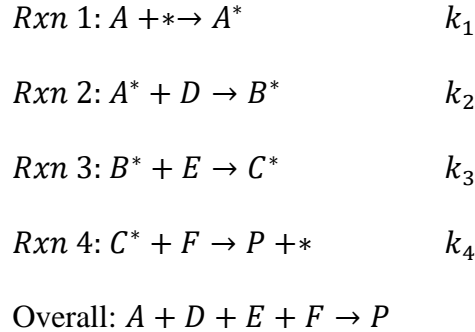
The degrees of rate control for the reaction network in Scheme 4.2 shown as a function of time in Figure 4.7c can be used to rationalize the observed transients after the step-change in the activity of D. The time at which the maximum rate is achieved during the transient when a_D is increased from 1 to 3 coincides with the time the elementary step involving the reactant D is rate-controlling (t ~ 6 au). These times coincide because the second step in the reaction sequence is first order in the step-changed reactant, D. This same phenomena is observed no matter which reactant is step-changed (see Section A4.5 in the Appendix for transient rate and degrees of rate control for other step-changed reactants). The rate through the step-change is also continuous at $t = 0$, in contrast to the
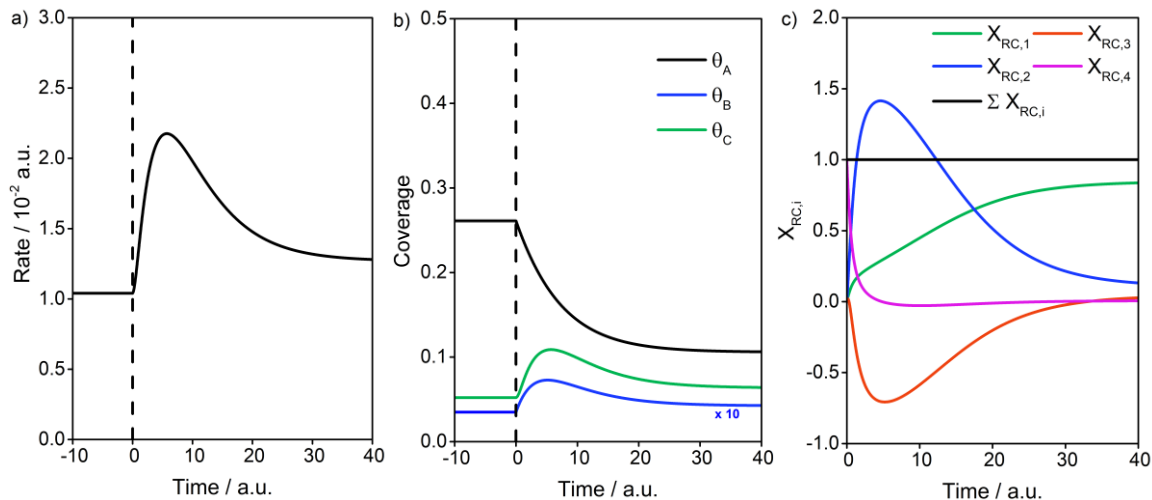
Figure 4.7: Analysis of the transient rate using degrees of rate control for the composite reaction in Scheme 4.2. $k_1 = 0.02$, $k_2 = 0.04$, $k_3 = 0.3$, $k_4 = 2$, $a_{A0} = a_{D0} = a_{E0} = a_{F0} = 1$. At time t = 0 au the activity of D is increased from $a_D = 1$ to $a_D = 3$ au a) Initial and transients rates through the step-change in the activity of D. b) Surface coverages before and after the step-change. c) Kinetic degrees of rate control after the step-change.

discontinuities observed when step-changing a_B for the reaction in Scheme 4.1. This is reflected in the sensitivities where $s_2 = 0$ at $t = 0$, and thus the reaction is zero-order in the step-changed reactant, D, at the time of the perturbation. At all times during the transient, the kinetic degrees of rate control sum to unity. This is always true and a proof is provided in Section A4.6 of the Appendix. During the transient, there is a step with a negative kinetic degree of rate control, in contrast to the transient degrees of rate control for Case 2 depicted in Figure 4.4. In Case 2, the transient rate was a sum of the contribution of the initial rate and the steady-state rate. In catalytic systems with more than two steps in series, there are additional terms that arise in the analytical transient rate functions, causing some steps to have negative contributions to the transient rate. Steps with negative kinetic degrees of rate control are referred to as "inhibition steps" because lowering the energy of their transition states leads to a decrease in the overall observed reaction rate.[56] It may seem counterintuitive that a network of irreversible reactions in

139

series can have inhibition steps, however, this can occur when the pseudo-steady-state approximation is invalid. This is demonstrated by example for a network of two irreversible fluid-phase reactions in series in Section A4.7 of the Appendix.

In experiments where transients are observed, we can now use the concept of rate-limiting steps during transients to acquire information that would otherwise be inaccessible by steady-state rate measurements alone. For example, consider the case where the overall reaction presented in Scheme 4.2 is known, but not the elementary steps that comprise the reaction network. During an experiment, when the activity of D is step-changed, the transient rate shown in Figure 4.7a is observed. Through the concept of rate-limiting steps during a transient, we can acquire new information about the reaction mechanism from this experiment. First, at the time of the step-change, we know that the only rate-limiting steps are those that form or consume the final product, P. From Figure 4.7a, we observe that the rate is zero-order in the activity of D at the time of the step-change, indicating that D is not involved in the elementary steps that form or consume the final product. Second, at the time of the maxima, we know that a step whose rate depends on the activity of D has a non-zero sensitivity. Because D is a reactant, the elementary step is likely positive order in D. The transient rate is also positive order in D (the rate reaches a maximum as opposed to a minimum), and thus we conclude that this unknown step has a positive sensitivity and is rate-limiting at the time of the maximum rate. Finally, the steady-state rate is nearly zero-order in D, suggesting that the step that is rate-limiting at the time of the maximum is different than the rate-limiting step(s) at steady-state at this reaction condition.

4.4 Conclusion

We introduce the concept of rate-controlling transition states and species during non(pseudo)steady-state reaction conditions by adapting the degree-of-rate-control formulae to quantify the rate-control of transition states and stable species during these transients. This modification involves reformulating the rate function so as to eliminate rate constants that multiply time, t, by identifying these factors as time constants, τ_j. The degree-of-rate-control formulae for non(pseudo)steady-state transients keep constant these τ_j when taking the partial derivative of the rate with respect to the rate constants or free energies. The utility of transient degrees of rate control for rationalizing features of the non(pseudo)steady-state rate is demonstrated in two case studies.

Chapter 5

Transient and steady-state kinetic study of formaldehyde alkylation of benzene to form diphenylmethane on HZSM-5 catalysts

5.1 Conspectus

A combined steady-state and transient kinetic study on the mechanism of diphenylmethane (DPM) formation in HZSM-5 from HCHO and benzene revealed two kinetically-relevant steps—the alkylation of benzene by HCHO and the deprotonation of a diphenylmethane benzenium ion (DPM^+) to form DPM. The functional dependence of the rate of each of these reactions was determined by observing the transient rate after a step-change in reactant partial pressures, specifically whether the rate was discontinuous through a step-change in partial pressure. Steady-state isotopic switching experiments revealed that a persistent surface intermediate with two aromatic rings, likely DPM+, is formed, and has a fractional coverage ranging from sparse (near zero) to complete (near one) that varies with process conditions. Reaction orders obtained from steady-state rate measurements suggest that HCHO, C_6H_6, and H_2O competitively adsorb on acid sites and that DPM^+ deprotonation is first-order in C_6H_6, suggesting that deprotonation is assisted by the presence of aromatics. Herein, we propose a complete mechanism for the condensation between HCHO and C_6H_6 to form DPM and from this mechanism a six parameter (three kinetic/thermodynamic parameters, three apparent activation/thermodynamic energies) kinetic model is derived that quantitatively describes the transient and steady-state rates and steady-state fractional coverages of DPM^+.

5.2 Introduction

Formaldehyde, formed by hydrogen transfer from methanol, is implicated as being potent in mediating the transformation of active hydrocarbon pool species (olefins and aromatics) to inactive polycyclic hydrocarbons during methanol-to-hydrocarbons (MTH) catalysis on microporous solid acid zeolite/zeotype catalysts.[66–69] Formaldehyde reacts with unsaturated hydrocarbons via sequential alkylation and dehydration reactions C_nH_x + $HCHO \rightarrow C_{n+1}H_x$ + H_2O, resulting in the addition of one degree of unsaturation to hydrocarbon pool chain carriers which shifts product selectivity and induces catalyst deactivation in microporous zeolite/zeotype materials.[66,70,71] Formaldehyde can react with any unsaturated hydrocarbon species during methanol-to-hydrocarbons catalysis, including olefins, dienes, and aromatics. Investigation of the mechanism and kinetics of each of these reactions is important for determining the relative contribution of each pathway to the consumption of HCHO and for elucidating deactivation mechanisms during MTH catalysis. Herein, we investigate the kinetics and mechanism of the reaction between HCHO and benzene to form diphenylmethane ($C_{13}H_{12}$) on the MTH catalyst HZSM-5.

Martinez-Espin et al.[72] proposed that diphenylmethane (DPM) is a product of the HCHO condensation with benzene (C_6H_6) during MTH catalysis on HZSM-5 at temperatures in the range 523-623 K. During co-reaction of C_6H_6 with CH_3OH, a kinetic isotope effect for DPM formation was observed when using CD_3OH as the reactant, suggesting C-D bond cleavage was the rate-determining step for DPM formation. These claims were corroborated by the authors by noting that the molecular weight of the DPM

product increased by two atomic mass units when using CD_3OH as the reactant instead of CH_3OH and by density functional theory (DFT) calculations which showed that a viable DPM formation pathway involves HCHO alkylation of benzene to form a benzyl alcohol intermediate followed by condensation with benzene to form DPM and water.[72] These observations led the authors to propose the reaction mechanism depicted in Scheme 5.1, where hydrogen abstraction from methanol to form formaldehyde is the rate-limiting step, followed by reaction with two benzene molecules and dehydration to form water and DPM. The work by Martinez-Espin et al.[72] determined that the rate-determining step for DPM formation was methanol dehydrogenation. We investigate here instead the kinetics and mechanism of the DPM formation reaction sequence after the genesis of the HCHO species. Prior reports that investigate HCHO-mediated alkylation rates and pathways identify DPM as the highest selectivity product in the reaction between HCHO and C_6H_6 on zeolite catalysts (HY and HZSM-5) during liquid-phase batch reactions.[73,74] Climent et al.[74] proposed a DPM formation mechanism on HY that is similar to the mechanism proposed by Martinez-Espin et al.[72] for HZSM-5, with the exception that benzyl alcohol dehydrates to form a phenylmethelium ion ($C_7H_7^+$) before reaction with C_6H_6 to form DPM^+ (dotted lines in Scheme 5.1). We report here the kinetics and mechanism of DPM at low partial pressures of HCHO (< 0.5 kPa) and C_6H_6 (< 5 kPa) during gas-phase reaction.

Specifically, we investigate the kinetics and mechanism of DPM formation from HCHO and C_6H_6 on self-pillared pentasil (SPP) HZSM-5 catalysts, a material with ~ 1.5 unit cell sheets of HZSM-5 chosen here to avoid complications due to diffusive transport.[75] We observe transients during reaction, which were not reported in previous

144

Scheme 5.1: Mechanism of DPM formation proposed by Martinez-Espin et al.[72] where the rate-limiting step (RLS) is CH_3OH dehrogenation. Climent et al.[74] proposed a pathway from HCHO and C_6H_6 involving a phenylmethelium ion intermediate (dashed lines).
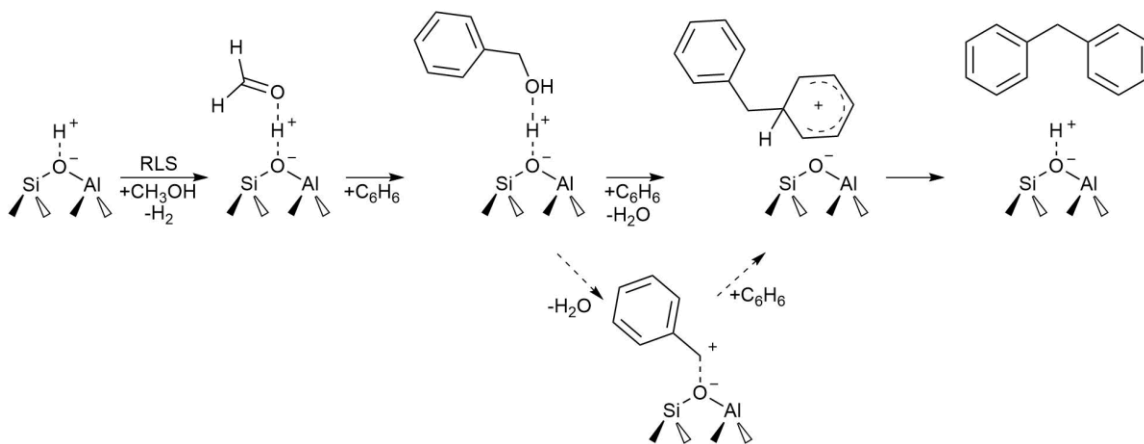
studies, and we demonstrate that these transients are the result of slowly evolving fractional coverage of DPM^+ during reaction. Further, we show that DPM^+ is a persistent species that is formed and consumed by irreversible reactions in series, either of which can be rate-controlling depending on the reaction conditions. The deprotonation of DPM^+ is facilitated by aromatic species, such that the proton-transfer from DPM^+ back to the zeolite is first-order in aromatics partial pressure via an adsorption-assisted desorption-like reaction.[76]

5.3 Methods

5.3.1 Catalyst Synthesis

Self-pillared pentasil (SPP) HZSM-5 was chosen for this study because of its ~3 nm diffusion length scales to reduce potential complications arising from transport limitations.[75,77] SPP-HZSM-5 was synthesized following a similar procedure reported previously,[75,77] with Si/Al ratio of 100 during synthesis. After synthesis, the zeolite was

dried at 343 K for 12 h, followed by oxidative thermal treatment at 823 K for 12 h in air. The zeolite was then washed with distilled water and thrice ion-exchanged with 1.0 mol L^{-1} ammonia nitrate solution at 353 K for 5 h, washed with water, dried at 343 K, and thermally treated in air at 823 K for 4 h to produce proton-form SPP-HZSM-5, assessed by amine titration and temperature-programmed desorption (see Section 5.3.2).

5.3.2 Ammonia and 2,6-di-tert-butylpyridine temperature-programmed desorption (TPD)

A gas stream containing 0.14 cm^3 s^{-1} NH$_3$ (Praxair, 1% in He) diluted in 1.42 cm^3 s^{-1} He and 0.167 cm^3 s^{-1} Ar (internal standard) was fed to a fixed bed of 0.093 g of SPP-HZSM-5 heated to 423 K until two hours after the NH$_3$ concentration in the reactor effluent was the same as the reactor influent. Adsorbing NH$_3$ at 423 K titrates only the Brønsted-acidic sites in the framework and will not adsorb to Lewis-acidic aluminum in the zeolite channels.[78,79] An online mass-spectrometer (MKS Instruments) was used to monitor the concentration of NH$_3$ (m/z = 16) and Ar (m/z = 40) in the reactor effluent. The reactor bed was flushed at 423 K with 1.56 cm^3 s^{-1} He and 0.167 cm^3 s^{-1} Ar for at least four hours to remove any physisorbed NH$_3$ before heating at 0.167 K s^{-1} to 723 K. The temperature was held at 723 K until the NH$_3$ concentration in the effluent reached zero. The amount of NH$_3$ that desorbed during the temperature ramp is considered to be stoichiometric with the number of Brønsted acid sites on the SPP-HZSM-5 catalyst. All gas flow rates in this study are at 298 K and atmospheric pressure.

A similar protocol was followed for the 2,6-di-*tert*-butylpyridine (DTBP) TPD experiments. A solution containing 0.048 g of DTBP ($\geq$ 97%, Sigma-Aldrich) was added

to 13.2 g of C_6H_6. The C_6H_6-DTBP solution was injected into a 1.12 cm^3 s^{-1} He and 0.073 cm^3 s^{-1} Ar (internal standard) stream via a syringe pump (KD Scientific) at a liquid flow rate of 3.5×10^{-4} cm^3 s^{-1}. The stream was fed to a fixed-bed reactor with 0.017 g SPP-HZSM-5 heated to 353 K for one hour after the concentration of DTBP in the effluent was the same as the DTBP concentration in the influent. The reactor effluent was monitored by injection into a gas-chromatograph (GC) equipped with a flame-ionization detector (FID) and a thermal conductivity detector (TCD). After adsorption, the reactor bed was flushed at 353 K with He (1.12 cm^3 s^{-1}) and Ar (0.073 cm^3 s^{-1}) for two hours. The reactor was then heated at 0.33 K s^{-1} to 873 K in He (1.12 cm^3 s^{-1}) and Ar (0.073 cm^3 s^{-1}) and the reactor effluent was monitored by GC-FID/TCD at one-minute intervals. The reactor temperature was held at 873 K until DTBP was no longer observed in the reactor effluent. The total moles of DTBP that desorbed during the temperature ramp was considered to be stoichiometric with the number of external Brønsted-acid sites because the bulky *tert*-butyl groups impede the diffusion of DTBP into the microporous channels of the SPP-HZSM-5 zeolite.[75,80]

5.3.3 Transient and steady-state diphenylmethane rate measurements

A solution of HCHO and H_2O was prepared by adding H_2O (Fisher Chemical, HPLC grade submicron filtered) to a HCHO/H_2O solution (Thermo Scientific, 16% w/v HCHO in H_2O, methanol-free) in ratios dependent on the reaction conditions. The HCHO/H_2O solution, additional H_2O feed, and C_6H_6 (Sigma Aldrich, ACS reagent, $\geq$ 99.0%) were injected via syringe pumps (KD Scientific, Cole-Parmer) into a stream of 2.07 cm^3 s^{-1} He, 0.073 cm^3 s^{-1} Ar (internal standard) via heated liquid injection ports. The temperature of

the injection ports varied with liquid flow rate and reactant to achieve stable flows. A 1000 cm^3 mixing volume located downstream of the liquid-injection ports was used to stabilize the concentrations of the reactor feed. The reactant stream was carried to and from one of two identical reactors via stainless steel lines heated to at least 353 K. The packed-bed reactor is an annulus (0.4 cm o.d.; 0.16 cm i.d.) with a thermowell containing a K-type thermocouple that measures the temperature at the radial and axial center of the packed bed. The outer wall of the annulus is borosilicate glass-lined stainless steel (SGE Analytical Science) and the inner wall is stainless steel. The reactor bed is heated externally by a resistive heating element (ARi Industries Inc.) controlled by a Watlow temperature controller. Reactant stream pressures are monitored by a pressure-transducer upstream of the reactor. Gas flows are controlled by mass-flow controllers (Brooks).

The SPP-HZSM-5 samples were crushed using a mortar and pestle and pressed to a pressure of 4000 psi, crushed again and sieved between mesh 40 and 80 to obtain catalyst pellets of size 180 to 420 microns. SPP-HZSM-5 catalyst particles (0.0109-0.0122 g) were physically mixed with quartz sand (~0.1 g, acid washed with 2 M HNO_3; rinsed with deionized water; heated to 1273 K in flowing air for 12 h) and loaded into a reactor. Quartz wool was loaded before and after the reactor bed to keep it in place. Diphenylmethane formation rates were measured from 353-393 K at differential conversion ($\leq 3.4\%$ conversion HCHO, $\leq 1\%$ C_6H_6) conditions. A discussion on heat and mass transport limitations can be found in Section A5.1 of the Appendix.

Diphenylmethane was the major product (typically > 99 mol% selectivity, at minimum 82 mol% selectivity) under all reaction conditions studied. The reactor effluent was monitored by an on-line Agilent 7890A gas chromatograph (GC) equipped with a

flame ionization detector (FID) and a thermal conductivity detector (TCD). Hydrocarbon species (HCHO, C_6H_6, DPM, etc.) were separated on an Agilent HP-1 column (50 m × 0.320 mm) and quantified in the FID. Non-hydrocarbon species (H_2O, Ar) were separated in a HP-Plot-Q (60 m × 0.320 mm) column and quantified in the TCD. The signal peaks in the FID and TCD chromatograms of the reactor effluent were assigned by comparison to chromatograms of known compounds injected into the GC, in addition to taking 10 cm^3 gaseous samples from the reactor effluent via a gas-tight syringe and injecting this sample into a GC-MS to obtain the mass spectra of the various products.

The catalyst bed was regenerated between successive experiments by oxidative thermal treatments by flowing 1.67 cm^3 s^{-1} zero grade air through the catalyst bed beginning at the reaction temperature and heating at 0.0167 K s^{-1} to 823 K and holding for 6 hours. The rate per mass of SPP-HZSM-5 degrades over repeated regenerations. This loss of activity is attributed to dealumination and collapse of the framework during thermal treatment, leading to the degradation of the catalyst and loss of active sites. To account for this loss of sites, a reference condition (0.010 kPa HCHO, 4 kPa H2O, 0.44 kPa C_6H_6, 393 K) was repeated regularly to determine the fractional activity remaining. The decrease in rate per mass catalyst was assumed to degrade linearly between reference tests. The change in rate per mass catalyst over time for each reactor bed is shown in Figure A5.3 of Section A5.2 in the Appendix. Typically, only one steady-state rate per reactor bed was measured per day. Sometimes more than one steady-state rate was obtained per experiment by changing the reactant pressures after acquiring a previous steady-state data point. During these experiments, the first reaction condition was

repeated at the end of the day to ensure the catalyst deactivated by less than 15% between the first and last steady-state rate measurements.

5.3.4 Steady state isotopic transient kinetic analysis (SSITKA)

SSITKA was used to determine the identity and fractional coverage of surface intermediates during steady-state reaction. During reaction, $^{12}C_6H_6$ and $^{13}C_6H_6$ ($\geq$ 99% ^{13}C, Sigma-Aldrich) were fed in parallel via syringe pumps into heated He carrier streams to opposite inlets of a Valco four-way valve (located downstream of mixing volumes varying in size from 100 cm^3 to 1000 cm^3) that selected which among the ^{12}C- or ^{13}C-labeled stream was fed to the reactor. After the four-way valve, the C_6H_6 stream sent to the reactor combined with the stream carrying HCHO, H_2O, 2.07 cm^3 s^{-1} He and 0.073 cm^3 s^{-1} Ar and this mixed gas stream was fed to the reactor. Initially $^{12}C_6H_6$ is fed to the reactor with HCHO and H_2O until the DPM formation rate was invariant in time for ~ 45 minutes (three consecutive GC injections), i.e. steady-state, as monitored by GC (Agilent 7890A) equipped with an HP-1 column connected to an Agilent 5975c mass spectrometer (MS). After the reaction was at steady-state, the four-way valve was flipped to feed $^{13}C_6H_6$ to the reactor and vent $^{12}C_6H_6$. The isotopologue distribution and reaction rate were monitored by GC-MS until the product isotopologue distribution reached steady-state. SSITKA was performed at two reaction conditions: 393 K, 0.02 kPa HCHO, 4 kPa H_2O, 0.4 kPa C_6H_6 and 393 K, 0.2 kPa HCHO, 2 kPa H_2O, 0.4 kPa C_6H_6.

5.3 Results and Discussion

5.3.1 Amine titration of acid sites

The density of internal and external acid sites on the SPP-HZSM-5 catalyst were assessed by NH_3 and 2,6-di-*tert*-butylpyridine (DTBP) temperature-programmed desorption (TPD). Ammonia adsorbs onto both internal and external Brønsted-acid sites, while the bulky *tert*-butyl groups on DTBP prevents the diffusion of DTBP into the micropores of the zeolite channels, and thus only titrates external Brønsted-acid sites.[75,80] The amount of adsorbed titrant for each amine is reported in Table 5.1. The amine desorption profiles are shown in Figure A5.3 in Section A5.3 of the Appendix. The small effective crystallite size of SPP-HZSM-5 results in a greater fraction of acid sites on the external surface of the catalyst compared to typical HZSM-5 catalyts.[75] For the material used in this study, ~40% of acid sites are on the external surface, in line with previous reports.[75] The DPM rate per acid site was slightly higher for internal + external acid sites than internal sites only, suggesting that external acid sites are more active than internal sites for DPM formation, as reported in Figure A5.4 in Section A5.4 of the Appendix. This effect may be a result of lower deprotonation energies or lower effective dielectric constants at the external surface compared to the internal sites or other electrostatic interactions that arise as a result of confining voids.[81,82]

Table 5.1: Moles of amine titrant adsorbed on SPP-HZSM-5

Amine Titrant	Moles Adsorbed / $\mu mol\ g^{-1}$
NH_3	141.2
DTBP	56.6

5.3.2 Transient Step-Change Measurements

Transients in the rate of diphenylmethane formation lasting several hours are observed during the reaction between HCHO and C_6H_6 on HZSM-5 when starting the reaction with fresh catalyst or when a reaction condition is changed. The transients observed when starting from a fresh catalyst (at time t = 0) and after step-changing the pressure of HCHO, H_2O, and C_6H_6 are depicted in Figure 5.1. When the partial pressure of HCHO or H_2O is step-changed (Figure 5.1a and 5.1b), the rate appears to change monotonically and continuously to a new steady-state value. In contrast, the rate appears to change discontinuously when the partial pressure of C_6H_6 is step-changed (Figure 5.1c). In these experiments, rate is not measured continuously and thus it is not possible to definitively determine whether the rate is continuous or discontinuous when each reactant pressure is step-changed, however it is clear that there are two important time-scales for the transient observed when step-changing C_6H_6 partial pressure—the time scale for partial pressure changes (within one GC injection, < 12 minutes) and the time-scale for reaching steady state (1-3 hours). Comparison of the transients strongly suggests that the rate is nearly discontinuous when changing the partial pressure of C_6H_6. The validity of this hypothesis is evaluated in Section 5.3.4.

Transients are ubiquitous in catalysis and provide essential information about the underlying reaction mechanism. These disparate time-scales in the transients observed during step-changes in partial pressures can be leveraged to elucidate the partial pressure dependencies of various steps in the DPM reaction mechanism as we discuss below. The
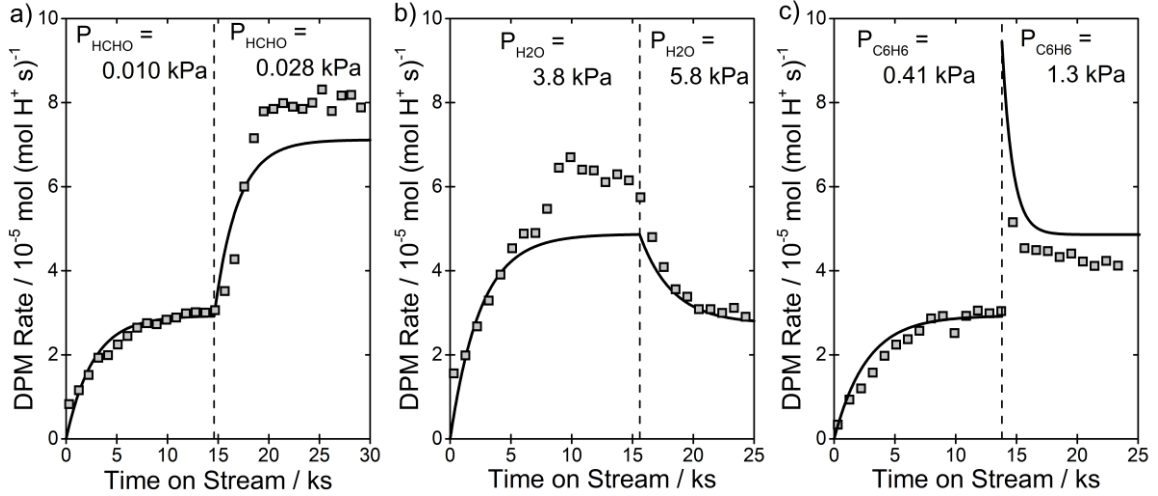
Figure 5.1: Transients observed starting from fresh catalyst (t = 0) and after step-changes in the partial pressure of a reactant (dashed line). Solid lines are predicted rates based on a model with two irreversible reactions in series using parameters estimated from steady-state rate measurements. a) Step-change in HCHO pressure from 0.010 to 0.028 kPa with T = 393 K, 0.41 kPa C_6H_6, 3.7 kPa H_2O, b) step-change in H_2O pressure from 3.8 to 5.8 kPa with T = 393 K, 0.41 kPa C_6H_6, 0.019 kPa HCHO, c) step-change in C_6H_6 pressure from 0.41 to 1.3 kPa with T = 393 K, 0.010 kPa HCHO, and 3.7 kPa H_2O.

observed rate of DPM formation is a sum of the rates of all elementary step reactions multiplied by the stoichiometric coefficient of DPM (eq. (5.1)):

$$r_{DPM}(t)/L = \sum_i v_{i,DPM} r_i(t)$$

$$= \sum_i v_{i,DPM} k_i \prod_{j^*} \left(\theta_{j^*}(t)\right)^{\alpha_{i,j^*}} \prod_j \left(P_j(t)\right)^{\alpha_{i,j}}$$

(5.1)

where L is the number of active sites, $v_{i,DPM}$ is the stoichiometric coefficient for DPM in reaction i, θ_{j^*} is the fractional coverage of surface intermediate j^*, P_j are the partial pressures for reactants j, and α_{i,j^*} and $\alpha_{i,j}$ are the reaction orders of surface intermediates j^* and reactants j for reaction i, respectively. In eq. (5.1), it is assumed that the number of active sites, rate constants, stoichiometric coefficients, and reaction orders are invariant in

153

time. The partial pressures only change at the start of the reaction and at the time of step-changes in partial pressures. In eq. (5.1), the partial pressures change on time-scales on the order of minutes while the fractional coverages of surface species change in time with time-scales that are dictated by the reaction kinetics and can be on the order of seconds to days. From eq. (5.1), if there is a transient in the formation rate of a product over several hours, this necessarily requires that the fractional coverages of surface species are changing in time. It is assumed that the number of active sites is constant, but this quantity can change if (i) active sites are lost to deactivation or (ii) the structure of the catalyst is evolving. The transients observed in this system often involve rate increasing in time (Figure 5.1) which would require a concomitant increase in the number of active sites with time on stream. Unmodified, well-defined proton-form zeolite catalysts do not form additional sites with time on stream except during oxidative thermal treatment to remove deposited carbon, and thus, for this system slowly evolving surface coverages with time on stream offer the most likely explanation for the transients observed.

The observed transients in rate are ~1-3 hours, suggesting that there is at least one kinetically-relevant surface intermediate that requires several hours to reach a steady-state fractional coverage. This occurs when the rates of the reactions that form and consume the reaction intermediate are "slow" (relative to other important time-scales in the reaction and to the data-sampling rate). Knowing that the formation and consumption of at least one reaction intermediate is slow compared to other reactions in the overall reaction network, we propose a mechanistic description where the overall reaction network can be separated into two sub-reaction networks depicted in Scheme 5.2. In this mechanism, the network of reactions that form (Reaction Network 1) and consume

154

(Reaction Network 2) the reaction intermediate, I*, reach pseudo-steady-state at much shorter time-scales than the time-scale required for the pseudo-steady-state assumption to be valid on the intermediate I*. Hence, we can treat the rate functions of the sub-reaction networks as pseudo-steady-state rate functions (r_1 for the formation of I* and r_2 for the consumption of I*), even during the transient when the pseudo-steady-state approximation on I* is invalid, such that eq. (5.2) describes the fractional coverage of I* in time:

$$\frac{d\theta_{I^*}}{dt} = \frac{r_1(t)}{L} - \frac{r_2(t)}{L} \tag{5.2}$$

The reaction rate for the consumption of I* is then equal to the rate of DPM formation (r_2), and can be written as eq. (5.3):

$$r_2(t)/L = \theta_{I^*}(t)f_2\left(k_j, K_j, P_{HCHO}(t), P_{C_6H_6}(t), P_{H_2O}(t)\right) \tag{5.3}$$

where r_2 is the rate of DPM formation, L is the number of active sites, k_j and K_j are the elementary step rate and equilibrium constants, θ_{I^*} is the fractional surface coverage of the reaction intermediate, I*, and f_2 is a function that describes the dependencies of the elementary step rate on k_j, K_j, and the reactant partial pressures, P_i. Equation (5.3) is written with only one surface species in the elementary step because zeolites do not typically catalyze reactions involving two sites, especially in high Si/Al materials like the catalyst used in this study. From eq. (5.3), the pressure dependencies of the rate function for the consumption of I* can be probed by studying the transient rate during step-changes in the partial pressure of each reactant as is demonstrated herein.

The continuity or discontinuity in the transient rate when step-changing the partial pressure of each reactant provides insights about the pressure dependencies of the steps comprising the composite reaction network. During the transient rate measurements shown in Figure 5.1, the reactant partial pressures only change at the start of the experiment ($t = 0$) and at the time of the step-change (indicated by dashed lines) and reach stable values within minutes. At the time of the step-change, the partial pressure of a species changes nearly *discontinuously* (e.g., benzene pressure changes from 0.41 to 1.3 kPa at the dashed line for the data shown in Figure 5.1c). If the function f_2 in eq. (5.3) depends on these partial pressures, its value will also change discontinuously, which in turn will result in a discontinuity in the rate of DPM formation, r_2, because the rate is changing on the time-scale that the partial pressures are changing. In this way, by monitoring whether the reaction rate undergoes a near discontinuous change when reactant partial pressures are step-changed, the functional dependence of f_2 can be ascertained. From Figure 5.1, the rate changes discontinuously only when the partial pressure of C_6H_6 is step-changed, and thus we conclude (eq. (5.4)):

$$f_2 = f_2\left(k_j, K_j, P_{C_6H_6}(t)\right) \tag{5.4}$$

such that the formation of the final DPM product, which is the net rate of Reaction Network 2 in Scheme 5.2, is a function only of the fractional coverage of I* and the partial pressure of C_6H_6 and does not depend on the partial pressures of H_2O or HCHO.

The steady-state DPM rate changes as a function of HCHO and H_2O partial pressures, as shown in Figures 5.1a and 5.1b. Because the rate r_2 does not depend on HCHO and H_2O partial pressure, the rate function for the formation of I*, r_1, must

Scheme 5.2: Proposed reaction mechanism based on transients in DPM rate with step-changes in reactant partial pressures, as shown in Figure 5.1. Reactions in Reaction Network 1 and Reaction Network 2 are assumed to be at pseudo-steady-state conditions at much shorter time scales than the pseudo-steady-state assumption is valid for the reaction intermediate I*.

$$r_1/L = \theta_* f_1(k_j, K_j, P_{HCHO}, P_{H_2O}, P_{C_6H_6}) \qquad r_2/L = \theta_{I^*} f_1(k_j, K_j, P_{C_6H_6})$$
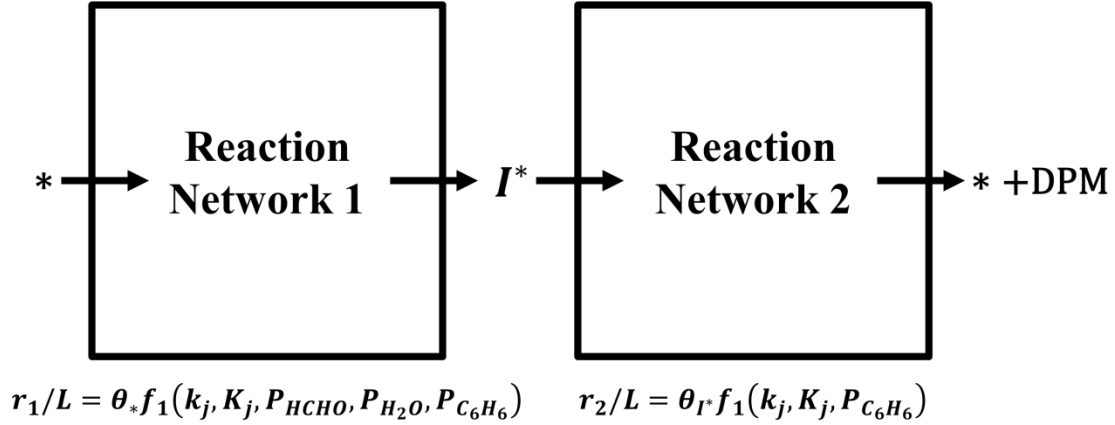
depend on the partial pressures of these reactants. During a step-change in C_6H_6 partial pressure, a discontinuity is observed if the rate function r_2 is a function of the benzene partial pressure, regardless of whether the rate function r_1 is a function of C_6H_6 partial pressure. Thus, from the transient data shown in Figure 5.1, it is not possible to determine with certainty whether the rate of formation of the surface intermediate, I*, depends on the partial pressure of C_6H_6; therefore, the formation rate of the surface intermediate (r_1) is assumed to be of the form given in eq. (5.5) to include the possibility of rates depending on C_6H_6 partial pressure:

$$r_1/L = \theta_*(t) f_1\left(k_j, K_j, P_{HCHO}(t), P_{H_2O}(t), P_{C_6H_6}(t)\right)$$

(5.5)

The dependency of this rate on the partial pressure of C_6H_6 is assessed by steady-state rate measurements by varying C_6H_6 pressure at conditions where the formation of I* is known to be rate-controlling for DPM formation (see Section 5.3.3).

In Chapter 4, we extended the concept of rate-controlling steps to non(pseudo)steady-state rates; the method developed therein enabled analytical relationships between features of the transient rate (e.g. discontinuities and extrema) during step-changes in reactant pressure and the pressure dependencies of the elementary-step reactions.[15] At the time of a step-change, only steps that consume or form the final product are rate-controlling because the fractional coverages depend solely on the initial condition at this time and are not functions of the rate constants,[15] such that the DPM rate is given by a function of the form (eq. (5.6)):

$$\frac{r_2(t = t_{0+})}{L} = f_2\big(k_j, K_j, P_j\big)\theta_{I^*,0} \qquad (5.6)$$

where t_{0+} is the time immediately after the step-change and $\theta_{I^*,0}$ is the fractional coverage of I* at the time of the step-change. For the transients observed in Figure 5.1, we see that the rate at the time of the step-change depends on the partial pressure of C_6H_6 but not on the partial pressures of HCHO or H_2O because a discontinuous change in the rate is observed only when step-changing the partial pressure of C_6H_6. Further, the step that is rate-controlling at the time of the step-change is likely not rate-controlling at steady-state at these reaction conditions, since the steady-state rate is a function of HCHO and H_2O pressures (Figure 5.1). Thus, at the reaction conditions in Figure 5.1 we conclude that the rate-controlling step is changing as a function of time, where (i) at the start of the transient, the consumption of I* to form DPM is rate-controlling and is a function only of C_6H_6 partial pressure and (ii) at steady-state the formation of I* is rate-controlling and is a function of HCHO and H_2O partial pressures. Thus, the partial pressure dependencies of the initial (at time $t = t_{0+}$ immediately after the step-change)

158

and steady-state rates and the observed transients during step-changes in partial pressure are rationalized by degrees of rate control at non(pseudo)steady-state conditions. Discussion on how the degrees of rate control for DPM formation evolve during each of the transients in Figure 5.1 can be found in Section A5.5 of the Appendix.

From transient step-change experiments, we identified that there are two rate functions that describe the rate of DPM formation—one function for the formation of a surface intermediate, I*, and another function for the consumption of the surface intermediate to form the final product, DPM. The surface intermediate, I*, does not rapidly reach a steady-state fractional coverage, but instead changes slowly in time with each change in the reaction condition, resulting in a transient in the DPM formation rate. In the next section, we report and discuss observations from measured steady-state reaction rates to obtain a detailed mechanistic description for Reaction Network 1 and 2 in Scheme 5.2 and identify potential rate-controlling transition states for DPM formation.

5.3.3 Steady-state rate measurements

The reaction temperature and partial pressures of HCHO, H_2O, and C_6H_6 were systematically varied to investigate the steady-state kinetics of DPM formation. The rate measurements were obtained under differential conversion conditions ($\leq$ 3.4% HCHO, $\leq$ 1% C_6H_6). In total, 153 independent steady-state rate measurements were obtained. These data are tabulated in Table A5.1 in Section A5.6 of the Appendix, and a subset of these data are reported in Figures 5.2 and 5.3.

In Figure 5.2a, at low HCHO pressures, the DPM formation rate is first-order in HCHO. From the transient step-change experiments, we determined that the rate of
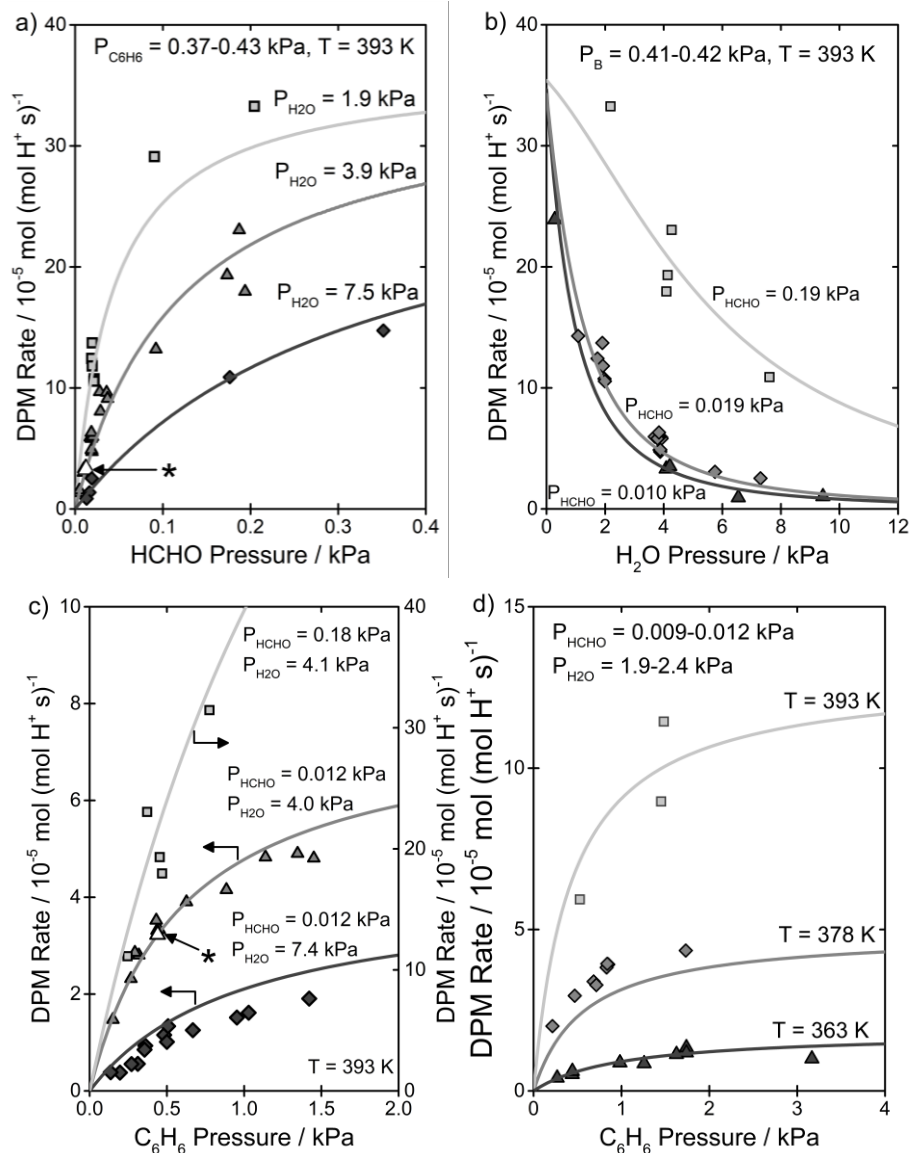
Figure 5.2: Steady-state rates at varying reaction conditions. a) Rate as a function of HCHO pressure with T=393 K, 0.37-0.43 kPa C_6H_6, with varying H_2O pressure (1.9, 3.9, and 7.5 kPa). b) Rate as a function of H_2O pressure with T=393 K, 0.41-0.42 kPa C_6H_6, and varying HCHO pressure (0.010, 0.019, and 0.19 kPa). c) Rate as a function of C_6H_6 pressure at T=393 K, at varying conditions: □ 0.18 kPa HCHO, 4.1 kPa H_2O, ◇0.012 kPa HCHO, 4.0 kPa H_2O, △0.012 kPa HCHO, 7.4 kPa H_2O. d) Rate as a function of C_6H_6 pressure at varying temperatures (T=363, 378, and 393 K) with 0.009-0.012 kPa HCHO, 1.9-2.4 kPa H_2O. Lines are model fits to the experimental data (see Section 5.3.5). Stars (*) pointing to unfilled symbols in a) and c) indicate the same experimental conditions.
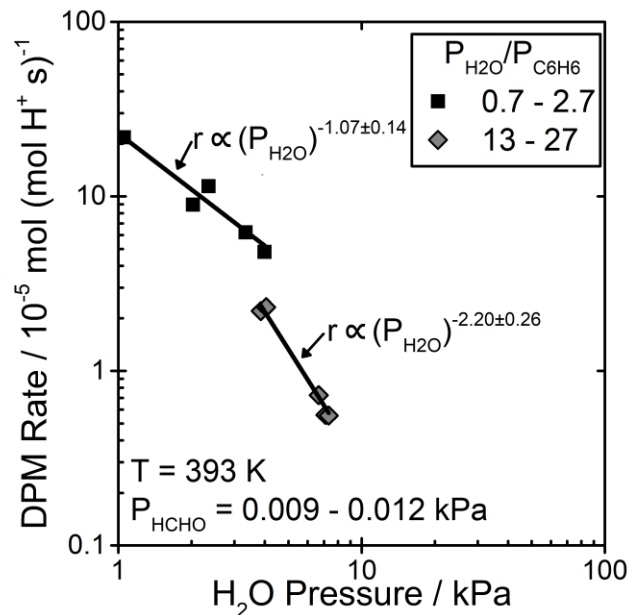
Figure 5.3: Plot of rate versus H_2O pressure at ($\square$) low and ($\diamond$) high $P_{H_2O}/P_{C_6H_6}$ ratios at 393 K, 0.009-0.012 kPa HCHO and ($\square$) 1.39-1.48 kPa C_6H_6, ($\diamond$) 0.27-0.31 kPa C_6H_6. Lines are power-law fits, where the power is the apparent reaction order of P_{H_2O}.

formation of the surface intermediate, I*, was a function of the partial pressure of HCHO, but the rate of consumption of this intermediate depends only on the C_6H_6 partial pressure. The rate of I* formation is likely at most first-order in HCHO because only one HCHO molecule appears in the overall reaction, and because the overall rate at low HCHO pressure is first-order in HCHO, the formation of the surface intermediate is likely the rate-controlling step at this condition. The unfilled data points indicated by the star in Figures 5.2a and 5.2c are at the same reaction condition, where the reaction is first-order in HCHO and also non-zero order in benzene. Thus, the rate of I* formation is a function of benzene pressure and the functional dependence of f_1 includes dependence on benzene partial pressure, as reported above in eq. (5.5).

Inhibition by H_2O is more significant at low benzene pressures (Figure 5.3) where the reaction is first-order in benzene (Figure 5.2c), than at high benzene pressures, where

the reaction order of benzene is zero. This simultaneous change in reaction orders suggests that H_2O and C_6H_6 both compete for the same site and, depending on their respective pressures, either H_2O* or C_6H_6* surface species dominate. A plausible mechanism that agrees with these steady-state and transient rate data is shown in Scheme 5.3, where adsorbed HCHO, which is in competition with the adsorption of C_6H_6 and H_2O, reacts with benzene to form the surface intermediate, I*, which further reacts with C_6H_6 (see eq. (5.4)) to form DPM. In addition to the inhibition by adsorption of H_2O on acid sites, the reaction is also inhibited by HCHO hydration by H_2O to form methane diol (CH_4O_2), as reported by Bollini et al.,[83] giving a minimum reaction order of -2 in water.

Methane diol was not observed, however the decomposition of CH_4O_2 to H_2O and HCHO occurs in the gas phase,[84–87] and may occur in the stainless steel lines (heated up to 473 K) or in the GC inlet (heated to 473 K), both maintained at elevated temperatures where HCHO becomes more thermodynamically favorable than methane diol.[83] An alternative explanation for the observed reaction orders in H_2O and C_6H_6 is the formation of H_2O-H_2O and C_6H_6-H_2O dimers instead of the formation of methane diol (Scheme 5.3), but these mechanistic hypotheses are kinetically indistinguishable. In Scheme 5.3, the equilibrium between HCHO and CH_4O_2 is described by eq. (5.7):

$$K_{hyd} = \frac{P_{CH_4O_2}}{P_{H_2O}P_{HCHO}} \tag{5.7}$$

where K_{hyd} is the pressure equilibrium constant for HCHO hydration and P_j are the equilibrium partial pressures of CH_4O_2, H_2O, and HCHO. By mole balance under differential conversion conditions, the partial pressures of HCHO and CH_4O_2 sum to the partial pressure of the inlet HCHO, $P_{HCHO,0}$ (eq. (5.8)):

$$P_{HCHO} + P_{CH_4O_2} = P_{HCHO,0} \tag{5.8}$$

Combining eqs. (5.7) and (5.8), the partial pressure of HCHO during reaction, P_{HCHO}, is related to the HCHO pressure fed to the reactor, $P_{HCHO,0}$, by eq. (5.9):

$$P_{HCHO} = \frac{P_{HCHO,0}}{1 + K_{hyd}P_{H_2O}} \tag{5.9}$$

where HCHO pressures reported in this work are $P_{HCHO,0}$. The rate function for the formation of I* from the reaction network shown in Scheme 5.3 (see Section A5.7 in the Appendix for derivation) is thus given by eq. (5.10):

$$r_1/L = \frac{k_1 K_{HCHO}\, P_{HCHO,0}P_{C_6H_6}/(1 + K_{hyd}P_{H_2O})}{1 + \dfrac{K_{HCHO}P_{HCHO,0}}{1 + K_{hyd}P_{H_2O}} + K_{C_6H_6}P_{C_6H_6} + K_{H_2O}P_{H_2O}}\, \theta_{*'} \tag{5.10}$$

where $\theta_{*'} = \theta_* + \theta_{HCHO^*} + \theta_{C_6H_6^*} + \theta_{H_2O^*} = 1 - \theta_{I^*}$ is the fractional coverage of all species that are equilibrated with vacant proton sites. The rate of I* consumption to form DPM in Scheme 5.3 is an elementary step with the rate given by eq. (5.11):

$$r_2/L = k_2 P_{C_6H_6}\theta_{I^*} \tag{5.11}$$

Combining eqs. (5.10) and (5.11) and noting that at steady-state $r_1 = r_2$ and at all times $\theta_{*'} = 1 - \theta_{I^*}$, the rate function for DPM formation for the composite reaction shown in Scheme 5.3 is (eq. (5.12)):

$$r_{DPM}/L$$

$$= \frac{k_1 k_2 K_{HCHO}\, P_{HCHO,0}P_{C_6H_6}/(1 + K_{hyd}P_{H_2O})}{\underbrace{\dfrac{k_1 K_{HCHO}P_{HCHO,0}}{1 + K_{hyd}P_{H_2O}}}_{I^*} + \underbrace{k_2}_{*} + \underbrace{\dfrac{k_2 K_{HCHO}P_{HCHO,0}}{1 + K_{hyd}P_{H_2O}}}_{HCHO^*} + \underbrace{k_2 K_{C_6H_6}P_{C_6H_6}}_{C_6H_6^*} + \underbrace{k_2 K_{H_2O}P_{H_2O}}_{H_2O^*}} \tag{5.12}$$

where each term in the denominator corresponds to the fractional coverage of a surface species, indicated by the brackets. Equation (5.12) shows the full rate function for the reaction in Scheme 5.3. Many terms in the denominator of eq. (5.12) are negligible because the corresponding species have low fractional coverages, and thus multiple kinetic/thermodynamic parameters are not estimable from the kinetic data, which requires us to simplify eq. (5.12) to only include relevant quantities.

At high HCHO pressures, the rate becomes zero order in HCHO (Figure 5.2a). This can occur because (i) the HCHO coverage approaches unity and the formation of I* is rate-controlling or (ii) the coverage of I* approaches unity and the consumption of I* becomes rate-controlling at high HCHO pressures, whose rate function depends on only the benzene partial pressure (eq. (5.11)). If (i) is true, then the third term in the denominator of eq. (5.12) becomes much larger than all other denominator terms, and eq. (5.12) simplifies to $r_{DPM}/L = k_1 P_{C_6H_6}$, which is order zero in water, order zero in HCHO, and order one in benzene. If (ii) is true, then the first term in the denominator of eq. (5.12) becomes much larger than all other denominator terms, and eq. (5.12) simplifies to $r_{DPM}/L = k_2 P_{C_6H_6}$, which is order zero in H_2O, order zero in HCHO, and order one in benzene. These cases are indistinguishable from steady-state rate measurements.

From steady-state rate measurements, we identified that the formation of a reaction intermediate, I*, is rate-controlling at least at low HCHO pressures, and that the rate function for the formation of I* depends on HCHO, H_2O, and C_6H_6 partial pressures. A plausible reaction network for the formation and consumption of I* was proposed (Scheme 5.3). Steady-state rate measurements were not able to ascertain whether the

formation or consumption of I* is rate-controlling at high HCHO pressures, where the reaction order of HCHO approaches zero. In the following section, we use isotopic switching experiments to assess the steady-state fractional coverage and identity of I^* to determine the rate-controlling steps of DPM formation.

Scheme 5.3: Proposed reaction network for the formation of DPM
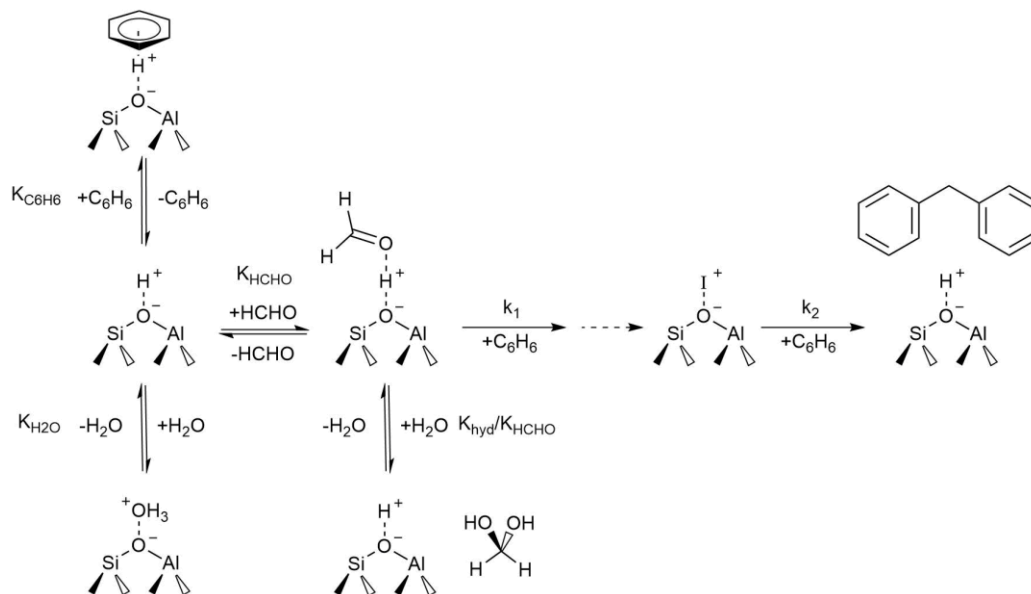
5.3.4 Steady-State Isotopic Transient Kinetic Analysis (SSITKA)

During SSITKA, the reactant feed was switched from $^{12}C_6H_6$ to $^{13}C_6H_6$ at steady state. After the isotopic switch, the surface intermediate formed prior to the switch will have ^{12}C-labeled six-membered rings. The isotopic content of the first DPM product formed immediately after the isotopic switch depends on the number of six-membered rings in the surface intermediate, I*, and the number of six-membered rings added to I* from the gas phase to form DPM. The number of ^{12}C-labeled aromatic rings in the first DPM product after the isotopic switch is equal to the number of six-membered rings in I*.

The results of the isotopic switching experiments at two different reaction conditions are shown in Figure 5.4. At both reaction conditions, the first DPM product

165

formed immediately after the switch has an m/z = 168, corresponding to entirely ^{12}C-labeled DPM. Only trace amounts of DPM product with one labeled aromatic ring (m/z = 174) was observed. These data suggest that the reaction intermediate, I*, has two six-membered rings. This is consistent with a protonated diphenylmethane benzenium ion ($C_{13}H_{13}^{+}$) as I*. Stable methylated DPM benzenium ions are important intermediates in alkylaromatic transalkylation pathways in zeolite catalysts,[88–95] including HZSM-5.[90,91] Computational calculations suggest deprotonation activation energies of methylated DPM^{+} in TON[94] and FAU[93] zeolite catalysts of 70 and 75 kJ mol^{-1}, respectively.
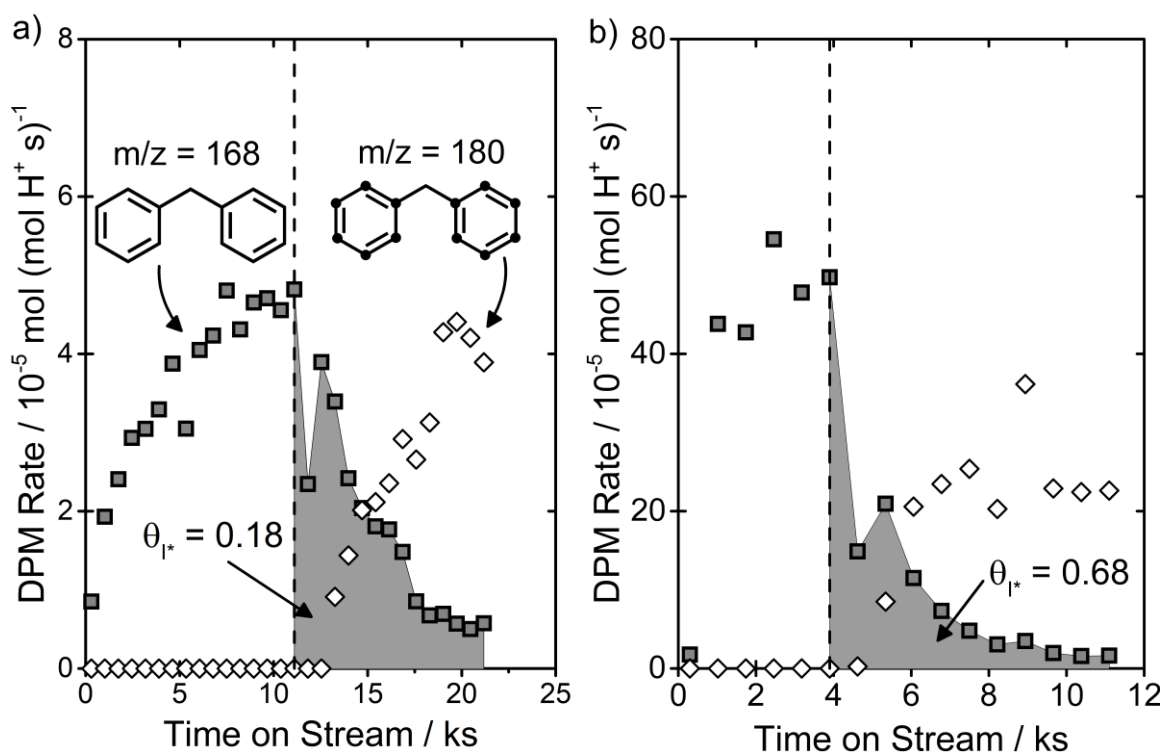
Figure 5.4: SSITKA experiments where ^{12}C$_6$H$_6$ is switched to ^{13}C$_6$H$_6$ at the dashed line. The shaded area under the curve is proportional to the fractional coverage of I* at steady state. a) 393 K, 0.02 kPa HCHO, 4 kPa H$_2$O, 0.4 kPa C$_6$H$_6$. Net rate of DPM is order ~1 in HCHO. b) 393 K, 0.2 kPa HCHO, 2 kPa H$_2$O, 0.4 kPa C$_6$H$_6$. Net rate of DPM is order < 1 in HCHO.

As the reaction progresses, all of the ^{12}C-labeled I* is consumed and replaced with ^{13}C-labeled I*, and an increase in DPM product with two ^{13}C-labeled aromatic rings (m/z = 180) is observed. The total amount of ^{12}C-labeled DPM product formed after the isotopic switch corresponds to the steady-state fractional coverage of I*. Figure 5.4a shows the SSITKA results for a steady-state reaction condition where the rate of DPM formation is order ~1 in HCHO (low HCHO pressure) and Figure 5.4b shows the SSITKA results where the steady-state rate is order < 1 in HCHO (high HCHO pressure). The corresponding steady-state fractional coverages of I* (DPM$^+$) for reaction order ~ 1 and < 1 are 0.18 and 0.68, respectively. This suggests that the reaction order of HCHO changes not because the fractional coverage of HCHO* is approaching unity, but because the fractional coverage of DPM$^+$ is approaching unity. For the irreversible formation (r_1) and consumption (r_2) of DPM$^+$, the steady-state fractional coverage of DPM$^+$ is related to the kinetic degrees of rate control by (eq. (5.13)):[60]

$$\theta_{DPM^+} = \frac{\sum_i s_i \nu_{iDPM^+} [\nu_{iDPM^+} < 0]}{\sum_{n^*} \sum_i s_i \nu_{in^*} [\nu_{in^*} < 0]} = \frac{s_2}{s_1 + s_2} = s_2 = X_{RC,2} \tag{5.13}$$

where eq. (5.13) was simplified because $\sum_i s_i = s_1 + s_2 = 1$ and related to $X_{RC,2}$ by noting $X_{RC,2} = s_2(1 - Z_2) = s_2$ since the consumption of DPM$^+$ is assumed irreversible ($Z_2 = 0$).[23,60] Equation (5.13) shows that the measured fractional coverage of DPM$^+$ is equal to the kinetic degree of rate control of reaction 2, the consumption of DPM$^+$. Thus, we conclude that the reaction order in HCHO is changing because the rate-controlling step is changing from the formation of DPM$^+$ at low HCHO pressures to the consumption of DPM$^+$ at high HCHO pressures.

The SSITKA results suggest that the reaction intermediate is DPM^+ and that, at high HCHO pressures, the consumption of the reaction intermediate to form the final product, DPM, is the rate-controlling step. However, transient rate measurements (Figure 5.1c) suggest that the rate of consumption of the reaction intermediate is a function of the benzene partial pressure. This is corroborated by steady-state rate measurements that show that at high HCHO pressures, the reaction order is ~ 1 in benzene (Figure 5.2c). These data suggest that the rate of proton-transfer from DPM^+ back to the zeolite framework is facilitated by benzene.

To determine whether deprotonation of DPM^+ is assisted by the presence of aromatics, HCHO and benzene were reacted on HZSM-5 at 353 K until reaching steady-state reaction conditions to form DPM^+ inside the zeolite catalyst (Phase I in Figure 5.5a). The reactor was then flushed with 2.07 cm^3 s^{-1} He for six hours at 353 K to remove any residual reactants and products. At the end of the He flush, no DPM was observed in the reactor effluent. After the He flush, a stream containing 0.4 kPa toluene was fed to the reactor. Immediately after introducing toluene to the reactor, unmethylated DPM was observed in the reactor effluent, demonstrating that the DPM^+ deprotonation is positive order in aromatics. The deprotonation of DPM^+ forms DPM, and thus the rate is indeed discontinuous through the step-change in the partial pressure of C_6H_6 (Figure 5.1c). The rate of DPM decreased with time on stream after introducing toluene as the fractional coverage of DPM^+ decayed to zero. In repeat experiments, toluene was replaced with cyclohexane after the He flush, but no DPM products were observed, suggesting that aromatics are necessary to facilitate the proton-transfer from DPM^+ to the zeolite framework. Lower proton-transfer energy barriers between aromatic molecules compared

168

to non-aromatic molecules have been reported previously.[96] If this is the prevalent mechanism for aromatic assisted proton transfer from DPM^+ to the zeolite, once the proton is transferred from DPM^+ to C_6H_6, the proton transfer to the zeolite framework must be spontaneous, as these benzenium ions are unstable in HZSM-5.[97,98] We hypothesize that a $C_6H_7^+$ carbenium ion is not formed but instead forms a transition state comparable to that of H/D exchange of C_6H_6 on zeolites, where the proton transfer to benzene from DPM^+ and from benzene to the zeolite are concerted.[99] During reaction, C_6H_6 may act as a proton shuttle between DPM^+ and the zeolite framework as an organic co-catalyst for the deprotonation of DPM^+ in HZSM-5. Alternatively, the π-system of aromatics may interact with the positively charged aromatic system in DPM^+ species, lowering the energy barrier for deportation. The DPM^+ surface species is persistent through a six hour He flush, suggesting that its formation is irreversible, in agreement with the mechanism proposed in Scheme 5.3. This is in contrast to what Clark et al.[95] proposed for DPM-mediated transalkylation mechanisms of *m*-xylene on FAU catalysts, where they suggested based on DFT calculations that the formation of a DPM^+ species is reversible, and will likely re-form the adsorbed alkylaromatic alkoxy species and gas-phase *m*-xylene many times before transferring the proton from DPM^+ to the zeolite. If this occurred during the present study, some DPM product with one ^{13}C-labeled aromatic ring would have been observed after the isotopic switch in the SSITKA experiment (Figure 5.4), and in Figure 5.5a a significant amount of methyl-DPM would be expected when feeding toluene after the 6 h helium flush. Thus, we conclude that at the reaction conditions in this study, DPM^+ formation is not reversible.
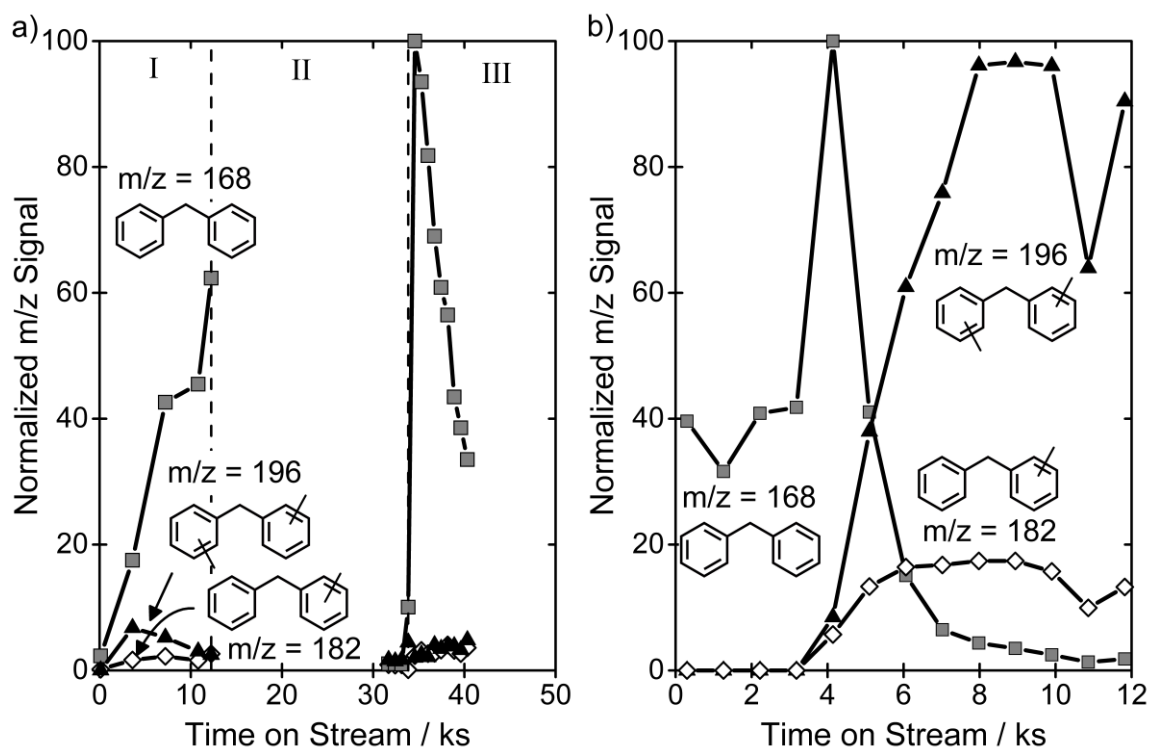
Figure 5.5: GC-MS data for DPM (m/z = 168), methylDPM (m/z = 182), and dimethylDPM (m/z = 196) normalized within each figure. a) During Phase I (0-12 ks time on stream), 0.4 kPa C_6H_6, 0.2 kPa HCHO, and 2.0 kPa H_2O are fed to the reactor heated to 353 K to build up a surface coverage of DPM^+ species. During Phase II (12-32 ks time on stream) the reactor was flushed with helium at 353 K. No DPM was observed at the end of the helium flush. During Phase III, 0.4 kPa toluene in helium was introduced to the reactor at 353 K. b) At time on stream = 0 ks, the reaction is at steady-state with T = 393 K, 0.4 kPa C_6H_6, 0.012 kPa HCHO, 4.0 kPa H_2O. At ~3 ks (dashed line) the feed was switched to a stream containing 0.4 kPa total aromatics with 2 toluene:1 benzene.

Svelle et al.[91] observed DPMs (methyl- and dimethyl-DPM) upon dissolution of HZSM-5 after reaction of toluene at 423 K for 16 h, demonstrating the importance of methylated DPM^+ intermediates in toluene disproportionation reactions. They examined the stability of the methylated DPM^+ intermediates by flushing several batches of pre-reacted catalyst at 473 K in N_2 for 5 min to 2 h, and dissolved each batch to liberate the entrained species. They observed a monotonic decrease in entrained DPMs and an initial increase in entrained xylenes with increasing flushing time, suggesting dimethyl-DPM^+

decomposed to toluene and formed an adsorbed xylene alkoxy species. They did not report whether dimethyl-DPM was observed in the reactor effluent during the N_2 flush, so the rate of DPM$^+$ deprotonation relative to the rate of decomposition at these conditions is unknown. Regardless, methylated DPM$^+$ likely decompose to single-ringed alkoxy aromatic species at temperatures elevated relative to those in the present study.

To ensure that no significant transport limitations impact the results of these transient experiments, we measured the rate of DPM products during a steady-state switch from a feed containing 0.4 kPa benzene to a feed containing 0.4 kPa aromatics with 2 toluene:1 benzene, while keeping the HCHO and H_2O pressures constant. After the feed was switched, the rate of DPM formation increased in the injection immediately after the switch (~ 12 minutes after switch), demonstrating that (i) toluene is more reactive for catalyzing the proton-transfer from DPM$^+$ to the framework and (ii) the rate senses the change in feed composition on much shorter time scales (< 12 minutes) than the time scale for transients in the observed rates (~1-3 hours), suggesting that the reactant concentration in the catalyst particle matches that of the reactant feed at short times on stream. Thus, we conclude that the transient kinetic measurements are not transport limited (see Section A5.8 of the Appendix for a detailed explanation on transport effects during transients). After the reaction reaches steady state with the toluene-benzene feed, methylated DPM products are observed. This confirms that during the reaction between toluene and DPM$^+$ after a He flush (Figure 5.5a), toluene is not incorporated into the final product, but instead only facilitates proton-transfer from DPM$^+$.

Through steady-state isotopic switching experiments, we determined that the reaction intermediate has two six-membered rings and is likely a diphenylmethane benzenium ion. The fractional coverage of this benzenium ion during steady-state catalysis varies with the reaction condition and the HCHO reaction order varies with the fractional coverage of DPM^+. At sparse DPM^+ coverages, the rate-controlling step is the formation of DPM^+ and the reaction is first-order in HCHO. At high coverages of DPM^+, the rate-controlling step becomes the deprotonation of DPM^+ to form DPM, and the net rate of DPM formation approaches zero-order in HCHO. Combining all this information, we propose a reaction mechanism and kinetic model for DPM formation that quantitatively describes the transient and steady state reaction rates with reactant partial pressures ranging from 0.005-0.35 kPa HCHO, 0.14-4.1 kPa C_6H_6, and 0.11-12.5 kPa H_2O and the temperature varying from 363-393 K.

5.3.5 Reaction Mechanism and Kinetic Model

The DPM formation mechanism presented in Scheme 5.4 arises from the combination of transient, steady-state, and isotopic data to complete the mechanistic description shown in Scheme 5.3. In Scheme 5.4, adsorbed HCHO reacts with benzene to form benzyl alcohol, as was proposed by Martinez-Espin et al.[72] and Climent et al.[74] However, benzyl alcohol was not observed in either of these studies. During reaction between 0.036 kPa benzyl alcohol (C_7H_7OH) and 7.2 kPa C_6H_6 on SPP-HZSM-5 at 353 K we did not observe any DPM product, despite nonzero rates of DPM formation during reaction between HCHO and C_6H_6 at 353 K (see Figure A5.4 in the Appendix). This suggests that there may be an alternative route to DPM formation that bypasses a benzyl alcohol intermediate or that

co-feeding of benzyl alcohol at pressures much higher than those present during HCHO reaction with C_6H_6 may significantly alter the reaction pathways such that no DPM product is formed. At reaction temperatures of 373 K and 393 K, DPM product was observed with 0.025 kPa C_7H_7OH and 4.0 kPa C_6H_6 at similar residence times as HCHO reactions with C_6H_6. At all temperatures, complete conversion of benzyl alcohol is observed. When feeding only benzyl alcohol, the only products observed are benzaldehyde and toluene, which are known products of benzyl alcohol disproportionation on zeolite catalysts.[100] At very few reaction conditions during HCHO reaction with C_6H_6, specifically when the coverage of DPM^+ is high (i.e. high HCHO pressures), a quantifiable amount of benzaldehyde (< 20 mol % of carbon containing products) is observed, suggesting that benzyl alcohol, which is not observed at any reaction conditions, is formed during these reactions (see Section A5.9 of the Appendix for benzaldehyde rates as a function of HCHO pressure). Benzyl alcohol is present in low enough pressures that it is not observed during reaction, suggesting that it is a reactive intermediate that is rapidly consumed by forward or reverse reaction. Decomposition of benzyl alcohol to benzene and HCHO was not observed when reacting only benzyl alcohol on SPP-HZSM-5, suggesting that benzyl alcohol must be consumed rapidly by forward reactions to form DPM^+ or benzaldehyde byproducts. From these data we conclude that the rate-controlling step of DPM^+ formation is C-C bond formation between HCHO and C_6H_6, in agreement with the steady-state kinetics being at most first-order in C_6H_6 when DPM^+ formation is rate-controlling, and in agreement with conclusions from previous studies.[72] Whether benzyl alcohol undergoes a concerted dehydration during C-C bond formation as proposed by Martinez-Espin et al.[72] or

dehydration to form a phenylmethelium cation surface species followed by C-C bond formation to form DPM$^+$, as proposed by Climent et al.,[74] cannot be ascertained from the experimental data presented here because these steps are kinetically irrelevant.

Scheme 5.4: Reaction mechanism for diphenylmethane formation.
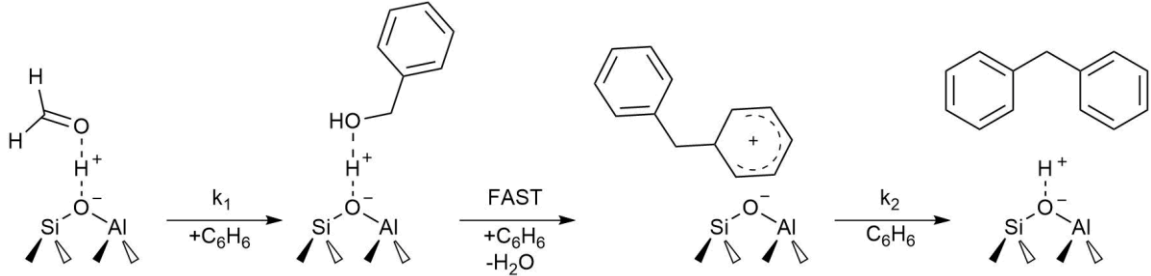
The second kinetically-relevant step in this reaction sequence is the benzene-catalyzed proton-transfer from DPM$^+$ to the zeolite framework to desorb the final product, DPM. From isotopic switching experiments, we determined that the reaction order in HCHO decreased because the fractional coverage of DPM$^+$ approached unity, not because the fractional coverage of HCHO approached unity. This suggests that the denominator term $K_{HCHO} P_{HCHO,0}/(1 + K_{hyd}P_{H_2O})$, which corresponds to the fractional coverage of HCHO, is negligible at the reaction conditions examined in this work. Parameter estimation results suggest that $K_{hyd}P_{H_2O} \gg 1$ and $K_{C_6H_6}P_{C_6H_6} + K_{H_2O}P_{H_2O} \gg 1$, such that the rate function for the formation of I* (eq. (5.10)) is rewritten to eliminate all negligible terms as (eq. (5.14)):

$$\frac{r_1}{L} = \frac{\frac{k_1 K_{HCHO}}{K_{hyd}K_{H_2O}}P_{HCHO,0}P_{C_6H_6}}{\frac{K_{C_6H_6}}{K_{H_2O}}P_{C_6H_6}P_{H_2O} + P_{H_2O}^2}\theta_{*'} = \frac{\alpha P_{HCHO,0}P_{C_6H_6}}{\beta P_{C_6H_6}P_{H_2O} + P_{H_2O}^2}\theta_{*'}$$

$$(5.14)$$

$$= f_1\left(P_{HCHO,0}, P_{C_6H_6}, P_{H_2O}\right)\theta_{*'}$$

where α and β are lumped kinetic/thermodynamic parameters and $\theta_{*'}$ is the fraction of sites without adsorbed DPM$^+$. The rate of consumption of DPM$^+$ is the rate of benzene-assisted proton-transfer to the zeolite framework, and is given by (eq. (5.15)):

$$r_2/L = k_2 P_{C_6 H_6} \theta_{DPM^+} = f_2\left(P_{C_6 H_6}\right)\theta_{DPM^+} \tag{5.15}$$

The steady-state rate is found by assuming $d\theta_{DPM^+}/dt = 0 = f_1\theta_{*'} - f_2\theta_{DPM^+}$, knowing that the fractional coverages sum to unity ($\theta_{*'} + \theta_{DPM^+} = 1$). From eqs. (5.14) and (5.15), the steady-state rate of DPM formation is (eq. (5.16)):

$$\frac{r_{DPM}}{L} = \frac{f_1 f_2}{f_1 + f_2} = \frac{\alpha k_2 P_{HCHO,0} P_{C_6 H_6}}{\alpha P_{HCHO,0} + \beta k_2 P_{C_6 H_6} P_{H_2 O} + k_2 P_{H_2 O}^2} \tag{5.16}$$

The kinetic parameters α, β, and k_2 were estimated using Athena Visual Studio. The temperature dependence for each parameter was assumed to be of Arrhenius form (eqs. (5.17)-(5.19)):

$$\alpha = \alpha_0 \exp\left(-\frac{E_{a,\alpha}}{R}\left(\frac{1}{T} - \frac{1}{363\ K}\right)\right) \tag{5.17}$$

$$\beta = \beta_0 \exp\left(-\frac{E_{a,\beta}}{R}\left(\frac{1}{T} - \frac{1}{363\ K}\right)\right) \tag{5.18}$$

$$k_2 = k_{2,0} \exp\left(-\frac{E_{a,k_2}}{R}\left(\frac{1}{T} - \frac{1}{363\ K}\right)\right) \tag{5.19}$$

where α_0, β_0, and $k_{2,0}$ are the values of the kinetic parameters at 363 K. The results of the parameter estimation fits are summarized in Table 5.2. The fits to steady-state rates using the parameters presented in Table 5.2 are shown in Figure 5.2 as solid curves for a

175

subset of the data, and a parity plot on linear and log scales are given in Figure 5.6 for all of the experimental data. All experimental conditions, measured rates, and predicted rates are tabulated in Table S1 of Section A5.6 of the Appendix. The six parameter kinetic model (eq. (5.16)) derived based on the proposed reaction mechanism presented in Schemes 5.3 and 5.4 quantitatively captures the trends in DPM formation rate with temperature and reactant partial pressures.

Table 5.2: Parameters estimated by fitting the model rate function (eq.(5.16)) to steady-state data.

Parameters	Estimated Values ± 95% Marginal HPD Intervals
$\log_{10}(\alpha_0 \ / \ \text{s}^{-1})$	-2.47 ± 0.17
$\log_{10}(\beta_0)$	0.33 ± 0.32
$\log_{10}(k_{2,0} \ / \ \text{s}^{-1} \ \text{kPa}^{-1})$	-3.41 ± 0.16
$E_{a,\alpha} \ / \ \text{kJ mol}^{-1}$	79. ± 17.
$E_{a,\beta} \ / \ \text{kJ mol}^{-1}$	51. ± 32.
$E_{a,k_2} \ / \ \text{kJ mol}^{-1}$	31. ± 15.

The model parameters in Table 5.2 were fit only to steady-state rate data, but also predicts the transients observed when starting the reaction from fresh catalyst or after step-changing the partial pressure of a reactant. The transient surface coverage of DPM$^+$ is found by solving the differential equation given in eq. (5.20):

$$\frac{d\theta_{DPM^+}}{dt} = f_1\big(P_{HCHO,0}, P_{C_6H_6}, P_{H_2O}\big)(1 - \theta_{DPM^+}) - f_2(P_{C_6H_6})\theta_{DPM^+} \qquad (5.20)$$

The transient rate is solved piecewise from the start of one change in the reaction condition to the start of the next change in the reaction condition. Each time the reaction condition is changed, it is assumed that θ_{DPM^+} an infinitesimal time before the change is
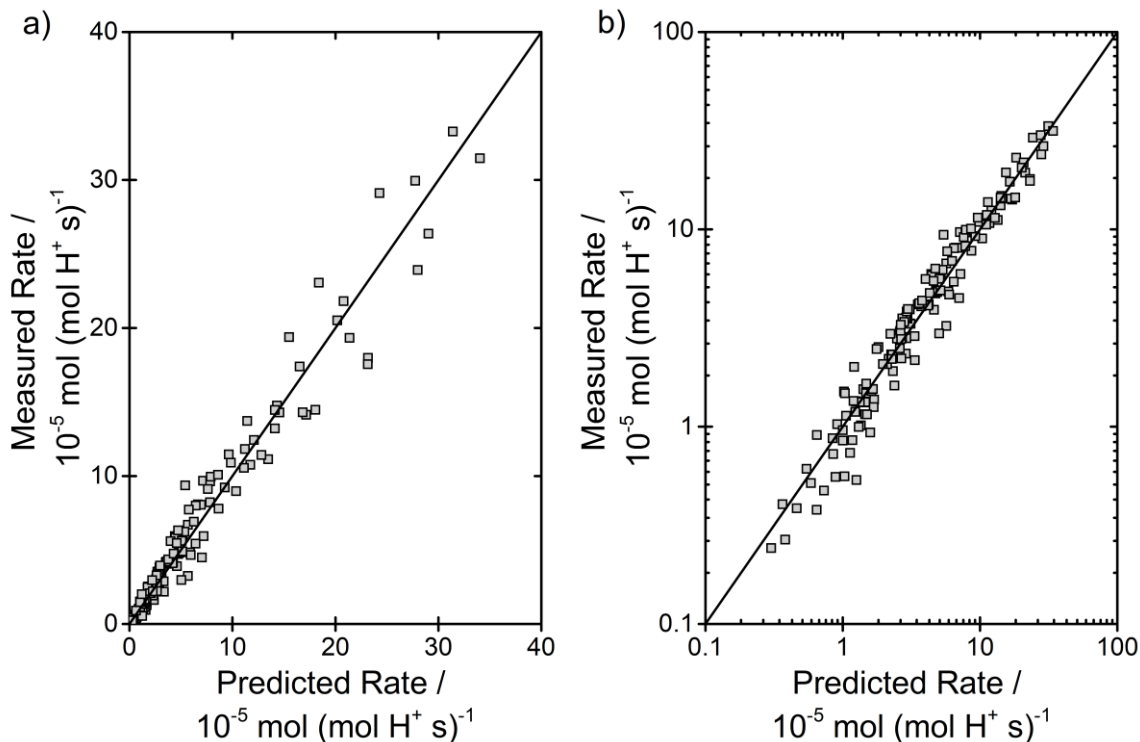
Figure 5.6: Measured versus predicted rate for all 153 rate measurements from 363-393 K, 0.005-0.35 kPa HCHO, 0.14-4.14 kPa C_6H_6, 0.11-12.5 kPa H_2O on a) a linear scale and b) a log scale to better visualize low rate data.

equal to θ_{DPM^+} an infinitesimal time after the change. The solution to eq. 15 with the initial condition $\theta_{DPM^+}(t = t_0) = \theta_{DPM^+,0}$ is (eq. (5.21)):

$$
\theta_{DPM^+}(t) = \frac{f_1}{f_1 + f_2}
$$

$$
+ \left(\theta_{DPM^+,0} - \frac{f_1}{f_1 + f_2} \right) \exp(-(f_1 + f_2)(t - t_0)) \quad \forall\, t \in [t_0, t_1]
$$

(5.21)

where f_1 and f_2 are functions that appear in eqs. (5.14) and (5.15), t_0 is the time at the start of the current reaction condition and t_1 is the starting time for the next reaction condition. The transient rate is simply given by multiplying eq. (5.21) by f_2 (see eq. (5.15)), as shown by eq. (5.22):

$$\frac{r_{DPM}(t)}{L} = \frac{f_1 f_2}{f_1 + f_2}$$

$$+ \left(f_2 \theta_{DPM^+,0} \right.$$

$$\left. - \frac{f_1 f_2}{f_1 + f_2} \right) \exp(-(f_1 + f_2)(t - t_0)) \quad \forall \, t \in [t_0, t_1] \tag{5.22}$$

Notice that the transient rate function (eq. (5.22)) requires only two additional parameters: the time since the previous change in reaction condition $(t - t_0)$ and the DPM$^+$ coverage at the time of the change in reaction condition, $\theta_{DPM^+,0}$. The quantity $\theta_{DPM^+,0}$ is zero if starting from fresh catalyst or the value of θ_{DPM^+} immediately before the step-change, found by evaluating eq. (5.21) at $t = t_1$ using the temperature and partial pressures from the previous condition. Thus, the transient can be modeled using the steady-state estimated parameters presented in Table 5.2. The model prediction for the transient rate (eq. (5.22)) when starting from a fresh catalyst and during the step-change in the partial pressure of each reactant are shown as solid curves in Figure 5.1. The model captures the time scales required to reach steady-state and the behavior through the step-change in reactant partial pressures. The steady-state kinetics accurately predict the transient rates, exemplifying the connection between these phenomena and affirming the validity of the proposed reaction mechanism for DPM formation.

The model predicts the transient and steady-state reaction rates, and from eq. (5.21), can also predict the steady-state and transient fractional coverages of DPM$^+$. The steady-state fractional coverage of DPM$^+$ was assessed at two reaction conditions using SSITKA (Figure 5.4). From eq. (5.21), the steady-state fractional coverage of DPM$^+$ is

$\theta_{DPM^+}(t \rightarrow \infty) = f_1/(f_1 + f_2)$. The predicted values for the steady-state coverages are in good agreement with the measured coverages, as shown in Table 5.3. Thus, the kinetic model quantitatively predicts transient rates, steady-state rates, and fractional coverages at a wide range of reaction conditions using only three fitted kinetic/thermodynamic parameters and three activation/thermodynamic energies.

Table 5.3: Measured and predicted steady-state fractional coverages of DPM^+.

T / K	$P_{HCHO,0}$ / kPa	$P_{C_6H_6}$ / kPa	$P_{C_6H_6}$ / kPa	Measured θ_{DPM^+}	Predicted θ_{DPM^+}
393	0.020	0.40	4.0	0.18	0.14
393	0.20	0.40	2.0	0.68	0.82

5.4 Conclusion

In this study, the mechanism of diphenylmethane (DPM) formation from HCHO and C_6H_6 on SPP-HZSM-5 zeolite catalysts in the presence of H_2O co-feeds is determined by combining transient and steady-state rate measurements and isotopic switching experiments. Transients lasting several hours were observed during experiments starting from freshly regenerated catalysts and for each change in the reaction condition. These were determined to result from the slowly evolving fractional coverage of a surface intermediate with time on stream. The isotopologue distribution of DPM products after a switch from ^{12}C- to ^{13}C-labeled C_6H_6 feed indicated that the surface intermediate has two six-membered rings and is likely a diphenylmethane benzenium ion (DPM^+). The steady-state coverage of DPM^+ was determined to vary significantly with reaction conditions, with increasing coverage corresponding to a shift in rate-controlling step from formation to consumption of DPM^+. Consumption of DPM^+ involves proton-transfer from DPM^+ to

the zeolite framework. This proton-transfer is assisted by the presence of aromatic species as evidenced by: (i) the rate being discontinuous in time when the partial pressure of C_6H_6 is step-changed, (ii) the steady-state rate of DPM formation being first-order in C_6H_6 at high fractional coverages of DPM^+, and (iii) DPM^+ surface species persisting on the zeolite during a He flush until the introduction of toluene. A mechanism consistent with observed trends in transient and steady-state reaction rates and the isotopic switching experiments was developed and a kinetic model based on this mechanism quantitatively captures all observations using three kinetic/thermodynamic parameters, each with an apparent activation energy to describe the temperature dependence.

Chapter 6

A method for assessing catalyst deactivation: A case study on methanol-to-hydrocarbons conversion

6.1 Conspectus

The decrease in conversion with time on stream in catalytic systems is referred to as the deactivation rate and is often described by empirical models that either have no chemical basis or assume *a priori* the kinetics of the reaction and the mechanism of deactivation. Herein, we develop metrics for assessing the rate, yield, and selectivity of deactivation reactions that can be measured with no assumptions of the reaction kinetics or underlying mechanism. These metrics are derived by treating active sites as species that are consumed in deactivation reactions, rendering them unavailable for catalysis. These metrics unable the study of deactivation mechanisms in the same way non-deactivation products are studied—by the direct measurements of rate, yield, and selectivity as a function of the reaction conditions. We demonstrate these methods in the study of deactivation during methanol-to-hydrocarbons catalysis on HZSM-5 and HSSZ-13 zeolite catalysts.

6.2 Introduction

Deactivation rate is a central metric in assessing viability of a catalyst for industrial practice.[101] Despite its significance, methods for assessing and definitions of deactivation rate in the literature offer conflicting interpretations. Herein, metrics for

assessing deactivation are derived by considering active sites consumable, akin to reacting species. This in turn allows us to define the rate, yield, and selectivity for the loss of sites during reaction. We contrast our approach to commonly used methods for assessing deactivation in flow systems—a change in conversion with time and $t_{0.5}$, the time required for the conversion to reach 50% starting from complete conversion—and discuss these existing metrics in context of methanol-to-hydrocarbons (MTH) chemistry. We illustrate the utility of metrics we propose in the context of the same chemistry for comparison but note that these assessors are not specific to this system.

6.3 Results and Discussion

An oft-used definition for deactivation rate is the rate of change of chemical conversion (X) with time on stream (t) with the instantaneous value of dX/dt being the numerical value of deactivation rate.[101] A loss in chemical conversion with time on stream is a result of either a decrease in the intrinsic per-site rate or a decrease in the number of active sites accessible for reaction.[101,102] For systems that experience *nonselective deactivation*—where the change in conversion and yield is entirely prescribed by a decrease in contact time, τ (moles of sites normalized by molar reactant flow rate), with time on stream (eq. (3.5))[103]—dX/dt can be written as a product of two derivatives using the chain rule (eq. (6.2)). Janssens[104] in his early and pioneering work on MTH noted that dX/dt conflates a decrease in the number of active sites with time on stream represented by $d\tau/dt$ and the reaction kinetics reflected by the quantity $dX/d\tau$.

$$X = X\big(\tau(t)\big) \tag{6.1}$$

$$\frac{dX}{dt} = \frac{dX}{d\tau}\frac{d\tau}{dt} \tag{6.2}$$

In Janssens's original work,[104] deactivation was assessed by choosing models to describe both $dX/d\tau = k(1-X)$ and $d\tau/dt = -aX$, where k is a first-order rate constant of reaction and a is the deactivation coefficient, and fitting these models to conversion versus time-on-stream data. The quantity $d\tau/dt$, with units of moles sites lost per mole reactant fed, was deemed the deactivation rate. Subsequent analysis of the model solutions allowed Janssens to specify the parameter $t_{0.5} \approx \tau_0/a$ as an assessor of the rate of catalyst deactivation, where τ_0 is the initial contact time.[104] We note first and foremost that these model fits are not unique. As a simple demonstration of this fact, if $dX/d\tau = f(\tau)$ and $d\tau/dt = g(\tau)$ fits the conversion versus time data, then by the symmetry of eq. (6.2), $dX/d\tau = g(\tau)$, $d\tau/dt = f(\tau)$ is an identical model fit. The model choices influence the values prescribed to $d\tau/dt$ and consequently, the interpretation of the deactivation rate.

Second, the use of models to define reaction kinetics, especially in systems of such complexity, results in simplistic descriptions of the chemistry and results in model-specific assessors of deactivation. Variation of such assessors now abound the MTH literature.[68,104,105] We note simply that numerous model-specific adaptations of Janssens's original formalism do not address the shortcoming that arises from the lack of uniqueness-of-fit of these models to conversion versus time-on-stream data. Instead, we seek an analytical formalism for assessing deactivation caused by a loss of sites accessible for reaction by use of eq. (6.2), where two of the three quantities, $dX/d\tau$ and

183

dX/dt, are measured such that the third, $d\tau/dt$, is determined. We then define site-loss rate, yield, and selectivity as model-agnostic assessors of deactivation.

The site-loss rate, yield, and selectivity are defined by considering active sites as consumable species in stoichiometric reactions (eq. (6.3)):

$$\nu_R R + \nu_* * \rightarrow \nu_C C \tag{6.3}$$

where ν_i are stoichiometric coefficients, R is the reactant species, $*$ is the active site, and C is coke. With this viewpoint, the site-loss rate, with units of moles sites lost per site per unit time, is given by eq. (6.4):

$$\text{Site-loss rate} = -\frac{1}{n_*}\frac{dn_*}{dt} = -\frac{1}{\tau}\frac{d\tau}{dt} \tag{6.4}$$

where n_* is the instantaneous number of active sites. The site-loss yield, with units of moles sites lost per mole reactant fed, is defined in eq. (6.5):

$$\text{Site-loss yield} = -\frac{1}{\dot{n}_R}\frac{dn_*}{dt} = -\frac{d\tau}{dt} \tag{6.5}$$

where $\dot{n}_R$ is the molar reactant flow rate. The site-loss selectivity, with units of moles sites lost per mole reactant converted, is described by eq. (6.6):

$$\text{Site-loss selectivity} = -\frac{1}{X\dot{n}_R}\frac{dn_*}{dt} = -\frac{1}{X}\frac{d\tau}{dt} \tag{6.6}$$

Each site-loss descriptor is simplified to an expression that contains the quantity $d\tau/dt$ (eqs. (6.4)-(6.6)). In the following sections, we first present an illustration of how eq. (6.2) is used to calculate $d\tau/dt$, and subsequently the deactivation assessors presented in eqs. (6.4)-(6.6), through a hypothetical example. Next, we demonstrate the power of our

approach in the context of MTH catalysis through three case studies. These case studies encompass (i) nonselective deactivation at subcomplete methanol conversion, (ii) nonselective deactivation at complete methanol conversion, and (iii) selective deactivation. Through these case studies, we investigate the relationship between site-loss yields and selectivities with varying co-feed pressures of formaldehyde, a known coking agent during MTH catalysis, to obtain mechanistic insights about the nature of catalyst deactivation.

6.3.1 Nonselective and Selective Deactivation

In this section, we describe briefly the distinction between nonselective and selective deactivation as it pertains to assessing catalyst deactivation. For nonselective deactivation, the change in conversion with time on stream is described by decreasing contact time with time on stream (eq. (3.5)). This implies that a partially deactivated catalyst bed will produce the same conversion and product yields as a fresh catalyst bed compared at identical contact times, i.e., losing X% of active sites is equivalent to decreasing the mass of catalyst in a fresh reactor bed by X%. Rigorously assessing this can be challenging as it requires enumerating sites in partially deactivated catalyst beds, however a close approximation for determining whether deactivation is nonselective is to compare product selectivity versus conversion data of partially deactivated catalyst beds to fresh catalyst beds—if deactivation is nonselective these data will be identical. We refer the reader to Figure 6.6 of reference [106] (Rojo-Gama et al., *Faraday Discuss.* **2017**, *197*, 421–446) for a clear demonstration of how this is appropriately assessed in systems with nonselective deactivation.

When conversion versus product selectivity curves differ between fresh and partially deactivated catalyst beds, the deactivation is selective. For these systems, losing X% of active sites is not equivalent to decreasing the mass of catalyst in a fresh reactor bed by X%. There are many reasons why this may occur, including time-dependent evolution of active sites and changes in catalyst properties relevant to the catalysis with time on stream because of coke deposition. We refer the reader to Figure 6.4 of reference [103] (Chen et al., *Ind. Eng. Chem. Res.* **1997**, *36*, 3473–3479) for an example of determining that deactivation is selective.

We note that the method of comparing product selectivities versus contact time does not guarantee that a reaction system is deactivating nonselectively, as it is possible that conversion versus contact time and product yields versus contact time both change with deactivation such that product yields versus conversion remain identical between a fresh and partially deactivated catalyst bed. For a reaction network as complicated as methanol-to-hydrocarbons conversion, it seems unlikely that deactivation could be selective while product yields versus conversion data remain unchanged during deactivation.

The examples chosen to illustrate the method we propose for assessing deactivation consider monofunctional catalytic systems, however, the methods are also applicable for polyfunctional catalysts. The assumptions for nonselective deactivation require the ratio of the different sites in the polyfunctional catalyst bed to remain constant as the catalyst deactivates, and this ratio needs to be reported in addition to the reaction conditions for the measurements of site-loss rate, yield, and selectivity. If the catalyst deactivates such that the ratio of various types of sites is not constant, then deactivation

186

will be selective and the initial ratio of sites need to be reported in addition to the initial reaction conditions.

We demonstrate utility of the method we prescribe for both selective and nonselective deactivation in context of methanol-to-hydrocarbons catalysis—specifically, we demonstrate availability of both instantaneous and cumulative metrics when deactivation in nonselective whereas only cumulative metrics are accessible when deactivation in selective.

6.3.2 Hypothetical Example

Consider catalysts A and B that differ kinetically, giving rise to dissimilar conversion versus contact time curves presented in Figure 6.1a. Conversion versus time-on-stream data are measured for each catalyst to assess deactivation, beginning at identical contact times τ_0 and conversions X_0 for both catalysts. Presume deactivation of catalysts A and B is nonselective and thus decreasing conversion with time on stream is entirely described by decreasing contact time as sites are lost to deactivation (eq. (3.5)). In this hypothetical scenario, catalysts A and B deactivate with identical, constant site-loss yields $(-d\tau/dt)$ such that τ decreases at the same constant rate for both catalysts during reaction. Subsequent time-on-stream measurements of conversion are thus taken at contact times that are identical for catalysts A and B, as indicated by the points in Figure 6.1a. These data are plotted versus time on stream in Figure 6.1b. The conversion versus time curves differ between catalysts A and B, despite beginning at identical contact times and identical conversions, and losing active sites at the same rate. This difference in conversion versus time on stream is caused by differences in the slopes of

the conversion versus contact time curves between the two materials, and not by differences in the frequency at which sites are lost in each catalyst. This clearly demonstrates that conversion versus time-on-stream measurements conflate deactivation and reaction kinetics, and thus are imperfect assessors of catalyst deactivation when deactivation is caused by decreasing numbers of active sites.
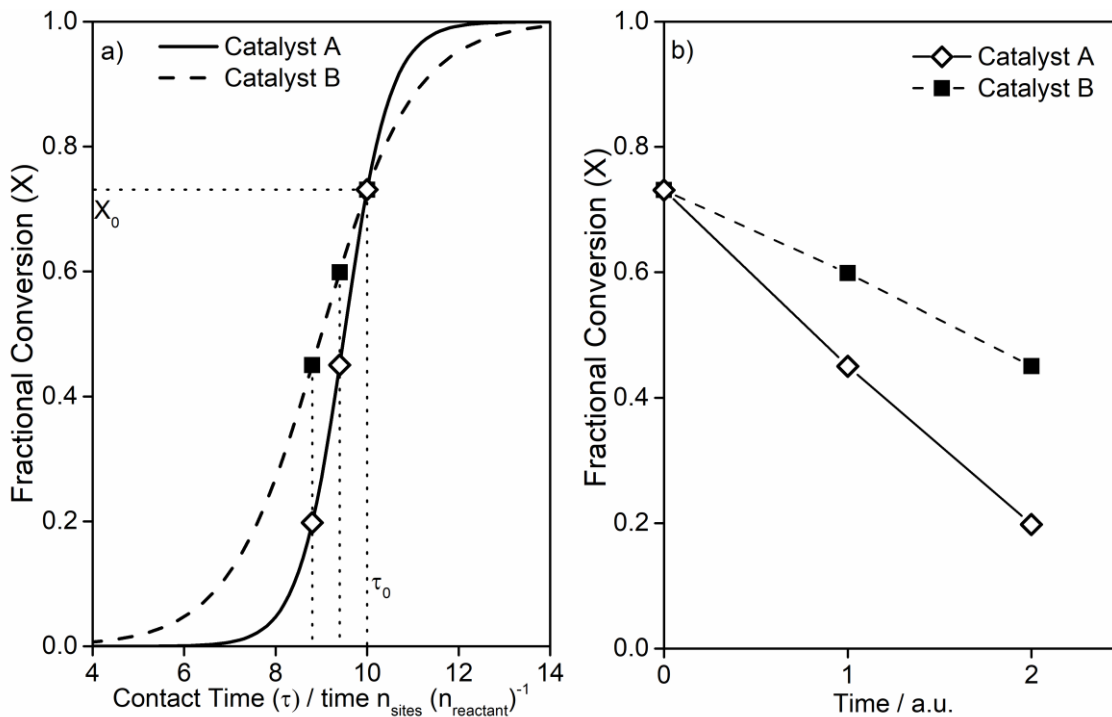
Figure 6.1: a) Fractional conversion versus contact time curves for catalysts A and B. Time-on-stream measurements were taken starting at identical contact times τ_0 and conversions X_0. Subsequent conversion measurements are indicated by points. b) Conversion versus time-on-stream measurements for catalysts A and B.

The calculation of site-loss yield requires the slopes of the conversion versus contact time and conversion versus time-on-stream data. The values for $dX/d\tau$ and dX/dt for each catalyst are approximated as the slopes of the linear fits of the data points in Figures 6.1a and 6.1b, respectively, and are reported in Figures 6.2a and 6.2b as

functions of conversion. With $dX/d\tau$ and dX/dt for catalysts A and B in hand, the site-loss yields $(-d\tau/dt)$ are easily calculated using eq. (6.2) over the conversion ranges of their respective experiments. Figure 6.3 shows that the site-loss yield for catalysts A and B are identical and constant, as was indicated in the setup of this hypothetical problem. This methodology analytically determines $-d\tau/dt$ and the accuracy of this measurement is not dependent on the models employed to fit conversion versus time-on-stream data. The site-loss selectivity and site-loss rate are found by dividing the site-loss yield by conversion and contact time, respectively.
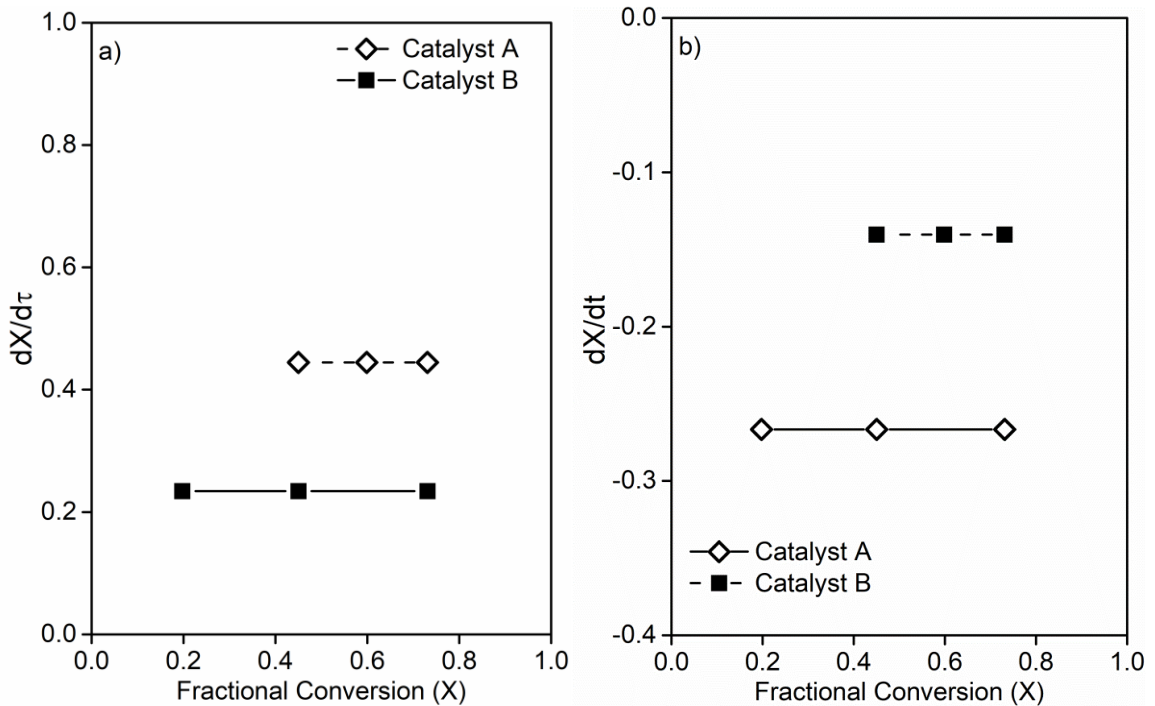
Figure 6.2: a) dX/dτ versus conversion for catalysts A and B as calculated by linear approximations of data in Figure 6.1a. b) dX/dt versus conversion for catalysts A and B as calculated by linear approximations of data in Figure 6.1b.
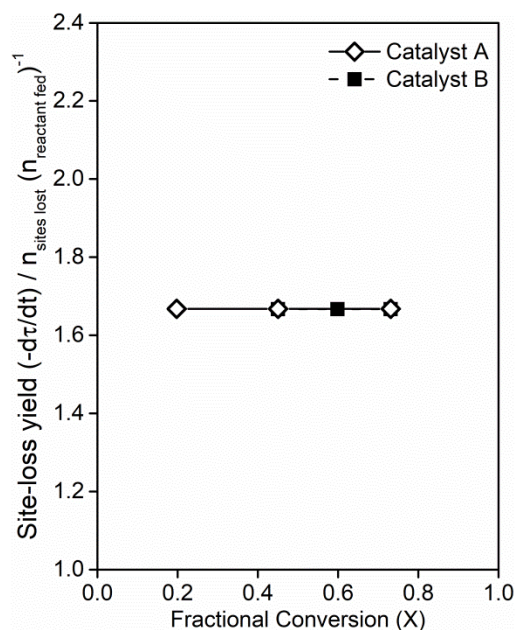
Figure 6.3: The site-loss yield versus conversion for hypothetical catalysts A and B calculated from eq. (6.2) using data reported in Figure 6.2.

6.3.2 Case 1: Nonselective Deactivation during MTH at Subcomplete Methanol Conversion

In systems that exhibit nonselective deactivation, contact time is the salient parameter describing the decrease in conversion with time on stream and eq. (6.2) can be used to calculate $d\tau/dt$. It has been previously reported that deactivation during MTH conversion is nonselective for ZSM-5,[107] ZSM-22, ZSM-23, EU-1,[108] and SAPO-5[109] catalysts in packed-bed reactors but is selective for SAPO-34[103] and ZSM-48[108] in packed-bed reactors, whose diffusive and shape-selective properties may be altered by coke deposition or the entrained organic co-catalysts may evolve with time on stream. We first demonstrate the measurement of site-loss yield in a system with nonselective deactivation: HZSM-5 during MTH catalysis in a packed-bed reactor.

190

Methanol-to-hydrocarbons conversion occurs through an autocatalytic mechanism on zeolite/zeotype catalysts.[110,111] Deactivation occurs at the front of the reactor bed during MTH catalysis in packed-bed reactors and formaldehyde (HCHO) is implicated as a chemical intermediate that mediates catalyst deactivation.[66–68,112,113] Conversion versus contact time and conversion versus time-on-stream data were measured during MTH catalysis with HCHO co-feeds for HZSM-5 (Zeolyst, CBV 8014) in a packed-bed reactor from 623–723 K. Physical and chemical characterization of the proton-form ZSM-5 material to assess porosity, crystal structure, and acid site density, and protocols for all experiments are provided in sections S2 and S6 of the Appendix. The X-ray diffraction pattern and scanning electron micrographs for this material have previously been reported in the Supporting Information by Ilias et al.[114] and Khare et al.[115], respectively. Conversion versus contact time data with 12 kPa methanol at 623–723 K on HZSM-5 measured in the absence of catalyst deactivation follow logistic curves characteristic of the autocatalytic MTH reaction, as shown in Figure 6.4a. To induce deactivation, HCHO was co-fed with methanol and the conversion was monitored with time on stream. Conversion versus time-on-stream data at 623 K with varying HCHO co-feed pressures are shown in Figure 6.4b. Following the methods described in the previous section, $dX/d\tau$ and dX/dt are approximated by the slopes of the linear fits depicted by the solid lines in Figure 6.4a and 6.4b, respectively. Note in Figure 6.4b that conversion versus time on stream appears to be linear even at methanol conversion near 100%, when an "S"-shaped curve is expected instead. Our inability to capture this shape for these data is attributed to small fluctuations in conversion, however this "S"-shaped curve was observed with 0.2 kPa HCHO at 12 kPa methanol, 673 K (see Figure A6.5b in the

Appendix). For systems with nonselective deactivation, an *instantaneous* site-loss yield is calculable, and thus a site-loss yield as a function of conversion, X, or contact time, τ, is determined, as opposed to *initial* conversion, X_0, or *initial* contact time, τ_0. The site-loss yields $(-d\tau/dt)$ calculated using eq. (6.2) are invariant with conversion at 623 K with HCHO co-feeds (Figure 6.4c). The data in Figure 6.4c considers that co-feeding HCHO negligibly changes $dX/d\tau$ as a function of methanol conversion, which is demonstrated for 0.2 kPa HCHO co-feed with 12 kPa methanol at 673 K in Figure A6.5a of the Appendix. Conversion versus time on stream and site-loss yield as a function of conversion for 673 K and 723 K are shown in Figures A6.1–A6.3 and the slope of the conversion versus contact time and conversion versus time-on-stream curves for 623–723 K are presented in Tables A6.1 and A6.2. Site-loss yield at ~50% conversion of methanol as a function of HCHO co-feed pressure is shown in Figure 6.4d for 623–723 K. Site-loss yield increases monotonically with HCHO co-feed pressure at all temperatures. Site-loss yield is invariant when temperature is increased from 623 to 673 K, but decreases from 673 to 723 K at identical HCHO co-feed pressure.

Co-fed HCHO is the primary chemical agent causing deactivation in these systems, as evidenced by the significantly lower site-loss yield in the absence of HCHO co-feeds (Figure 6.4d). Formaldehyde is completely consumed during MTH catalysis, even at contact times corresponding to ~20% conversion of methanol. This results in a site-loss yield that is invariant with contact time (and methanol conversion), as shown in Figure 6.4c, since increasing contact time beyond what is required to achieve complete HCHO conversion leads to minimal carbon deposition. Tripling the HCHO co-feed pressure from 0.2 kPa to 0.6 kPa increased the site-loss yield at 623 K from 5.9 x 10^{-5} to

3.7 x 10^{-4} mol H_{lost}^+ (mol MeOH)$^{-1}$ as shown in Figure 6.4d, a greater than six-fold increase. This greater than one-to-one increase in site-loss yield with increasing HCHO conversion can be rationalized by considering the site-loss selectivity of HCHO. The selectivity of HCHO to site-loss can be calculated by multiplying the site-loss yield calculated for methanol (eq. (6.7)) by the ratio of the methanol molar flow rate to the HCHO molar flow rate and dividing by the conversion of HCHO (eq. (6.8)).

$$\text{Site-loss yield of MeOH} = -\frac{d\tau_{MeOH}}{dt} = -\frac{1}{\dot{n}_{MeOH}}\frac{dn_*}{dt} \tag{6.7}$$

$$\begin{aligned}\text{Site-loss selectivity of HCHO} &= -\frac{1}{X_{HCHO}\dot{n}_{HCHO}}\frac{dn_*}{dt} \\ &= \frac{\dot{n}_{MeOH}}{X_{HCHO}\dot{n}_{HCHO}}\left(-\frac{d\tau_{MeOH}}{dt}\right)\end{aligned} \tag{6.8}$$

The selectivity of HCHO to site-loss at 623 K with 0.2 and 0.6 kPa HCHO co-feed pressure is shown in Table 6.1. Increasing the HCHO co-feed pressure from 0.2 to 0.6 kPa not only increases the amount of HCHO that can consume active sites, but also increases the propensity of HCHO to do so, as evidenced by the increase in HCHO site-loss selectivity with increasing HCHO co-feed pressure. These data suggest that there are competing pathways of HCHO consumption: one pathway that primarily leads to carbon deposition and a second pathway where the product is a non-coke species, and that the coke formation pathway is enhanced relative to the non-coke pathway by increasing HCHO pressure. This observation is in agreement with previous reports that HCHO alters the distribution of active hydrocarbon pool chain carriers and causes deactivation during MTH catalysis.[66,70] A mathematical explanation of this claim is provided in Section A6.3 of the Appendix.
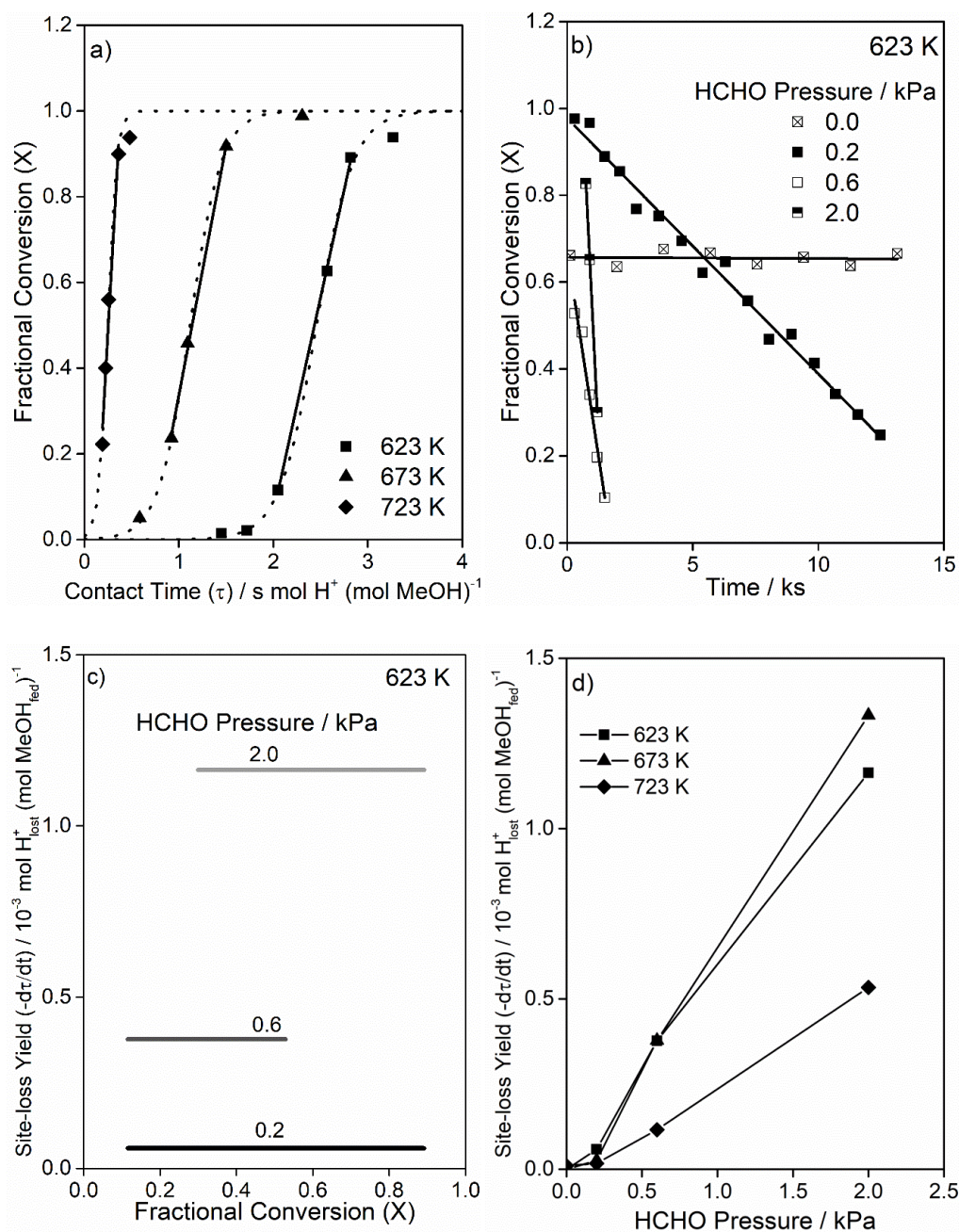
Figure 6.4: a) Fractional conversion versus contact time on HZSM-5 with 12 kPa methanol from 623–723 K. Dotted lines highlight the logistic shape of the conversion versus contact time curves. Solid lines are linear fits of the selected data. b) Fractional conversion versus time on stream with 12 kPa methanol and 0.0–2.0 kPa HCHO at 623 K. c) Site-loss yield versus methanol conversion with 12 kPa methanol and 0.2–2.0 kPa HCHO at 623 K. d) Site-loss yield at ~50% methanol conversion as a function of HCHO pressure with 12 kPa methanol from 623–723 K.

Table 6.1: Site-loss selectivity of formaldehyde at 623 K with 12 kPa methanol

Temperature / K	HCHO Pressure / kPa	Site-loss selectivity $(-1/X \, d\tau/dt)$ / 10^{-3} mol H^+_{lost} (mol HCHO consumed)$^{-1}$
623	0.2	3.5
623	0.6	7.5

6.3.3 Case 2: Nonselective Deactivation during MTH at Complete Methanol Conversion

The site-loss yield can be assessed at complete methanol conversion by recognizing that X in eq. (6.2) is not limited to conversion, but can be any quantity Y whose relationships with contact time and time on stream are known. In example, at complete methanol conversion with 12 kPa methanol and 0.2 kPa HCHO at 623 K on HZSM-5 the ethane/ethene ratio is linear with contact time from 6.2 to 12.4 s mol H^+ (mol MeOH)$^{-1}$, as shown in Figure 6.5a. Figure 6.5b shows that the ethane/ethene ratio decreases linearly with time on stream with 12 kPa methanol and 0.2 kPa HCHO at 623 K. The values for $dY/d\tau$ and dY/dt at complete methanol conversion are determined by the slopes of the linear fits in Figure 6.5a and 5b, respectively, and the site-loss yields are calculated using eq. (6.2). The site-loss yield at subcomplete and complete methanol conversion at 623 K with 0.2 kPa HCHO and 12 kPa methanol are compared in Table 6.2. As discussed in the previous section, site-loss yield is invariant with contact time because HCHO, which mediates the consumption of active sites, is completely consumed at short contact times (e.g., at less than 20% methanol conversion for the process conditions described above). Thus, if the presence of formaldehyde is what primarily determines site-loss yields, then it is expected that these yields will be largely invariant at subcomplete and complete methanol conversion. Site-loss yields measured at subcomplete and complete methanol conversion indeed agree within ~25%.
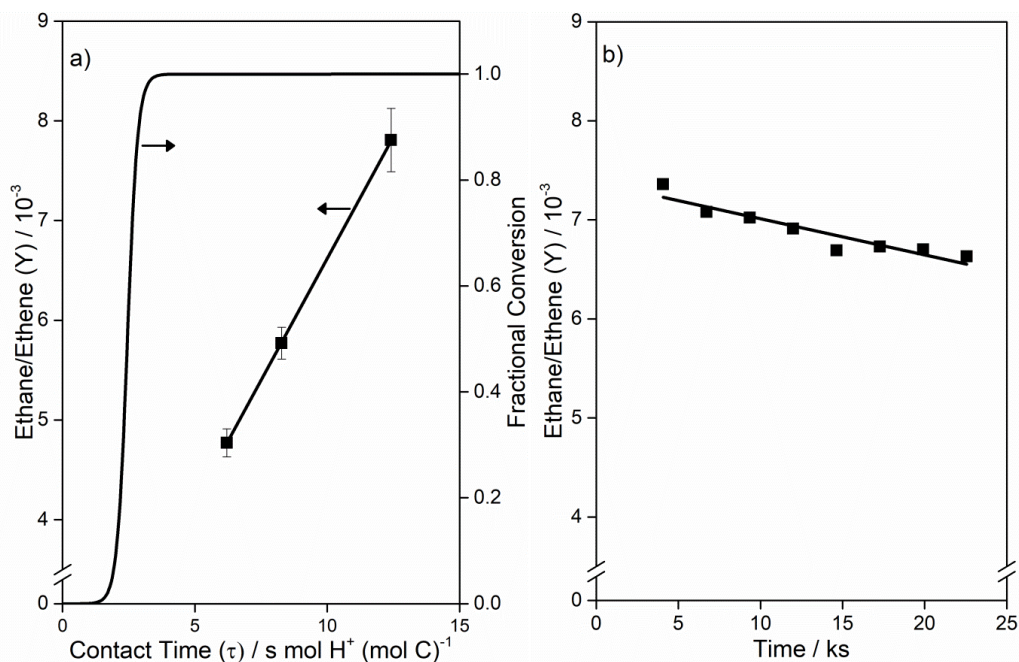
Figure 6.5: a) Ethane/ethene ratio versus contact time with 12 kPa methanol and 0.2 kPa HCHO at 623 K. Error bars represent two standard deviations of repeat experiments. b) Ethane/ethene ratio versus time with 12 kPa methanol and 0.2 kPa HCHO at 623 K. Solid lines represent linear fits.

Table 6.2: Site-loss yield calculated at subcomplete and complete methanol conversion.

Contact Time / s mol H^+ (mol MeOH)$^{-1}$	Conversion	Site-loss Yield ($-d\tau/dt$) / 10^{-4} mol H^+_{lost} (mol MeOH$_{fed}$)$^{-1}$
2.2 – 2.8	25 – 89%	0.59
6.2 – 12.4	100%	0.75

6.3.4 Case 3: Selective Deactivation during MTH

Instantaneous yields and selectivities for catalysts that undergo selective deactivation are difficult to interpret because fresh catalyst beds behave differently than partially deactivated beds. For such systems, cumulative selectivities are used to compare different reaction conditions.[66] Analogously, we posit that a quantitative assessment of deactivation for catalysts that do not undergo *nonselective* deactivation is the *cumulative*

site-loss selectivity defined in eq. (6.9). Cumulative site-loss selectivity has units of either (i) total moles sites lost per total moles reactant converted to effluent hydrocarbons, if omitting conversion to entrained hydrocarbons; or (ii) total moles sites lost per total moles reactant consumed, if including conversion to entrained hydrocarbons. The inverse of the cumulative site-loss selectivity is related to the inverse of the (i) total turnovers or (ii) total conversion capacity, which are already employed as metrics for catalyst lifetime.[27,67,116–118] In Figure 6.6, the cumulative site-loss selectivity on HSSZ-13, an MTH zeolite catalyst analogous in structure to HSAPO-34, is reported as a function of the initial contact time and the HCHO co-feed pressure based on the data reported by Hwang et al.[66] The cumulative site-loss selectivity increased monotonically with decreasing initial contact time and increasing HCHO co-feed pressures on HSSZ-13, similar to the monotonic increase in site-loss yield observed with increasing HCHO co-feed pressure observed on HZSM-5 (Figure 6.4d).

$$\text{Cumulative Site-loss Selectivity} = \frac{\int_0^\infty -\frac{dn_*}{dt}\,dt}{\int_0^\infty X\dot{n}_{R,0}\,dt} = \frac{n_{*,0}}{\int_0^\infty X\dot{n}_{R,0}\,dt} = \frac{\tau_0}{\int_0^\infty X\,dt} \qquad (6.9)$$

For systems with nonselective deactivation, the instantaneous site-loss selectivity/yield is a function of contact time and does not depend on the initial contact time, whereas the cumulative site-loss selectivity is a complex function of the instantaneous site-loss selectivity/yield, the *initial* contact time, and the reaction kinetics over the life of the catalyst. As a demonstration of this, consider a reaction system with n[th] order kinetics and constant site-loss yield γ described by eqs. (6.10) and (6.11), where k is the rate constant for the nth order reaction, X is conversion, P_R is the reactant

197
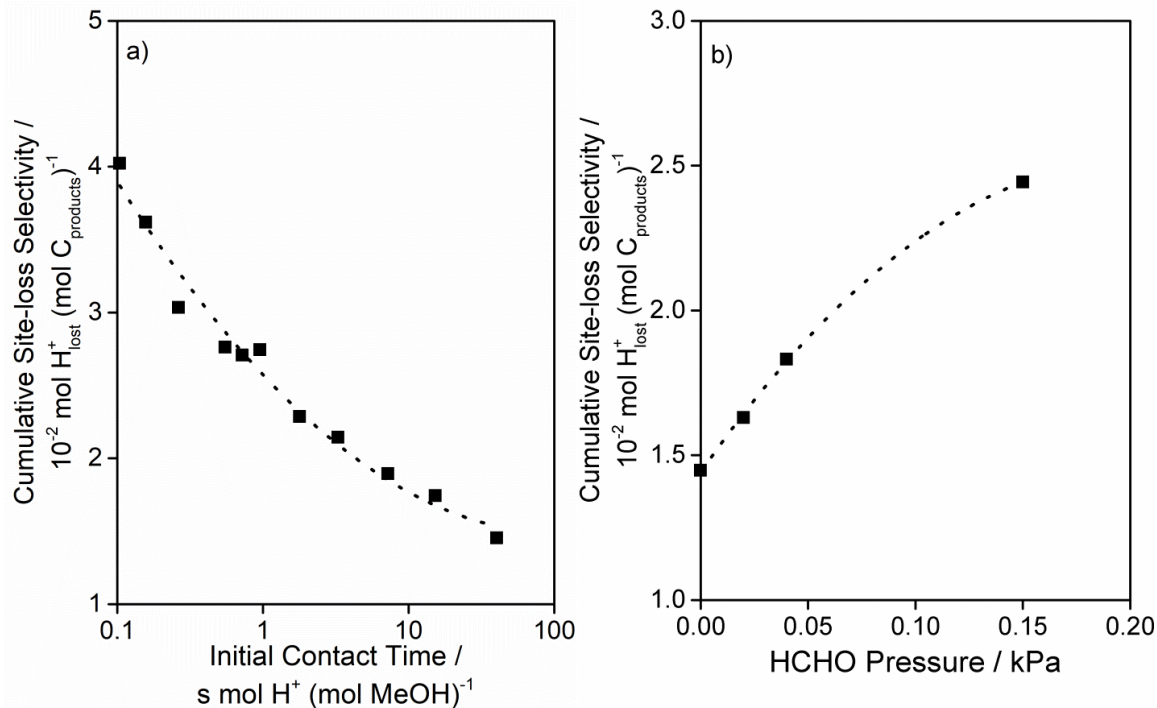
Figure 6.6: a) Cumulative site-loss selectivity as a function of the initial contact time on HSSZ-13 (Si/Al 8.4) with 22 kPa methanol at 623 K. b) Dependence of cumulative site-loss selectivity on HCHO co-feed pressure (9:1 mol H_2O:mol HCHO solution) on HSSZ-13 with 23 kPa methanol at 623 K. Dotted lines are to guide the eye. These data were reported by Hwang et al. in Journal of Catalysis **2017**, 346, 154–160.[66]

pressure, and τ_0 is the initial contact time. The cumulative site-loss selectivity for this system, given in eq. (6.12) (derived in Section A6.4 of the Appendix), is not only a function of the site-loss yield (γ), but also depends on the reaction kinetics and the initial contact time. The cumulative site-loss selectivity is a measure of the average frequency of deactivation events relative to the average frequency of product formation events over the life of the catalyst. In contrast, instantaneous site-loss rate, yield, and selectivity are quantitative measures of the instantaneous frequency of deactivation events normalized by the number of sites, molar reactant flow rate, and the instantaneous frequency of reaction events, respectively. In this way, instantaneous site-loss measures contain more

information about catalyst deactivation than cumulative site-loss selectivity and are the preferred assessors of deactivation when deactivation is nonselective.

$$\frac{dX}{kP_R^n} = d\tau \tag{6.10}$$

$$\tau = \tau_0 - \gamma t \tag{6.11}$$

Cumulative Site-loss Selectivity

$$= \tau_0 \left(\int_0^{\frac{\tau_0}{\gamma}} 1 - [(n-1)kP_{R0}^n(\tau_0 - \gamma t) + 1]^{\frac{1}{1-n}} dt \right)^{-1} \tag{6.12}$$

6.4 Conclusion

When deactivation is caused by the loss of active sites, conversion versus time-on-stream measurements are insufficient assessors of deactivation because these data conflate the reaction kinetics and the rate-of-change of contact time. Instead, we consider active sites as consumable akin to reacting species and on this basis propose that definitions of rate, yield, and selectivity, commonly used for describing transformations of reactants can be transposed to describe catalyst deactivation, which we refer to as the *site-loss* rate, *site-loss* yield, and *site-loss* selectivity. For reaction systems where deactivation is nonselective, that is, systems where product yields at a given contact time do not differ between fresh and partially deactivated catalysts, *instantaneous* site-loss rate, yield, and selectivity are assessors of deactivation. For systems where deactivation is selective, it is instead necessary to use *cumulative* site-loss selectivity, the ratio of total

199

sites lost to total moles reactant consumed or converted to effluent products, to assess deactivation, a metric inversely related to the total conversion capacity and total turnovers of a catalyst.

We demonstrate the utility of quantifying deactivation using the newly defined deactivation assessors by obtaining mechanistic insights into catalyst deactivation during methanol-to-hydrocarbons conversion with formaldehyde co-feeds. Site-loss selectivity of HCHO increases with increasing HCHO co-feed pressure, suggesting the existence of competing HCHO consumption pathways and suggesting that the pathways toward active site consumption are enhanced with increasing HCHO co-feed pressure.

Chapter 7

A kinetic evaluation of deactivation pathways in methanol-to-hydrocarbons catalysis on HZSM-5 with formaldehyde, olefinic, dieneic, and aromatic co-feeds

7.1 Conspectus

The dominant mechanism of formaldehyde-mediated deactivation during MTH catalysis on HZSM-5 is assessed by measuring site-loss yields and selectivities when co-feeding mixtures of formaldehyde, olefins, dienes, and aromatics with methanol. Site-loss selectivity of formaldehyde (HCHO) increases with increasing HCHO co-feed pressures, implying there is a deactivation pathway that is second-order in HCHO in competition with HCHO-consuming reactions that are first-order in HCHO and do not lead to deactivation, suggesting that HCHO reacts with itself or with a HCHO-derived species en route to deactivation. Co-feeding the HCHO-derived species in this selectivity-determining step should result in the site-loss selectivity becoming zero-order in HCHO since selectivity would no longer be limited about the formation of the HCHO-derived species. Reactions between HCHO-derived aromatics and HCHO as the predominant selectivity-determining steps leading to deactivation are ruled out on the basis that site-loss selectivity increases with HCHO co-feed partial pressure even with a 1.0 kPa co-feed of toluene, suggesting the prevalent deactivation pathway involves non-aromatic species that are (i) derived from HCHO and (ii) react with HCHO to cause deactivation. Dienes are known Prins-condensation products between HCHO and olefins, and co-feed experiments with 1.0 kPa of 1,3-butadiene increases the site-loss selectivity of 0.2 kPa HCHO from less than 0.01 mol H^+ mol $HCHO^{-1}$ to 0.4 mol H^+ mol $HCHO^{-1}$, compared to

0.005 and 0.0003 mol H^{+} mol HCHO[-1] with combined HCHO-toluene an HCHO-propylene co-feeds, respectively, implicating diene-based mechanisms as prevalent deactivation pathways during MTH catalysis with HCHO co-feeds.

7.2 Introduction

Formaldehyde (HCHO), formed in transfer dehydrogenation of methanol, has been implicated in shifting product selectivity towards unsaturated species, including polycyclic aromatic species, that cause deactivation of zeolite/zeotype materials during methanol-to-hydrocarbons (MTH) catalysis.[66–68,70,111,113,119–124] The network of reaction pathways that describe HCHO-mediated deactivation are, however, not yet well understood. Deactivation by polycyclic aromatics formation on solid-acid zeolite/zeotype catalyst during hydrocarbon/oxygenate chemistry at MTH relevant reaction temperatures are categorized into three general mechanisms (see Scheme 7.1): (i) alkyl-aromatics mechanism, (ii) diphenylmethane mechanism, and (iii) diene oligomerization mechanism.[125] The precise mechanism and relative importance of each of these deactivation pathways depends on the specific chemistry and relative rates of reactions, which vary with reaction conditions and zeolite topology.[125–130] In mechanism (i), a benzenium ion undergoes alkyl-chain growth and eventual dehydrocyclization to form polycyclic aromatic species.[20] An analogous HCHO-mediated alkyl-aromatics mechanism was proposed by Hwang and Bhan for MTH on CHA zeolite/zeotype materials as a potential HCHO-mediated deactivation pathway, where dehydrative alkylation of aromatics with HCHO forms a benzenium ion that can undergo secondary reactions to form polycyclic aromatics species via mechanism (i) (see Scheme 7.2(i)).[66]

In the diphenylmethane (DPM) mechanism (mechanism (ii)), a benzyl cation undergoes electrophilic substitution with an aromatic to form DPM, which undergoes dehydrogenative coupling to form polyaromatic speces.[125] This mechanism was proposed as a potential HCHO-mediated deactivation pathway during MTH catalysis by Martinez-Espin et al.,[72] who observed methyl-DPMs during MTH catalysis with benzene co-feeds. They proposed that HCHO alkylation of aromatics forms an aryl alcohol that can undergo dehydrative benzylation to form DPM, which can either form poly(DPM) by homologation or undergo dehydrogenative coupling to form polycyclic aromatic species (Scheme 7.2(ii)).[72] In mechanism (iii), dienes, especially cyclopentadienes, which have a propensity to form organic deposits in zeolites and other solid-acid catalysts,[125,131–134] oligomerize to form polycyclic aromatics. Dienes, including cyclopentadienes, are observed during MTH catalysis and non-cyclic dienes are products of Prins-condensation between HCHO and olefins on solid acid catalysts (Scheme 7.2 (iiia)),[70,135–137] and we further propose that the highly reactive cyclopentadiene species can be formed by dehydrative reaction with HCHO via a 2,4-diene-1-ol intermediate (Scheme 7.2 (iiib)). Cyclopentadienes have been shown to be active hydrocarbon pool chain carriers[86,138–140] and a recent report by Wang et al.[141] postulates that reactions between cyclopentadienes and aromatics lead to formation of polycyclic aromatics in HSSZ-13 based on π-bond interactions observed in solid-state two-dimensional NMR spectroscopy. It has also been demonstrated previously that acid-catalyzed reactions between aromatics and dienes leads to the formation of alkenyl-aromatics and diarylalkanes, which are intermediates in mechanism (i) and (ii) in Scheme 7.1, respectively.[142,143] Close proximity between cyclopentadiene and aromatics were not observed on HZSM-5 zeolite catalysts, which

Wang et al.[141] suggest may be why HZSM-5 has a lower susceptibility to form polycyclic aromatics than other MTH catalysts. Many different pathways likely simultaneously contribute to deactivation during MTH catalysis, but it is of interest to identify and understand the prominent deactivation pathways under MTH reaction conditions.[106,126]

Scheme 7.1: Polycyclic aromatic formation pathways on solid acid catalysts. Adapted from Guisnet and Magnoux.[125]
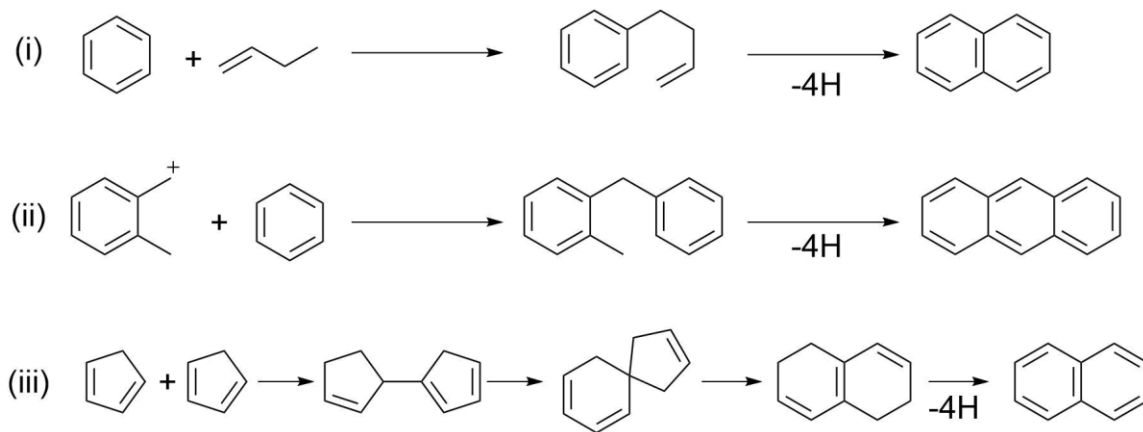
Scheme 7.2: Proposed HCHO-mediated deactivation pathways during MTH catalysis.
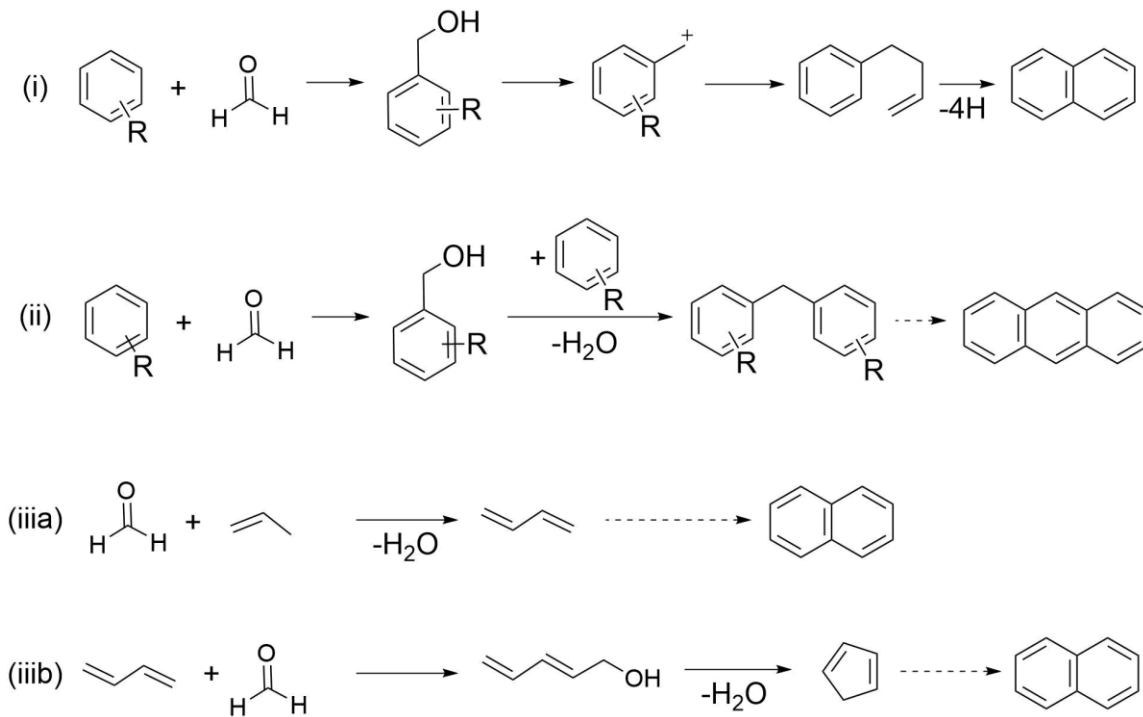
In Chapter 6, we defined metrics of yield, selectivity, and rate of deactivation for catalytic processes based on the concept of treating active sites as species that are consumed stoichiometrically in deactivation reactions.[144] These metrics are termed the *site-loss* yield, selectivity, and rate defined as (eqs. (7.1)-(7.3))[144]:

$$\text{Site-loss yield} = -\frac{d\tau}{dt} \ [=] \ \frac{\text{mol sites lost}}{\text{mol reactant fed}} \tag{7.1}$$

$$\text{Site-loss selectivity} = -\frac{1}{X}\frac{d\tau}{dt} \ [=] \ \frac{\text{mol sites lost}}{\text{mol reactant consumed}} \tag{7.2}$$

$$\text{Site-loss rate} = -\frac{1}{\tau}\frac{d\tau}{dt} \ [=] \ \frac{\text{mol sites lost}}{\text{s mol sites}} \tag{7.3}$$

where X is conversion, τ is contact time, defined as number of sites divided by the molar reactant flow rate, and t is time. These metrics enable the model-free assessment of deactivation as a function of reaction conditions (e.g., no assumptions regarding linear or exponential changes in rates with time or conversion are invoked), which allows the study of deactivation reactions with minimal assumptions regarding the precise deactivation and product-forming mechanisms. These metrics are assessed instantaneously, i.e., at a specified conversion or contact time, in reaction systems that exhibit nonselective deactivation, which is when conversion changes as a function of time exclusively because the contact time is decreasing with time on stream as active sites are consumed by deactivation reactions. For reaction systems that deactivate nonselectively, conversion is written as (eq. (7.4))[103,104,144]:

$$X = X\big(\tau(t)\big) \tag{7.4}$$

205

By taking the derivative of both sides of eq. (7.4) and rearranging we derive an equation for the site-loss yield (eq. (7.5))[104,144]:

$$-\frac{d\tau}{dt} = -\frac{dX}{dt}\left(\frac{dX}{d\tau}\right)^{-1} \tag{7.5}$$

The site-loss yield, $-d\tau/dt$, cannot be directly measured but is related to two measurable quantities, the change in conversion with time on stream, dX/dt, and the change in conversion (in the absence of deactivation) with contact time, $dX/d\tau$, by eq. (7.5).

Herein, we probe the mechanisms of deactivation by measuring the site-loss yield and selectivity while co-feeding combinations of representative species formed during MTH catalysis including formaldehyde, ethylene, propylene, 1,3-butadiene, and toluene under MTH reaction conditions on HZSM-5. We assess the functional dependence of rates of deactivation events on the partial pressure of HCHO with and without toluene co-feeds to elucidate potential HCHO-mediated deactivation pathways during MTH catalysis and determine the propensity of olefins, aromatics, and dienes to participate in these HCHO-mediated deactivation pathways.

7.3 Methods

7.3.1 Experimental methods for assessing conversion versus contact time and conversion versus time on stream

Formaldehyde trimers (1,3,5-trioxane, ≥99%, Sigma-Aldrich) were dissolved in methanol (Chromosolv, ≥99% purity, Sigma-Aldrich) and fed via syringe pump (Cole Parmer 78-0100C) into a heated stream of helium carrier gas (≥99.997%, Matheson).

Toluene (≥99.9, Sigma Aldrich) was fed via a separate syringe pump into the same helium carrier gas stream. Ethene (≥99.999%, Praxair), propylene (≥99.83%, Sigma-Aldrich) and 1,3-butadiene (≥99%, Sigma-Aldrich) and helium flow rates were regulated by mass flow controllers (Brooks SLA5850). The reactant flow rates were adjusted to achieve desired contact times and reactant partial pressures for each experiment. The reactant stream was fed to a quartz tube reactor (0.4–1 cm i.d.) containing HZSM-5 (Zeolyst, CBV8014, 0.012 g) zeolite catalysts (pressed, crushed and sieved into 177–400 μm aggregates) diluted with quartz sand (~0.1 g, 2 M HNO_3 washed, rinsed with deionized water, heated to 1273 K in flowing air for 12 h). Physical and chemical characterization of the HZSM-5 catalyst used in this study to assess porosity, crystal structure, and acid site density, and can be found in prior reports .[114,115,144] The quartz tube reactors were heated to reaction temperature (673 K) by a resistively heated furnace (National Element FA120) equipped with a PID controller (Watlow 96). A K-type thermocouple (Omega) monitored the temperature at the axial center of the reactor bed on the outside of the quartz tube reactor. Before each reaction the catalyst was regenerated by oxidative thermal treatment in air (Matheson, Ultra Zero Certified, 1.67 cm^3 s^{-1}) at 823 K for 6 h. The fractional conversion is defined such that methanol and dimethyl ether (DME) are both reactants, and is given by the total carbon molar flow rate minus the molar flow rate of non-methanol co-feeds (HCHO, ethylene, propylene, toluene, 1,3-butadiene), as shown in eq. (7.6), where $n_{C,i}$ and $\dot{n}_{i,out}$ ($\dot{n}_{i,in}$) are the carbon number and the molar effluent (influent) flow rates of species i, respectively.

Fractional Conversion

$$= \frac{\sum_i n_{C,i} \dot{n}_{i,out} - \left(2\dot{n}_{DME,out} + \dot{n}_{CH_3OH,out} + \sum_{i=\text{co-feeds}} n_{C,i}\dot{n}_{i,in}\right)}{\sum_i n_{C,i}\dot{n}_i - \sum_{i=\text{co-feeds}} n_{C,i}\dot{n}_{i,in}} \quad (7.6)$$

Conversion versus contact time $(dX/d\tau)$ data were obtained by measuring the conversion at 180 s time on stream for each reactant composition at three different initial contact times that spanned methanol conversion ranging from ~20% to ~80%. The 180 s time on stream was chosen because it was after the initiation of the hydrocarbon pool but before substantial deactivation reduced the number of active sites in the reactor bed. In each of these experiments, the conversion was also monitored with time on stream to obtain dX/dt for each reaction condition. The reactor effluent composition was determined by a gas chromatograph (Agilent 7890) equipped with an HP-Plot/Q column (30 m $\times$ 0.530 mm $\times$ 40 μm) in series with a CP-Molsieve 5Å column (25 m $\times$ 0.530 mm $\times$ 40 μm). The column outlets were connected to a thermal conductivity detector (TCD) preceding an oxidation-methanation reactor (Polyarc®, Activated Research Company) and a flame ionization detector (FID). The reactor effluent stream was injected directly into the GC or stored in 250 μL heated (373 K) stainless steel sample loops using a multi-position valve and analyzed shortly after the reaction.

7.3.2 Analysis of site-loss yields

To understand how site-loss yields change as a function of feed compositions, we separate the site-loss yield into the contributions of the individual deactivation pathways, as illustrated by eq. (7.7):

$$-\left(\frac{d\tau}{dt}\right)_{total} = -\sum_i \left(\frac{d\tau}{dt}\right)_{i=pathways} - \sum_i \sum_{j \neq i} \left(\frac{d\tau}{dt}\right)_{i+j}$$

$$-\sum_i \sum_{j \neq i} \sum_{\substack{k \neq \\ \{i,j\}}} \left(\frac{d\tau}{dt}\right)_{i+j+k} - \cdots \qquad (7.7)$$

where $-\left(\frac{d\tau}{dt}\right)_{total}$ is the total site-loss yield, $\left(\frac{d\tau}{dt}\right)_i$ is the site-loss yield as a result of

pathways originating solely from reactant i, $\left(\frac{d\tau}{dt}\right)_{i+j}$ is the site-loss yield of pathways

involving species that originated from both reactant i and j, etc. For example, site-loss

yields for deactivation during MTH catalysis without co-feeds and with HCHO co-feeds

are given by eqs. (7.8) and (7.9), respectively:

$$\left[-\left(\frac{d\tau}{dt}\right)_{total}\right]_{\text{no co-feed}} = \left[-\left(\frac{d\tau}{dt}\right)_{CH_3OH}\right]_{\text{no co-feed}} \qquad (7.8)$$

$$-\frac{d\tau}{dt}\bigg|_{HCHO} = \left[-\left(\frac{d\tau}{dt}\right)_{CH_3OH} - \left(\frac{d\tau}{dt}\right)_{HCHO} - \left(\frac{d\tau}{dt}\right)_{HCHO+CH_3OH}\right]_{HCHO} \qquad (7.9)$$

where $-\left(\frac{d\tau}{dt}\right)_{CH_3OH}$ is the contribution to site-loss yield of reaction pathways originating

solely from methanol reactants, $-\left(\frac{d\tau}{dt}\right)_{HCHO}$ is the contribution to site-loss yield of

reaction pathways originating solely from HCHO reactants, which does not include

HCHO formed *in situ* from CH_3OH, and $-\left(\frac{d\tau}{dt}\right)_{HCHO+CH_3OH}$ is the site-loss yield of

reaction pathways originating from both HCHO and CH_3OH reactant species. The

brackets in eqs. (7.8) and (7.9) indicate that the site-loss yields for each pathway

(CH_3OH, HCHO, or HCHO+CH_3OH pathway) are during the experiment with no co-

feed or with 0.2 kPa HCHO co-feed, respectively. The co-feed pressures are dropped for clarity, but unless explicitly stated, it is 0.2 kPa HCHO and 1.0 kPa for all other co-feeds. A schematic explaining the difference in deactivation pathways is depicted in Scheme 7.3, where HCHO+A causes deactivation, but HCHO can either originate from CH_3OH or from the HCHO co-feed. In Scheme 7.3, when HCHO originates from CH_3OH and reacts with A, it is part of the CH_3OH deactivation pathway. When co-fed HCHO causes deactivation by reaction with A, which originates exclusively from CH_3OH, then this deactivation is part of the CH_3OH+HCHO pathway.

Scheme 7.3: Hypothetical deactivation reaction scheme with CH_3OH, HCHO, and CH_3OH+HCHO deactivation pathways.

In general, we posit that the site-loss yield of a given pathway will decrease by increasing the number of co-feeds such that (eq. (7.10)):

$$\left[-\left(\frac{d\tau}{dt}\right)_{pathway\ A}\right]_{i\ co-feed} \geq \left[-\left(\frac{d\tau}{dt}\right)_{pathway\ A}\right]_{i+j\ co-feed} \tag{7.10}$$

Equation (7.10) states that co-feeding i and j has a lower site-loss yield for pathway A than when only co-feeding i. Under most conditions, eq. (7.10) holds because if co-feed j reacts with any species in pathway A, that reaction becomes part of pathway A+j, decreasing the yield of products in pathway A. For example, by co-feeding HCHO during methanol-to-hydrocarbon catalysis, it is unlikely that HCHO consumes a species

in a way that increases the likelihood that methanol causes deactivation, which mathematically gives eq. (7.11):

$$\left[-\left(\frac{d\tau}{dt}\right)_{CH_3OH}\right]_{no\ co-feed} \geq \left[-\left(\frac{d\tau}{dt}\right)_{CH_3OH}\right]_{HCHO} \tag{7.11}$$

and thus an increase in site-loss yield with the addition of HCHO co-feeds is attributed to HCHO-mediated deactivation pathways and not via mechanism where HCHO increases the site-loss yield of CH_3OH-only deactivation pathways. Similar arguments can be made for co-feeding, for example, toluene with HCHO. Our data suggests that olefins react with HCHO in routes that suppress deactivation.

The rationale for the assumption that site-loss yields for a particular pathway decrease with increasing co-feeds is discussed in the following example. In Scheme 7.4, we illustrate three scenarios where adding an additional co-feed (i) does not change, (ii) decreases, and (iii) increases the yield of product D from reactant A when adding the co-feed F, where D can be a stable product species or may itself represent the consumption of an active site. In (i), F does not react with A or with any other species in the network and is thus completely independent and non-interacting and therefore does not change the yield of A to D. In (ii), F reacts with B, an intermediate that reacts with A to form D, thus decreasing the amount of D that is formed from A because F intercepts a key reaction intermediate. In (iii), F reacts with C, a species that reacts with A to form a product E. By reaction with C, F decreases the concentration of C and thus limits how much A is consumed by reaction with C, which increases the yield of the pathway where A reacts with B to form D. If F reacted with A, B, and C, we would likely decrease the yield of A

to D, and only under serendipitous conditions where F selectively removes intermediate C will we expect an increase in the yield of A to D by addition of co-feed F.

Scheme 7.4: Change in yield of A to D when co-feeding another reactant, F.
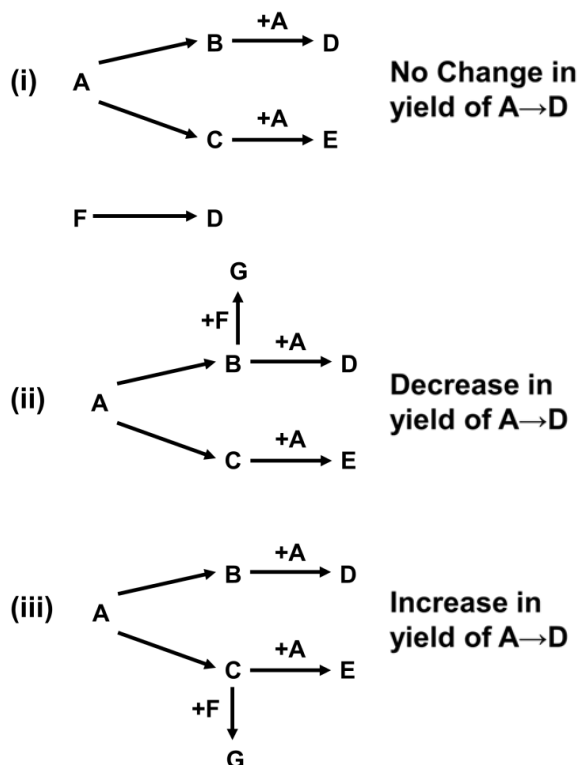
7.3.3 Analysis of site-loss selectivities

The site-loss selectivity of HCHO given in eq. (7.12) is a sum of the site-averaged rates of each deactivation reaction ($\langle r_{*,i} \rangle$) multiplied by the stoichiometric number for sites, $\nu_{*,i}$, in each overall reaction i, divided by the site-averaged rates of all reactions that consume HCHO, either deactivation reactions ($\langle r_{*,i} \rangle$) or product-forming reactions

$(\langle r_{P,i} \rangle)$, multiplied by the respective stoichiometric numbers of HCHO, $\nu_{HCHO,*,i}$, and $\nu_{HCHO,P,i}$:

$$\text{Site-loss selectivity of HCHO} = -\frac{1}{X_{HCHO}}\frac{d\tau_{HCHO}}{dt}$$

$$= \frac{\sum_i \nu_{*,i}\langle r_{*,i}\rangle}{\sum_i \nu_{HCHO,*,i}\langle r_{*,i}\rangle + \sum_i \nu_{HCHO,P,i}\langle r_{P,i}\rangle} \tag{7.12}$$

$$= \frac{\bar{\nu}_*\langle r_*\rangle}{\bar{\nu}_{HCHO,*}\langle r_*\rangle + \bar{\nu}_{HCHO,P}\langle r_P\rangle}$$

where $\bar{\nu}_*$, $\bar{\nu}_{HCHO,*}$, and $\bar{\nu}_{HCHO,P}$ are the weighted-average stoichiometric numbers for sites in site-loss reactions, HCHO consumption via site-loss reactions, and HCHO consumption via product-forming reactions, respectively, where the weights are the site-averaged rates, as illustrated in eq. (7.13) for $\bar{\nu}_*$:

$$\bar{\nu}_* = \frac{\sum_i \nu_{*,i}\langle r_{*,i}\rangle}{\sum_i \langle r_{*,i}\rangle} = \frac{\sum_i \nu_{*,i}\langle r_{*,i}\rangle}{\langle r_*\rangle} \tag{7.13}$$

and $\langle r_*\rangle$ and $\langle r_P\rangle$ are the sum of the site-averaged rates of each overall deactivation pathway. In this work, we assume that the average stoichiometric numbers (eq. (7.13)) are not strong functions of the reaction conditions, such that observed changes in selectivity (eq. (7.12)) primarily reflect changes in the site-averaged rates of deactivation and product-forming reactions. For example, if the site-loss selectivity of HCHO increases with HCHO, we presume that this is not because the average stoichiometry of deactivation reactions increased with increased HCHO pressures, but instead that the rate of deactivating reactions increased relative to the rate of non-deactivating reactions.

213

Herein, we investigate the relationship between the site-loss selectivity of HCHO as a function of HCHO co-feed pressure, and we assume that $\bar{v}_*$, $\bar{v}_{HCHO,*}$, and $\bar{v}_{HCHO,P}$ are weak functions of HCHO pressure, which means that the mechanisms of deactivation and HCHO incorporation into products are relatively invariant with HCHO pressure during MTH catalysis.

7.4 Results

Under typical MTH conditions, HCHO is formed *in situ* and reacts with unknown species to cause deactivation by formation of polycyclic aromatic species. We probe HCHO-mediated deactivation mechanisms during MTH catalysis on HZSM-5 by co-feeding species that are representative of the MTH hydrocarbon pool: ethylene and propylene for olefins, toluene for aromatics, and 1,3-butadiene for polyunsaturated non-aromatic species. By co-feeding hydrocarbon pool species with HCHO during MTH catalysis, we enhance the relative consumption of HCHO via that pathway. The quantitative comparison of site-loss yields with varying co-feeds enables determination of the propensity of various HCHO-mediated pathways to cause deactivation.

The site-loss yields for each reaction condition were assessed by measuring independently the slopes of the deactivation-free conversion versus contact time curves (dX/dτ) and the conversion versus time curves (dX/dt) during MTH catalysis with formaldehyde, olefinic, dienic, and aromatic co-feeds as reported in Table 7.1. The conversion versus contact time slopes with 1,3-butadiene co-feeds were not measured because deactivation was too rapid to identify a deactivation-free conversion for each reaction condition. Instead, dX/dτ during MTH with 1,3-butadiene co-feeds are taken as the average of the dX/dτ for all other co-feed conditions shown in Table 7.1 (no co-feed,

propylene, ethylene, toluene, HCHO, and combinations thereof) which are relatively invariant with co-feed, varying at most by 50% between the smallest (Propylene+Toluene+HCHO) and largest (Propylene+HCHO) dX/dτ.

Table 7.1: Slope of conversion versus contact time, conversion versus time curves, and site-loss yield with various co-feeds with 12 kPa methanol at 673 K and ~50% conversion in methanol.

Co-feeds[a]	dX/dτ / mol MeOH (mol H$^+$)$^{-1}$ s^{-1}	–dX/dt / 10^{-6} s^{-1}	Site-loss yield (–dτ/dt) / μmol H$^+_{lost}$ mol MeOH^{-1}
No co-feed	1.16	1.0	0.9
Propene	1.25	5.7	4.6
Toluene	1.19	15.	12.
HCHO	1.31	51.	39.
1,3-butadiene	1.23^b	880	720
Propene+HCHO	1.67	8.8	5.3
Propene+Toluene	1.15	12.	10.
Ethene+HCHO	1.28	36.	29.
Toluene+HCHO	1.27	100	81.
1,3-butadiene+HCHO	1.23^b	8000	6500
Propene+Toluene+HCHO	1.12	53.	47.

[a]Propylene, toluene, ethylene and butadiene co-feeds are 1 kPa, HCHO co-feed is 0.2 kPa
[b]Not measured. Taken as the average of all other dX/dτ values.

By comparison of the site-loss yields with and without HCHO co-feeds from the data reported in Table 7.1, we determine that the difference between the total site-loss yield when co-feeding 0.2 kPa HCHO and when there is no co-feed is (eq. (7.14)):

$$\left[-\left(\frac{d\tau}{dt}\right)_{total}\right]_{HCHO} - \left[-\left(\frac{d\tau}{dt}\right)_{total}\right]_{no\ co-feed}$$

$$= (39 - 0.9)\ \mu mol\ H^+_{lost}\ mol\ MeOH^{-1}_{fed} \qquad (7.14)$$

$$= 38\ \mu mol\ H^+_{lost}\ mol\ MeOH^{-1}_{fed}$$

demonstrating that HCHO co-feeds do increase the site-loss yield during MTH catalysis. We assess the contribution of each deactivation pathway (CH$_3$OH only, HCHO only, and

HCHO+CH$_3$OH) by writing the total site-loss yields shown in eq. (7.14) as a sum of each

deactivation pathway (see eq. (7.7)), such that (eqs. (7.15) and (7.16)):

$$\left[-\left(\frac{d\tau}{dt}\right)_{total}\right]_{HCHO} = \left[-\left(\frac{d\tau}{dt}\right)_{CH_3OH} - \left(\frac{d\tau}{dt}\right)_{HCHO} - \left(\frac{d\tau}{dt}\right)_{HCHO+CH_3OH}\right]_{HCHO} \quad (7.15)$$

$$\left[-\left(\frac{d\tau}{dt}\right)_{total}\right]_{no\ co-feed} = \left[-\left(\frac{d\tau}{dt}\right)_{CH_3OH}\right]_{no\ co-feed} \quad (7.16)$$

where the brackets indicate which co-feeds are present in the reaction and the subscripts

on $(d\tau/dt)$ indicates which reactants each site-loss yield originates from. We posit that

the site-loss yield of the CH$_3$OH pathway with no co-feed is greater than or equal to the

site-loss yield of the CH$_3$OH pathway during MTH with a HCHO co-feed (see eq. (7.10))

such that (eq. (7.17)):

$$\left[-\left(\frac{d\tau}{dt}\right)_{CH_3OH}\right]_{no\ co-feed} \geq \left[-\left(\frac{d\tau}{dt}\right)_{CH_3OH}\right]_{HCHO} \quad (7.17)$$

By combination of eqs. (7.14)-(7.17), we can estimate the site-loss yields of HCHO-

mediated pathways when co-feeding HCHO at the reaction conditions shown in Table 7.1

as eq. (7.18):

$$38\ \mu mol\ H^+_{lost}\ mol\ MeOH^{-1}_{fed} \leq \left[-\left(\frac{d\tau}{dt}\right)_{HCHO} - \left(\frac{d\tau}{dt}\right)_{HCHO+CH_3OH}\right]_{HCHO}$$
$$\leq 39\ \mu mol\ H^+_{lost}\ mol\ MeOH^{-1}_{fed} \quad (7.18)$$

Equation (7.18) demonstrates that deactivation events originating from HCHO co-feeds

(38-39 μmol H$^+_{lost}$ mol MeOH$^{-1}_{fed}$) accounts for between 97% and 100% of the total site-

loss yield (39 μmol H^+_{lost} mol $MeOH^{-1}_{fed}$) when co-feeding HCHO. Thus we conclude that HCHO increases the site-loss yield during MTH either by HCHO-only deactivation pathways or via reaction pathways involving both HCHO and CH_3OH as the originating reactants, as is expected because HCHO has been implicated as a key chemical intermediate for causing deactivation during MTH catalysis.[66–68,70,113,119,120,124]

The site-loss yield for MTH catalysis with 0.2 kPa HCHO and 1.0 kPa toluene (C_7H_8) co-feeds (81 μmol H^+_{lost} mol $MeOH^{-1}$) is larger than the sum of the independent site-loss yields for 0.2 kPa HCHO (39 μmol H^+_{lost} mol $MeOH^{-1}$) and 1.0 kPa toluene (12 μmol H^+_{lost} mol $MeOH^{-1}$) co-feeds. The difference between the site-loss yields for HCHO+toluene co-feeds and for HCHO and toluene co-feeds independently gives eq. (7.19):

$$
\begin{aligned}
&\left[-\left(\frac{d\tau}{dt}\right)_{CH_3OH} - \left(\frac{d\tau}{dt}\right)_{HCHO} - \left(\frac{d\tau}{dt}\right)_{C_7H_8} - \left(\frac{d\tau}{dt}\right)_{CH_3OH+HCHO} \right.\\
&\qquad - \left(\frac{d\tau}{dt}\right)_{CH_3OH+C_7H_8} - \left(\frac{d\tau}{dt}\right)_{HCHO+C_7H_8} \\
&\qquad \left. - \left(\frac{d\tau}{dt}\right)_{CH_3OH+HCHO+C_7H_8}\right]_{HCHO+C_7H_8} \\
&\quad - \left[-\left(\frac{d\tau}{dt}\right)_{CH_3OH} - \left(\frac{d\tau}{dt}\right)_{HCHO} - \left(\frac{d\tau}{dt}\right)_{CH_3OH+HCHO}\right]_{HCHO} \\
&\quad - \left[-\left(\frac{d\tau}{dt}\right)_{CH_3OH} - \left(\frac{d\tau}{dt}\right)_{C_7H_8} - \left(\frac{d\tau}{dt}\right)_{CH_3OH+C_7H_8}\right]_{C_7H_8} \\
&= 30\ \mu\text{mol}\ H^+_{lost}\ \text{mol}\ MeOH^{-1}_{fed}
\end{aligned}
\tag{7.19}
$$

A range for the values of site-loss yields of combined HCHO+C_7H_8 pathways is assessed using eq. (7.10), from which eq. (7.19) simplifies to eq. (7.20):

30 μmol H_{lost}^+ mol $MeOH_{fed}^{-1}$

$$\leq \left[-\left(\frac{d\tau}{dt}\right)_{HCHO+C_7H_8} - \left(\frac{d\tau}{dt}\right)_{CH_3OH+HCHO+C_7H_8} \right]_{HCHO+C_7H_8} \quad (7.20)$$

$$\leq 81 \ \mu mol \ H_{lost}^+ \ mol \ MeOH_{fed}^{-1}$$

Equation (7.20) shows that the fraction of the site-loss yield caused by $HCHO+C_7H_8$ pathways (30-81 μmol H_{lost}^+ mol $MeOH_{fed}^{-1}$) accounts for between 37% and 100% of the total site-loss yield when co-feeding HCHO and C_7H_8 (81 μmol H_{lost}^+ mol $MeOH_{fed}^{-1}$) during MTH catalysis. Thus, we conclude that when co-feeding HCHO and C_7H_8 during MTH catalysis the site-loss yield of the combined $HCHO+C_7H_8$ is significant; it is on the order or larger than the site-loss yield expected for the $CH_3OH+HCHO$ pathway ($\leq$ 39 μmol H_{lost}^+ mol $MeOH_{fed}^{-1}$) at this reaction condition, clearly demonstrating that reaction between HCHO and aromatics can lead to deactivation during MTH catalysis on HZSM-5, but HCHO pathways not involving toluene that lead to deactivation may still account for as much as 63% of the total site-loss yield when co-feeding $HCHO+C_7H_8$. By a similar analysis for 1,3-butadiene and HCHO co-feeds, we find from the data in Table 7.1 that (eq. (7.21)):

5700 μmol H_{lost}^+ mol $MeOH_{fed}^{-1}$

$$\leq \left[-\left(\frac{d\tau}{dt}\right)_{HCHO+C_4H_4} - \left(\frac{d\tau}{dt}\right)_{CH_3OH+HCHO+C_4H_4} \right]_{HCHO+C_4H_4} \quad (7.21)$$

$$\leq 6500 \ \mu mol \ H_{lost}^+ \ mol \ MeOH_{fed}^{-1}$$

implicating reactions between HCHO and polyunsaturated non-aromatic species such as 1,3-butadiene as potential deactivation pathways during MTH catalysis. Equation (7.21) suggests that when co-feeding both HCHO+C_4H_4, combined HCHO+C_4H_4 deactivation pathways account for at least 88% of the total site-loss yield, while the C_4H_4 deactivation pathways account for at most 720 μmol H^+_{lost} mol $MeOH^{-1}_{fed}$ (see Table 7.1) or 11% of the total site-loss yield observed at these conditions. Finally, we consider the deactivation pathways between HCHO and olefins by co-reacting HCHO and propylene with methanol. We find that the total site-loss yield for HCHO+propylene is lower than the total site-loss yield with HCHO co-feed, suggesting that propylene decreases the propensity of HCHO to cause deactivation. This is in agreement with previous results that demonstrate that co-feeding olefins during MTH catalysis mitigates deactivation.[145,146] Because site-loss is a terminal reaction product, the site-loss yields of each pathway must be non-negative, and thus the site-loss yield of HCHO deactivation pathways must be decreased by propylene co-feeds. This suggests that there are competing pathways for HCHO consumption: reactions between HCHO with aromatics or dienes to cause deactivation and reaction between HCHO and olefins to form non-deactivation products. This analysis delineates these competing pathways that determine the fate of HCHO to either consume active sites and cause deactivation or be incorporated into non-deactivation products, but does not shed light on the relative importance of each pathway during MTH catalysis. By measuring how site-loss yields and selectivities vary as functions of HCHO co-feed partial pressures, we can eliminate mechanisms that are incongruent with these experimental observations to determine which pathways,

aromatic-based or diene-based deactivation pathways, are more prevalent during deactivation on HZSM-5 when co-feeding HCHO. Specifically, we will

The site-loss yield as a function of HCHO co-feed pressure with and without a 1 kPa C_7H_8 co-feed is shown in Figure 7.1a, and the difference between these two curves is shown in Figure 7.1b. The trend in Figure 7.1a suggests that the total site-loss yields when co-feeding only HCHO or HCHO+C_7H_8 are both proportional to formaldehyde to powers greater than one (eqs. (7.22) and (7.23)):

$$\left[-\left(\frac{d\tau}{dt}\right)_{total}\right]_{HCHO} \propto P_{HCHO}^{\alpha}, \alpha > 1 \tag{7.22}$$

$$\left[-\left(\frac{d\tau}{dt}\right)_{total}\right]_{HCHO+C_7H_8} \propto P_{HCHO}^{\beta}, \beta > 1 \tag{7.23}$$

The trend in Figure 7.1b shows that the difference between the total site-loss yield with HCHO+C_7H_8 and the total site-loss yield with just HCHO co-feed is approximately proportional to the co-feed pressure of HCHO (eqs. (7.24)):

$$\left[-\left(\frac{d\tau}{dt}\right)_{total}\right]_{HCHO+C_7H_8} - \left[-\left(\frac{d\tau}{dt}\right)_{total}\right]_{HCHO} \overset{\propto}{\sim} P_{HCHO} \tag{7.24}$$

From eq. (7.12), we also calculate the site-loss selectivity of HCHO (mol sites lost per mol HCHO consumed) with and without a toluene co-feed, as shown in Figure 7.1c. In all experiments with HCHO+C_7H_8 co-feeds, assuming a stoichiometry of 1 HCHO:1 site-loss, the site-loss selectivity of HCHO is $\lesssim$ 1%, suggesting that most of the HCHO consumed does not lead to deactivation. The site-loss selectivity increases with increasing HCHO pressure (Figure 7.1c), such that (eq. (7.25)):

$$-\frac{1}{X_{HCHO}}\frac{d\tau_{HCHO}}{dt} = \frac{\bar{v}_*\langle r_*\rangle}{\bar{v}_{HCHO,*}\langle r_*\rangle + \bar{v}_{HCHO,P}\langle r_P\rangle} \overset{\propto}{\sim} P_{HCHO} \tag{7.25}$$

Because the site-loss selectivity is approximately proportional to the HCHO pressure (eq. (7.25)), we conclude that (i) $\bar{v}_{HCHO,*}\langle r_*\rangle \ll \bar{v}_{HCHO,P}\langle r_P\rangle$ such that most of the HCHO is consumed in non-deactivating reactions, because if $\bar{v}_{HCHO,*}\langle r_*\rangle \gg \bar{v}_{HCHO,P}\langle r_P\rangle$ then the left-hand side of eq. (7.25) would simplify to $\bar{v}_*/\bar{v}_{HCHO,*}$ which is not a function of HCHO pressure, and (ii) the ratio of the rate of deactivation reactions divided by the rate of HCHO-consuming product formation reactions is proportional to HCHO pressure (eq. (7.26)):

$$\frac{\langle r_*\rangle}{\langle r_P\rangle} \overset{\propto}{\sim} P_{HCHO} \tag{7.26}$$

Conclusion (i) is further supports the hypothesis that most of the HCHO co-fed in these experiments is incorporated into products and do not lead to deactivation. Thus far, we have investigated quantitatively the impact of varying the co-feed identities on the site-loss yield (Table 7.1) and how the site-loss yield and selectivities change as functions of HCHO co-feed pressure (Figure 7.1 and eqs. (7.22)-(7.26)), next we will rationalize these data with potential deactivation mechanisms.

With only HCHO co-feeds, the prevailing site-loss pathways are HCHO and HCHO+CH_3OH pathways (eq. (7.18)), and the site-loss yields of these pathways is greater than order one in HCHO co-feed pressure (eq. (7.22)) and the site-loss rate, $\langle r_*\rangle$, is higher order in HCHO pressure than the rate of the competing reaction pathway to incorporate HCHO into products, $\langle r_P\rangle$ (eq. (7.26)). The simplest explanation for this observation is that the rate of the deactivation pathway is order ~2 in HCHO, while the
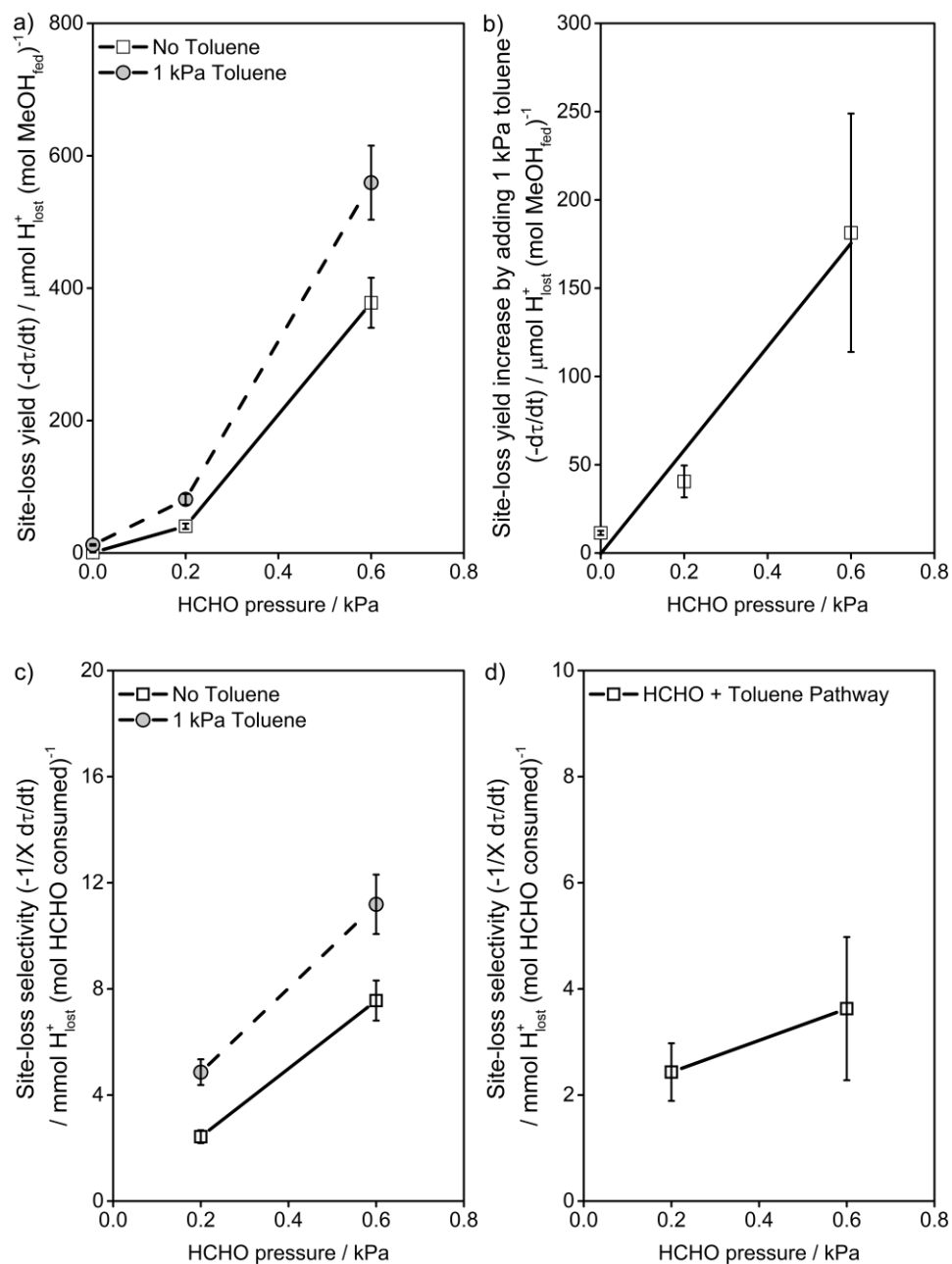
Figure 7.1: a) Site-loss yield of methanol as a function of HCHO co-feed pressure with and without a 1 kPa C_7H_8 co-feed, b) the increase in the site-loss yield when adding 1 kPa C_7H_8 as a function of HCHO co-feed pressure, c) the site-loss selectivity of HCHO as a function of HCHO co-feed pressure with and without 1 kPa C_7H_8 co-feed, and d) site-loss selectivity of the HCHO+Toluene pathway if it is merely additive to the HCHO deactivation pathway, at 673 K with 12 kPa CH_3OH and 50% conversion of CH_3OH, 100% conversion of HCHO.

rate of HCHO incorporation into products is order ~1 in HCHO. This implies that HCHO either reacts with itself to cause deactivation or reacts with a species whose concentration increases with increasing HCHO partial pressure. For example, in Scheme 7.2 the alkylaromatic and diphenylmethane deactivation mechanisms both involve the reaction between HCHO and an aromatic, and thus if this step is the selectivity-determining step for whether HCHO forms a product or causes deactivation, we might expect the rate of this step to be given by $\langle r_* \rangle \propto P_{HCHO} P_{aromatic}$. It has been demonstrated previously that HCHO increases the selectivity towards aromatic species during MTH catalysis on HZSM-5, and thus it is plausible that $P_{aromatic} \propto P_{HCHO}$ and thus $\langle r_* \rangle \propto (P_{HCHO})^2$ while HCHO incorporation into products by reaction with other hydrocarbon species, such as olefins, is only first-order in HCHO such that $\langle r_P \rangle \propto P_{HCHO}$. The ratio of these two rates, $\langle r_* \rangle / \langle r_P \rangle$, would then increase with increasing HCHO pressure, as observed in Figure 7.1a and shown in eq. (7.26). However if this were the case, then co-feeding aromatics would lead to $\langle r_* \rangle \propto P_{HCHO} P_{aromatic}$ where $P_{aromatic}$ is approximately the co-feed pressure of aromatics and would not be a function of HCHO, and thus $\langle r_* \rangle / \langle r_P \rangle \propto (P_{HCHO})^0$ since the rate of both reactions would now be first-order in HCHO partial pressure, which is not the trend observed in Figure 7.1c. In addition, if $\langle r_* \rangle \propto P_{HCHO} P_{aromatic}$ as expected for the alkylaromatic or diphenylmethane deactivation pathways and reaction of HCHO with a non-aromatic species lead to incorporation into products, then $\langle r_* \rangle / \langle r_P \rangle \propto (P_{aromatic})^1$ is expected. However, co-feeding 0.2 kPa HCHO+1.0 kPa C_7H_8 increases the aromatics pressure by many orders of magnitude relative to co-feeding only 0.2 kPa HCHO (< 0.1 kPa aromatics at < 20% CH_3OH conversion, where deactivation occurs), but the site-loss selectivity only increases by a

factor of ~2. This suggests that the ratio of the rates of site-loss and product formation from HCHO in selectivity-determining steps is nearly invariant with aromatics pressures, $\langle r_* \rangle / \langle r_P \rangle \overset{\propto}{\sim} (P_{aromatics})^0$. This is inconsistent with HCHO alkylation of aromatics as a selectivity-determining reaction. Instead, a different non-aromatic species that is derived from co-fed HCHO but leads to deactivation must be involved in the reaction that determines whether HCHO causes deactivation instead of being incorporated into products.

Dehydrative Prins-condensation of HCHO with olefin forms dienes, as illustrated in mechanism (iiia) in Scheme 7.2.[66,70,71] Dienes are precursors to species that can undergo dehydrocyclization to form aromatics and dienes are formed as products of HCHO-olefin reactions, such that diene partial pressure may be a positive order function of HCHO.[124] If the selectivity-determining step is the reaction between HCHO and dienes, and $P_{diene} \propto P_{HCHO}$ as a result of dienes being Prins-condensation products of HCHO, the rate of the selectivity determining step would be expected to be second-order in P_{HCHO} ($\langle r_* \rangle \propto P_{HCHO} P_{diene} = (P_{HCHO})^2$), and would be consistent with eq. (7.26) with or without aromatic co-feeds. Co-feeding 1.0 kPa 1,3-butadiene with 0.2 kPa HCHO results in a site-loss yield for HCHO+C_4H_4 pathways that are in excess of 5700 μmol H_{lost}^+ mol $MeOH_{fed}^{-1}$, compared to the maximum site-loss yield for HCHO+C_7H_8 pathways when co-feeding 1.0 kPa toluene with 0.2 kPa HCHO of 81 μmol H_{lost}^+ mol $MeOH_{fed}^{-1}$. In Figure 7.2, we compare the site-loss selectivity of 0.2 kPa HCHO with no additional co-feed or with 1.0 kPa of toluene, propylene, or 1,3-butadiene, where the site-loss selectivity is less than 0.01 mol H^+ mol $HCHO^{-1}$ in all

cases except when co-feeding 1,3-butadiene, where the site-loss selectivity is nearly 0.4 mol H^+ mol $HCHO^{-1}$. We postulated above that aromatics or dienes formation may be limiting the selectivity of HCHO to site-loss as an explanation for why site-loss selectivity increases with increasing HCHO co-feed pressure. If this is the case, we expect that co-feeding the limiting species will then significantly enhance the site-loss selectivity of HCHO, which is observed when co-feeding 1,3-butadiene but not when co-feeding toluene. This result combined with the trend in site-loss selectivity with HCHO pressure when co-feeding aromatics (Figure 7.1c and eq. (7.26)) suggests that reaction of HCHO with aromatics is not likely the predominant deactivation pathway when co-feeding HCHO during MTH catalysis (mechanisms (i) and (ii) in Scheme 7.2). We instead propose that diene-mediated pathways, such as mechanisms (iiia) and (iiib) in Scheme 7.2, are the primary deactivation pathways at these reaction conditions.
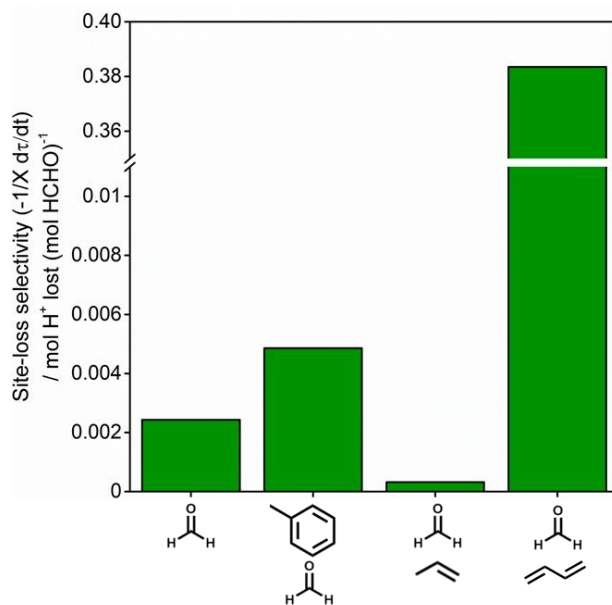
Figure 7.2: Site-loss selectivity of HCHO with varying co-feed combinations during methanol-to-hydrocarbons conversion on HZSM-5 at 673 K with 12 kPa CH_3OH, 50% conversion of CH_3OH and 100% conversion of HCHO.

We propose a plausible deactivation mechanism in Scheme 7.5 to rationalize experimental measurements of site-loss yields and selectivities. HCHO is consumed via reaction with aromatics, olefins, or dienes. When HCHO reacts with olefins, dienes are formed and no deactivation occurs. This dienic species can then react via one of two competitive pathways to cause deactivation by reaction with HCHO or to form aromatics by reaction with olefins or methanol. Alternatively, deactivation can occur via reaction of aromatics with HCHO. When only HCHO is co-fed with CH_3OH, non-deactivating consumption of HCHO by reaction with olefins predominates, and a small amount of HCHO is consumed via reaction with dienic species or with aromatic species to consume active sites. Both aromatic and dienic species are formed from HCHO, and thus the selectivity of each of these pathways increases with HCHO pressure because they are both second-order in HCHO while the non-deactivating reaction pathway with olefins is only first-order in HCHO. When aromatics are co-processed with HCHO and CH_3OH, the selectivity of the aromatics deactivation pathway is increased, but the site-loss selectivity of HCHO increases with HCHO co-feed pressure because the pathway involving reaction of HCHO with dienic species contributes non-negligibly to the site-loss yield. This also suggests that when co-feeding aromatics with HCHO, most of the HCHO is consumed via non-deactivation pathways, since the site-loss selectivity increases with HCHO pressure, in agreement with the site-loss selectivities reported for 0.2 kPa HCHO co-feed with various additional co-feeds shown in Figure 7.2.

Scheme 7.5: Potential deaction pathways that qualitatively agree with observed trend in site-loss yield and site-loss selectivities during methanol-to-hydrocarbons conversion with co-feeds.
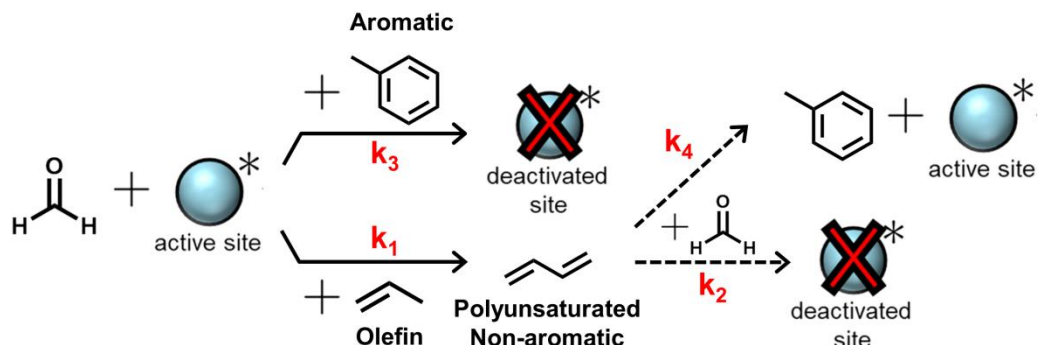
The relationship between site-loss yield and HCHO pressure with and without a toluene co-feed is quantitatively similar (Figure 7.1a and eqs. (7.22) and (7.23)) suggesting that the prevailing deactivation mechanism is unchanged by co-feeding toluene. The difference between the site-loss yield with and without C_7H_8 co-feed is positive order in HCHO pressure (Figure 7.1b). In Scheme 7.5, this is rationalized by the fact that with or without the aromatic co-feed, the diene-based deactivation pathway dominates, and the selectivity of this pathway increases with increasing HCHO pressure, in agreement with the increasing site-loss selectivity with increasing HCHO co-feed pressure, as observed in Figure 7.1c. The difference in site-loss yield increases proportionally to HCHO pressure (Figure 7.1d) because an additional pathway, the aromatic-based pathway, contributes to deactivation when toluene is co-fed, and the yield of this pathway is first-order in HCHO pressure when co-feeding toluene. The non-deactivating pathway is the reaction between HCHO and olefins to form aromatics via diene intermediates and is also first-order in HCHO, and thus the selectivity of the HCHO+C_7H_8 pathway is nearly invariant with HCHO co-feed pressure, in agreement with the experimental results shown in Figure 7.1d.

227

We demonstrate that the experimental observations are described qualitatively for the reaction network in Scheme 7.5 with rate constants chosen to obtain the trends that agree qualitatively with the experimental data ($k_1 = 1$, $k_2 = 10$, $k_3 = 0.01$, and $k_4 = 100$ au), as shown in in Figure 7.3, where the site-loss yield increases greater than proportionally as a function of HCHO co-feed pressure with and without a 1 kPa toluene co-feed, and the increase resulting from the addition of 1 kPa toluene is proportional to the HCHO co-feed pressure. The site-loss selectivity predicted by this model is reported in Figure 7.4, where co-feeding 0.2 kPa HCHO has much lower site-loss selectivity than 0.2 kPa HCHO with 1.0 kPa 1,3-butadiene, but adding 1.0 kPa toluene only marginally increases the site-loss selectivity relative to the 0.2 kPa HCHO case.
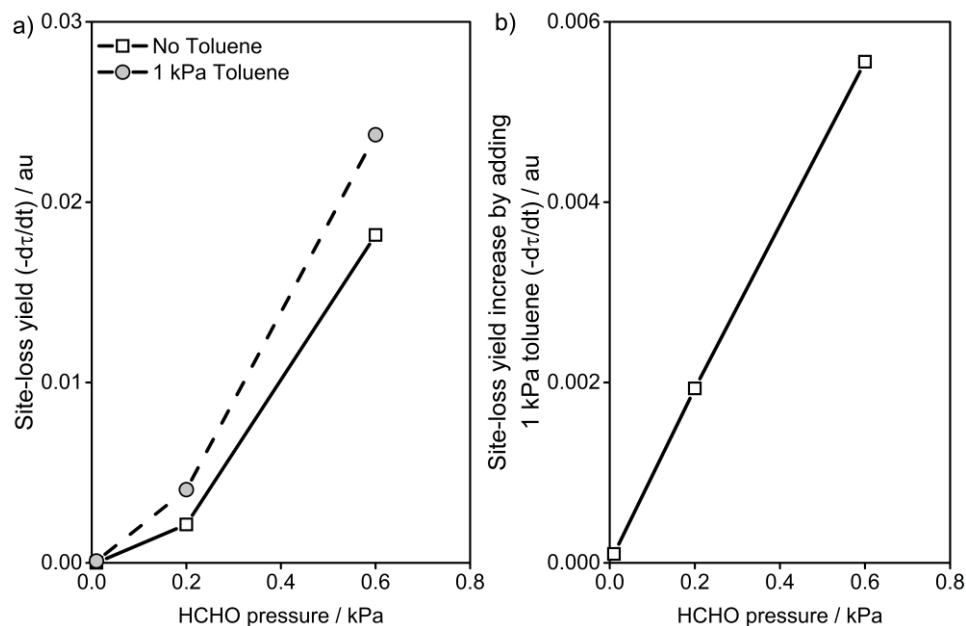
Figure 7.3: a) Site-loss yield as a function of HCHO pressure with and without a 1 kPa toluene co-feed and b) the increase in site-loss yield by addition of 1 kPa toluene co-feed as a function of HCHO pressure. These results are based on the reaction network depicted in Scheme 7.5 with rate constants $k_1 = 1$, $k_2 = 10$, $k_3 = 0.01$, and $k_4 = 100$ a.u.
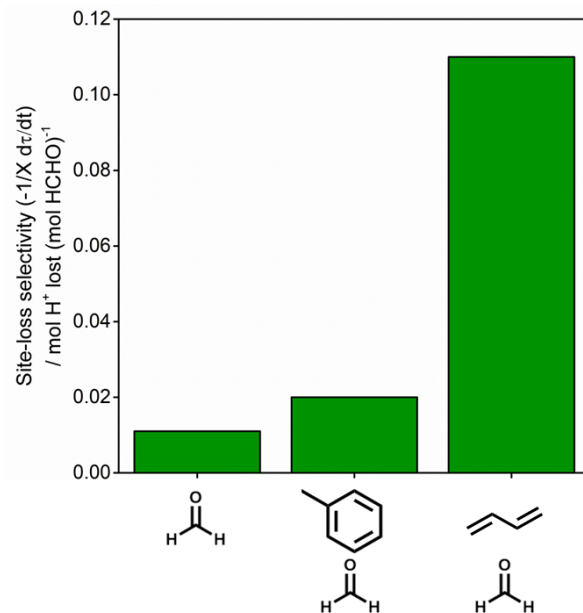
Figure 7.4: Site-loss selectivity of HCHO with various co-feed combinations based on the reaction network depicted in Scheme 7.5 with rate constants $k_1 = 1$, $k_2 = 10$, $k_3 = 0.01$, and $k_4 = 100$ a.u and $P_{HCHO} = 0.2$ kPa, $P_{C_7H_8} = 1.0$ kPa, and $P_{C_4H_4} = 1.0$ kPa.

7.5 Discussion

We propose that the site-loss yield and selectivities as a function of feed composition suggest that direct reaction between HCHO and aromatics is not the prevailing deactivation pathway during MTH catalysis on HZSM-5 when co-feeding HCHO, specifically because the site-loss selectivity increases with increases in HCHO co-feed pressure, even with a 1.0 kPa toluene co-feed. Co-feeding 1,3-butadiene increased the site-loss yield more than an equivalent mole fraction co-feed of toluene, suggesting that dienes may be important intermediates to causing deactivation. It has been shown that high pressure H_2 co-feeds during MTH catalysis increases catalyst lifetime on MFI, CHA, AEI, FER and BEA zeolite/zeotype frameworks and it has been proposed that the mechanistic basis for this increased lifetime lies in the propensity of H_2

to hydrogenate dienes over olefins, evidenced by second order rate constants that are 1-2 orders of magnitude higher for 1,3-butadiene hydrogenation compared to propylene hydrogenation.[117,147,148] Hydrogenation of dienes may prevent deactivation by preventing them from forming aromatics, or, as our data suggests, dienes are involved in critical elementary steps for polycyclic aromatics formations that bypass monocyclic aromatic intermediates. This is not to suggest that polycyclic aromatics are not formed from aromatics via reaction between an aromatic and a diene. This only implies that dienes are critically involved in the polycyclic aromatics formation such that if they are eliminated, the rate of polycyclic aromatics formation will be decreased, even if aromatics are still present.

The importance of dienes in causing deactivation during MTH catalysis is exemplified by co-feeding both 1,3-butadiene and HCHO simultaneously and observing a site-loss yield of 0.2 kPa HCHO+1.0 kPa C_4H_4 pathway between 5700 and 6500 µmol H_{lost}^+ mol $MeOH_{fed}^{-1}$, which are significantly higher than the site-loss yields of 39 and 720 for the 0.2 kPa HCHO-only and 1.0 kPa C_4H_4-only co-feeds, respectively, suggesting that HCHO and 1,3-butadiene react via overall reaction to cause deactivation, possibly by direct reaction to form cyclopentadiene. During MTH catalysis on HZSM-5, at the front of the reactor bed where deactivation occurs, HCHO is a primary product of methanol disproportionation and transfer dehydrogenation, and, at 748 K on HZMS-5, is one of the first products observed followed by light olefins that undergo subsequent reaction to form aromatics, likely through diene and cyclodiene intermediates.[66,70,121,149,150] We surmise that this mixture of HCHO with olefins leads to the formation of reactive unsaturated non-aromatic compounds that cause deactivation.

Thus, we conclude that dienes play a critical role in deactivation during MTH catalysis, either by diene oligomerization, including cyclopentadienes that may be products of diene reaction with HCHO, or by reaction with olefins and aromatics. Diels-alder-like reactions between HCHO and dienes could also lead to the formation of oxygen containing six-member rings[151] that can undergo further reaction to polycyclic aromatic species, and may be the source of oxygen-containing coke species that are observed in HZSM-5.[119,152]

7.6 Conclusion

We probe the mechanism of catalyst deactivation during methanol-to-hydrocarbons catalysis on HZSM-5 by measuring site-loss yields and selectivities as functions of reactant composition. Through co-feed experiments, we determine that it is unlikely for the reaction between HCHO and aromatics to be the predominant HCHO-mediated deactivation pathway during MTH catalysis on HZSM-5. With a 1.0 kPa toluene co-feed, the site-loss yield was greater than first-order in the HCHO co-feed pressure, suggesting that an alternative deactivation pathway requiring multiple species that originate from HCHO contributes non-negligibly to deactivation. We propose that reactions involving polyunsaturated non-aromatic species, such as aliphatic or cyclodienes, are strong candidates for key species that mediate deactivation during MTH catalysis on HZSM-5. This proposal is supported by a 190x increase in the site-loss selectivity of HCHO upon co-feeding 1.0 kPa 1,3-butadiene with 0.2 kPa HCHO, compared to only a ~2x increase when co-feeding 1.0 kPa toluene with 0.2 kPa HCHO.

Bibliography

(1)   Logadóttir, Á.; Nørskov, J. K. Ammonia Synthesis over a Ru(0001) Surface Studied by Density Functional Calculations. *J. Catal.* **2003**, *220*, 273–279.

(2)   Chamberlain, T. W.; Biskupek, J.; Skowron, S. T.; Markevich, A. V.; Kurasch, S.; Reimer, O.; Walker, K. E.; Rance, G. A.; Feng, X.; Müllen, K.; Turchanin, A.; Lebedeva, M. A.; Majouga, A. G.; Nenajdenko, V. G.; Kaiser, U.; Besley, E.; Khlobystov, A. N. Stop-Frame Filming and Discovery of Reactions at the Single-Molecule Level by Transmission Electron Microscopy. *ACS Nano* **2017**, *11*, 2509–2520.

(3)   Skowron, S. T.; Chamberlain, T. W.; Biskupek, J.; Kaiser, U.; Besley, E.; Khlobystov, A. N. Chemical Reactions of Molecules Promoted and Simultaneously Imaged by the Electron Beam in Transmission Electron Microscopy. *Acc. Chem. Res.* **2017**, *50*, 1797–1807.

(4)   Laidler, K. J. *Chemical Kinetics*, Third.; Berger, L. S., Pisano, S., Eds.; Prentice-Hall, Inc.: Upper Saddle River, NJ, 1987.

(5)   Boudart, M. *Kinetics of Chemical Processes*; Amundson, N. R., Ed.; Prentice-Hall, Inc.: Englewood Cliffs, N.J., 1968.

(6)   Waage, P.; Guldberg, C. M. Studier over Affiniteten. *Forh. Vid. Selsk. Christ.* **1864**, 35–45.

(7)   Guldberg, C. M.; Waage, P. *Études Sur Les Affinités Chimiques*; Brøgger & Christie: Oslo, Norway, 1867.

(8)   Wynne-Jones, W. F. K.; Eyring, H. The Absolute Rate of Reactions in Condensed Phases. *J. Chem. Phys.* **1935**, *3*, 492–502.

(9)   Laidler, K. J.; Glasstone, S.; Eyring, H. Application of the Theory of Absolute Reaction Rates to Heterogeneous Processes. II. Chemical Reactions on Surfaces. *J. Chem. Phys.* **1940**, *8*, 667–676.

(10)   Mahan, B. H. Activated Complex Theory of Bimolecular Gas Reactions. *J. Chem. Educ.* **1974**, *51*, 709–711.

(11)   Stegelmann, C.; Andreasen, A.; Campbell, C. T. Degree of Rate Control: How Much the Energies of Intermediate and Transition States Control Rates. *J. Am. Chem. Soc.* **2009**, *131*, 8077–8082.

(12)   Campbell, C. T. The Degree of Rate Control: A Powerful Tool for Catalysis Research. *ACS Catal.* **2017**, *7*, 2770–2779.

(13)   Campbell, C. T. Micro- and Macro-Kinetics : Their Relationship in Heterogeneous

Catalysis. *Top. Catal. I* **1994**, 353–366.

(14) Foley, B. L.; Bhan, A. Thermodynamically Consistent Forward and Reverse Degrees of Rate Control in Reversible Reactions. *J. Catal.* **2020**.

(15) Foley, B. L.; Bhan, A. Degrees of Rate Control at Non(Pseudo)Steady-State Conditions. *ACS Catal.* **2020**, No. 4, 2556–2564.

(16) Dumesic, J. A.; Huber, G. W.; Boudart, M. Rates of Catalytic Reactions. In *Handbook of Heterogeneous Catalysis*; Ertl, G., Knözinger, H., Schüth, F., Weitkamp, J., Eds.; Wiley-VCH: Weinheim, Germany, 2008; pp 1445–1462.

(17) Baranski, A. On the Usefulness of Campbell's Concept of the Rate-Determining Step. *Solid State Ionics* **1999**, *117*, 123–128.

(18) Kozuch, S.; Shaik, S. A Combined Kinetic - Quantum Mechanical Model for Assessment of Catalytic Cycles: Application to Cross-Coupling and Heck Reactions. **2006**, No. 4, 3355–3365.

(19) Dumesic, J. A. Reply to Finding the Rate-Determining Step in a Mechanism: Comparing DeDonder Relations with the "Degree of Rate Control." *J. Catal.* **2001**, *204*, 525–529.

(20) Dumesic, J. A. Analyses of Reaction Schemes Using De Donder Relations. *J. Catal.* **1999**, *505*, 496–505.

(21) Campbell, C. T. Finding the Rate-Determining Step in a Mechanism: Comparing DeDonder Relations with the "Degree of Rate Control." *J. Catal.* **2001**, *204*, 520–524.

(22) Motagamwala, A. H.; Dumesic, J. A. Analysis of Reaction Schemes Using Maximum Rates of Constituent Steps. *Proc. Natl. Acad. Sci.* **2016**, *113*, E2879–E2888.

(23) Cortright, R. D.; Dumesic, J. A. Kinetics of Heterogeneous Catalytic Reactions: Analysis of Reaction Schemes. In *Advances in Catalysis*; Gates, B., Knoezinger, H., Eds.; Academic Press: Cambridge, MA, 2001; Vol. 46, pp 161–264.

(24) Kozuch, S.; Martin, J. M. L. The Rate-Determining Step Is Dead. Long Live the Rate- Determining State! *ChemPhysChem* **2011**, *5017*, 1413–1418.

(25) Wolcott, C. A.; Medford, A. J.; Studt, F.; Campbell, C. T. Degree of Rate Control Approach to Computational Catalyst Screening. *J. Catal.* **2015**, *330*, 197–207.

(26) Razdan, N. K.; Kumar, A.; Foley, B. L.; Bhan, A. Influence of Ethylene and Acetylene on the Rate and Reversibility of Methane Dehydroaromatization on Mo/H-ZSM-5 Catalysts. *J. Catal.* **2020**, *381*, 261–270.

(27) Boudart, M. Turnover Rates in Heterogeneous Catalysis. *Chem. Rev.* **1995**, *95*, 661–666.

(28) Harris, J. W.; Arvay, J.; Mitchell, G.; Delgass, W. N.; Ribeiro, F. H. Propylene Oxide Inhibits Propylene Epoxidation over Au/TS-1. *J. Catal.* **2018**, *365*, 105–114.

(29) Gokhale, A. A.; Dumesic, J. A.; Mavrikakis, M. On the Mechanism of Low-Temperature Water Gas Shift Reaction on Copper. *J. Am. Chem. Soc.* **2008**, *130*, 1402–1414.

(30) Meskine, H.; Matera, S.; Scheffler, M.; Reuter, K.; Metiu, H. Examination of the Concept of Degree of Rate Control by First-Principles Kinetic Monte Carlo Simulations. *Surf. Sci.* **2009**, *603*, 1724–1730.

(31) Stangeland, K.; Li, H.; Yu, Z. Thermodynamic Analysis of Chemical and Phase Equilibria in CO2 Hydrogenation to Methanol, Dimethyl Ether, and Higher Alcohols. *Ind. Eng. Chem. Res.* **2018**, *57*, 4081–4094.

(32) Arena, F.; Mezzatesta, G.; Zafarana, G.; Trunfio, G.; Frusteri, F.; Spadaro, L. Effects of Oxide Carriers on Surface Functionality and Process Performance of the Cu-ZnO System in the Synthesis of Methanol via CO2 Hydrogenation. *J. Catal.* **2013**, *300*, 141–151.

(33) Dubois, J.-L.; Sayama, K.; Arakawa, H. Conversion of CO 2 to Dimethylether and Methanol over Hybrid Catalysts . *Chemistry Letters*. 1992, pp 1115–1118.

(34) Boudart, M. Consistency between Kinetics and Thermodynamics. *J. Phys. Chem.* **1976**, *80*, 2869–2870.

(35) Horiuti, J.; Nakamura, T. Stoichiometric Number and the Theory of Steady Reaction. *Zeitshrift für Phys. Chemie* **1957**, 358–365.

(36) Horiuti, J. Rates Relation Between Rate Coefficients and Equilibrium Constants. *Adv. Catal.* **1957**, *9*, 339–342.

(37) Enomoto, S.; Horiuti, J. Determination of Stoichiometric Number of Ammonia Synthesis Reaction. *J. Res. Inst. Catal. Hokkaido Univ.* **1953**, *2*, 87–104.

(38) Horiuti, J. Significance and Experimental Determination of Stoichiometric Number. *J. Catal.* **1962**, *1*, 199–207.

(39) Horiuti, J.; Takezawa, N. Stoichiometric Number of the Rate-Determining Step and the Mechanism of Catalyzed Ammonia Synthesis in the Presence of Commercial Iron Catalyst. *J. Res. Inst. Catal. Hokkaido Univ.* **1960**, *8*, 127–150.

(40) Kaneko, Y.; Oki, S. On the Mechanism of Water Gas Shift Reaction: Part III :

Determination of Stoichiometric Number of Rate-Determining Step in the Neighbourhood of Equilibrium of the Reaction. *J. Res. Inst. Catal. Hokkaido Univ.* **1968**, *15*, 185–192.

(41) Kaneko, Y.; Oki, S. On the Mechanism of Water Gas Shift Reaction: Part II. Determination of Stoichiometric Number of Rate-Determining Step by Means of ^{13}C as Tracer. *J. Res. Inst. Catal. Hokkaido Univ.* **1966**, *13*, 169–186.

(42) Masuda, M. Application of the Theory of Stoichiometric Number Determination of the Rate-Determining Step: The Mechanism of Water-Gas Shift Reaction Catalyzed by Platinum. *J. Res. Inst. Catal. Hokkaido Univ.* **1977**, *24*, 83–101.

(43) Kaneko, Y.; Odanaka, H. On the Mechanism of the Oxidation of Sulfur Dioxide Part I: Determination of the Stoichiometric Number by Means of 35S. *J. Res. Inst. Catal. Hokkaido Univ.* **1965**, *13*, 29–43.

(44) Happel, J. Study of Kinetic Structure Using Marked Atoms. *Catal. Rev.* **1972**, *6*, 221–260.

(45) Boudart, M.; Djega-Mariadassou, G. *Kinetics of Heterogeneous Catalytic Reactions*; Prausnitz, J. M., Brewer, L., Eds.; Princeton University Press: Princeton, New Jersey, 1984.

(46) Happel, J.; Atkins, R. S. Rate-Controlling Path for Catalytic Butane Dehydrogenation. *Ind. Eng. Chem. Fundam.* **1970**, *9*, 11–14.

(47) Happel, J.; Atkins, R. S.; Tanaka, K. Stoichiometric Number of the Rate-Determining Steps for Dehydrogenation of Butane and Butenes over Chromia and Chromia-Alumina Catalysts: Analysis of Data of Balandin and His Collaborators. *J. Res. Inst. Catal. Hokkaido Univ.* **1969**, *17*, 197–212.

(48) Balandin, A. A.; Neiman, M. B.; Bogdanova, O. K.; Isagulyants, G. V.; Shcheglova, A. P.; Popov, E. I. Dehydrogenation of Butane-Butene Mixtures Investigated with the Aid of C14. *Bull. Acad. Sci. USSR, Div. Chem. Sci.* **1957**, 167–175.

(49) Razdan, N. K.; Kumar, A.; Bhan, A. Controlling Kinetic and Diffusive Length-Scales during Absorptive Hydrogen Removal in Methane Dehydroaromatization on MoCx/H-ZSM-5 Catalysts. *J. Catal.* **2019**, *372*, 370–381.

(50) Kumar, A.; Song, K.; Liu, L.; Han, Y.; Bhan, A. Absorptive Hydrogen Scavenging for Enhanced Aromatics Yield During Non-Oxidative Methane Dehydroaromatization on Mo/H-ZSM-5 Catalysts. *Angew. Chemie - Int. Ed.* **2018**, *57*, 15577–15582.

(51) Bedard, J.; Hong, D. Y.; Bhan, A. CH4 Dehydroaromatization on Mo/H-ZSM-5: 1. Effects of Co-Processing H2 and CH3COOH. *J. Catal.* **2013**, *306*, 58–67.

(52) Borry, R. W.; Kim, Y. H.; Huffsmith, A.; Reimer, J. A.; Iglesia, E. Structure and Density of Mo and Acid Sites in Mo-Exchanged H-ZSM5 Catalysts for Nonoxidative Methane Conversion. *J. Phys. Chem. B* **1999**, *103*, 5787–5796.

(53) Temkin, M. I. The Kinetics of Stationary Reactions. *Dokl. Akad. Nauk SSSR* **1963**, *152*, 156–159.

(54) Temkin, M. I. The Kinetics of Transfer of Labeled Atoms By Reaction. *Ann. N. Y. Acad. Sci.* **1973**, *213*, 79–89.

(55) Krupka, R. M.; Kaplan, H.; Laidler, K. J. Kinetic Consequences of the Principle of Microscopic Reversibility. *Trans. Faraday Soc.* **1966**, *62*, 2754–2859.

(56) Campbell, C. T. The Degree of Rate Control: A Powerful Tool for Catalysis Research. *ACS Catal.* **2017**, *7*, 2770–2779.

(57) Kozuch, S.; Shaik, S. A Combined Kinetic-Quantum Mechanical Model for Assessment of Catalytic Cycles: Application to Cross-Coupling and Heck Reactions. *J. Am. Chem. Soc.* **2006**, *128*, 3355–3365.

(58) Ray, W. J. Rate-Limiting Step: A Quantitative Definition. Application to Steady-State Enzymic Reactions. *Biochemistry* **1983**, *22*, 4625–4637.

(59) Laidler, K. J. Rate-Controlling Step: A Necessary or Useful Concept? *J. Chem. Educ.* **1988**, *65*, 250–254.

(60) Foley, B. L.; Bhan, A. Degree of Rate Control and De Donder Relations – an Interpretation Based on Transition State Theory. *J. Catal.* **2020**, *384*, 231–251.

(61) Lewis, G. N. A New Principle of Equilibrium. **1925**.

(62) Horiuti, J.; Nakamura, T. On the Theory of Heterogeneous Catalysis. *Adv. Catal.* **1967**, *17*, 1–74.

(63) Mao, Z.; Campbell, C. T. Apparent Activation Energies in Complex Reaction Mechanisms: A Simple Relationship via Degrees of Rate Control. *ACS Catal.* **2019**, *9*, 9465–9473.

(64) Mao, Z.; Campbell, C. T. The Degree of Rate Control of Catalyst-Bound Intermediates in Catalytic Reaction Mechanisms: Relationship to Site Coverage. *J. Catal.* **2020**, *381*, 53–62.

(65) Boisen, A.; Dahl, S.; Nørskov, J. K.; Christensen, C. H. Why the Optimal Ammonia Synthesis Catalyst Is Not the Optimal Ammonia Decomposition Catalyst. *J. Catal.* **2005**, *230*, 309–312.

(66) Hwang, A.; Kumar, M.; Rimer, J. D.; Bhan, A. Implications of Methanol

Disproportionation on Catalyst Lifetime for Methanol-to-Olefins Conversion by HSSZ-13. *J. Catal.* **2017**, *346*, 154–160.

(67) Hwang, A.; Bhan, A. Bifunctional Strategy Coupling Y_2O_3-Catalyzed Alkanal Decomposition with Methanol-to-Olefins Catalysis for Enhanced Lifetime. *ACS Catal.* **2017**, *7*, 4417–4422.

(68) Martinez-Espin, J. S.; Mortén, M.; Janssens, T. V. W.; Svelle, S.; Beato, P.; Olsbye, U. New Insights into Catalyst Deactivation and Product Distribution of Zeolites in the Methanol-to-Hydrocarbons (MTH) Reaction with Methanol and Dimethyl Ether Feeds. *Catal. Sci. Technol.* **2017**, *7*, 2700–2716.

(69) Müller, S.; Liu, Y.; Kirchberger, F. M.; Tonigold, M.; Sanchez-Sanchez, M.; Lercher, J. A. Hydrogen Transfer Pathways during Zeolite Catalyzed Methanol Conversion to Hydrocarbons. *J. Am. Chem. Soc.* **2016**, *138*, 15994–16003.

(70) Arora, S. S.; Bhan, A. The Critical Role of Methanol Pressure in Controlling Its Transfer Dehydrogenation and the Corresponding Effect on Propylene-to-Ethylene Ratio during Methanol-to-Hydrocarbons Catalysis on H-ZSM-5. *J. Catal.* **2017**, *356*, 300–306.

(71) Vasiliadou, E. S.; Gould, N. S.; Lobo, R. F. Zeolite-Catalyzed Formaldehyde–Propylene Prins Condensation. *ChemCatChem* **2017**, *9*, 4417–4425.

(72) Martinez-Espin, J. S.; De Wispelaere, K.; Westgård Erichsen, M.; Svelle, S.; Janssens, T. V. W.; Van Speybroeck, V.; Beato, P.; Olsbye, U. Benzene Co-Reaction with Methanol and Dimethyl Ether over Zeolite and Zeotype Catalysts: Evidence of Parallel Reaction Paths to Toluene and Diphenylmethane. *J. Catal.* **2017**, *349*, 136–148.

(73) Hou, Z.; Okuhara, T. Catalytic Synthesis of Diphenylmethane from Benzene and Formalin with Water-Tolerant Solid Acids. *Appl. Catal. A Gen.* **2001**, *216*, 147–155.

(74) Climent, M. J.; Corma, A.; García, H.; Primo, J. Zeolites in Organic Reactions. Condensation of Formaldehyde with Benzene in the Presence of HY Zeolites. *Appl. Catal.* **1989**, *51*, 113–125.

(75) Zhang, X.; Liu, D.; Xu, D.; Asahina, S.; Cychosz, K. A.; Agrawal, K. V.; Al Wahedi, Y.; Bhan, A.; Al Hashimi, S.; Terasaki, O.; Thommes, M.; Tsapatsis, M. Synthesis of Self-Pillared Zeolite Nanosheets by Repetitive Branching. *Science* **2012**, *336*, 1684–1687.

(76) Veefkind, V. A.; Lercher, J. A. On the Elementary Steps of Acid Zeolite Catalyzed Amination of Light Alcohols. **1999**, *181*, 245–255.

(77) Swindlehurst, G. R.; Kumar, P.; Xu, D.; Alhassan, S. M.; Mkhoyan, K. A.;

Tsapatsis, M. Nucleation, Growth, and Robust Synthesis of SPP Zeolite: Effect of Ethanol, Sodium, and Potassium. *Top. Catal.* **2015**, *58*, 545–558.

(78)   Bates, S. A.; Delgass, W. N.; Ribeiro, F. H.; Miller, J. T.; Gounder, R. Methods for NH_3 Titration of Brønsted Acid Sites in Cu-Zeolites That Catalyze the Selective Catalytic Reduction of NO_x with NH_3. *J. Catal.* **2014**, *312*, 26–36.

(79)   Bagnasco, G. Improving the Selectivity of NH3 TPD Measurements. *J. Catal.* **1996**, *159*, 249–252.

(80)   Khare, R.; Bhan, A. Mechanistic Studies of Methanol-to-Hydrocarbons Conversion on Diffusion-Free MFI Samples. *J. Catal.* **2015**, *329*, 218–228.

(81)   Rybicki, M.; Sauer, J. Acidity of Two-Dimensional Zeolites. *Phys. Chem. Chem. Phys.* **2015**, *17*, 27873–27882.

(82)   Gounder, R.; Iglesia, E. The Catalytic Diversity of Zeolites: Confinement and Solvation Effects within Voids of Molecular Dimensions. *Chem. Commun. (Camb).* **2013**, *49*, 3491–3509.

(83)   Bollini, P.; Chen, T. T.; Neurock, M.; Bhan, A. Mechanistic Role of Water in HSSZ-13 Catalyzed Methanol-to-Olefins Conversion. *Catal. Sci. Technol.* **2019**, *9*, 4374–4383.

(84)   Böhm, S.; Navrátil, R.; Kuthan, J. A Theoretical Study of the Methanediol Decomposition Mechanism. *J. Mol. Struct.* **1991**, *227*, 277–283.

(85)   Iv, D. R. K.; Widicus, S. L.; Iii, W. A. G. A Theoretical Study of the Conversion of Gas Phase Methanediol to Formaldehyde. *J. Chem. Phys.* **2003**, *119*, 5117–5129.

(86)   Hazra, M. K.; Francisco, J. S.; Sinha, A. Gas Phase Hydrolysis of Formaldehyde to Form Methanediol: Impact of Formic Acid Catalysis. *J. Phys. Chem. A* **2013**, *117*, 11704–11710.

(87)   Kumar, M.; Anglada, J. M.; Francisco, J. S. Role of Proton Tunneling and Metal-Free Organocatalysis in the Decomposition of Methanediol: A Theoretical Study. *J. Phys. Chem. A* **2017**, *121*, 4318–4325.

(88)   Min, H. K.; Cha, S. H.; Hong, S. B. Mechanistic Insights into the Zeolite-Catalyzed Isomerization and Disproportionation of m-Xylene. *ACS Catal.* **2012**, *2*, 971–981.

(89)   Margarit, V. J.; Osman, M.; Al-Khattaf, S.; Martínez, C.; Boronat, M.; Corma, A. Control of the Reaction Mechanism of Alkylaromatics Transalkylation by Means of Molecular Confinement Effects Associated to Zeolite Channel Architecture. *ACS Catal.* **2019**, *9*, 5935–5946.

(90) Cha, S. H.; Hong, S. B. Reaction Intermediates and Mechanism of the Zeolite-Catalyzed Transalkylation of 1,2,4-Trimethylbenzene with Toluene. *J. Catal.* **2018**, *357*, 1–11.

(91) Svelle, S.; Olsbye, U.; Lillerud, K. P.; Kolboe, S.; Bjørgen, M. Diphenylmethane-Mediated Transmethylation of Methylbenzenes over H-Zeolites. *J. Am. Chem. Soc.* **2006**, *128*, 5618–5619.

(92) Huang, J.; Jiang, Y.; Marthala, V. R. R.; Hunger, M. Insight into the Mechanisms of the Ethylbenzene Disproportionation: Transition State Shape Selectivity on Zeolites. *J. Am. Chem. Soc.* **2008**, *130*, 12642–12644.

(93) Clark, L. A.; Sierka, M.; Sauer, J. Stable Mechanistically-Relevant Aromatic-Based Carbenium Ions in Zeolite Catalysts. *J. Am. Chem. Soc.* **2003**, *125*, 2136–2141.

(94) Demuth, T.; Raybaud, P.; Lacombe, S.; Toulhoat, H. Effects of Zeolite Pore Sizes on the Mechanism and Selectivity of Xylene Disproportionation - A DFT Study. *J. Catal.* **2004**, *222*, 323–337.

(95) Clark, L. A.; Sierka, M.; Sauer, J. Computational Elucidation of the Transition State Shape Selectivity Phenomenon. *J. Am. Chem. Soc.* **2004**, *126*, 936–947.

(96) Bernasconi, C. F.; Wenzel, P. J.; Ragains, M. L. Proton Transfers in Aromatic and Antiaromatic Systems. How Aromatic or Antiaromatic Is the Transition State? An Ab Initio Study. *J. Am. Chem. Soc.* **2008**, *130*, 4934–4944.

(97) Haw, J. F. Zeolite Acid Strength and Reaction Mechanisms in Catalysis. *Phys. Chem. Chem. Phys.* **2002**, *4*, 5431–5441.

(98) Fang, H.; Zheng, A.; Xu, J.; Li, S.; Chu, Y.; Chen, L.; Deng, F. Theoretical Investigation of the Effects of the Zeolite Framework on the Stability of Carbenium Ions. *J. Phys. Chem. C* **2011**, *115*, 7429–7439.

(99) Beck, L. W.; Xu, T.; Haw, J. F.; Nicholas, J. B. Kinetic NMR and Density Functional Study of Benzene H/D Exchange in Zeolites, the Most Simple Aromatic Substitution. *J. Am. Chem. Soc.* **1995**, *117*, 11594–11595.

(100) Sreekumar, R.; Pillai, C. N. Reactions of Benzyl Alcohol and Dibenzyl Ether over Zeolites. *Catal. Letters* **1993**, *19*, 281–291.

(101) Scott, S. L. A Matter of Life(Time) and Death. *ACS Catal.* **2018**, *8*, 8597–8599.

(102) Argyle, M.; Bartholomew, C. Heterogeneous Catalyst Deactivation and Regeneration: A Review. *Catalysts* **2015**, *5*, 145–269.

(103) Chen, D.; Rebo, H. P.; Moljord, K.; Holmen, A. Influence of Coke Deposition on

Selectivity in Zeolite Catalysis. *Ind. Eng. Chem. Res.* **1997**, *36*, 3473–3479.

(104) Janssens, T. V. W. A New Approach to the Modeling of Deactivation in the Conversion of Methanol on Zeolite Catalysts. *J. Catal.* **2009**, *264*, 130–137.

(105) Janssens, T. V. W.; Svelle, S.; Olsbye, U. Kinetic Modeling of Deactivation Profiles in the Methanol-to-Hydrocarbons (MTH) Reaction: A Combined Autocatalytic-Hydrocarbon Pool Approach. *J. Catal.* **2013**, *308*, 122–130.

(106) Rojo-Gama, D.; Etemadi, S.; Kirby, E.; Lillerud, K. P.; Beato, P.; Svelle, S.; Olsbye, U. Time- and Space-Resolved Study of the Methanol to Hydrocarbons (MTH) Reaction-Influence of Zeolite Topology on Axial Deactivation Patterns. *Faraday Discuss.* **2017**, *197*, 421–446.

(107) Bleken, F. L.; Janssens, T. V. W.; Svelle, S.; Olsbye, U. Product Yield in Methanol Conversion over ZSM-5 Is Predominantly Independent of Coke Content. *Microporous Mesoporous Mater.* **2012**, *164*, 190–198.

(108) Teketel, S.; Skistad, W.; Benard, S.; Olsbye, U.; Lillerud, K. P.; Beato, P.; Svelle, S. Shape Selectivity in the Conversion of Methanol to Hydrocarbons: The Catalytic Performance of One-Dimensional 10-Ring Zeolites: ZSM-22, ZSM-23, ZSM-48, and EU-1. *ACS Catal.* **2012**, *2*, 26–37.

(109) Westgård Erichsen, M.; Svelle, S.; Olsbye, U. H-SAPO-5 as Methanol-to-Olefins (MTO) Model Catalyst: Towards Elucidating the Effects of Acid Strength. *J. Catal.* **2013**, *298*, 94–101.

(110) Ilias, S.; Bhan, A. Mechanism of the Catalytic Conversion of Methanol to Hydrocarbons. *ACS Catal.* **2013**, *3*, 18–31.

(111) Haw, J. F.; Song, W.; Marcus, D. M.; Nicholas, J. B. The Mechanism of Methanol to Hydrocarbon Catalysis. *Acc. Chem. Res.* **2003**, *36*, 317–326.

(112) Müller, S.; Liu, Y.; Vishnuvarthan, M.; Sun, X.; Van Veen, A. C.; Haller, G. L.; Sanchez-Sanchez, M.; Lercher, J. A. Coke Formation and Deactivation Pathways on H-ZSM-5 in the Conversion of Methanol to Olefins. *J. Catal.* **2015**, *325*, 48–59.

(113) Rojo-Gama, D.; Mentel, L.; Kalantzopoulos, G. N.; Pappas, D. K.; Dovgaliuk, I.; Olsbye, U.; Lillerud, K. P.; Beato, P.; Lundegaard, L. F.; Wragg, D. S.; Svelle, S. Deactivation of Zeolite Catalyst H-ZSM-5 during Conversion of Methanol to Gasoline: Operando Time- and Space-Resolved X-Ray Diffraction. *J. Phys. Chem. Lett.* **2018**, *9*, 1324–1328.

(114) Ilias, S.; Khare, R.; Malek, A.; Bhan, A. A Descriptor for the Relative Propagation of the Aromatic- and Olefin-Based Cycles in Methanol-to-Hydrocarbons Conversion on H-ZSM-5. *J. Catal.* **2013**, *303*, 135–140.

(115) Khare, R.; Millar, D.; Bhan, A. A Mechanistic Basis for the Effects of Crystallite Size on Light Olefin Selectivity in Methanol-to-Hydrocarbons Conversion on MFI. *J. Catal.* **2015**, *321*, 23–31.

(116) Bjørgen, M.; Joensen, F.; Spangsberg, M.; Olsbye, U.; Lillerud, K.; Svelle, S. Applied Catalysis A : General Methanol to Gasoline over Zeolite H-ZSM-5 : Improved Catalyst Performance by Treatment with NaOH. **2008**, *345*, 43–50.

(117) Arora, S. S.; Nieskens, D. L. S.; Malek, A.; Bhan, A. Lifetime Improvement in Methanol-to-Olefins Catalysis over Chabazite Materials by High-Pressure H_2 Co-Feeds. *Nat. Catal.* **2018**, *1*, 666–672.

(118) Bollini, P.; Bhan, A. Improving HSAPO-34 Methanol-to-Olefin Turnover Capacity by Seeding the Hydrocarbon Pool. *ChemPhysChem* **2018**, *19*, 479–483.

(119) Müller, S.; Liu, Y.; Vishnuvarthan, M.; Sun, X.; Van Veen, A. C.; Haller, G. L.; Sanchez-Sanchez, M.; Lercher, J. A. Coke Formation and Deactivation Pathways on H-ZSM-5 in the Conversion of Methanol to Olefins. *J. Catal.* **2015**, *325*, 48–59.

(120) Grundner, S.; Luo, W.; Sanchez-Sanchez, M.; Lercher, J. Synthesis of Single-Site Copper Catalysts for Methane Partial Oxidation. *Chem. Commun.* **2015**, *52*, 1–17.

(121) Olsbye, U.; Svelle, S.; Lillerud, K. P.; Wei, Z. H.; Chen, Y. Y.; Li, J. F.; Wang, J. G.; Fan, W. B. The Formation and Degradation of Active Species during Methanol Conversion over Protonated Zeotype Catalysts. *Chem. Soc. Rev.* **2015**, *44*, 7155–7176.

(122) Olsbye, U.; Svelle, S.; Bjrgen, M.; Beato, P.; Janssens, T. V. W.; Joensen, F.; Bordiga, S.; Lillerud, K. P. Conversion of Methanol to Hydrocarbons: How Zeolite Cavity and Pore Size Controls Product Selectivity. *Angew. Chemie - Int. Ed.* **2012**, *51*, 5810–5831.

(123) Tian, P.; Wei, Y.; Ye, M.; Liu, Z. Methanol to Olefins (MTO): From Fundamentals to Commercialization. *ACS Catal.* **2015**, *5*, 1922–1938.

(124) Hwang, A.; Bhan, A. Deactivation of Zeolites and Zeotypes in Methanol-to-Hydrocarbons Catalysis: Mechanisms and Circumvention. *Acc. Chem. Res.* **2019**.

(125) Guisnet, M.; Magnoux, P. Organic Chemistry of Coke Formation. *Appl. Catal. A Gen.* **2001**, *212*, 83–96.

(126) M. Guisnet; Ribeiro, F. R. *Deactivation and Regeneration of Zeolite Catalysts*; Hutchings, G. J., Ed.; Imperial College Press: London, 2011.

(127) Rojo-Gama, D.; Signorile, M.; Bonino, F.; Bordiga, S.; Olsbye, U.; Lillerud, K. P.; Beato, P.; Svelle, S. Structure–Deactivation Relationships in Zeolites during the

Methanol–to-Hydrocarbons Reaction: Complementary Assessments of the Coke Content. *J. Catal.* **2017**, *351*, 33–48.

(128) Pinilla-Herrero, I.; Olsbye, U.; Márquez-Álvarez, C.; Sastre, E. Effect of Framework Topology of SAPO Catalysts on Selectivity and Deactivation Profile in the Methanol-to-Olefins Reaction. *J. Catal.* **2017**, *352*, 191–207.

(129) Goetze, J.; Meirer, F.; Yarulina, I.; Gascon, J.; Kapteijn, F.; Ruiz-Martínez, J.; Weckhuysen, B. M. Insights into the Activity and Deactivation of the Methanol-to-Olefins Process over Different Small-Pore Zeolites As Studied with Operando UV-Vis Spectroscopy. *ACS Catal.* **2017**, *7*, 4033–4046.

(130) Park, J. W.; Lee, J. Y.; Kim, K. S.; Hong, S. B.; Seo, G. Effects of Cage Shape and Size of 8-Membered Ring Molecular Sieves on Their Deactivation in Methanol-to-Olefin (MTO) Reactions. *Appl. Catal. A Gen.* **2008**, *339*, 36–44.

(131) Anderson, J. R.; Chang, Y. F.; Western, R. J. Retained and Desorbed Products from Reaction of 1-Hexene over H-ZSM5 Zeolite: Routes to Coke Precursors. *J. Catal.* **1989**, *118*, 466–482.

(132) Anderson, J. R.; Chang, Y. F.; Western, R. J. The Effect of Acidity on the Ormation of Retained Residue From-1-Hexene over Usy Zeolite Catalysts. *Stud. Surf. Sci. Catal.* **1991**, *68*, 745–751.

(133) Barbier, J. Deactivation of Reforming Catalysts by Coking - a Review. *Appl. Catal.* **1986**, *23*, 225–243.

(134) Guisnet, M.; Costa, L.; Ramôa, F. Journal of Molecular Catalysis A : Chemical Prevention of Zeolite Deactivation by Coking. **2009**, *305*, 69–83.

(135) Sushkevich, V. L.; Ordomsky, V. V; Ivanova, I. I. Synthesis of Isoprene from Formaldehyde and Isobutene over Phosphate Catalysts. *Appl. Catal. A Gen.* **2012**, 441–442.

(136) Arundale, E.; Mikeska, L. A. The Olefin-Aldehyde Condensation. The Prins Reaction. *Chem. Rev.* **1952**, *51*, 505–555.

(137) Adams, D. R.; Bhatnagar, S. P. The Prins Reaction. *Synthesis* **1977**, *1977*, 661–672.

(138) Chua, Y. T.; Stair, P. C. An Ultraviolet Raman Spectroscopic Study of Coke Formation in Methanol to Hydrocarbons Conversion over Zeolite H-MFI. *J. Catal.* **2003**, *213*, 39–46.

(139) Haw, J. F.; Nicholas, J. B.; Song, W.; Deng, F.; Wang, Z.; Xu, T.; Heneghan, C. S. Roles for Cyclopentenyl Cations in the Synthesis of Hydrocarbons from Methanol on Zeolite Catalyst HZSM-5. *J. Am. Chem. Soc.* **2000**, *122*, 4763–4775.

(140) Wang, C.; Xu, J.; Qi, G.; Gong, Y.; Wang, W.; Gao, P.; Wang, Q.; Feng, N.; Liu, X.; Deng, F. Methylbenzene Hydrocarbon Pool in Methanol-to-Olefins Conversion over Zeolite H-ZSM-5. *J. Catal.* **2015**, *332*, 127–137.

(141) Wang, C.; Hu, M.; Chu, Y.; Zhou, X.; Wang, Q.; Qi, G.; Li, S.; Xu, J.; Deng, F. π-Interactions between Cyclic Carbocations and Aromatics Cause Zeolite Deactivation in Methanol-to-Hydrocarbon Conversion. *Angew. Chemie - Int. Ed.* **2020**, *59*, 7198–7202.

(142) Pines, H.; Pines, H. Reaction of Benzene with Butadiene in the Presence of Sulfuric Acid and Hydrogen. **1986**, *478*, 1–2.

(143) Schaad, R. E.; Pines, H.; Monroe, G. S.; Ipatieff, B. V. N.; Schaad, R. E.; Pines, H.; Monroe, G. S. Reaction between Benzene and Butadiene in the Presence of Silico-Phosphoric Acid Catalyst. **1944**, *316*, 1944–1946.

(144) Foley, B. L.; Johnson, B. A.; Bhan, A. A Method for Assessing Catalyst Deactivation: A Case Study on Methanol-to-Hydrocarbons Conversion. *ACS Catal.* **2019**, *9*, 7065–7072.

(145) Teketel, S.; Olsbye, U.; Lillerud, K. P.; Beato, P.; Svelle, S. Co-Conversion of Methanol and Light Alkenes over Acidic Zeolite Catalyst H-ZSM-22: Simulated Recycle of Non-Gasoline Range Products. *Appl. Catal. A Gen.* **2015**, *494*, 68–76.

(146) Sun, X.; Mueller, S.; Liu, Y.; Shi, H.; Haller, G. L.; Sanchez-Sanchez, M.; Van Veen, A. C.; Lercher, J. A. On Reaction Pathways in the Conversion of Methanol to Hydrocarbons on HZSM-5. *J. Catal.* **2014**, *317*, 185–197.

(147) Arora, S. S.; Shi, Z.; Bhan, A. Mechanistic Basis for Effects of High-Pressure H2 Cofeeds on Methanol-to-Hydrocarbons Catalysis over Zeolites. *ACS Catal.* **2019**, *9*, 6407–6414.

(148) DeLuca, M.; Janes, C.; Hibbitts, D. Contrasting Arene, Alkene, Diene, and Formaldehyde Hydrogenation in H-ZSM-5, H-SSZ-13, and H-SAPO-34 Frameworks during MTO. *ACS Catal.* **2020**, *10*, 4593–4607.

(149) Liu, Y.; Kirchberger, F. M.; Müller, S.; Eder, M.; Tonigold, M.; Sanchez-Sanchez, M.; Lercher, J. A. Critical Role of Formaldehyde during Methanol Conversion to Hydrocarbons. *Nat. Commun.* **2019**, *10*, 1–9.

(150) Chang, C. D.; Silvestri, A. J. The Conversion of Methanol and Other O-Compounds to Hydrocarbons over Zeolite Catalysts. *J. Catal.* **1977**, *47*, 249–259.

(151) Dermer, O. C.; Kohn, L.; Nelson, W. J. The Reaction of 1,3-Butadiene with Formaldehyde. *J. Am. Chem. Soc.* **1951**, *73*, 5869–5870.

(152) Hutchings, G. J.; Hunter, R. Hydrocarbon Formation from Methanol and Dimethyl

Ether: A Review of the Experimental Observations Concerning the Mechanism of Formation of the Primary Products. *Catal. Today* **1990**, *6*, 279–306.

(153) Anderson, J. B. Statistical Theories of Chemical Reactions. Distributions in the Transition Region Region. *J. Chem. Phys.* **1973**, *58*, 4684–4692.

(154) Keck, J. C. Variational Theory of Reaction Rates. In *Advances in Chemical Physics*; Prigogine, I., Ed.; John Wiley & Sons, Inc.: Hoboken, NJ, 1967; Vol. 13, pp 85–121.

Appendix

A1 Introduction

The following appendices provide detailed calculations, experimental methods, programming codes, raw experimental data, and more detailed explanations to supplement the discussions in Chapters 2-7. They are ordered in correspondence to the preceding and are written such that they are standalone, but reference previous chapters as necessary.

A2 Degree of rate control and De Donder relations – An interpretation based on transition state theory

A2.1 Writing the overall rate function with elementary step rate functions as the independent variables

We demonstrate in this section how the overall rate can be written as a function of the elementary step rate functions, r_i, and how the sensitivities of each step i are calculated as a derivative of the function $\ln r$ with respect to $\ln r_i$. We define the rate, r, as the solution of a system of equations (eq. (A2.1)):

$$r(r_1, r_{-1}, r_2, r_3)$$

$$= \begin{cases} \dfrac{d\theta_*}{dt} = 0 = r_3(\boldsymbol{\theta}) - r_1(\boldsymbol{\theta}) + r_{-1}(\boldsymbol{\theta}) \\[2mm] \dfrac{d\theta_{A^*}}{dt} = 0 = r_1(\boldsymbol{\theta}) - r_{-1}(\boldsymbol{\theta}) - r_2(\boldsymbol{\theta}) \\[2mm] \dfrac{d\theta_{B^*}}{dt} = 0 = r_2(\boldsymbol{\theta}) - r_3(\boldsymbol{\theta}) \\[2mm] \theta_* + \theta_{A^*} + \theta_{B^*} = 1 \\[1mm] vary\ \boldsymbol{\theta}\ such\ that\ the\ above\ equations\ are\ true, then: \\[1mm] \qquad output = r_3(\boldsymbol{\theta}) \end{cases} \qquad (A2.1)$$

where $\boldsymbol{\theta}$ is a vector containing the fractional coverages of surface species, which are adjusted to solve the system of algebraic equations. Equation (A2.1) shows a system of mass balance equations for a catalytic reaction as an example, but a similar system of equations can be written for a system of fluid-phase reactions or a combination of catalytic and fluid-phase reactions, where a vector of the activities of reaction intermediates would be included. The vector $\boldsymbol{\theta}$ that satisfies the system of equations is the steady-state fractional coverage of surface species. The value of the function r is equal to the function r_3 evaluated at this steady-state vector of fractional coverages, and thus *output* is the output of function r for a given set of inputs r_i. The inputs into the function

246

r are the rate functions for the elementary steps, which have not yet been specified and can take on any functional form. To demonstrate this, we choose nonsensical functions to represent r_i that are not in the form of a TST rate function. The Matlab code for this function is copied here and available for download online at https://github.com/foley352/JCat-DoRC-1:

```
function [output,theta_SS]=rate(r1,rr1,r2,r3)
[t,x]=ode23s(@(t,x)[r3(x)-r1(x)+rr1(x);r1(x)-rr1(x)-r2(x);r2(x)-
r3(x)],[0,100],[0.998,0.001,0.001]); %forward integration of the rate until a
long      t=100      which      is      assumed      to      be      steady-state,
x=theta=[theta_*,theta_A^*,theta_B^*]
theta_SS=x(end,:);%theta_SS is the steady-state coverages
output=r3(theta_SS); %output is the rate
end
```

We define the functions r_i as (eqs. (A2.2)-(A2.5)):

$$r_1 = \frac{\theta_*}{\theta_{A^*}} \frac{k_1^2}{k_{-1}} - e^{-\theta_{B^*}} * (1\ s^{-1}) \tag{A2.2}$$

$$r_{-1} = (\theta_A^*)^{0.5}(\theta_{B^*}) * (1\ s^{-1}) \tag{A2.3}$$

$$r_2 = \frac{\theta_A}{\theta_{B^*}^{0.1}} * (1\ s^{-1}) \tag{A2.4}$$

$$r_3 = (\theta_{B^*}^4 - \theta_{A^*}) * (1\ s^{-1}) \tag{A2.5}$$

We multiply where necessary by $1\ s^{-1}$ so each equation still has units of rate. For $k_1 = 1\ s^{-1}$, $k_{-1} = 0.4\ s^{-1}$ the rate is (eq. (A2.6)):

$$r(r_1, r_{-1}, r_2, r_3) = 0.1742\ s^{-1} \tag{A2.6}$$

and the steady-state surface coverages are (eq. A2.7):

$$\boldsymbol{\theta} = [\theta_*, \theta_{A^*}, \theta_{B^*}] = [0.0647, 0.1696, 0.7657] \tag{A2.7}$$

We can numerically calculate the sensitivities derived in eq. (2.31) using eq. (A2.8):

$$s_i = \left(\frac{\partial \ln r}{\partial \ln r_i}\right)_{r_{n \neq i}}$$

$$= \lim_{\delta \to 0} \frac{r_i}{r(r_1, r_{-1}, r_2, r_3)} \frac{\left((1 + \delta)r(r_i, r_{j \neq i}) - r(r_1, r_{-1}, r_2, r_3)\right)}{(1 + \delta)r_i - r_i}$$

$$\approx \frac{r_i}{r(r_1, r_{-1}, r_2, r_3)} \frac{\left(r(1.0001r_i, r_{j \neq i}) - r(r_1, r_{-1}, r_2, r_3)\right)}{1.0001r_i - r_i} \tag{A2.8}$$

$$= \frac{\left(r(1.0001r_i, r_{j \neq i}) - r(r_1, r_{-1}, r_2, r_3)\right)}{0.0001 * r(r_1, r_{-1}, r_2, r_3)}$$

The sensitivities calculated by eq. (A2.8) are given by eq. (A2.9)-(A2.12):

$$s_1 = 0.0728 \tag{A2.9}$$

$$s_{-1} = -0.0469 \tag{A2.10}$$

$$s_2 = 0.7527 \tag{A2.11}$$

$$s_3 = 0.2214 \tag{A2.12}$$

These are sensitivities of the overall rate function to the elementary step rate functions r_i.

We define the sensitivities with respect to the rate constants k_i as $s_{k_i} = \left(\frac{\partial \ln r}{\partial \ln k_i}\right)_{k_{n \neq i}}$.

Numerically calculating s_{k_1} we find it is equal to (eq. (A2.13)):

$$s_{k_1} = 0.2838 \tag{A2.13}$$

Here $s_1 \neq s_{k_1}$ because r_1 is not($\propto$) k_1. However, we can determine the relationship between s_{k_1} and s_1 by substitution of $x = \ln k_1$ into eq. (2.35) and changing the total derivative to a partial derivative, which is given by eq. (A2.14):

$$s_{k_1} = \left(\frac{\partial \ln r}{\partial \ln k_1}\right)_{k_{j \neq 1}} = \sum_{i=rxn} s_i \left(\frac{\partial \ln r_i}{\partial \ln k_1}\right)_{k_{j \neq 1}} = s_1 \left(\frac{\partial \ln r_1}{\partial \ln k_1}\right)_{k_{j \neq 1}}$$

$$= \frac{2 \dfrac{\theta_*}{\theta_{A^*}} \dfrac{k_1^2}{k_{-1}}}{\dfrac{\theta_*}{\theta_{A^*}} \dfrac{k_1^2}{k_{-1}} - e^{-\theta_{B^*}}(s^{-1})} = 0.2838$$

(A2.14)

which agrees with the numerically calculated value (eq. (A2.13)). Any functions r_i can be inputs to the overall rate function r in eq. (A2.1). In the case where the functional form of r_i is a transition-state theory rate function ($r_i = k_i \prod_j a_j^{\psi_{ij}}$), then the sensitivity of the rate with respect to r_i is equal to the sensitivity of the rate constant of step i (k_i), as derived in eq. (2.31). This occurs because $r_i \propto k_i$. The Matlab script for these calculations is copied below—it references the previous Matlab function defined for rate, above. Both are available online at https://github.com/foley352/JCat-SI-DoRC-1:

```
%definiton of ki and ri
k1=1;kr1=0.4
r1=@(x) x(1)/x(2)*k1^2/kr1-exp(-x(3));
rr1=@(x) sqrt(x(2))*x(3);
r2=@(x) x(2)/(x(3))^0.1;
r3=@(x) x(3)^4-x(2);

[rxnrate0,thetaSS]=rate(r1,rr1,r2,r3);%rate with unperturbed inputs, output of
steady-state coverages

[rxnrate1,~]=rate(@(x) 1.0001*r1(x),rr1,r2,r3);%rate with r1 perurbed
[rxnrater1,~]=rate(r1,@(x) 1.0001*rr1(x),r2,r3);%rate with r-1 perturbed
[rxnrate2,~]=rate(r1,rr1,@(x) 1.0001*r2(x),r3);%rate with r2 perturbed
[rxnrate3,~]=rate(r1,rr1,r2,@(x) 1.0001*r3(x));%rate with r3 perturbed

%calulation of sensitivities
s1=(rxnrate1-rxnrate0)/0.0001/rxnrate0;
sr1=(rxnrater1-rxnrate0)/0.0001/rxnrate0;
s2=(rxnrate2-rxnrate0)/0.0001/rxnrate0;
s3=(rxnrate3-rxnrate0)/0.0001/rxnrate0;

%calculation of s_k1
k1=1.0001;
r1=@(x) x(1)/x(2)*k1^2/kr1-exp(-x(3));
[rxnratek1,~]=rate(r1,rr1,r2,r3);
sk1=(rxnratek1-rxnrate0)/0.0001/rxnrate0;
```

```
%output of sensitivities
sensitivities=[s1,sr1,s2,s3]
total=sum([s1,sr1,s2,s3]) %the total still sums to one because of units
[sk1,sensitivities(1)*((2*x(1)/x(2)*k1^2/kr1)/(x(1)/x(2)*k1^2/kr1-exp(-x(3))))]
%output of s_k1 and the calculated value from eq. 36
```

A2.2 Comparison of r_{TST} to r for a simple two-step catalytic reaction

In this section, we illustrate that the transition-state theory function, r_{TST}, is tangent to the rate function, r, about a specified point that the sensitivities are calculated (see eq. (2.38)). Consider the catalytic reaction scheme shown in Table A2.1 with the reaction parameters also shown in Table A2.1. The rate functions of the elementary steps are of the forms given in eqs. (A2.15)-(A2.17):

$$r_1 = k_1 a_A \theta_* L \tag{A2.15}$$

$$r_2 = k_2 a_B \theta_{A^*} L \tag{A2.16}$$

$$r_{-1} = k_{-1} \theta_{A^*} L \tag{A2.17}$$

where L is the number of catalytic active sites. The steady-state overall reaction rate is given by eq. (A2.18):

$$r = \frac{k_1 a_A k_2 a_B}{k_1 a_A + k_{-1} + k_2 a_B} L \tag{A2.18}$$

Each rate constant is of the form (eq. (A2.19)):

$$k_i = \frac{k_B T}{h} e^{\frac{\Delta S_i^{o \neq}}{R}} e^{\frac{-\Delta H_i^{o \neq}}{RT}} \tag{A2.19}$$

At T = 300 K, a_A = 100 and a_B = 1, the rate/L is equal to 1.79 x 10^{-2} s^{-1} and the sensitivities as calculated by eq. (2.4) are given by eqs. (A2.20)-(A2.22):

$$s_1 = \frac{k_2 a_B + k_{-1}}{k_1 a_A + k_{-1} + k_2 a_B} = 0.967 \tag{A2.20}$$

$$s_2 = \frac{k_1 a_A + k_{-1}}{k_1 a_A + k_{-1} + k_2 a_B} = 0.332 \tag{A2.21}$$

$$s_{-1} = \frac{-k_{-1}}{k_1 a_A + k_{-1} + k_2 a_B} = -0.300 \tag{A2.22}$$

From eq. (2.39), the transition-state theory rate function for the composite reaction is (eq. (A2.23):

$$r_{TST} = C \prod_i r_i^{s_i} = C r_1^{s_1} r_2^{s_2} r_{-1}^{s_{-1}} = C(k_1 a_A \theta_* L)^{s_1} (k_2 a_B \theta_{A^*} L)^{s_2} (k_{-1} \theta_{A^*} L)^{s_{-1}}$$

$$\tag{A2.23}$$

$$= C k_1^{s_1} k_2^{s_2} a_A^{s_1} a_B^{s_2} \theta_*^{s_1} \theta_{A^*}^{s_2 + s_{-1}} L$$

From eq. (2.76), because the surface species behave ideally in this example, the surface coverages of empty sites and A* are given by eq. (A2.24) and eq. (A2.25):

$$\theta_* = \sum_{i=rxn} s_i \nu_{i*} [\nu_{i*} < 0] \bigg/ \sum_{\substack{j^*=surface \\ species}} \sum_{i=rxn} s_i \nu_{ij^*} [\nu_{ij^*} < 0] = \frac{s_1}{s_1 + s_{-1} + s_2}$$

$$\tag{A2.24}$$

$$= 0.967$$

$$\theta_{A^*} = \frac{s_{-1} + s_2}{s_1 + s_{-1} + s_2} = 0.033 \tag{A2.25}$$

The arbitrary constant C is calculated using eq. (2.34) (eq. (A2.26)):

$$C = \frac{r|_X}{\prod_i r_i^{s_i}|_X} = \frac{(1.79 \times 10^{-2} \ s^{-1})L}{k_1^{s_1} k_2^{s_2} a_A^{s_1} a_B^{s_2} \theta_*^{s_1} \theta_{A^*}^{s_2 + s_{-1}} L} = 0.550 \tag{A2.26}$$

With the arbitrary constant determined, the transition-state theory rate function (r_{TST}) is defined. The overall rate, r, is plotted with r_{TST} as a function of temperature (Figure A2.1), the activity of A (Figure A2.2), and the activity of B (Figure A2.3). The function

r_{TST} is the transition-state theory-form rate function for r at the point indicated by the circle in Figures A2.1-A2.3. The function r_{TST} is tangent to r with respect to every variable—including the physical variables that determine the reaction condition, such as temperature and activities of fluid-phase species, but also with respect to fundamental constants such as the gas constant R, as shown in Figure A2.4.

The TST-form rate function, r_{TST}, is equal to the overall rate function, r, with respect to differential changes in every variable about a point, $\boldsymbol{X}$, which represents the reaction condition at steady-state. At this reaction condition, the sensitivities, s_i, are calculated to define r_{TST} as a sensitivity-weighted-average function of the rate function of the elementary steps $\left(r_{TST} = C \prod_i r_i^{s_i}\right)$.

Table A2.1: Reaction parameters for a simple catalytic reaction

Reaction	$\Delta S_i^{o\neq}$ / J (mol K)$^{-1}$	$\Delta H_i^{o\neq}$ / kJ (mol)$^{-1}$
$A + * \rightarrow A^*, k_1$	20	100
$A^* \rightarrow A + *, k_{-1}$	10	-80
$A^* + B \rightarrow C + *, k_2$	-250	0
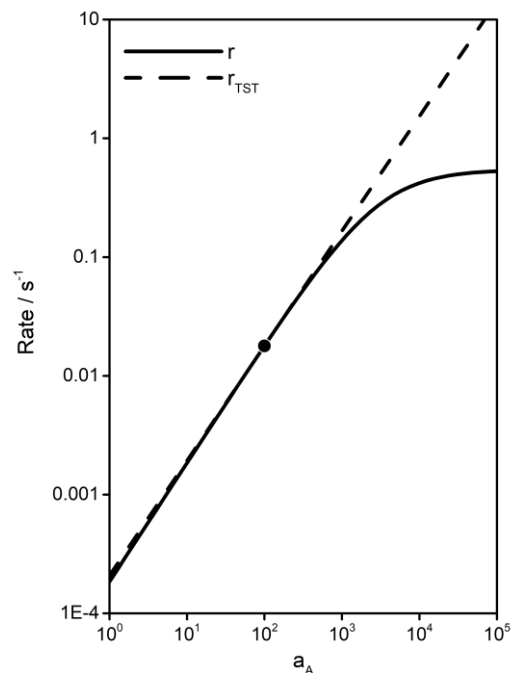
Figure A2.1: r and r_{TST} versus the activity of A for the reaction scheme shown in Table A2.1 with $a_B = 1$ and T = 300 K.
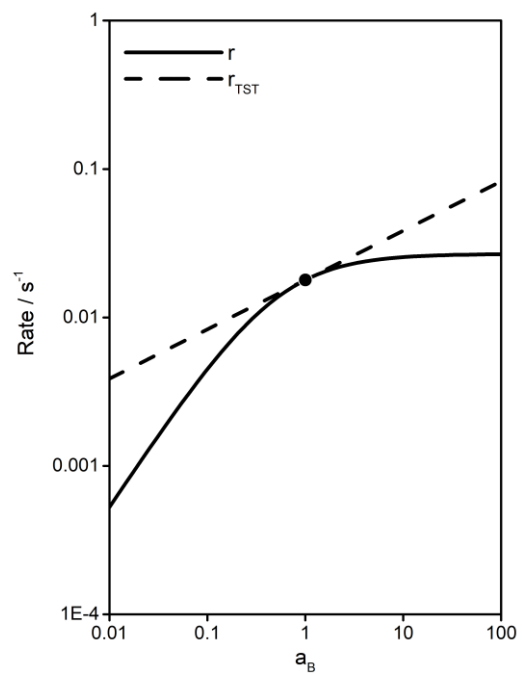
Figure A2.2: r and r_{TST} versus the activity of B for the reaction scheme shown in Table A2.1 with $a_A = 100$ and T = 300 K.
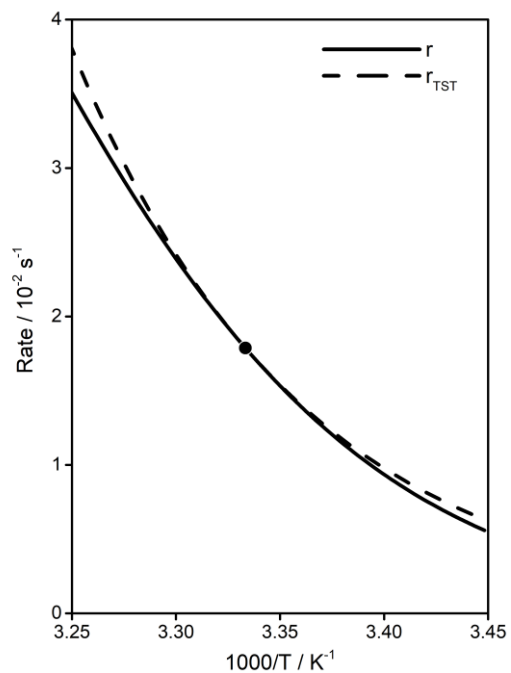
Figure A2.3: r and r_{TST} versus 1000/T for the reaction scheme shown in Table A2.1 with $a_A = 100$ and $a_B = 1$.
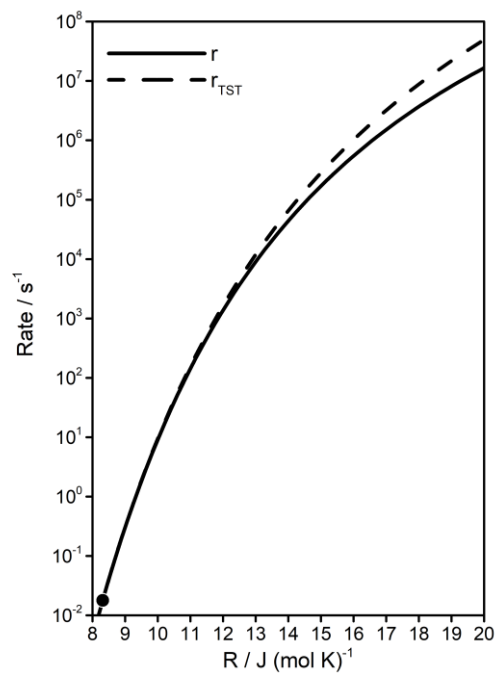
Figure A2.4: r and r_{TST} versus R for the reaction scheme shown in Table A2.1 with $a_A = 100$, $a_B = 1$ and T = 300 K.

A2.3 Relating apparent reaction orders of species to sensitivities using the formal definition of the derivative as a limit

Here we show that the relationship between reaction orders and sensitivities can be realized using Taylor-series expansions and the formal definition of the derivative as a limit. As discussed in Section A2.1, the rate of a catalytic reaction can be written as a function of the rate functions of the elementary steps, as is illustrated more generally here for a combined system of fluid-phase and catalytic reactions (eq. (A2.27)):

$$r(r_1, r_{-1}, \ldots, r_i, r_{-i}, \ldots, r_N, r_{-N})$$

$$
= \left\{
\begin{array}{c}
\dfrac{d\boldsymbol{\theta}}{dt} = 0 = \displaystyle\sum_i \nu_{ij^*} r_i(\boldsymbol{a}, \boldsymbol{\theta}) \\[2ex]
\dfrac{d\boldsymbol{a}}{dt} = 0 = \displaystyle\sum_i \nu_{ij} r_i(\boldsymbol{a}, \boldsymbol{\theta}) \\[2ex]
\displaystyle\sum_{j^*} \theta_{j^*} = 1 \\[2ex]
vary\ \boldsymbol{a}\ and\ \boldsymbol{\theta}\ such\ that\ the\ above\ equations\ are\ true, then: \\[1ex]
r = \displaystyle\sum_i \nu_{ip} r_i(\boldsymbol{a}, \boldsymbol{\theta})
\end{array}
\right.
\tag{A2.27}
$$

where $\boldsymbol{\theta}$ is a vector of all surface species (including vacant sites), and $\boldsymbol{a}$ is a vector of the activities of all fluid-phase reaction intermediates, ν_{ip} is the stoichiometric coefficient for the product in reaction i. The rate functions of the elementary steps are of the form (eq. (A2.28)):

$$r_i = k_i \prod_j a_j^{\psi_{ij}} \prod_{j^*} \theta_{j^*}^{\psi_{ij^*}} \tag{A2.28}$$

For this example, we consider only the case where activities of fluid-phase species are ideal and where surface species behave ideally. The sensitivity is defined in eq. (2.4) as (eq. (A2.29)):

255

$$s_i = \left(\frac{\partial \ln r}{\partial \ln k_i}\right)_{k_{j \neq i}}$$

$$= \lim_{\delta \to 0} \frac{k_i}{r(k_i)} \frac{r\big((1+\delta)k_i\big) - r(k_i)}{(1+\delta)k_i - k_i} \tag{A2.29}$$

$$= \lim_{\delta \to 0} \frac{r\big((1+\delta)k_i\big) - r(k_i)}{\delta r(k_i)}$$

The apparent reaction order of the activity of species m $\left(\psi_{m,app}\right)$ is defined in eq. (2.36) as (eq. (A2.30)):

$$\psi_{m,app} = \left(\frac{d \ln r}{d \ln a_m}\right) = \lim_{\delta \to 0} \frac{r\left((1+\delta)a_m, a_{j \neq m}\right) - r\left(a_m, a_{j \neq m}\right)}{\delta r(a_m, a_{j \neq m})} \tag{A2.30}$$

If we substitute $(1+\delta)a_m$ into the rate function for an elementary step, we find (eq. (A2.31)):

$$r_i\big(k_i, (1+\delta)a_m, a_{j \neq m}, \theta_{j^*}\big) = k_i\big((1+\delta)a_m\big)^{\psi_{im}} \prod_{j \neq m} a_j^{\psi_{ij}} \prod_{j^*} \theta_{j^*}^{\psi_{ij^*}}$$

$$= (1+\delta)^{\psi_{im}} k_i \prod_j a_j^{\psi_{ij}} \prod_{j^*} \theta_{j^*}^{\psi_{ij^*}} \tag{A2.31}$$

The Taylor-series expansion of $(1+\delta)^{\psi_{ij}}$ about the point $\delta = 0$ noting that $\delta \ll 1$ is (eq. (A2.32)):

$$(1+\delta)^{\psi_{ij}} = 1 + \psi_{ij}\delta + O(0) \tag{A2.32}$$

where $O(0)$ represents order-zero terms. Then eq. (A2.31) becomes eq. (A2.33):

$$r_i\big(k_i, (1+\delta)a_j, \theta_{j^*}\big) = (1 + \psi_{ij}\delta)k_i \prod_j a_j^{\psi_{ij}} \prod_{j^*} \theta_{j^*}^{\psi_{ij^*}} \tag{A2.33}$$

It follows from eq. (A2.33) that a $1 + \delta$ factor multiplying the activity is the same as a $(1 + \psi_{ij}\delta)$ factor multiplying the rate constant (eq. (A2.34)):

$$r_i\big(k_i, (1 + \delta)a_j, \theta_{j^*}\big) = r_i\left((1 + \psi_{ij}\delta)k_i, a_j, \theta_{j^*}\right) \tag{A2.34}$$

We show in eq. (A2.27) that the rate can be written with rate functions for elementary reaction steps as the independent variables. Thus we can write (eq. (A2.35)):

$$r\big(\boldsymbol{k}, (1 + \delta)a_j\big) = r\big(r_i(k_i, (1 + \delta)a_j), r_{-i}(k_{-i}, (1 + \delta)a_j), \dots\big) \tag{A2.35}$$

where $\boldsymbol{k}$ is a vector of all rate constants. From eq. (A2.34) we obtain eq. (A2.36):

$$
\begin{aligned}
r\big(r_i(k_i, (1 + \delta)a_j), r_{-i}(k_{-i}, (1 + \delta)a_j), \dots\big) \\
= r\left(r_i\left((1 + \psi_{ij}\delta)k_i, a_j\right), r_{-i}\left((1 + \psi_{-ij}\delta)k_{-i}, a_j\right), \dots\right)
\end{aligned}
\tag{A2.36}
$$

Thus, we can relate the apparent reaction order of the activity of species a_j to the limit in eq. (A2.37):

$$
\begin{aligned}
\frac{d \ln r}{d \ln a_j} &= \lim_{\delta \to 0} \frac{\left(r\big(r_i(k_i, (1 + \delta)a_j), \dots\big) - r\big(r_i(k_i, a_j), \dots\big)\right)}{\delta r\big(r_i(k_i, a_j), \dots\big)} \\[2mm]
&= \lim_{\delta \to 0} \frac{\left(r\big(r_i((1 + \psi_{ij}\delta)k_i, a_j), \dots\big) - r\big(r_i(k_i, a_j), \dots\big)\right)}{\delta r\big(r_i(k_i, a_j), \dots\big)}
\end{aligned}
\tag{A2.37}
$$

Equation (A2.37) can be simplified by noting the form of the multivariable Taylor-series expansion (eq. (A2.38)):

$$f(x + \Delta x, y + \Delta y) = f(x, y) + f'_x(x, y)(\Delta x) + f'_y(x, y)(\Delta y) \tag{A2.38}$$

Thus, eq. (A2.38) can be written in terms of the sensitivities (eq. (A2.39)):

$$\psi_{j,app} = \frac{d \ln r}{d \ln a_j}$$

$$= \lim_{\delta \to 0} \frac{\left(r\left(r_i\left((1 + \psi_{ij}\delta)k_i, a_j\right), \dots\right) - r\left(r_i(k_i, a_j), \dots\right)\right)}{\delta r\left(r_i(k_i, a_j), \dots\right)} \tag{A2.39}$$

$$= \frac{\sum_i \psi_{ij}\delta k_i \left.\frac{dr}{dk_i}\right|_{k_i,a_j}}{\delta r\left(r_i(k_i, a_j), \dots\right)} = \sum_i \psi_{ij} \left.\frac{d \ln r}{d \ln k_i}\right|_{k_i,a_j} = \sum_i \psi_{ij} s_i$$

and we find that the apparent reaction order of the overall rate is a sensitivity-weighted average of the reaction orders of the elementary steps. The same procedure can be followed to determine that (eq. (A2.40)):

$$\psi_{j^*,app} = \left(\frac{\partial \ln r}{\partial \ln \theta_{j^*}}\right)_{\theta_{n \neq j^*}} = \sum_i \psi_{ij^*} s_i \tag{A2.40}$$

Notice that eq. (A2.39) is written as a total derivative while eq. (A2.40) is written as a partial derivative while keeping constant all other surface species. This is because there is no constraint on the values of the fluid-phase activities, whether they are reactants, products, or reaction intermediates. There is, however, a constraint that the fractional coverages of surface species must sum to unity $\left(\sum_{j^*} \theta_{j^*} = 1\right)$. Finally, in eq. (2.31) the sensitivity was redefined as a partial derivative with respect to the rate function of an elementary step. This is easily proven by recognizing that multiplying the rate constant k_i by $(1 + \delta)$ is equivalent to multiplying the rate function of an elementary step by $(1 + \delta)$ because $r_i \propto k_i$ (eq. (A2.41)):

$$s_i = \left(\frac{\partial \ln r}{\partial \ln k_i}\right)_{k_{j \neq i}} = \lim_{\delta \to 0} \frac{r\big(r_i\big((1 + \delta)k_i\big), \dots\big) - r\big(r_i(k_i), \dots\big)}{\delta r\big(r_i(k_i), \dots\big)}$$

$$= \lim_{\delta \to 0} \frac{r\big((1 + \delta)r_i(k_i), \dots\big) - r\big(r_i(k_i), \dots\big)}{\delta r\big(r_i(k_i), \dots\big)} = \left(\frac{\partial \ln r}{\partial \ln r_i}\right)_{r_{j \neq i}}$$

<div align="right">(A2.42)</div>

A2.4 Analogy between the constant of integration C in r_{TST} and the conversion coefficient, ξ

Here we draw analogy between the arbitrary constant of integration that appears in the TST-form rate function of the composite reaction (eq. (2.33)) and the conversion coefficient, ξ, which appears as a multiplicative factor in transition-state theory.[1] The basis for this analogy becomes apparent for the case study described herein. The TST-form rate function of a composite reaction is (eq. (A2.43))

$$r_{TST} = C \prod_i r_i^{s_i}$$

$$= C \frac{k_B T}{h} e^{-\sum_i \left(s_i G_{TS,|i|}^o + \sum_j s_i v_{ij}[v_{ij} < 0]G_j^o\right)/k_B T} \prod_j a_j^{-\sum_i s_i v_{ij}[v_{ij} < 0]}$$

<div align="right">(A2.43)</div>

eq. (A2.43) is similar to the form of a transition-state theory rate function of an elementary step, with the exception of a constant of integration, C. The transition-state theory rate functions of elementary steps can have multiplicative factors such as the conversion coefficient, ξ_i, such that the TST rate function of the elementary step, i, is (eq. (A2.44)):

$$r_i = \xi_i \frac{k_B T}{h} e^{-\Delta G_i^{o \neq}/k_B T} \prod_j a_j^{-\Sigma_i \nu_{ij}[\nu_{ij}<0]} \qquad (A2.44)$$

where ξ_i is determined from combined phase-space/trajectory analysis (CPS/T).[153,154] The

conversion coefficient is a factor that accounts for scenarios when each crossing of the

transition state in the forward direction does not necessarily lead to products because the

activated complex can return over the transition state in the reverse direction before

forming the products of the elementary step. In CPS/T analysis, the conversion

coefficient is determined by sampling trajectories originating from reactants and dividing

the number of successful trajectories that form products by the number of crossings of a

dividing surface, preferably located at the transition state saddle point, in the forward

direction.[153,154] We extend this concept by analogy to the TST-form rate function of a

composite reaction by defining an apparent conversion coefficient, ξ_{app}, of the apparent

rate-determining step of the composite reaction.

Within the framework of this analogy, we show by example that when the

crossings of rate-limiting transition states have a one-to-one correspondence with the

formation of the product(s) of interest, the constant of integration, C, is unity, and when

the crossings of rate-limiting transition states do not always lead to formation of the

products of interest, then this multiplicative factor can be calculated using combined

phase-space/trajectory analysis (CPS/T). Consider the three-step reaction sequence in

Scheme A2.1, where species A and B are in equilibrium and $k_3 \gg k_2$, such that the

pseudo-steady-state assumption on intermediate C is valid. The pseudo-steady-state rate

of D formation for this composite reaction is given by eq. (A2.45):

$$r = \frac{k_1 k_2}{k_{-1}} a_A \tag{A2.45}$$

By applying TST to the equilibrium between the apparent initial and transition states in Scheme A2.1, the TST-form rate function of the composite reaction is equal to eq. (A2.46):

$$r_{TST} = C \frac{k_B T}{h} a_A^{s_1} a_B^{s_{-1}+s_2} a_C^{s_3}$$

$$\times e^{-\left((s_1+s_{-1})G_{TS,1}^o + s_2 G_{TS,2}^o + s_3 G_{TS,3}^o - (s_1 G_A^o + (s_{-1}+s_2)G_B^o + s_3 G_C^o)\right)/k_B T} \tag{A2.46}$$

$$= C k_1^{s_1} k_{-1}^{s_{-1}} k_2^{s_2} k_3^{s_3} a_A^{s_1} a_B^{s_{-1}+s_2} a_C^{s_3}$$

The sensitivities calculated by applying the formula $s_i = (\partial \ln r / \partial \ln k_i)_{k_{j \neq i}}$ to eq. (A2.45) gives $s_1 = 1, s_{-1} = -1, s_2 = 1$, and $s_3 = 0$. Substitution of these values into eq. (A2.46) arrives at eq. (A2.47):

$$r = C \frac{k_B T}{h} a_A e^{-(G_{TS,2}^o - G_A^o)/RT} = C \frac{k_1 k_2}{k_{-1}} a_A \tag{A2.47}$$

which is identical to the rate function shown in eq. (A2.47) when $C = 1$.

Scheme A2.1: Three-step fluid-phase reaction sequence. (Left) Elementary reaction steps with stoichiometric coefficients to sum to the overall reaction.(Right) Equilibrium reactions between initial states and transition states of elementary reactions with stoichiometric numbers equal to the sensitivity. The overall equilibrium reaction between the apparent initial and apparent transition state is equal to the sum of the equilibrium reactions between the initial and transition states of each elementary step with stoichiometric numbers equal to the sensitivities.

$$A \leftrightarrow B, \quad k_1, k_{-1} \quad \sigma = 1 \qquad\qquad A \leftrightarrow TS_1, \quad \sigma = s_1$$

$$B \rightarrow C, \quad k_2 \qquad\quad \sigma = 1 \qquad\qquad B \leftrightarrow TS_1, \quad \sigma = s_{-1}$$

$$C \rightarrow D, \quad k_3 \qquad\quad \sigma = 1 \qquad\qquad B \leftrightarrow TS_2, \quad \sigma = s_2$$

$$\qquad\qquad\qquad\qquad\qquad\qquad\qquad\qquad C \leftrightarrow TS_3, \quad \sigma = s_3$$

$$\text{Overall:} \quad A \rightarrow D \qquad\qquad s_1 A + (s_{-1} + s_2)B + s_3 C$$

$$\qquad\qquad\qquad\qquad\qquad\qquad\qquad \leftrightarrow (s_1 + s_{-1})TS_1 + s_2 TS_2 + s_3 TS_3$$
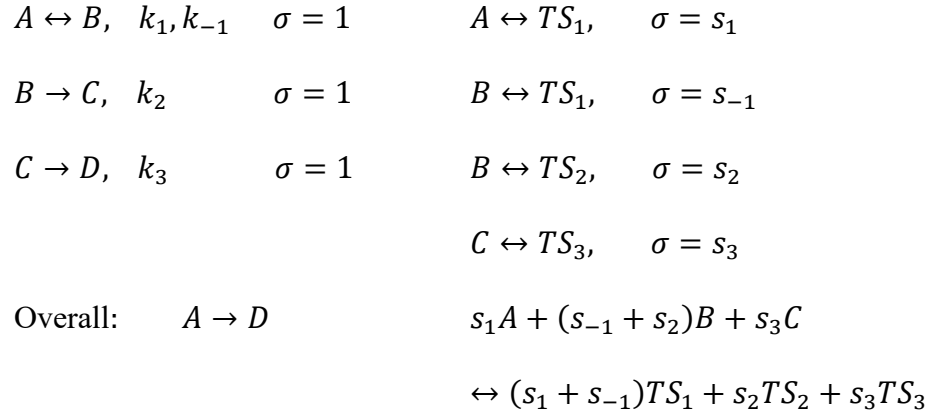
The above example assumes that A and B are equilibrated. In this next example, the same composite reaction network illustrated in Scheme A2.1 is considered, but the equilibrium assumption is relaxed and instead the pseudo-steady-state assumption is applied to species B. The rate function is now given by eq. (A2.48):

$$r = \frac{k_1 k_2}{k_{-1} + k_2} a_A \qquad\qquad\qquad\qquad (A2.48)$$

The TST-form rate function is still given by eq. (A2.46) because the network connectivity remains unchanged, but the sensitivities corresponding to eq. (A2.48) are now (eqs. (A2.49)-(A2.52)):

$$s_1 = 1 \qquad\qquad\qquad\qquad (A2.49)$$

$$s_{-1} = -\frac{k_{-1}}{k_{-1} + k_2} \qquad\qquad\qquad\qquad (A2.50)$$

$$S_2 = \frac{k_{-1}}{k_{-1} + k_2} \tag{A2.51}$$

$$S_3 = 0 \tag{A2.52}$$

The constant of integration is found by eq. (A2.53):

$$C = \frac{r|_X}{\prod_i r_i^{s_i}|_X} \tag{A2.53}$$

Note that the denominator in eq. (A2.53) is the TST-form rate function r_{TST} (eq. (A2.46)) taking $C = 1$. The rate of the composite/overall reaction from eq. (A2.48) divided by the TST-form rate equation (taking $C = 1$) gives the value of the arbitrary constant, C. This is plotted as a function of the reversibility of the first reaction, $Z_1 = r_{-1}/r_1$, in Figure A2.5 with $k_1 = 1, k_2 = 10, k_3 = 100$ and k_{-1} varied from 0 to 10^4 for illustration. When the first reaction is equilibrated or irreversible, the constant C is equal to unity. However, when the first reaction is reversible but not equilibrated, the constant C takes on values less than one. This difference is caused by a non-one-to-one correspondence between crossings of the rate-limiting transition states and formation of the final products.
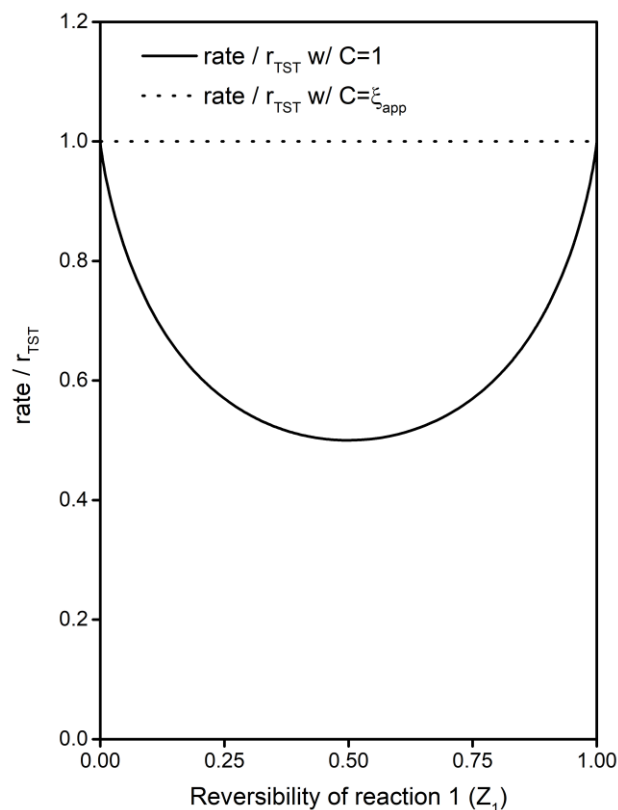
Figure A2.5: The rate (eq. (A4.48)) of a composite reaction with a reversible step divided by r_{TST} with $C = 1$ (eq. (A2.46), solid line) or r_{TST} with $C = \xi_{app}$ (eq. (A2.58)), dotted line).

To determine the value of C, we extend the concept of the conversion coefficient by analogy to composite/overall reaction networks where we redefine a successful trajectory as one that forms the final product(s) of interest instead of the product(s) of the elementary step. In our definition, the conversion coefficient of an elementary step, ξ_i, is defined as the ratio of the successful trajectories that form the final products divided by the number of crossings of transition state i, where crossing the transition state in the reverse direction is considered crossing transition state $-i$ (eq. (A2.54)):

$$\xi_i = \frac{trajectories\ that\ form\ final\ products}{number\ of\ crossings\ of\ transition\ state\ i} \tag{A2.54}$$

The conversion coefficient is schematically illustrated in Figure A2.6, which depicts three trajectories on a potential energy surface where reactions are reversible. In Figure A2.6, there are three successful trajectories that form the product, C, six crossings of TS_1 in the forward direction, three crossings of TS_1 in the reverse direction, and three crossings of TS_2 in the forward direction. In this example, $\xi_1 = 3/6 = 1/2$, $\xi_{-1} = 3/3 = 1$, $\xi_2 = 3/3 = 1$. For a system of reactions in series where the pseudo-steady-state approximation is valid, the conversion coefficient, ξ_i, is a function of the reversibility, Z_i, as we discuss below. For a forward reaction, the probability that a given crossing of TS_i is successful is equal to $(1 - Z_i)$, since the probability of returning over TS_{-i} and therefore, not forming products, is Z_i (eq. (A2.55)):

$$\xi_i = (1 - Z_i), i > 0 \tag{A2.55}$$

The conversion coefficient of a reverse reaction is determined by calculating the expectation value for the number of crossings of the reverse transition state per successful trajectory. The probability of crossing that transition state zero times is equal to $(1 - Z_i)$, the probability of crossing precisely one time is equal to the probability of reflecting back over TS_i in the reverse direction once (Z_i) multiplied by the probability of not reflecting again $(1 - Z_i)$, etc., forming the infinite series shown in eq. (A2.56):

$$\xi_{-i} = \underbrace{\sum_{j=0}^{\infty}}_{number\ of\ crossings} Z_i^j (1 - Z_i) * j = \frac{1 - Z_i}{Z_i} \tag{A2.56}$$

The apparent transition state is a sensitivity-weighted average of the transition states of elementary steps and there is one ξ_i associated with each r_i, thus ξ_{app} is a geometric average of the ξ_i of elementary steps by eq. (A2.57):

$$\xi_{app} = \prod_{i=rxn} \xi_i^{s_i} \tag{A2.57}$$

The TST-form rate function of the composite reaction with ξ_{app} is eq. (A2.58):

$$r_{TST} = \xi_{app} k_1^{s_1} k_{-1}^{s_{-1}} k_2^{s_2} k_3^{s_3} a_A^{s_1} a_B^{s_{-1}+s_2} a_C^{s_3} \tag{A2.58}$$

Figure A2.5 shows that the ratio of the rate (eq. (A2.48)) divided by r_{TST} with $C = \xi_{app}$ (eq. (A2.58)) is always equal to unity for the case study considered. Hence, the arbitrary constant C is analogous to the conversion coefficient ξ.
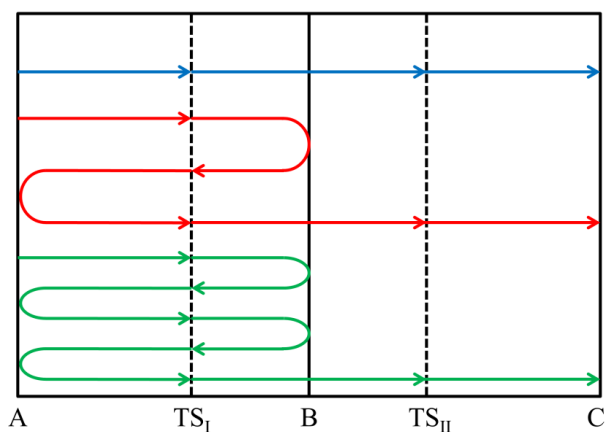
Figure A2.6: A trajectory along the reaction coordinate with reversible reactions. Modified from Anderson, J. B. J. Chem. Phys. **1973**, 58, 4684–4692.[153]

A2.5 Proof that sums of sensitivities are constrained because of units

In Section 2.3.3, we noted that the power of $k_B T/h$ in eq. (2.39) is equal to unity because rate has units of s^{-1}, and that the power of $k_B T/h$ is equal to the sum of the sensitivites, which must therefore be equal to unity. In this section, we provide a more general proof that units are why the sums of sensitivites and sums of degrees of rate control are constrained. Take a generic function $f = f(x_1, x_2, \dots)$ that depends on indefinitely many variables, x_i. The units of f are units of rate, s^{-1}. It is possible to prove on the basis of

units that the sum of the sensitivities of a subset of the variables of the function must sum

to one by redefining each variable as a unitless component, x_i', and a unitted component,

u_j, where the subscript j corresponds to the unit. For example, if $x_1 = 3\ m/s^2$, this can

be rewritten as (eq. (A2.59)):

$$x_1 = x_1' u_m / u_s^2 \tag{A2.59}$$

where $x_1' = 3$, $u_m = 1\ m$, and $u_s = 1\ s$. The function f, because it has only units of s^{-1},

must be able to be written in the form (eq. (A2.60)):

$$f(x_1, x_2, \dots) = f'(x_1', x_2', \dots) / u_s \tag{A2.60}$$

where all $u_{i \neq s}$ cancel out, and thus f' is only a function of x_i'. Thus, taking the derivative

of $\ln f$ with respect to $\ln u_s$ on both sides of eq. (A2.60) we find (eq. (A2.61)):

$$\frac{d \ln f}{d \ln u_s} = \sum_i \left(\frac{\partial \ln f}{\partial \ln x_i} \right)_{x_{j \neq i}} \frac{d \ln x_i}{d \ln u_s} = -1 \tag{A2.61}$$

Now consider the case where f is the overall rate r and x_i are the rate functions for

elementary steps, r_i, the equation becomes (eq. (A2.62)):

$$\frac{d \ln r}{d \ln u_s} = \sum_i \left(\frac{\partial \ln r}{\partial \ln r_i} \right)_{r_{j \neq i}} \frac{d \ln r_i}{d \ln u_s} = -\sum_i s_i = -1 \tag{A2.62}$$

The partial derivative is the sensitivity (eq. (2.31)), s_i, and the total derivative is -1 for

each r_i because each rate function has units of s^{-1}. Equation (A2.62) proves that the

sensitivities sum to unity. The conservation of units offers a constraint on the values that

the sensitivites sum to. This should not be surprising because the sensitivity is a measure

of the apparent power to which a variable is taken to, and hence, the sums are constrained

by the units of the overall function. We demonstrate that units dictate the sum of sensitivities with a simple example, one in which f is not a rate function.

Consider the function f with units of m/s^2 where (eq. (A2.63)):

$$f(x_1, x_2, x_3, x_4, x_5) = \frac{(x_1 x_2)^{\frac{1}{3}}}{\dfrac{x_3}{x_4} + \dfrac{x_3^2 x_5}{x_2}} \tag{A2.63}$$

and x_i have units of: $x_1[=]m/s^2$, $x_2[=]m^2/s$, $x_3[=]m$, $x_4[=]m/s$, and $x_5[=]unitless$. On the basis of units, we expect that since f has units of m^1, then (eq. (A2.64)):

$$s_1 + 2s_2 + s_3 + s_4 = 1 \tag{A2.64}$$

where the coefficients that multiply the sensitivities are determined by the power to which each x_i depends on m. Likewise, because f has units of s^{-2}, then (eq. (A2.65)):

$$-2s_1 - s_2 - s_4 = -2 \tag{A2.65}$$

The sensitivities are given by eq. (A2.66)-(A2.70):

$$s_1 = \left(\frac{\partial \ln f}{\partial \ln x_1} \right)_{x_{j \neq 1}} = \frac{1}{3} \tag{A2.66}$$

$$s_2 = \left(\frac{\partial \ln f}{\partial \ln x_2} \right)_{x_{j \neq 2}} = \frac{4}{3} - \frac{x_2}{x_2 + x_3 x_4 x_5} \tag{A2.67}$$

$$s_3 = \left(\frac{\partial \ln f}{\partial \ln x_3} \right)_{x_{j \neq 3}} = \frac{x_2}{x_2 + x_3 x_4 x_5} - 2 \tag{A2.68}$$

$$s_4 = \left(\frac{\partial \ln f}{\partial \ln x_4}\right)_{x_{j \neq 4}} = \frac{x_2}{x_2 + x_3 x_4 x_5} \tag{A2.69}$$

$$s_5 = \left(\frac{\partial \ln f}{\partial \ln x_5}\right)_{x_{j \neq 5}} = \frac{-x_3^2 x_5 / x_2}{\dfrac{x_3}{x_4} - x_3^2 x_5 / x_2} \tag{A2.70}$$

Substituting eqs. (A2.66)-(A2.70) into eqs. (A2.64) and (A2.65) (eqs. (A2.71) and (A2.72)):

$$s_1 + 2s_2 + s_3 + s_4$$

$$= \frac{1}{3} + 2\left(\frac{4}{3} - \frac{x_2}{x_2 + x_3 x_4 x_5}\right) + \frac{x_2}{x_2 + x_3 x_4 x_5} - 2 \tag{A2.71}$$

$$+ \frac{x_2}{x_2 + x_3 x_4 x_5} = 1$$

$$-2s_1 - s_2 - s_4 = -2\left(\frac{1}{3}\right) - \left(\frac{4}{3} - \frac{x_2}{x_2 + x_3 x_4 x_5}\right) - \frac{x_2}{x_2 + x_3 x_4 x_5} = -2 \tag{A2.72}$$

in agreement with what were expected based on units.

A2.6 Sensitivities for mass-transfer limited reactions

We demonstrated in Section A2.5 above that the only constraint for the sum of sensitivities and the kinetic degrees of rate control is imposed by the units—the rates of the elementary steps have the same units as the rate of the overall reaction, and thus the sensitivities must sum to unity. In this way, there is nothing inherently special about a reaction system that causes the sum of the sensitivities and kinetic degrees of rate control to sum to unity, but it is convenient, as the sensitivity thus becomes a measure of the relative contribution of an elementary step rate function to the TST-from rate function.

Because there is nothing inherently unique about composite reaction systems, the concept of sensitivities can be applied to other systems as we demonstrate by example for an external mass-transfer limited catalytic reaction system.

Consider a first-order reaction with external mass transfer limitations and no internal mass transfer limitations. The rate of external mass transfer (r_m) is described by (eq. (A2.73)):

$$r_m = \bar{k}_c (a_{A,B} - a_{A,S}) A \tag{A2.73}$$

where $\bar{k}_c$ is the external mass transfer coefficient with units of cm/s, $a_{A,B}$ is the activity of species A in the bulk phase, $a_{A,S}$ is the activity of A at the surface (which is equal to the activity of A throughout the entire particle), and A is the surface area (cm^2). The reaction rate (r_r) is given by (eq. (A2.74)):

$$r_r = k a_{A,S} V \tag{A2.74}$$

where V is volume of particle (cm^3) and k is the intrinsic rate constant (s^{-1}). At steady-state, the mass transfer rate must equal the reaction rate, $r_m = r_r$ and thus at steady state (eq. (A2.75)):

$$\bar{k}_c (a_{A,B} - a_{A,S}) A = k a_{A,S} V \tag{A2.75}$$

The solution of this equation gives the observed steady-state reaction rate, r (eq. (A2.76)):

$$r = \frac{k \bar{k}_c \left(\frac{A}{V}\right)}{k + \bar{k}_c \left(\frac{A}{V}\right)} a_{A,B} V = \frac{k \bar{k}_c (3/R)}{k + \bar{k}_c (3/R)} a_{A,B} V \tag{A2.76}$$

where R is the radius of a spherical catalyst particle. The steady-state reaction rate is a function of the mass transfer rate function and the reaction rate function, such that (eq. (A2.77)):

$$r = r\left(r_m(\bar{k}_c, R), r_r(k, R)\right) \tag{A2.77}$$

We can then define sensitivities for the rate of mass transfer and the rate of reaction as eqs. (A2.78) and (A2.79):

$$s_m = \left(\frac{\partial \ln r}{\partial \ln r_m}\right)_{r_r} \tag{A2.78}$$

$$s_r = \left(\frac{\partial \ln r}{\partial \ln r_r}\right)_{r_m} \tag{A2.79}$$

By integrating eqs. (A2.78) and (A2.79), a function for the curve tangent to r/V at a point is derived, denoted $r_{tangent}$ (eq. (A2.80)):

$$r_{tangent} = C r_m^{s_m} r_r^{s_r} = C\left(\bar{k}_c\left(a_{A,B} - a_{A,S}\right)A\right)^{s_k}\left(k a_{A,S} V\right)^{s_r} \tag{A2.80}$$

Both r_m and r_r have units of s^{-1}, thus $s_m + s_r = 1$. Unlike the case where there are no mass transfer limitations, this function $r_{tangent}$ does not resemble a TST-form rate function. Instead, it takes on a mixed-form rate function that is a product of the mass-transfer rate function and the TST-form rate function, the contributions of which are determined by the sensitivities s_m and s_r. Both the chemical reaction and mass transfer are *resistances* to the overall rate, and the sensitivities for this system quantify how much each of these rate processes is limiting the observed rate. For $k = 2.36 \, s^{-1}$, $\bar{k}_c = 1.77 \, cm/s$, $R = 3.54 \, cm$, $a_A = 4.11$, then $C = 1$ (from eq. (2.35)), and $r_{tangent}$ is tangent to r with respect to each variable (Figure A2.7). At this condition, we find that

271

$s_m = 0.611$ and $s_r = 0.389$, implying that the reaction has severe external mass transfer limitations at this condition.
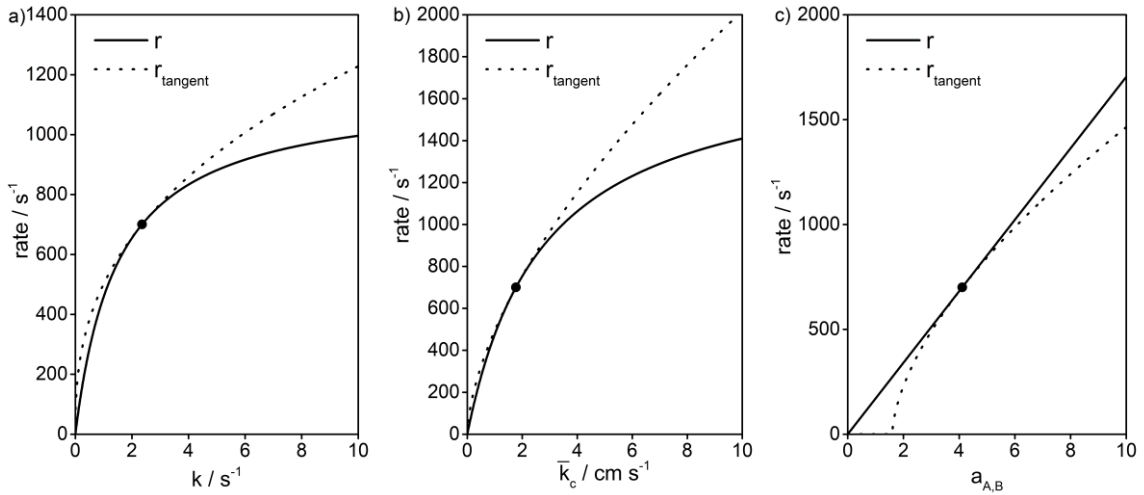
Figure A2.7: a) Rate as a function of the intrinsic rate constant k, b) rate as a function of the external mass transfer coefficient $\overline{k}_c$, and c) rate as a function of the bulk activity of A, $a_{A,B}$. Solid lines are the actual rates (eq. (A2.76)) and the dotted line is $r_{tangent}$ (eq. (A2.80)), with $s_m = 0.611$ and $s_r = 0.389$). If unspecified by the x-axis, $k = 2.36$ s^{-1}, $\overline{k}_c = 1.77$ cm s^{-1}, R = 3.54 cm, and $a_{A,B} = 4.11$. The location $r_{tangent}$ is tangent to r is specified by the circular point.

A3 Thermodynamically consistent forward and reverse degrees of rate control in reversible reactions

A3.1 Proofs of sensitivity and degree of rate control relationships

In this section, we prove various relationships between forward, reverse, and net rate sensitivities and degrees of rate control. We note that many of these proofs are identical to those presented in previous work, which will be referenced throughout this section, which is separated into subsections for each proof.

A3.1.1 Proof that $\vec{X}_{RC,i} = \vec{s}_i + \vec{s}_{-i}$ (eq. (3.15))

This proof follows analogously to proofs presented previously by Dumesic and coworkers (eq. (A3.1))[19,23]:

$$
\begin{aligned}
\vec{X}_{RC,i} &= \left(\frac{\partial \ln \vec{r}}{\partial (-G^o_{TS,i}/k_BT)} \right)_{G^o_{j \neq TS,i}} \\
&= \sum_n \left(\frac{\partial \ln \vec{r}}{\partial \ln k_n} \right)_{k_{m \neq n}} \left(\frac{\partial \ln k_n}{\partial (-G^o_{TS,i}/k_BT)} \right)_{G^o_{j \neq TS,i}} = \sum_n \vec{s}_n \delta_{i|n|} \qquad (A3.1) \\
&= \vec{s}_i + \vec{s}_{-i}
\end{aligned}
$$

where $\delta_{i|n|}$ is the Krönecker delta which is equal to one if $i = |n|$ and zero otherwise. This term arises because only the rate constants k_i and k_{-i} are function of $G^o_{TS,i}$. The one-line proof presented in eq. (A3.1) assumes the elementary step rate constants are in the form of transition-state theory rate constants (eq. (A3.2)):

$$k_i = \frac{k_B T}{h} \exp\left(-\frac{G^o_{TS,|i|} + v_{ij}[v_{ij} < 0]G^o_j}{k_B T}\right)$$

(A3.2)

where $[v_{ij} < 0]$ is one if true and zero if false such that only reactant standard-state free energies appear in eq. (A3.2). The transition state of a reverse reaction (negative i) is the same as the transition state for a forward reaction (positive i), which is why the transition state energy in eq. (A3.2) has an absolute value "$|i|$" in the subscript.

A3.1.2 Proof that $\vec{X}_{TRC,j} = \sum_i v_{ij}\vec{s}_i[v_{ij} < 0]$ (eq. (3.16))

This proof follows analogously to a proof presented in Chapter 2 (eq. (A3.3)):

$$\vec{X}_{TRC,j} = \left(\frac{\partial \ln \vec{r}}{\partial(-G^o_j/k_B T)}\right)_{G^o_{i \neq j}} = \sum_n \left(\frac{\partial \ln \vec{r}}{\partial \ln k_n}\right)_{k_{m \neq n}} \left(\frac{\partial \ln k_n}{\partial(-G^o_j/k_B T)}\right)_{G^o_{i \neq j}}$$

$$= \sum_n \vec{s}_n v_{ij}[v_{ij} < 0]$$

(A3.3)

The stoichiometric coefficients appear in eq. (A3.3) because the standard-state free energies of species are multiplied by stoichiometric coefficients in elementary step rate constants when species j is a reactant (see eq. (A3.2)).

A3.1.3 Proof that $\left(\frac{\partial \ln r}{\partial \ln \vec{r}}\right)_{\vec{r}}/\left(\frac{\partial \ln r}{\partial \ln \vec{r}}\right)_{\vec{r}} = -Z_{eff}$ (eq. (3.34))

This proof follows analogously to a proof presented in Chapter 2. The net rate of a reaction is defined as eq. (A3.4):

$$r = \vec{r} - \overleftarrow{r}$$

(A3.4)

The total derivative of the net rate is (eq. (A3.5)):

$$d \ln r = \left(\frac{\partial \ln r}{\partial \ln \vec{r}}\right)_{\overleftarrow{r}} d \ln \vec{r} + \left(\frac{\partial \ln r}{\partial \ln \overleftarrow{r}}\right)_{\vec{r}} d \ln \overleftarrow{r} \tag{A3.5}$$

We use eq. (A3.5) to find the partial derivative of $\ln r$ with respect to $\ln \vec{r}$ while keeping r constant (eq. (A3.6)):

$$\left(\frac{\partial \ln r}{\partial \ln \vec{r}}\right)_{r} = \left(\frac{\partial \ln r}{\partial \ln \vec{r}}\right)_{\overleftarrow{r}} \left(\frac{\partial \ln \vec{r}}{\partial \ln \vec{r}}\right) + \left(\frac{\partial \ln r}{\partial \ln \overleftarrow{r}}\right)_{\vec{r}} \left(\frac{\partial \ln \overleftarrow{r}}{\partial \ln \vec{r}}\right)_{r} \tag{A3.6}$$

which simplifies to eq. (A3.7):

$$0 = \left(\frac{\partial \ln r}{\partial \ln \vec{r}}\right)_{\overleftarrow{r}} + \left(\frac{\partial \ln r}{\partial \ln \overleftarrow{r}}\right)_{\vec{r}} \left(\frac{\partial \ln \overleftarrow{r}}{\partial \ln \vec{r}}\right)_{r} \tag{A3.7}$$

By rearranging eq. (A3.7) we find the ratio of the relative change in the net rate with respect to relative changes in the forward and reverse rates is given by eq. (A3.8):

$$\left(\frac{\partial \ln r}{\partial \ln \overleftarrow{r}}\right)_{\vec{r}} \Big/ \left(\frac{\partial \ln r}{\partial \ln \vec{r}}\right)_{\overleftarrow{r}} = -\left(\frac{\partial \ln \vec{r}}{\partial \ln \overleftarrow{r}}\right)_{r} \tag{A3.8}$$

The reverse rate as a function of the forward and net rate is $\overleftarrow{r} = \vec{r} - r$, and the derivative on the right-hand side of eq. (A3.8) is (eq. (A3.9)):

$$-\left(\frac{\partial \ln \vec{r}}{\partial \ln \overleftarrow{r}}\right)_{r} = -\frac{\overleftarrow{r}}{\vec{r}} \frac{\partial}{\partial \overleftarrow{r}} (\vec{r} - r)_{r} = -\frac{\overleftarrow{r}}{\vec{r}} = -Z_{eff} \tag{A3.9}$$

Thus by substitution of the result from eq. (A3.9) into eq. (A3.8) we arrive at the final result (eq. (A3.10)):

$$\left(\frac{\partial \ln r}{\partial \ln \overleftarrow{r}}\right)_{\vec{r}} \Big/ \left(\frac{\partial \ln r}{\partial \ln \vec{r}}\right)_{\overleftarrow{r}} = -Z_{eff} \tag{A3.10}$$

A3.1.4 Proof that $\left(\frac{\partial \ln r}{\partial \ln \vec{r}}\right)_{\overleftarrow{r}} + \left(\frac{\partial \ln r}{\partial \ln \overleftarrow{r}}\right)_{\vec{r}} = 1$

The net rate is written as the difference of the forward and reverse rates (eq. (A3.4)), and the partial derivatives of net rate with respect to forward/reverse rate while keeping the reverse/forward rate functions constant are sensitivities of the net rate to the forward/reverse rates, as opposed to sensitivities of the net rate to the rates of elementary steps. When the net rate is written in the form of eq. (A3.4), the net rate has two sensitivities, one for the sensitivity to the forward rate and one for the sensitivity to the reverse rate, and thus they are all of the sensitivities in the system, which must sum to unity. This is proven by defining the forward and reverse sensitivities as (eqs. (A3.11) and (A3.12)):

$$\vec{s} = \left(\frac{\partial \ln r}{\partial \ln \vec{r}}\right)_{\overleftarrow{r}} \tag{A3.11}$$

$$\overleftarrow{s} = \left(\frac{\partial \ln r}{\partial \ln \overleftarrow{r}}\right)_{\vec{r}} \tag{A3.12}$$

By integration of eqs. (A3.11) and (A3.12) and treating the sensitivities as constant, we derive an alternative function for rate, denoted r', is (eq. (A3.13)):

$$r' = C\vec{r}^{\vec{s}}\overleftarrow{r}^{\overleftarrow{s}} \tag{A3.13}$$

where C is a unitless arbitrary constant of integration. Since both sides of eq. (A3.13) have units of rate, it follows that (eq. (A3.14)):

$$\vec{s} + \overleftarrow{s} = \left(\frac{\partial \ln r}{\partial \ln \vec{r}}\right)_{\overleftarrow{r}} + \left(\frac{\partial \ln r}{\partial \ln \overleftarrow{r}}\right)_{\vec{r}} = 1 \tag{A3.14}$$

276

A3.1.5 Proof that $\vec{X}_{TRC,j^*} = -\vec{\sigma}_{*,app}\theta_{j^*}$ (eq. (3.53))

The proof of the relationship between forward thermodynamic degrees of rate control and steady-state fractional coverages is analogous to the proof for net rate thermodynamic degrees of rate control, as was presented in Chapter 2. The proof begins with a cyclic-chain rule identity (eq. (A3.15)):

$$\left(\frac{\partial \vec{r}}{\partial \theta_{1^*}}\right)_{\theta_{m\neq 1^*}} \left(\prod_{n=1}^{N-1}\left(\frac{\partial \theta_{n^*}}{\partial \theta_{(n+1)^*}}\right)_{r,\theta_{m\neq\{n^*,(n+1)^*\}}}\right)\left(\frac{\partial \theta_{N^*}}{\partial \vec{r}}\right)_{\theta_{m\neq N^*}} = (-1)^{N+1} \qquad (A3.15)$$

where species are randomly assigned values from 1 to N. Because the sum of the fractional coverages equals unity, $(\sum_j \theta_{j^*} = 1)$, the partial derivatives of one fractional coverage (n^*) with respect to another fractional coverage $((n+1)^*)$ while keeping all fractional coverages constant is (eq. (A3.16)):

$$\left(\frac{\partial \theta_{n^*}}{\partial \theta_{(n+1)^*}}\right)_{r,\theta_{m\neq(n^*,(n+1)^*)}} = -1 \qquad (A3.16)$$

Substitution of eq. (A3.16) into eq. (A3.15) gives eq. (A3.17):

$$\left(\frac{\partial \vec{r}}{\partial \theta_{1^*}}\right)_{\theta_{m\neq 1^*}} (-1)^{N-1}\left(\frac{\partial \theta_{N^*}}{\partial \vec{r}}\right)_{\theta_{m\neq N^*}} = (-1)^{N+1} \qquad (A3.17)$$

After dividing both sides by $(-1)^{N-1}$ and multiplying both sides by $\vec{r}/\vec{r}$ and $\theta_{1^*}/\theta_{N^*}$ and defining the partial derivative of the forward rate with respect to the fractional coverage of a species as the reaction order with respect to the fractional coverage, $\vec{\alpha}_{\theta j^*}$ (eq. (A3.18)):

$$\frac{\theta_{1^*}}{\vec{r}}\left(\frac{\partial \vec{r}}{\partial \theta_{1^*}}\right)_{\theta_{m\neq 1^*}} \frac{\vec{r}}{\theta_{N^*}}\left(\frac{\partial \theta_{N^*}}{\partial \vec{r}}\right)_{\theta_{m\neq N^*}} = \left(\frac{\partial \ln \vec{r}}{\partial \ln \theta_{1^*}}\right)_{\theta_{m\neq 1^*}} \left(\frac{\partial \ln \theta_{N^*}}{\partial \ln \vec{r}}\right)_{\theta_{m\neq N^*}} = \frac{\vec{\alpha}_{\theta 1^*}}{\vec{\alpha}_{\theta N^*}}$$

$$= \frac{\theta_{1^*}}{\theta_{N^*}}$$

(A3.18)

Because the numbers between 1 and N were randomly assigned to species, eq. (A3.18) shows that the ratio of any two $\vec{\alpha}_{\theta j^*}$ is equal to the ratio of the fractional coverages. From this we can write eq. (A3.19):

$$\frac{\vec{\alpha}_{\theta N^*}}{\sum_{j^*} \vec{\alpha}_{\theta j^*}} = \left(\sum_{j^*} \frac{\vec{\alpha}_{\theta j^*}}{\vec{\alpha}_{\theta N^*}}\right)^{-1} = \left(\sum_{j^*} \frac{\theta_{j^*}}{\theta_{N^*}}\right)^{-1} = \left(\frac{1}{\theta_{N^*}}\right)^{-1} = \theta_{N^*}$$

(A3.19)

where we find that the fractional coverage of a species is equal to the forward reaction order for that species' fractional coverage divided by the sum of the forward reaction orders for all surface species. The apparent reaction order of the fractional coverage of a species is related to the sensitivities by the chain rule (eq. (A3.20)):

$$\vec{\alpha}_{\theta j^*} = \left(\frac{\partial \ln \vec{r}}{\partial \ln \theta_{j^*}}\right)_{\theta_{m\neq j^*}} = \sum_i \left(\frac{\partial \ln \vec{r}}{\partial \ln r_i}\right)_{r_{m\neq i}} \left(\frac{\partial \ln r_i}{\partial \ln \theta_{N^*}}\right)_{\theta_{m\neq N^*}}$$

$$= \sum_i \vec{s}_i \left(\frac{\partial \ln r_i}{\partial \ln \theta_{N^*}}\right)_{\theta_{m\neq N^*}}$$

(A3.20)

and thus we re-write eq. (A3.20) in terms of sensitivities as eq. (A3.21):

$$\frac{\vec{\alpha}_{\theta N^*}}{\sum_{j^*} \vec{\alpha}_{\theta j^*}} = \frac{\sum_i \vec{s}_i \left(\frac{\partial \ln r_i}{\partial \ln \theta_{N^*}}\right)_{\theta_{m\neq N^*}}}{\sum_{j^*} \sum_i \vec{s}_i \left(\frac{\partial \ln r_i}{\partial \ln \theta_{j^*}}\right)_{\theta_{m\neq j^*}}} = \theta_{N^*}$$

(A3.21)

When standard-state free energies are not functions of fractional coverages, the relative change in the rate of an elementary step with respect to a relative change in the fractional

coverage is equal to negative the stoichiometric coefficient of species j^* in elementary step i where j^* is a reactant ($\nu_{ij^*} < 0$) (eq. (A3.22)):

$$\left(\frac{\partial \ln r_i}{\partial \ln \theta_{j^*}}\right)_{\theta_{n \neq j^*}} = -\nu_{ij^*}[\nu_{ij^*} < 0] \tag{A3.22}$$

Substitution of eq. (A3.22) into eq. (A3.21) gives eq. (A3.23):

$$\frac{-\sum_i \vec{s}_i \nu_{iN^*}[\nu_{iN^*} < 0]}{-\sum_{j^*} \sum_i \vec{s}_i \nu_{ij^*}[\nu_{ij^*} < 0]} = \frac{\vec{X}_{TRC,N^*}}{\sum_{j^*} \vec{X}_{TRC,j^*}} = \theta_{N^*} \tag{A3.23}$$

where the sum of the forward thermodynamic degrees of rate control of all surface species is (eq. (A3.24)):

$$\sum_{j^*} \vec{X}_{TRC,j^*} = \sum_{i=rxn} \vec{s}_i \sum_{j^*} \nu_{ij^*} = -\sum_{i=rxn} \vec{s}_i \sigma_{*,i} = -\vec{\sigma}_{*,app} \tag{A3.24}$$

where $\sigma_{*,i}$ is the number of surface species reacting in elementary step i, and $\vec{\sigma}_{*,app}$ is the forward-sensitivity-weighted-average of the number of surface species reacting in each elementary step. Substitution of eq. (A3.24) into eq. (A3.23) and rearrangement gives the final equation (eq. (A3.25)):

$$\vec{X}_{TRC,N^*} = -\vec{\sigma}_{*,app} \theta_{N^*} \tag{A3.25}$$

A3.2 Experimental assessment of forward and reverse sensitivities and degrees of rate control

In Chapter 2, we showed that all sensitivities and degrees of rate control for net rates can be determined by measuring the steady-state elementary step reversibilities for single-path reactions. A similar approach can be applied to experimentally assess forward and reverse sensitivities and degrees of rate control, however, in general the measurement

of only the steady-state reversibilities is insufficient for determining all forward/reverse sensitivities. This is because elementary step reversibilities are a function of two net rate sensitivities, but four forward/reverse rate sensitivities, as shown in eq. (A3.26):

$$-Z_i = \frac{S_{-i}}{S_i} = \frac{\vec{S}_{-i} - Z_{eff}\overleftarrow{S}_{-i}}{\vec{S}_i - Z_{eff}\overleftarrow{S}_i} \tag{A3.2627}$$

introducing more unknowns without a congruent increase in the number of equations to solve for them. Thus, to completely determine all forward and reverse rate sensitivities, it is also necessary to experimentally assess the forward/reverse reaction orders, which are related to the forward/reverse sensitivities by eq. (A3.27):

$$\vec{\alpha}_j = -\vec{X}_{TRC,j} = -\sum_j \vec{s}_i v_{ij}[v_{ij} < 0] \tag{A3.27}$$

and the reaction orders of fluid-phase intermediates are zero (eq. (A3.28)):

$$\vec{\alpha}_j = -\vec{X}_{TRC,j} = -\sum_j \vec{s}_i v_{ij}[v_{ij} < 0] \tag{A3.28}$$

$$= 0 \text{ for fluid-phase reaction intermediates}$$

The proof for eq. (A3.28) is shown in Section A3.3. For surface species, the fractional coverages are related to sensitivities by eq. (A3.23). Isotopic labeling experiments can supply additional information to reduce the number of reaction order measurements required, as it enables the experimental assessment of the "forward/reverse rate reversibilities of elementary steps," defined as $\vec{Z}_i = \vec{r}_{-i}/\vec{r}_i$, where $\vec{r}_i$ is the rate of elementary step i for reaction trajectories that originate from reactants. This is most easily discussed by considering the reaction network shown in Scheme A3.1.

Scheme A3.1: Sequence of fluid-phase reactions

$$A \underset{k_{-1}}{\overset{k_1}{\rightleftarrows}} B + C \qquad\qquad \sigma_1 = 2$$

$$2B \underset{k_{-2}}{\overset{k_2}{\rightleftarrows}} D \qquad\qquad \sigma_2 = 1$$

Overall: $2A \Rightarrow 2C + D$

There are 8 forward/reverse sensitivities that we would like to determine:

$$\vec{s}_1, \vec{s}_{-1}, \vec{s}_2, \vec{s}_{-2}, \overleftarrow{s}_1, \overleftarrow{s}_{-1}, \overleftarrow{s}_2, \overleftarrow{s}_{-2}$$

The equations we have to determine sensitivities from reversibilities are (eqs. (A3.29)-(A3.32)):

$$\frac{\overrightarrow{s_{-1}} - Z_{eff}\overleftarrow{s_{-1}}}{\overrightarrow{s_1} - Z_{eff}\overleftarrow{s_1}} = -Z_1 \tag{A3.29}$$

$$\frac{\overrightarrow{s_{-2}} - Z_{eff}\overleftarrow{s_{-2}}}{\overrightarrow{s_2} - Z_{eff}\overleftarrow{s_2}} = -Z_2 \tag{A3.30}$$

$$\vec{s}_{-1} + 2\overrightarrow{s_2} = 0 \tag{A3.31}$$

$$\overleftarrow{s}_{-1} + 2\overleftarrow{s}_2 = 0 \tag{A3.32}$$

which is only four equations. Unlike sensitivities for net rate, the ratio $\overrightarrow{s_{-i}}/\overrightarrow{s_i}$ is not a meaningful quantity, limiting the number of independent equations we have. However,

we can measure the reaction order for the forward and reverse reactions with respect to A, C, and D, since (eqs. (A3.33)-(A3.38)):

$$\overrightarrow{\alpha_A} = \overrightarrow{s_1} \tag{A3.33}$$

$$\overleftarrow{\alpha_A} = \overleftarrow{s_1} \tag{A3.34}$$

$$\overrightarrow{\alpha_C} = \overrightarrow{s_{-1}} \tag{A3.35}$$

$$\overleftarrow{\alpha_C} = \overleftarrow{s_{-1}} \tag{A3.36}$$

$$\overrightarrow{\alpha_D} = \overleftarrow{s_{-2}} \tag{A3.37}$$

$$\overleftarrow{\alpha_D} = \overleftarrow{s_{-2}} \tag{A3.38}$$

These give six more equations for a total of ten equations. Thus, we only need to measure two forward rate reaction orders and two reverse rate reaction orders to know all forward and reverse sensitivities, but this is still more information than what is necessary for net reaction rates. However, we can reduce the number of reaction orders that need to be known by defining new reversibilities—the reversibilities of the forward and reverse rates.

Consider the reaction in Scheme A3.1 at equilibrium where $r_1 = r_{-1} = 0.8, r_2 = r_{-2} = 0.2$ and $\vec{r} = \overleftarrow{r} = \frac{2}{15}$ (this is following the example presented in Section 3.3.2). Imagine that the reactant A is unlabeled and D is labeled, though this need not be physically the case. The forward rate of step one makes 6 B in the same amount of time as the reverse rate of step two makes 3 B (note that $D \rightarrow 2B$ is reverse step two). Reactions involving unlabeled species are represented by black lines and reactions

involving labeled species are represented by red dotted lines. In Figure A3.1 below, it is clear that while the net rate of step 1 is zero, not all of the reverse reactions are reverse reactions of the forward rate (black lines).
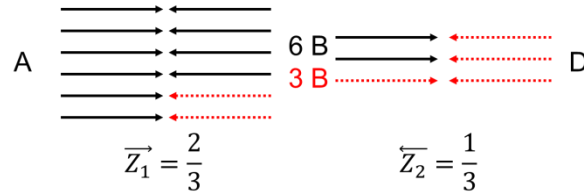
Figure A3.1: Relative reaction rates of elementary steps where reactions corresponding to the composite forward rate are represented by solid black arrow and reactions correspond to the composite reverse rate are represented by dotted red arrows. Each line represents a rate of 2/15 au on the basis of forming or consuming 1 B, or 1/15 au on the basis of forming or consuming 1 D.

The "net" forward rate is envisioned as the net number of black arrows in the forward direction at each step: for step 1, there are net two black arrows in the forward direction, and for step 2, there are also net two black arrows in the forward direction, which is the same as for step 1 as required by steady state. This corresponds to a forward rate of 2/15. This is represented mathematically as (eq. (A3.39)):

$$\vec{r} = \frac{1}{\sigma_i}(\vec{r}_i - \vec{r}_{-i}) = \frac{\vec{r}_i}{\sigma_i}\left(1 - \frac{\vec{r}_{-i}}{\vec{r}_i}\right) = \frac{\vec{r}_i}{\sigma_i}(1 - \vec{Z}_i) \qquad (A3.39)$$

where $\vec{r}_i$ are the black lines in the forward direction and $\vec{r}_{-i}$ are the black lines in the reverse and $\vec{Z}_i$ is the reversibility of step i for the forward rate. For example, for $i = 1$, we have $\overrightarrow{Z_1} = \frac{4}{6} = \frac{2}{3}$ from counting the number of black lines in the quantitatively accurate Figure A3.1. Thus, by substitution of this into eq. (A3.40) we find the forward rate is (eq. (A3.40)):

$$\vec{r} = \frac{\vec{r_1}}{\sigma_1}\left(1 - \vec{Z}_1\right) = \frac{0.8}{2}\left(1 - \frac{2}{3}\right) = \frac{2}{15} \tag{A3.40}$$

Likewise, for the reverse rate, we have $\overleftarrow{Z_2} = \frac{1}{3}$, and thus the reverse rate is (eq. (A3.41)):

$$\overleftarrow{r} = \frac{\overleftarrow{r_i}}{\sigma_i}\left(1 - \overleftarrow{Z}_2\right) = \frac{0.2}{1}\left(1 - \frac{1}{3}\right) = \frac{2}{15} \tag{A3.41}$$

which is equal to the forward rate, consistent with the fact that we are at equilibrium. These reversibilities are also related to forward and reverse sensitivities, but not to the forward and reverse sensitivities discussed above ($\vec{s}_1, \vec{s}_{-1}, \vec{s}_2, \vec{s}_{-2}, \overleftarrow{s}_1, \overleftarrow{s}_{-1}, \overleftarrow{s}_2, \overleftarrow{s}_{-2}$).

When considering the forward and reverse reactions, it is important to know where the intermediates came from – reactants or products. Let us pretend that reactant A is "labelled" "*" and the product D is "unlabeled" and C does not contain labeled or unlabeled components. In this system, the forward/reverse rates are the forward/reverse exchange rates, and our simple four reaction systems becomes a 10 reaction system, represented in Scheme A3.2 ("**" indicates two labels). In this network, stoichiometric numbers cannot be assigned to elementary steps because there are multiple paths in which a labeled reactant can form a labeled product, either going through reaction 4 or reaction 5 in Scheme A3.2.

Scheme A3.2: Network of fluid-phase reactions with labeled reactants.

    1. $A \rightleftarrows B + C$

    2. $A^* \rightleftarrows B^* + C$

    3. $2B \rightleftarrows D$

$$4. \quad 2B^* \rightleftarrows D^{**}$$

$$5. \quad B^* + B \rightleftarrows D^*$$
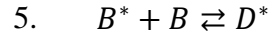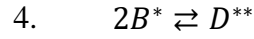
Each reaction contains two sensitivities, one for forward rate and one for reverse rate, listed below (number of "*" indicate number of labels in the reaction, "o" indicates no labels in the reaction):

$$\vec{s}_{1^o}, \overleftarrow{s}_{1^o}, \vec{s}_{-1^o}, \overleftarrow{s}_{-1^o}$$

$$\vec{s}_{1^*}, \overleftarrow{s}_{1^*}, \vec{s}_{-1^*}, \overleftarrow{s}_{-1^*}$$

$$\vec{s}_{2^o}, \overleftarrow{s}_{2^o}, \vec{s}_{-2^o}, \overleftarrow{s}_{-2^o}$$

$$\vec{s}_{2^{**}}, \overleftarrow{s}_{2^{**}}, \vec{s}_{-2^{**}}, \overleftarrow{s}_{-2^{**}}$$

$$\vec{s}_{2^*}, \overleftarrow{s}_{2^*}, \vec{s}_{-2^*}, \overleftarrow{s}_{-2^*}$$

For a total of 20 sensitivities. These sensitivities are related to forward and reverse sensitivities for unlabeled reactions by their sums (eq. (A3.42)):

$$\vec{s}_i = \sum_{j=\{o,*,**\}} \vec{s}_{ij} \tag{A3.42}$$

which for the reaction network represented by Schemes A3.1 and A3.2 gives eqs. (A3.43)-(A3.46):

$$\vec{s}_1 = \vec{s}_{1^o} + \vec{s}_{1^*} \tag{A3.43}$$

$$\vec{s}_{-1} = \vec{s}_{-1^o} + \vec{s}_{-1^*} \tag{A3.44}$$

$$\vec{s}_2 = \vec{s}_{2^o} + \vec{s}_{2^*} + \vec{s}_{2^{**}} \tag{A3.45}$$

$$\vec{s}_{-2} = \vec{s}_{-2^o} + \vec{s}_{-2^*} + \vec{s}_{-2^{**}} \tag{A3.46}$$

Following an analogous proof to that in Section A3.1.3, the forward/reverse labeled sensitivities are related to the forward/reverse reversibilities by eq. (A3.47):

$$\frac{\vec{s}_{-i\ominus}}{\vec{s}_{i\ominus}} = -Z_{i\ominus}, \qquad \ominus = \{o \quad * \quad **\} \tag{A3.47}$$

In this example, $Z_{1^*} = \vec{Z}_1$. This gives ten more equations that relate labeled forward/reverse sensitivities to reversibilities (eqs. (A3.48)-(A3.52)):

$$\frac{\vec{s}_{-1^*}}{\vec{s}_{1^*}} = \frac{\overleftarrow{s}_{-1^*}}{\overleftarrow{s}_{1^*}} = -Z_{1^*} \tag{A3.48}$$

$$\frac{\vec{s}_{-1^o}}{\vec{s}_{1^o}} = \frac{\overleftarrow{s}_{-1^o}}{\overleftarrow{s}_{1^o}} = -Z_{1^o} \tag{A3.49}$$

$$\frac{\vec{s}_{-2^o}}{\vec{s}_{2^o}} = \frac{\overleftarrow{s}_{-2^o}}{\overleftarrow{s}_{2^o}} = -Z_{2^o} \tag{A3.50}$$

$$\frac{\vec{s}_{-2^*}}{\vec{s}_{2^*}} = \frac{\overleftarrow{s}_{-2^*}}{\overleftarrow{s}_{2^*}} = -Z_{2^*} \tag{A3.51}$$

$$\frac{\vec{s}_{-2^{**}}}{\vec{s}_{2^{**}}} = \frac{\overleftarrow{s}_{-2^{**}}}{\overleftarrow{s}_{2^{**}}} = -Z_{2^{**}} \tag{A3.52}$$

Each of these reversibilities are experimentally measureable when using isotopic labels. The relationships between forward and reverse sensitivities and the net rate reversibilities still hold for reactions with isotopic labels (eqs. (A3.29) and (A3.30)). Further, the thermodynamic degrees of rate control for reaction intermediates B and B* must be 0 for both forward and reverse reactions, such that (eq. (A3.53)):

$$\sum_i \vec{s}_{i\ominus} v_{ij} [v_{ij} < 0] = 0 \quad \ominus = \{o \quad * \quad **\} \tag{A3.53}$$

Which, for the examples in Schemes A3.1 and A3.2 are (eqs. (A3.54)-(A3.57)):

$$\vec{s}_{-1^o} + 2\vec{s}_{2^o} + \vec{s}_{2^*} = 0 \tag{A3.54}$$

$$\vec{s}_{-1^*} + 2\vec{s}_{2^{**}} + \vec{s}_{2^*} = 0 \tag{A3.55}$$

$$\overleftarrow{s}_{-1^o} + 2\overleftarrow{s}_{2^o} + \overleftarrow{s}_{2^*} = 0 \tag{A3.56}$$

$$\overleftarrow{s}_{-1^*} + 2\overleftarrow{s}_{2^{**}} + \overleftarrow{s}_{2^*} = 0 \tag{A3.57}$$

Finally, the sum of all of the forward sensitivities must equal unity, and the sum of all of the reverse sensitivities must equal unity, such that (eqs. (A3.58) and (A3.59)):

$$\vec{s}_{1^o} + \vec{s}_{1^*} + \vec{s}_{-1^o} + \vec{s}_{-1^*} + \vec{s}_{2^o} + \vec{s}_{2^*} + \vec{s}_{2^{**}} + \vec{s}_{-2^o} + \vec{s}_{-2^*} + \vec{s}_{-2^{**}} = 1 \tag{A3.58}$$

$$\overleftarrow{s}_{1^o} + \overleftarrow{s}_{1^*} + \overleftarrow{s}_{-1^o} + \overleftarrow{s}_{-1^*} + \overleftarrow{s}_{2^o} + \overleftarrow{s}_{2^*} + \overleftarrow{s}_{2^{**}} + \overleftarrow{s}_{-2^o} + \overleftarrow{s}_{-2^*} + \overleftarrow{s}_{-2^{**}} = 1 \tag{A3.59}$$

This gives a total of 18 equations for 20 unknown sensitivities. The final two equations are obtained by experimentally measuring one forward and one reverse reaction order. Thus, through the use of isotopic labels, it is possible to reduce the number of reaction orders that need to be experimentally measured to determine all forward and reverse sensitivities in the reaction system ($\vec{s}_1, \vec{s}_{-1}, \vec{s}_2, \vec{s}_{-2}, \overleftarrow{s}_1, \overleftarrow{s}_{-1}, \overleftarrow{s}_2, \overleftarrow{s}_{-2}$). Unlike the net rate sensitivities of single-path reactions, all forward and reverse sensitivities cannot necessarily be determined because the forward/reverse reactions cannot be represented as

a single path, as illustrated by the fact that stoichiometric numbers cannot be assigned to the elementary step reactions in Scheme A3.2, namely that the exchange of labeled/unlabeled species can occur through two labeled/unlabeled B species (reactions 3 and 4 in Scheme A3.2), or through a reaction with one labeled and one unlabeled B species (reaction 5 in Scheme A3.2), making the forward and reverse overall reactions non-single-path, despite the overall reaction being single-path when not considering the origin (reactants or products) of reaction intermediates, as shown in Scheme A3.1.

A3.3 Proof that $X_{TRC,j} = 0$ for fluid-phase intermediates

Proving that the thermodynamic degrees of rate control of fluid-phase intermediates equals zero is the same as proving that the steady-state reaction order of fluid-phase intermediates is zero, since the reaction order is equal to negative the thermodynamic degree of rate control. It is typically assumed that because the activities of reaction intermediates are eliminated from overall rate functions by solving for them in terms of the activities of reactants and products, they necessarily have reaction orders equal to zero. However, in Chapter 2 we proved[60] that surface species in composite catalytic reactions have non-zero reaction orders, despite not appearing in a typical steady-state rate function. Thus, the argument that one can derive a rate function without the appearance of species is not sufficient evidence that the reaction order of that species is zero. For example, consider the simple catalytic reaction shown in Scheme A3.3. The rate

function of each elementary step is first order in either vacant sites, $*$, or adsorbed A, A^*, yet no surface species appear in our *chosen* overall rate function, and thus we would erroneously conclude that all reaction intermediates do not have reaction orders, despite each elementary step having non-zero reaction orders for surface species.

Scheme A3.3: Two-step catalytic transformation of A to B

$$A +* \underset{k_{-1}}{\overset{k_1}{\rightleftharpoons}} A^*$$

$$r_1/L = k_1 a_A \theta_*$$

$$r_{-1}/L = k_{-1}\theta_{A^*}$$

$$A^* \overset{k_2}{\rightarrow} * + B$$

$$r_2/L = k_2 \theta_{A^*}$$

Overall: $\qquad A \Rightarrow B \qquad \dfrac{r}{L} = \dfrac{k_1 k_2 a_A}{k_1 a_A + k_{-1} + k_2}$

In Chapter 2 we proved that the overall rates can be written as transition-state-theory (TST) form rate functions of the forms given in eqs. (A3.60) and (A3.61), respectively:

$$r = k_{app} \prod_{j=fluid\ phase} a_j^{\alpha_j} \tag{A3.60}$$

$$\frac{r}{L} = k_{app} \prod_{j=fluid\ phase} a_j^{\alpha_j} \prod_{j^*=surface} \theta_{j^*}^{\alpha_{j^*}} \tag{A3.61}$$

where k_{app} is the apparent rate constant, a_j are the activities of fluid-phase species j, L are the number of active sites, θ_{j^*} are the fractional coverages of surface species j^*, and

α_j and α_{j^*} are the apparent reaction orders of fluid-phase and surface species. When the rate of a composite catalytic reaction is of the form given by eq. (A3.61), the rates are non-zero-order in surface species because their thermodynamic degrees of rate control are non-zero (see eq. (A3.25)). From eq. (A3.25), we concluded in Chapter 2 that a species that is a reactive intermediate, meaning that it is an unstable species that is rapidly consumed after it is formed, and thus has low steady-state concentrations/coverages, has a $X_{TRC,j^*} \approx 0$, and thus has a reaction order that is near zero.[60] We extended this to fluid-phase species, where we assumed that in order to have a closed-form rate function, it was necessary that fluid-phase intermediates be reactive such that the pseudo-steady-state approximation was valid. However, this was only necessary because we were considering the reaction rates as measured in ideal plug-flow reactors, but it is not necessary to simulate a particular unit operation to simulate a reaction rate. We have found since that the thermodynamic degrees of rate control for fluid-phase intermediates are zero regardless of their reactivity, which we prove herein.

The steady-state concentration of a fluid-phase reaction intermediate, j, is found by the steady-state assumption (eq. (A3.62)):

$$\frac{d[j]}{dt} = \sum_{i=rxn} \nu_{ij} r_i [\nu_{ij} > 0] + \sum_{i=rxn} \nu_{ij} \exp(\nu_{ij} G_j^o / k_B T)[j]^{-\nu_{ij}} f_i [\nu_{ij} < 0] = 0 \quad \text{(A3.62)}$$

where f_i are functions of all other species and energies that do not include j, $[\nu_{ij} > 0]$ is unity if true and zero if false, such that the first summation corresponds to elementary-step reactions where j is a product and the second summation corresponds to elementary-step reactions where j is a reactant. For reactions where j is a product, $\nu_{ij} > 0$, the

reaction rates do not depend on G_j^o of reaction intermediate j. To find how the stead-state

concentration of species j changes as a function of G_j^o, we take the total differential of eq.

(A3.62) (eq. (A3.63)):

$$
0 = [v_{ij} > 0]d\left(\sum_{i=rxn} v_{ij}r_i\right)
$$

$$
+ \sum_i f_i v_{ij}^2 [v_{ij} < 0] \exp\left(-v_{ij}G_j^o/k_BT\right)[j]^{-v_{ij}} d\left(-\frac{G_j^o}{k_BT}\right) \quad \text{(A3.63)}
$$

$$
- \sum_i f_i v_{ij}^2 [v_{ij} < 0] \exp\left(-v_{ij}G_j^o/k_BT\right)[j]^{-v_{ij}} d\ln[j]
$$

From eq. (A3.63), the relative change in the steady-state concentration of species j per

k_BT decrease in the standard-state free energy of an intermediate j is equal to one (eq.

(A3.64)):

$$
\frac{d\ln[j]}{d\left(-G_j^o/k_BT\right)} = 1 \quad \text{(A3.64)}
$$

The rates of all elementary step reactions are considered to be TST-form rate functions

given by eqs. (A3.65)(A3.65) and (A3.66):

$$
r_i = k_i[j]^{-v_{ij}} \quad \text{(A3.65)}
$$

$$
k_i = \frac{k_BT}{h}\exp\left(-\frac{\left(G_{TS,i}^o + \sum_n v_{in}[v_{in} < 0]G_n^o\right)}{k_BT}\right) \quad \text{(A3.66)}
$$

For rates of this form, we can calculate the relative change in the rate of an elementary

step per k_BT decrease in G_j^o (j is an intermediate) using the chain rule (eq. (A3.67)):

$$\frac{d \ln r_i}{d\left(-G_j^o/k_B T\right)} = \frac{d \ln r_i}{d \ln[j]} \frac{d \ln[j]}{d\left(-G_j^o/k_B T\right)} + \frac{d \ln r_i}{d \ln k_i}\left(\frac{d \ln k_i}{d\left(-G_j^o/k_B T\right)}\right) \qquad \text{(A3.67)}$$

By evaluating the derivatives in eq. (A3.67) (see eqs. (A3.64)-(A3.66)) we find that the rates of all elementary steps are unchanged when the energy of a fluid-phase intermediate is perturbed (eq. (A3.68)):

$$\frac{d \ln r_i}{d\left(-G_j^o/k_B T\right)} = -v_{ij}\left[v_{ij} < 0\right] * 1 + 1 * v_{ij}\left[v_{ij} < 0\right] = 0 \qquad \text{(A3.68)}$$

If the rates of no elementary steps change, then the steady-state concentration of all other reaction intermediates remain unchanged, and the rate of the overall reaction is unchanged. Thus, $X_{TRC,j} = 0$ for fluid-phase intermediates, as does the reaction order. This is true for fluid-phase intermediates because perturbations in the standard-state free energy of a fluid-phase intermediate alters the steady-state concentration such that the effects of both changes on elementary step reaction rates cancel out. This proof is valid not only for net rates, but also to the overall forward and reverse rates of composite reactions. For surface intermediates, the above proof does not apply because the rates of formation of surface intermediates (see eq. (A3.63)) are not independent of the fractional coverage of the intermediate. For example, in Scheme A3.3, the rate of formation of A* is first-order in $\theta_* = 1 - \theta_{A^*}$, and thus the proof detailed above applies only to fluid-phase reaction intermediates.

A3.4 Matlab code for forward and reverse sensitivity calculations

This section includes Matlab code used to calculate forward and reverse sensitivities for the uncatalyzed and catalyzed reactions in Schemes 3.1 and 3.2. They are copied in the sections below and available for download at https://github.com/foley352/DoRC-3.

A3.4.1 Example for uncatalyzed reaction network shown in Scheme 3.1.

```matlab
close all
clear

k00=[1,20,20,1]; %values of rate constants [k1, kr1, k2, kr2] where "r"
means "reverse"
a=0;

for
q=[0.0001,0.001,0.01:0.01:0.09,0.1,0.11,0.12,0.13,0.14,0.15,0.16,0.17,0
.18,0.19,0.199,0.1999,0.19999,0.20001,0.2001,0.201,0.21:0.01:0.59,0.599
,0.5999]
    %for loop varying extent of reaction, q
    a=a+1;
    x0=[1.2-2*q,0,2*q,q,0];    %vary   concentrations   with   extent   of
reaction, x0=[[A],0,[C],[D],0]
    for b=1:5 %for  loop  for  calculating  sensitivites,  each  loop
perturbs a different k, b=1 is unperturbed
    clear x Zeff t rfwdcalc rfwdreal z

    k0=k00;

    if b==1
    else
    k0(b-1)=1.00001*k0(b-1);  %perturbe  one  of  the  k's  by  a  small
multiplicative factor
    end

    k1=k0(1);
    kr1=k0(2);
    k2=k0(3);
    kr2=k0(4);

    %solve for the steady-state concentration of B [B] by forward
    %integration
[t,x]=ode23s(@(t,x) [0;
    k1*x(1)-kr1*x(2)*x(3)-2*k2*x(2)^2+2*kr2*x(4);
    0;
    0;
    k2*x(2)^2-kr2*x(4)],[0,100],x0);
%calculate Z's, sigmabar, and the forward and reverse rates, the fifth
```

293

```matlab
%position  is the change in a fictitious product to measure the
%steady-staete rate
Z1=kr1*x(end,2).*x(end,3)./(k1*x(end,1));
Z2=kr2.*x(end,4)./(k2*x(end,2).^2);
Zeff=kr1*x(end,2).*x(end,3)./(k1*x(end,1)).*kr2.*x(end,4)./(k2*x(end,2)
.^2);
sigmabar=real((2*log(Z1)+log(Z2))/(log(Z1)+log(Z2)));
fwd(b)=(x(end,5)-x(end-1,5))./(t(end)-t(end-1))./(1-(Zeff));
rvs(b)=(x(end,5)-x(end-1,5))./(t(end)-t(end-1))./(1-(Zeff)).*((Zeff));

if b==1 %store unperturbed concentration of A-D at steady-state
    A=x(end,1);
    B=x(end,2);
    C=x(end,3);
    D=x(end,4);
end

    end
    %calc net rate
    net=fwd-rvs;

    %calc forward and reverse sensitivities
    s1for=(fwd(2)-fwd(1))/(fwd(1))/0.00001;
    sr1for=(fwd(3)-fwd(1))/(fwd(1))/0.00001;
    s2for=(fwd(4)-fwd(1))/(fwd(1))/0.00001;
    sr2for=(fwd(5)-fwd(1))/(fwd(1))/0.00001;

    s1rev=(rvs(2)-rvs(1))/(rvs(1))/0.00001;
    sr1rev=(rvs(3)-rvs(1))/(rvs(1))/0.00001;
    s2rev=(rvs(4)-rvs(1))/(rvs(1))/0.00001;
    sr2rev=(rvs(5)-rvs(1))/(rvs(1))/0.00001;

    s1=(net(2)-net(1))/(net(1))/0.00001;
    sr1=(net(3)-net(1))/(net(1))/0.00001;
    s2=(net(4)-net(1))/(net(1))/0.00001;
    sr2=(net(5)-net(1))/(net(1))/0.00001;

    %calcualte Cfwd and Crev

Cfwd=fwd(1)/((k1*A)^(s1for)*(kr1*B*C)^(sr1for)*(k2*B^2)^(s2for)*(kr2*D)
^(sr2for));

Crvs=rvs(1)/((k1*A)^(s1rev)*(kr1*B*C)^(sr1rev)*(k2*B^2)^(s2rev)*(kr2*D)
^(sr2rev));

    %calculate kfwd and krev

kfor=Cfwd*((k1)^(s1for)*(kr1)^(sr1for)*(k2)^(s2for)*(kr2)^(sr2for));

krev=Crvs*((k1)^(s1rev)*(kr1)^(sr1rev)*(k2)^(s2rev)*(kr2)^(sr2rev));

    %store data in matrices that can be copied to excel
    data1(a,:)=[q,fwd(1),rvs(1),fwd(1)-rvs(1),Zeff,
s1for,sr1for,s2for,sr2for,s1for+sr1for,s2for+sr2for,s1rev,sr1rev,s2rev,
```

```
sr2rev,s1rev+sr1rev,s2rev+sr2rev,s1,sr1,s2,sr2,sigmabar,Cfwd,Crvs,Z1,Z2
,kfor,krev];

data2(a,:)=[Z1,Z2,Zeff,s1,sr1,s2,sr2,s1for,sr1for,s2for,sr2for,s1rev,sr
1rev,s2rev,sr2rev];
end
```

A3.4.2 Example for catalyzed reaction network presented in Scheme 3.2.

```
close all
clear
j=0;

k00=[1,20,20,1];  %assign  k's  k00=[k1,kr1,k2,kr2]  where  r  indicates
reverse

a=0;
for q=[0.001,0.01:0.01:0.92,0.92:0.001:0.999,0.9999,0.99999]
    %for loop for varying extent of reaction, q
    a=a+1; %step counting variable

    %calc concentrations of A and B
    A=1-q;
    B=0.5*q;

    for b=1:5 %for loop for pertrubing k's to calc sensitivities
    clear x Zeff t rfwdcalc rfwdreal z

    k0=k00;

    if b==1 %if b==1 don't perturb any k's
    else
    k0(b-1)=1.0001*k0(b-1);  %perturb  k's  by  a  small  multiplicative
factor
    end

    k1=k0(1);
    kr1=k0(2);
    k2=k0(3);
    kr2=k0(4);

    %solve for steady-state fractional coverages by forward integration
    %from clean surface
[t,x]=ode23s(@(t,x) [-k1*A*x(1)+kr1*x(2)+2*k2*x(2).^2-2*kr2*B*x(1)^2;
    k1*A*x(1)-kr1*x(2)-2*k2*x(2).^2+2*kr2*B*x(1)^2;
    k2*x(2).^2-kr2*B*x(1)^2],[0,100],[1,0,0]);

%calc Z's
Z1=kr1*x(end,2)/(k1*A*x(end,1));
```

```
Z2=kr2*B*x(end,1)^2/(k2*x(end,2)^2);
Zeff=Z1*Z2;

%calc sigma bar, steady-state surface coverages for unperturbed
condition
if b==1
sigmabar=(2*log(Z1)+log(Z2))/(log(Z1)+log(Z2));
thetastar=x(end,1);
thetaA=x(end,2);
end

%calc fwd and rvs rates
fwd(b)=(x(end,3)-x(end-1,3))./(t(end)-t(end-1))./(1-(Zeff));
rvs(b)=(x(end,3)-x(end-1,3))./(t(end)-t(end-1))./(1-(Zeff)).*((Zeff));
    end

%calc net rate
    net=fwd-rvs;

%calc sensitities
    s1for=(fwd(2)-fwd(1))/(fwd(1))/0.0001;
    sr1for=(fwd(3)-fwd(1))/(fwd(1))/0.0001;
    s2for=(fwd(4)-fwd(1))/(fwd(1))/0.0001;
    sr2for=(fwd(5)-fwd(1))/(fwd(1))/0.0001;

    s1rev=(rvs(2)-rvs(1))/(rvs(1))/0.0001;
    sr1rev=(rvs(3)-rvs(1))/(rvs(1))/0.0001;
    s2rev=(rvs(4)-rvs(1))/(rvs(1))/0.0001;
    sr2rev=(rvs(5)-rvs(1))/(rvs(1))/0.0001;

    s1=(net(2)-net(1))/(net(1))/0.0001;
    sr1=(net(3)-net(1))/(net(1))/0.0001;
    s2=(net(4)-net(1))/(net(1))/0.0001;
    sr2=(net(5)-net(1))/(net(1))/0.0001;

%store data in a matrix that can be copied to excel
    data1(a,:)=[q,fwd(1),rvs(1),fwd(1)-
rvs(1),rvs(1)/fwd(1),s1for,sr1for,s2for,sr2for,s1for+sr1for,s2for+sr2fo
r,s1rev,sr1rev,s2rev,sr2rev,s1rev+sr1rev,s2rev+sr2rev,s1,sr1,s2,sr2,sig
mabar,thetastar,thetaA];
end
```

A3.5 Forward and Reverse Constants as a function of Z_{eff} for the uncatalyzed reaction network presented in Scheme 3.1.

Figure A3.2 below shows how the constants $\vec{C}$ and $\overleftarrow{C}$ vary as a function of Z_{eff} for the

uncatalyzed reaction network shown in Scheme 3.1, and demonstrates that they are equal

at equilibrium, as required by eq. (3.50).

296
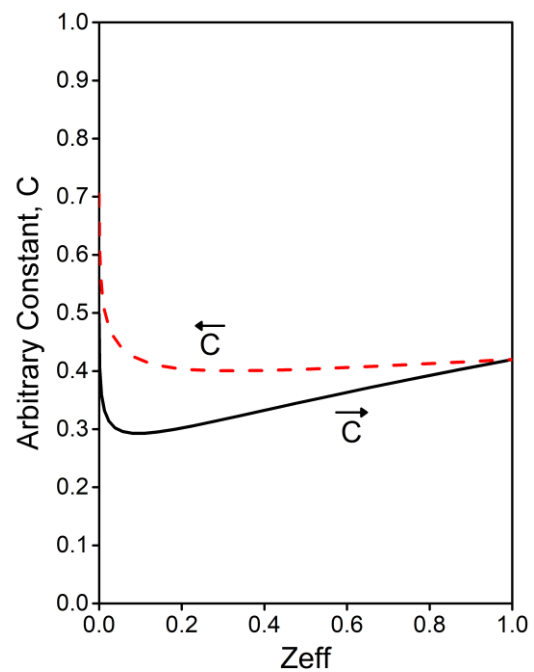
Figure A3.2: Forward (solid lines) and reverse (dashed lines) arbitrary constants of integration as a function of Z_{eff} for the reaction shown in Scheme 1 with $[A]_0 = 1.2$ au.

A3.6 Microkinetic model for NH₃ synthesis on Ru(0001) step sites

A3.6 Microkinetic model for NH$_3$ synthesis on Ru(0001) step sites

The microkinetic model for NH$_3$ synthesis/decomposition on Ru(0001) step sites are based on density functional theory calculations reported by Logadóttir and Nørskov.[1] The elementary step rate constants for these reactions are summarized in Table A3.1. The microkinetic model used mass-action rate functions for each forward and reverse elementary step. The steady-state fractional coverages and rate were determined by forward integration from a clean surface ($\theta_* = 1$). Statistical factors arising from elementary step-reactions involving multiple sites were ignored. Sensitivities and degrees of rate control were numerically calculated at each reaction condition.

Table A3.1: Kinetic parameters used in the microkinetic model for NH$_3$ synthesis on Ru(0001) step sites based on density functional theory calculations from Logadóttir and Nørskov.[1]

Reaction	$A_{fwd}{}^a$ / s^{-1}	$A_{rev}{}^a$ / s^{-1}	$E_{a,fwd}$ / eV	$E_{a,rev}$ / eV	k_i / s^{-1}	k_{-i} / s^{-1}
1. N$_2$+*⇄ 2N*	2.39 x 10^4	1.46 x 10^{14}	0.4	1.2	3.16 x 10^1	3.35 x 10^5
2. N*+H*⇄NH*+*	1.46 x 10^{13}	1.46 x 10^{13}	1.1	1.1	1.76 x 10^5	1.76 x 10^5
3. NH*+H*⇄NH$_2$*+*	1.46 x 10^{13}	1.46 x 10^{13}	1.3	1.46	6.38 x 10^3	4.50 x 10^2
4. NH$_2$*+H*⇄NH$_3$*+*	1.46 x 10^{13}	1.46 x 10^{13}	1.2	0.75	3.35 x 10^4	5.81 x 10^7
5. NH$_3$*⇄NH$_3$+*	1.46 x 10^{13}	2.46 x 10^3	0.85	0	1.11 x 10^7	2.46 x 10^3
6. H$_2$+2*⇄2H*	3.89 x 10^6	1.46 x 10^{13}	0	1.1	3.89 x 10^6	1.76 x 10^5

^{a}Pre-exponential factors are calculated with a 1 bar reference pressure at 700 K using the partition functions reported in Table A3.2.

The elementary step rate constants were assumed to be of the form derived from statistical mechanics (eq. (A3.69)):

$$k_i' = \frac{k_B T}{h} \frac{q_{TS,i}}{q_{IS,i}} \exp\left(-\frac{E_{TS,i} - E_{IS,i}}{k_B T}\right) \tag{A3.69}$$

where $q_{\text{TS,i}}$ and $q_{\text{IS,i}}$ are the partition function for the transition state and the initial state of the elementary step reaction, respectively, and $E_{\text{TS},i}$ and $E_{\text{IS},i}$ are the electronic energies of the transition and initial states, respectively, and k_i' is the elementary step rate constant when the rate function is in terms of concentration. Later we will convert k_i', which has a reference of 1 mol L^{-1}, to k_i, which has a reference of 1 bar. The total partition functions are products of the vibrational, translation, and rotational partition functions for the species in the initial and transition states (eq. (A3.70)):

$$q_{j,\text{tot}} = q_{j,\text{rot}} \times q_{j,\text{vib}} \times q_{j,\text{trans}} \tag{A3.70}$$

For the diatomic gas-phase molecules H_2 and N_2, the rotational partition function is given by (eq. (A3.71)):

$$q_{diatomic,\text{rot}} = \frac{8\pi^2 I k_B T}{2h^2} \tag{A3.71}$$

where I is the moment of inertia of the molecule. For NH_3, the rotational partition function is given by (eq. (A3.72)):

$$q_{NH_3,\text{rot}} = \frac{8\pi^2 (8\pi^3 I_A I_B I_C)^{\frac{1}{2}} (k_B T)^{\frac{3}{2}}}{3h^3} \tag{A3.72}$$

where I_A, I_B, and I_C are the moments of inertia about three orthogonal rotational axes. The vibrational partition functions are given by (eq. (A3.73)):

$$q_{j,\text{vib}} = \frac{1}{1 - \exp\left(-\frac{h\nu}{k_B T}\right)} \tag{A3.73}$$

For each vibrational mode in the molecule, where ν is the frequency of the vibration. Finally, the translational partition function is given by (eq. (A3.74)):

$$q_{j,\text{trans}} C^{\ominus} = \frac{1}{(1000\ L/m^3)N_A} \frac{(2\pi m k_B T)^{\frac{3}{2}}}{h^3} \tag{A3.74}$$

for a molecule with mass m with three translational degrees of freedom with $N_A = 6.022 * 10^{23}$ is Avogadro's number and 1000 is L/m^3, taking the right fraction to have units of m^{-3}, and where $C^{\ominus} = 1\ \text{mol}\ L^{-1}$ is the reference concentration. Typically $q_{j,\text{trans}}$ has units, but here we assign the units to $C^{\ominus}$ to make more suggestive the origin of the reference condition. As written in eq. (A3.74), $1/1000N_A$ gives $C^{\ominus} = 1\ \text{mol}\ L^{-1}$. The rate function written in this way is thus in terms of concentration (eq. (A3.75)):

$$\frac{r_i}{L} = k_i' \prod_j \left(\frac{C_j}{C^{\ominus}}\right)^{-\nu_j} \prod_{j^*} \theta_{j^*}^{-\nu_{j^*}} \tag{A3.75}$$

but we would like inputs of pressure for the gas-phase reaction for convenience. $P_j/RT = C_j$, so substitution of this quantity into eq. (A3.75) we have (eq. (A3.76)):

$$\frac{r_i}{L} = k_i' \prod_j \left(\frac{P_j}{C^{\ominus}RT}\right)^{-\nu_j} \prod_{j^*} \theta_{j^*}^{-\nu_{j^*}} \tag{A3.76}$$

We want a reference $P^{\ominus} = 1$ bar, so we rewrite this as $C^{\ominus}RT = \frac{C^{\ominus}RT}{P^{\ominus}} P^{\ominus}$ where the fraction is unitless. Substitution and rearrangement into eq. (A3.76) we have (A3.77):

$$\frac{r_i}{L} = k_i' \left(\frac{P^{\ominus}}{C^{\ominus}RT}\right)^{-\Sigma_j \nu_j} \prod_j \left(\frac{P_j}{P^{\ominus}}\right)^{-\nu_j} \prod_{j^*} \theta_{j^*}^{-\nu_{j^*}} = k_i \prod_j \left(\frac{P_j}{P^{\ominus}}\right)^{-\nu_j} \prod_{j^*} \theta_{j^*}^{-\nu_{j^*}} \tag{A3.77}$$

where the reference is $P^{\ominus} = 1$ bar and $C^{\ominus} = 1$ mol L^{-1} is the previous reference

condition and k_i is the rate constant when the reference is $P^{\ominus} = 1$ bar which is given by

eq. (A3.78):

$$k_i = A \exp\left(-\frac{E_{\text{TS},i} - E_{\text{IS},i}}{k_B T}\right) = \frac{k_B T}{h}\left(\frac{P^{\ominus}}{C^{\ominus}RT}\right)^{-\Sigma_j v_j} \frac{q_{\text{TS},i}}{q_{\text{IS},i}} \exp\left(-\frac{E_{\text{TS},i} - E_{\text{IS},i}}{k_B T}\right) \quad \text{(A3.78)}$$

where A is the pre-exponential factor with units of s^{-1}. We demonstrate the calculation of

the pre-exponential factor for the dissociative adsorption of N_2. The vibrational frequency

of the N-N stretching mode is 2744 cm^{-1}, which gives the vibrational partition function

(eq. (A3.79)):

$$q_{N_2,\text{vib}} = \frac{1}{1 - \exp\left(-\dfrac{h(2744\ cm^{-1})(3*10^{10}cm/s)}{k_B(700\ K)}\right)} \approx 1 \quad \text{(A3.79)}$$

where $h = 6.63*10^{-34}\ J\ s$ and $k_B = 1.38*10^{-23}\ J\ K^{-1}$ are used through these

calculations. N_2 has a moment of inertia of 1.41 x 10^{-46} kg m^2 and from eq. (A3.71) the

rotational partition function for N_2 is (eq. (A3.80)):

$$q_{N_2,\text{rot}} = \frac{8\pi^2(1.41*10^{-46}\ kg\ m^2)k_B(700\ K)}{2h^2} \approx 122 \quad \text{(A3.80)}$$

Finally the mass of an N_2 molecule is 4.65 x 10^{-26} kg giving a translational partition

function (eq. (A3.80)):

$$q_{N_2,\text{trans}}C^{\ominus} = \frac{1}{(1000\ L/m^3)N_A} \frac{(2\pi(4.65\ \text{x}\ 10^{-26}\ kg\ )k_B(700\ K))^{\frac{3}{2}}}{h^3} \quad \text{(A3.80)}$$

$$\approx 8.55*10^5\ mol\ L^{-1}$$

This give a $q_{N_2,\text{tot}}$ of (eq. (A3.81)):

$$q_{N_2,\text{tot}} = 1 * 122 * 8.55 * 10^5 = 1.05 * 10^8 \tag{A3.81}$$

Surface species and the surface transition states are assumed to have no translational and rotational degrees of freedom such that $q_{j,\text{trans}} = q_{j,\text{rot}} = 1$. Logadóttir and Nørskov[1] reported that $q_{j,\text{vib}} = 10$ for the transition state of step 1, and we assume all other $q_{j,\text{vib}} = 1$ for surface species and transition states. With this information we calculate the rate constant for N_2 dissociation as (eq. (A3.82)):

$$A = \frac{k_B T}{h} \frac{q_{\text{TS1,tot}}}{q_{N_2,\text{tot}}}$$

$$= \frac{k_B (700\ K)}{h} \frac{10}{1.05 * 10^8} \left(\frac{bar}{mol\ L^{-1} \left(0.08314\ bar\ \frac{L}{mol\ K} \right)(700\ K)} \right) \tag{A3.82}$$

$$= 2.39 * 10^4\ s^{-1}$$

This is five orders of magnitude larger than the pre-exponential factor reported by Logadóttir and Nørskov.[1] For N_2, we have identical rotational and vibrational partition functions and our translational partition functions both agree when expressed in units of m^{-3}, and thus we surmise that the discrepancy arises when adjusting the standard-state reference condition from 1 molecule m^{-3} to 1 bar. The masses, moments of inertia, and partition function for the three gas-phase species are reported in Table A3.2. All transition states and surface species besides that for N_2 dissociation (TS1) were assumed to have total partition functions equal to unity.

Table A3.2: Partition function calculations for gas-phase species.

Species	Mass / kg	Moments of Inertia / kg m^2	$q_{j,\text{trans}}$[a]	$q_{j,\text{rot}}$	$q_{j,\text{vib}}$	$q_{j,\text{tot}}$[a]
N$_2$ (g)	4.65 x 10^{-26}	1.41 x 10^{-46}	8.55 x 10^5	1.22 x 10^2	1	1.05 x 10^8
TS1	-	-	1	1	10.0	10.0
NH$_3$ (g)	2.82 x 10^{-26}	4.41 x 10^{-47} 2.81 x 10^{-47} 2.81 x 10^{-47}	4.04 x 10^5	2.52 x 10^2	1	1.02 x 10^8
H$_2$ (g)	3.32 x 10^{-27}	4.55 x 10^{-48}	1.63 x 10^4	3.95	1	6.44 x 10^4

[a]The total and translational partition functions for gas-phase species have a reference condition of $C^{\ominus} = 1$ mol L^{-1}.

A4 Degrees of rate control non(pseudo)steady-state conditions

A4.1 Derivation of the relationship between reaction orders and sensitivites (eq. (4.20))

In this section, we restate the derivation of eq. (4.20) which is reported in Chapter 2. The rate of an overall reaction is a function of the rate functions for each elementary step in the composite reaction network, such that (eq. (A4.1)):

$$r = r\big(r_1(k_1, a_j), r_{-1}(k_{-1}, a_j), r_2(k_2, a_j), r_{-2}(k_{-2}, a_j), \dots \big) \tag{A4.1}$$

where r is the overall rate, r_i are the rate functions for elementary step i, k_i are the rate constants for elementary step i, and a_j are the activities of species j. The reaction order for a composite reaction, α_j, is defined as (eq. (A4.2)):

$$\alpha_j = \left(\frac{d \ln r}{d \ln a_j} \right) \tag{A4.2}$$

Using the chain rule, the derivative in eq. (A4.2) can be written as (eq. (A4.3)):

$$\alpha_j = \left(\frac{d \ln r}{d \ln a_j} \right) = \sum_i \left(\frac{d \ln r}{d \ln k_i} \right) \left(\frac{d \ln k_i}{d \ln r_i} \right) \left(\frac{d \ln r_i}{d \ln a_j} \right) = \sum_i \left(\frac{d \ln r}{d \ln k_i} \right) \left(\frac{d \ln r_i}{d \ln a_j} \right) \tag{A4.3}$$

In eq. (A4.3), it is assumed that the elementary step rate function is first-order in k_i, such that $r_i \propto k_i$, and thus $\left(\frac{d \ln k_i}{d \ln r_i} \right) = 1$, which is consistent with reaction rate theories for elementary step reactions. The derivative of the log of the rate with respect to the log of the elementary step rate constant is equal to the sensitivity (eq. (A4.4)):

$$\frac{d \ln r}{d \ln k_i} = \sum_j \left(\frac{\partial \ln r}{\partial \ln k_j} \right)_{k_{n \neq j}} \left(\frac{d \ln k_j}{d \ln k_i} \right) = \sum_j \left(\frac{\partial \ln r}{\partial \ln k_j} \right)_{k_{n \neq j}} \delta_{ij} = \left(\frac{\partial \ln r}{\partial \ln k_i} \right)_{k_{n \neq i}} \tag{A4.4}$$

$$= s_i$$

where δ_{ij} equals one if $i = j$ and is zero otherwise. Substitution of eq. (A4.4) into eq.

(A4.3) and noting that $\left(\frac{d \ln r_i}{d \ln a_j}\right) = \alpha_{ij}$ is the reaction order for species j in elementary step

i by definition, we derive eq. (A4.5), which is identical to eq. (4.20):

$$\alpha_j = \left(\frac{d \ln r}{d \ln a_j}\right) = \sum_i s_i \alpha_{ij} \qquad (A4.5)$$

A4.2 Derivation of transient rate equation (eq. (4.21)) for Scheme 4.1.

In this section, we derive the transient rate equation for the reaction depicted in Scheme

A4.1:

Scheme A4.1: Two-step catalytic reaction

$$A + * \rightleftarrows A^* \qquad\qquad k_1, k_{-1}$$

$$A^* + B \rightarrow C + * \qquad\qquad k_2$$

The rate of reaction is equal to (eq. (A4.6)):

$$\frac{r(t)}{L} = k_1 a_B \theta_{A^*}(t) \qquad (A4.6)$$

where k_i are rate constants for step i, a_i are activities of species i, and θ_i is the fractional

coverage of species i. The fractional coverage of A as a function of time is described by

the differential equation (eq. (A4.7)):

$$\frac{d\theta_{A^*}(t)}{dt} = k_1 a_A \theta_* - k_{-1} \theta_{A^*} - k_2 a_B \theta_{A^*} \qquad (A4.7)$$

with the initial condition (eq. (A4.8)):

$$\theta_{A^*}(t = 0) = \theta_{A^*,0} \qquad (A4.8)$$

The sum of the fractional coverages equals unity ($\theta_{A^*} + \theta_* = 1$); substitution of this equation into eq. (A4.7) gives eq. (A4.9):

$$\frac{d\theta_{A^*}(t)}{dt} = k_1 a_A (1 - \theta_{A^*}) - k_{-1}\theta_{A^*} - k_2 a_B \theta_{A^*}$$

$$= k_1 a_A - (k_1 a_A + k_{-1} + k_2 a_B)\theta_{A^*}$$

(A4.9)

Equation A4.9 is rearranged to give eq. (A4.10):

$$(k_1 a_A - (k_1 a_A + k_{-1} + k_2 a_B)\theta_A)^{-1} d\theta_{A^*} = dt$$

(A4.10)

which is integrated to give eq. (A4.11):

$$\frac{\ln(k_1 a_A - (k_1 a_A + k_{-1} + k_2 a_B)\theta_{A^*})}{(k_1 a_A + k_{-1} + k_2 a_B)} = t + C$$

(A4.11)

where C is the constant of integration. Solving eq. (A4.11) for θ_{A^*} gives eq. (A4.12):

$$\theta_{A^*}(t) = \frac{k_1 a_A}{k_1 a_A + k_{-1} + k_2 a_B} - C e^{-(k_1 a_A + k_{-1} + k_2 a_B)t}$$

(A4.12)

Substitution of the initial condition (eq. (A4.8)) into eq. (A4.12):

$$\theta_{A^*}(t) = \frac{k_1 a_A}{k_1 a_A + k_{-1} + k_2 a_B}$$
$$- \left(\frac{k_1 a_A}{k_1 a_A + k_{-1} + k_2 a_B} - \theta_{A^*,0}\right) e^{-(k_1 a_A + k_{-1} + k_2 a_B)t}$$

(A4.13)

Finally combining eq. (A4.13) and eq. (A4.6) gives eq. (A4.14), which is identical to eq. (4.21):

$$\frac{r(t)}{L} = \frac{k_1 a_A k_2 a_B}{k_1 a_A + k_{-1} + k_2 a_B}\left(1 - e^{-(k_1 a_A + k_{-1} + k_2 a_B)t}\right)$$
$$+ k_2 a_B \theta_{A^*,0} e^{-(k_1 a_A + k_{-1} + k_2 a_B)t}$$

(A4.14)

A4.3 Derivation of the relationship between transient degrees of rate control and transient sensitivities (eqs. (4.29) and (4.30))

For the derivation of eq. (4.29), by the multivariable chain-rule (eq. (A4.15)):

$$X_{RC,i}(t) = \left(\frac{\partial \ln r(t)}{\partial \ln k_i}\right)_{k_{j\neq i},K_i,\tau_j}$$

$$= \sum_n \left(\frac{\partial \ln r(t)}{\partial \ln k_n}\right)_{k_{j\neq n},\tau_j} \left(\frac{\partial \ln k_n}{\partial \ln k_i}\right)_{k_{j\neq i},K_i,\tau_j}$$

$$+ \sum_n \left(\frac{\partial \ln r(t)}{\partial \ln \tau_n}\right)_{k_j,\tau_{j\neq n}} \left(\frac{\partial \ln \tau_n}{\partial \ln k_i}\right)_{k_{j\neq i},K_i,\tau_j} \qquad (A4.15)$$

Most of the terms in eq. (A4.15) are eliminated by noting that they are equal to zero. $\left(\frac{\partial \ln k_n}{\partial \ln k_i}\right)_{k_{j\neq i},K_i,\tau_j}$ is equal to one if $n = i$, negative one if $n = -i$, and is zero otherwise, so the first summation in eq. (A4.15) simplifies to (eq. (A4.16)):

$$\sum_n \left(\frac{\partial \ln r(t)}{\partial \ln k_n}\right)_{k_{j\neq n},\tau_j} \left(\frac{\partial \ln k_n}{\partial \ln k_i}\right)_{k_{j\neq i},K_i,\tau_j} = \left(\frac{\partial \ln r(t)}{\partial \ln k_i}\right)_{k_{j\neq n},\tau_j} - \left(\frac{\partial \ln r(t)}{\partial \ln k_{-i}}\right)_{k_{j\neq n},\tau_j}$$

$$= s_i(t) - s_{-i}(t) \qquad (A4.16)$$

The second summation in eq. (A4.15) is eliminated because the derivative of τ_n while keeping all τ_j constant is zero, such that $\left(\frac{\partial \ln \tau_n}{\partial \ln k_i}\right)_{k_{j\neq i},K_i,\tau_j} = 0$ and the second summation is equal to zero, and thus eq. (A4.15) becomes eq. (A4.17):

$$X_{RC,i}(t) = \left(\frac{\partial \ln r(t)}{\partial \ln k_i}\right)_{k_{j\neq i}, K_i, \tau_j} = s_i(t) - s_{-i}(t) \tag{A4.17}$$

which is identical to eq. (4.29).

For eq. (4.30) we again use the multivariable chain-rule to write (eq. (A4.18)):

$$X_{TRC,j}(t) = \left(\frac{\partial \ln r(t)}{\partial(-G_j^o/k_BT)}\right)_{G_{n\neq j}^o, \tau_n}$$

$$= \sum_i \left(\frac{\partial \ln r(t)}{\partial \ln k_i}\right)_{k_{n\neq i}, \tau_n} \left(\frac{\partial \ln k_i}{\partial(-G_j^o/k_BT)}\right)_{G_{n\neq j}^o, \tau_n} \tag{A4.18}$$

$$+ \sum_i \left(\frac{\partial \ln r(t)}{\partial \ln \tau_i}\right)_{k_n, \tau_{n\neq i}} \left(\frac{\partial \ln \tau_i}{\partial(-G_j^o/k_BT)}\right)_{G_{n\neq j}^o, \tau_n}$$

Again the derivative of τ_i while keeping τ_n constant is zero, so $\left(\frac{\partial \ln \tau_i}{\partial(-G_j^o/k_BT)}\right)_{G_{n\neq j}^o, \tau_n} = 0$, and

thus the second summation in eq. (A4.18) is zero. The elementary step rate constants for

transition-state theory are of the form (eq. (A4.19)):

$$k_i = \frac{k_BT}{h} \exp\left(-\frac{\left(G_{TS,i}^{o\ddagger} + \sum_j v_{ij}G_j^o[v_{ij} < 0]\right)}{k_BT}\right) \tag{A4.19}$$

Thus, the derivative of log of the rate constant with respect to the free energy of a species

is (eq. (A4.20)):

$$\left(\frac{\partial \ln k_i}{\partial(-G_j^o/k_BT)}\right)_{G_{n\neq j}^o, \tau_n} = v_{ij}[v_{ij} < 0] \tag{A4.20}$$

and since $\left(\frac{\partial \ln r(t)}{\partial \ln k_i}\right)_{k_{n\neq i}, \tau_n} = s_i(t)$ by definition, then eq. (A4.18) simplifies to eq. (A4.21):

$$X_{TRC,j}(t) = \sum_i \left(\frac{\partial \ln r(t)}{\partial \ln k_i}\right)_{k_{n \neq i}, \tau_n} \left(\frac{\partial \ln k_i}{\partial(-G_j^o/k_B T)}\right)_{G_{n \neq j}^o, \tau_n} = \sum_i \nu_{ij} s_i(t)[\nu_{ij} < 0] \qquad \text{(A4.21)}$$

which is identical to eq. (4.30).

A4.4 Matlab code for calculating transient degrees of rate control for Scheme 4.2

The Matlab script calculating the analytical transient rate function for the reaction in Scheme 4.2 (eqs. (4.34)-(4.36)) and the sensitivities (eqs. (4.25)-(4.26)) is available for download at:

https://github.com/foley352/Transient-DoRC

A4.5 Transients when step-changing activities of A, E, and F in Scheme 4.2

The transient rates, surface coverages, and kinetic degrees of rate control when step-changing the activities of A, E, and F from 1 to 3 for the four reactions in series depicted by Scheme A4.2 are shown in Figures A4.1-A4.3.

Scheme A4.2: Four irreversible Eley-Rideal elementary surface reactions in series to produce product P.

$$Rxn\ 1: A + * \rightarrow A^* \qquad k_1$$

$$Rxn\ 2: A^* + D \rightarrow B^* \qquad k_2$$

$$Rxn\ 3: B^* + E \rightarrow C^* \qquad k_3$$

$$Rxn\ 4: C^* + F \rightarrow P + C^* \qquad k_4$$
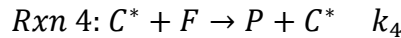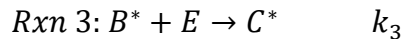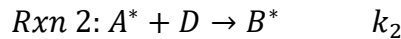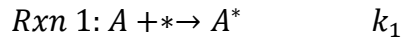
In each case, if there is an extrema in the transient rate, it occurs when there is an extrema in the degree of rate control for the step whose rate depends on the reactant activity that was step-changed. The rate is continuous through the step-change except when the

activity of F is step-changed (Figure A4.3a). At the time of the step-change, the kinetic degree of rate control of step 4 is always one, and thus, because this step is irreversible and is first-order in the activity of F, the rate at the time of the step-change is also first-order in the activity of F and zero-order in all other reactant activities.
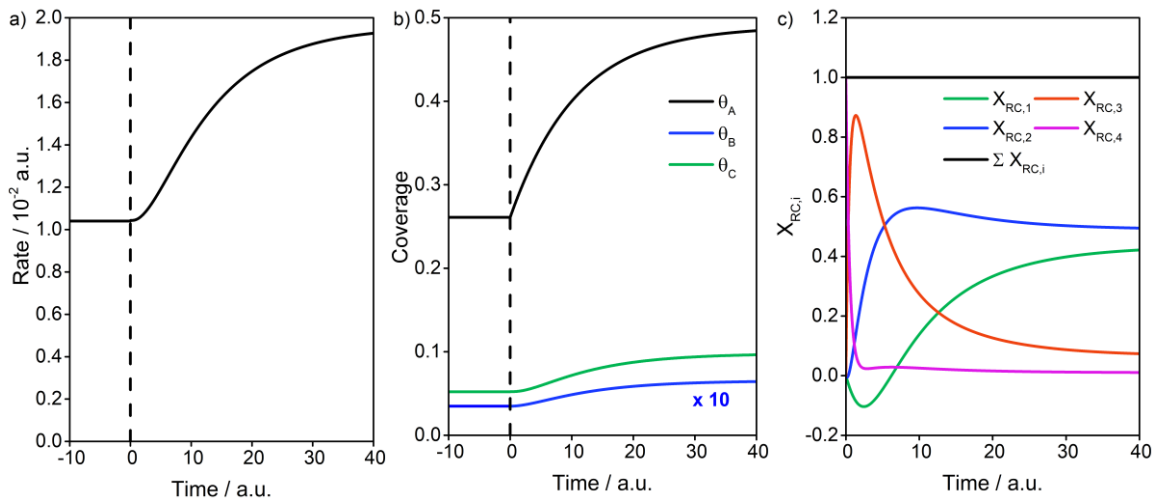
Figure A4.1: Analysis of the transient rate using degrees of rate control for the composite reaction in Scheme A4.2. $k_1 = 0.02$, $k_2 = 0.04$, $k_3 = 0.3$, $k_4 = 2$, $a_{A0} = a_{D0} = a_{E0} = a_{F0} = 1$. At time $t = 0$ au the activity of A is increased from $a_A = 1$ to $a_A = 3$ a) Initial and transients rates through the step-change in the activity of D. b) Surface coverages before and after the step-change. c) Kinetic degrees of rate control after the step-change. The vertical dotted line indicates the time of the step-change.
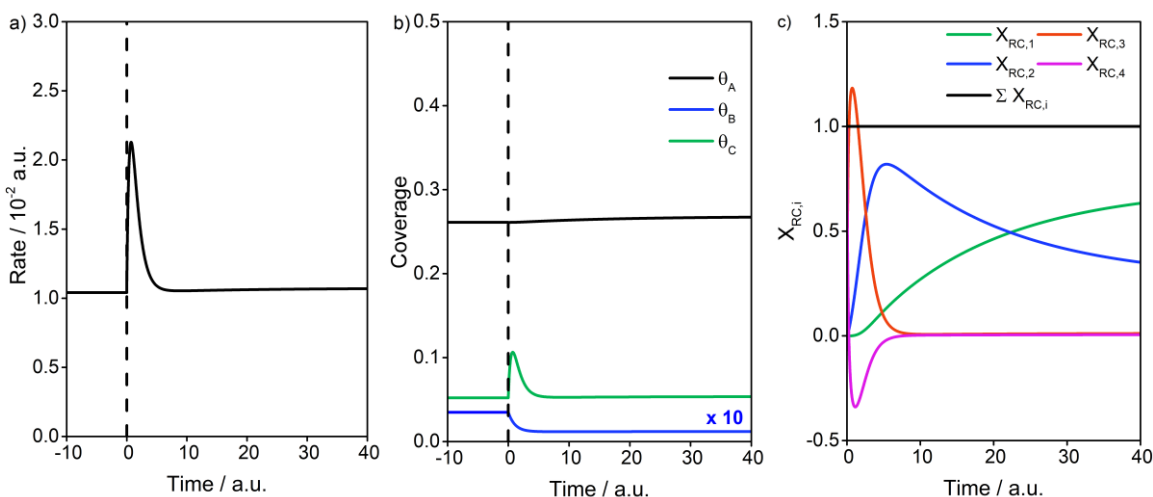
Figure A4.2: Analysis of the transient rate using degrees of rate control for the composite reaction in Scheme A4.2. $k_1 = 0.02$, $k_2 = 0.04$, $k_3 = 0.3$, $k_4 = 2$, $a_{A0} = a_{D0} = a_{E0} = a_{F0} = 1$. At time $t = 0$ au the activity of E is increased from $a_E = 1$ to $a_E = 3$ au a) Initial and transients rates through the step-change in the activity of D. b) Surface coverages before and after the step-change. c) Kinetic degrees of rate control after the step-change. The vertical dashed line indicates the time of the step-change.

311
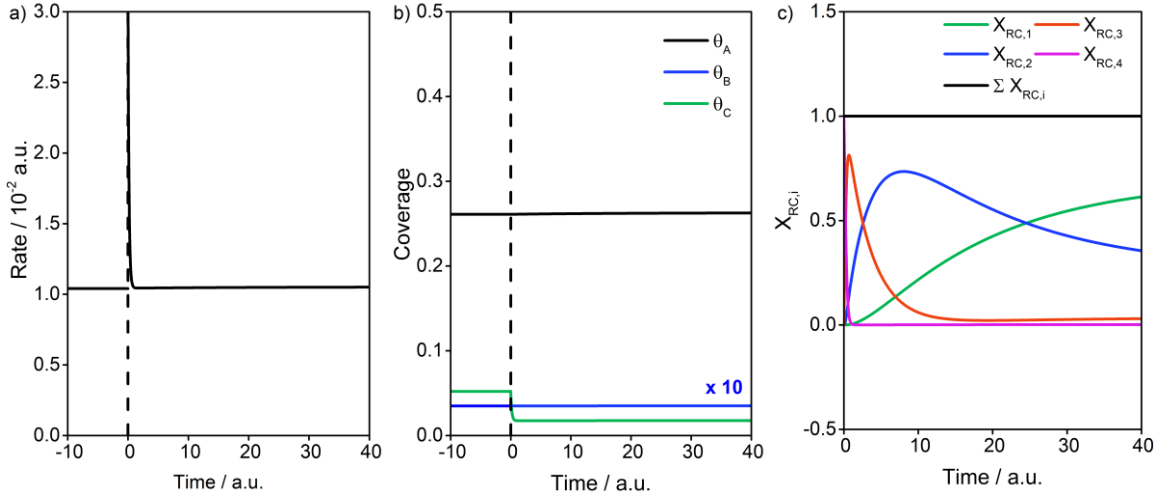
Figure A4.3: Analysis of the transient rate using degrees of rate control for the composite reaction in Scheme A4.2. $k_1 = 0.02$, $k_2 = 0.04$, $k_3 = 0.3$, $k_4 = 2$, $a_{A0} = a_{D0} = a_{E0} = a_{F0} = 1$. At time $t = 0$ au the activity of F is increased from $a_F = 1$ to $a_F = 3$ au a) Initial and transients rates through the step-change in the activity of D. b) Surface coverages before and after the step-change. c) Kinetic degrees of rate control after the step-change. The vertical dotted line indicates the time of the step-change.

A4.6 Proof that the sensitivities (and kinetic degrees of rate control) sum to unity during the transient

The transient rate is a function of the rate constants of elementary steps (k_i), the activities of reactant and product species (a_j), the initial fractional coverages of surface species $(\theta_{j,0})$, and time (t). Each variable can be separated into a unitless component, designated by primes $(')$ and a unitted component, designated by the variable u_i where the subscript on i corresponds to the units of u_i. For example, k_1 can be rewritten as $k_1 = k_1'/u_s$ where $u_s = 1\ s$ and $k_1' = k_1 * u_s$. Doing this for each variable we can write the rate as a function of dimensional quantities, f', divided by the unitted quantity u_s so that the rate has units of inverse time (eq. (A4.22)):

312

$$r = f(k_i, a_j, \theta_{j,0}, t) = f'(k_i', a_j', \theta_{j,0}', t')/u_s \tag{A4.22}$$

The total derivative of the log of the rate with respect to the log of the variable u_s is thus (eq. (A4.23)):

$$\frac{d \ln r}{d \ln u_s} = \frac{u_s}{r} \frac{dr}{du_s} = \frac{u_s}{f'/u_s} \frac{d}{du_s} f'(k_i', a_j', \theta_{j,0}', t')/u_s = -1 \tag{A4.23}$$

Using the chain rule, the total derivative of the rate is related to the partial derivatives by eq. (A4.24):

$$\begin{aligned}
\frac{d \ln r}{d \ln u_s} &= \sum_i \left(\frac{\partial \ln r}{\partial \ln k_i}\right)_{k_{n \neq i}, a_j, \theta_{j,0}, t} \left(\frac{d \ln k_i}{d \ln u_s}\right) \\
&+ \sum_j \left(\frac{\partial \ln r}{\partial \ln a_j}\right)_{k_i, a_{n \neq j}, \theta_{j,0}, t} \left(\frac{d \ln a_j}{d \ln u_s}\right) \\
&+ \left(\frac{\partial \ln r}{\partial \ln t}\right)_{k_n, a_j, \theta_{j,0}} \left(\frac{d \ln t}{d \ln u_s}\right) \\
&+ \sum_j \left(\frac{\partial \ln r}{\partial \ln \theta_{j,0}}\right)_{k_{n \neq i}, a_j, \theta_{n \neq j, t}} \left(\frac{d \ln \theta_{j,0}}{d \ln u_s}\right) \\
&= -\sum_i \left(\frac{\partial \ln r}{\partial \ln k_i}\right)_{k_{n \neq i}, a_j, \theta_{j,0}, t} + \left(\frac{\partial \ln r}{\partial \ln t}\right)_{k_n, a_j, \theta_{j,0}}
\end{aligned} \tag{A4.24}$$

where derivatives of activity and fractional coverage with respect to u_s are zero. Since the activities, coverages, and time, t, are not functions of the rate constants, the partial derivatives in eq. (A4.24) can be related to the sensitivities (eq. (A4.25)):

$$\left(\frac{\partial \ln r}{\partial \ln k_i}\right)_{k_{n \neq i}, a_j, \theta_{j,0}, t} = \left(\frac{\partial \ln r}{\partial \ln k_i}\right)_{k_{n \neq i}} = s_i \tag{A4.25}$$

and the partial derivative with time is defined as the sensitivity, s_t. Combination of eqs. (A4.23)-(A4.25) gives eq. (A4.26):

313

$$-\sum_i s_i + s_t = -1 \tag{A4.26}$$

and thus, when the transient rate is of the form given by eq. (A4.22), $\sum_i s_i \neq 1$ for all t.

By identifying the time constants, τ_j, and rewriting the rate as eq. (A4.27):

$$r = g\big(k_i, a_j, t'_j = t/\tau_j, \theta_{j,0}\big) = g'\big(k'_i, a'_j, t'_j = t/\tau_j, \theta'_{j,0}\big)/u_s \tag{A4.27}$$

the time variable, t' is already dimensionless. The total derivative of the log of the rate with respect to the log of the variable u_s is still eq. (A4.23), but now using the chain rule for eq. (A4.27), this derivative is related to the partial derivatives by eq. (A4.28):

$$\frac{d \ln r}{d \ln u_s} = \sum_i \left(\frac{\partial \ln r}{\partial \ln k_i}\right)_{k_{n\neq i}, a_j, \theta_{j,0}, t'} \left(\frac{d \ln k_i}{d \ln u_s}\right)$$

$$+ \sum_j \left(\frac{\partial \ln r}{\partial \ln a_j}\right)_{k_i, a_{n\neq j}, \theta_{j,0}, t'} \left(\frac{d \ln a_j}{d \ln u_s}\right)$$

$$+ \left(\frac{\partial \ln r}{\partial \ln t'}\right)_{k_n, a_j, \theta_{j,0}} \left(\frac{d \ln t'}{d \ln u_s}\right) \tag{A4.28}$$

$$+ \sum_j \left(\frac{\partial \ln r}{\partial \ln \theta_{j,0}}\right)_{k_{n\neq i}, a_j, \theta_{n\neq j, t'}} \left(\frac{d \ln \theta_{j,0}}{d \ln u_s}\right)$$

$$= -\sum_i \left(\frac{\partial \ln r}{\partial \ln k_i}\right)_{k_{n\neq i}, a_j, \theta_{j,0}, t'} = -\sum_i s_i$$

By combining eq. (A4.28) with eq. (A4.23), it is clear that $\sum_i s_i = 1$ for all times when the rate is written in the form given by eq. (A4.27).

A4.7 Rate of non-pseudo-steady-state reaction with irreversible steps in series with apparent inhibition

We demonstrate by example that for non-pseudo-steady irreversible reactions in series, increasing the rate constant of a step can decrease the reaction rate at certain times on stream, congruent with steps that are inhibition steps. Consider the two-step fluid-phase reactions in series illustrated in Scheme A4.3. The reaction begins at time $t = 0$ with an initial activity A equal to a_0 and the initial activity of B equal to zero. The rate of C formation as a function of time is given by eq. (A4.29):

$$r = \frac{k_1 k_2 a_{A0}}{k_2 - k_1}(e^{-k_1 t} - e^{-k_2 t}) \qquad (A4.29)$$

The rate as a function of time for $a_{A0} = 1$ and $k_2 = 1$ au and $k_1 = 2$ or $k_1 = 6$ au is shown in Figure A4.4. Notice that the rate at the times shown in Figure A4.4 decreases when the rate constant k_1 is increased, demonstrating that even for irreversible reactions in series, a step can be inhibiting.

Scheme A4.3: Hypothetical reaction network with two irreversible reaction steps in series

$$Rxn\ 1{:}\ A \rightarrow B \qquad\qquad k_1$$

$$Rxn\ 2{:}\ B \rightarrow C \qquad\qquad k_2$$
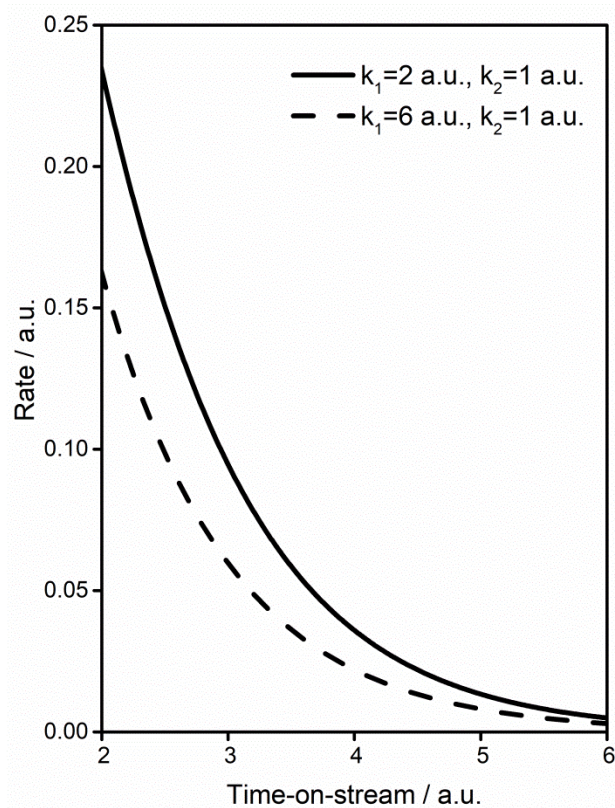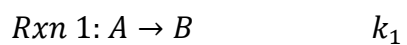
Figure A4.4: Rate for the reaction network in Scheme A4.3 as given by eq. (A4.29).

A5 Transient and steady-state kinetic study of formaldehyde alkylation of benzene to form diphenylmethane on HZSM-5 catalysts

A5.1 Discussion on Heat- and Mass-Transfer Limitations

Intra-crystallite mass transfer limitations are assessed by the Weisz-Prater criterion, which state that intra-crystallite mass transfer limitations are negligible if the inequality given by eq. (A5.1) is satisfied:[1]

$$\frac{r_V R_p^2}{C_s D_{eff}} \leq 3\beta \tag{A5.1}$$

where r_V is the rate per volume of catalyst, R_p is the radius of the catalyst particle, C_s is the concentration of the reactant at the catalyst surface, D_{eff} is the effective diffusivity, and β is approximately related to the effectiveness, η by eq. (A5.2):

$$\eta = 1 - \frac{n\beta}{4} \tag{A5.2}$$

where n is the reaction order. The potential for intra-crystallite mass transfer limitations is typically greatest when the rate is highest. We assess mass transport limitations when DPM$^+$ consumption is rate-limiting and the rate is first-order in C_6H_6 (n=1). For $\eta = 0.95$, from eq. (A5.2) $\beta = 0.2$. The rate per volume catalyst $r_V \approx 35 * 10^{-9}$ mol cm^{-3} and the effective particle radius is $R_p = 3$ nm $= 3 * 10^{-7}$ cm. The concentration of benzene at a partial pressure of 0.4 kPa at 393 K is given by the ideal gas law as $C_s = 1.2 * 10^{-7}$ mol cm^{-3}. The diffusion coefficient at 393 K is approximately $D_{eff} = 10^{-9}$ cm^2 s^{-1}.[3] For these conditions, we find the inequality for the Weisz-Prater criterion to be (eq. (A5.3)):

$$\frac{r_V R_p^2}{C_s D_{eff}} = 1.3 * 10^{-5} \leq 3\beta = 0.6 \qquad \text{(A5.3)}$$

and thus the criterion is satisfied and intra-crystallite mass transfer limitation are not expected.

External heat and mass transfer limitations can be assessed by varying the interfacial velocity of the fluid in the reactor bed. **Figure A5.1** shows the DPM rate as a function of total flow through the reactor bed at a reaction condition where the rate is high, where external transport limitations should be most severe. When there are no external transport limitations, the rate should be invariant with space velocity. The DPM rate increases monotonically with flow rate in Figure A5.1, suggesting that there may be slight external transport limitations. An alternative explanation is that the rate of DPM formation is inhibited by a product of the reaction. Most of the reaction conditions in this study are at much lower reaction rates, and the effect of total flow rate on the measure of DPM rate is relatively modest, increasing from 30.6 x 10^{-5} mol (mol s)$^{-1}$ at a flow rate of 2.3 cm^3 s^{-1} to 32.7 10^{-5} mol (mol s)$^{-1}$ at 3.3 cm^3 s^{-1}. For the reactions in this study, the flow rate is typically ~2.5 cm^3 s^{-1}. These data suggest at high reaction rates, the steady-state rate may be slightly underestimated. Despite this, the agreement between transient and steady-state reaction rate and steady-state fractional coverages using the same kinetic model suggests that the slight underestimation of the steady-state rate at select reaction conditions has negligible impact on the dataset as a whole.
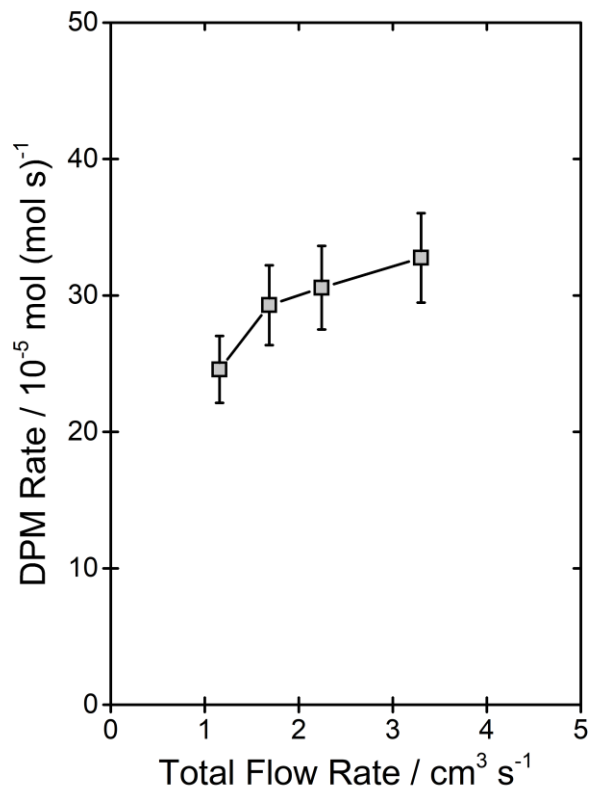
Figure A5.1: DPM rate with varying total flow rate at 3.4-4.0 kPa H_2O, 0.17-0.19 kPa HCHO, 0.62-0.74 kPa C_6H_6 at 393 K for a catalyst bed with 0.0105 g SPP-HZSM-5 and ~0.1 g sand.

A5.2 Degradation in activity of SPP-HZSM-5 with repeated regeneration cycles

The rate per mass of SPP-HZSM-5 degrades over successive oxidative thermal treatments to remove coke deposits. This decrease in rate was attributed to hydrolysis of framework Al and local collapse of the zeolite framework. To account for catalyst degradation over time, a reference condition (0.010 kPa HCHO, 4 kPa H_2O, 0.44 kPa C_6H_6, 393 K) was repeated regularly to assess the loss of active sites over time. The measured rate in any given experiment was normalized by the remaining number of active sites in the reactor bed based on the data shown in Figure A5.2. Two different

319

reactor beds were used in this study, and each experienced different reaction conditions and were regenerated with different frequencies, and thus the fraction of sites remaining in each reactor are not expected to be the same.
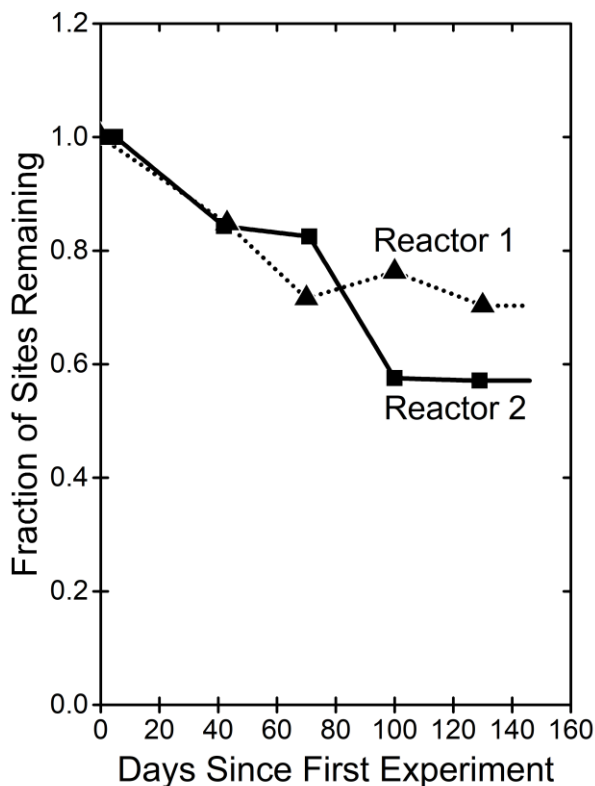
Figure A5.2: The fraction of sites remaining for each reactor bed as determined by repeating reference reaction conditions (0.010 kPa HCHO, 4 kPa H_2O, 0.44 kPa Benzene, 393 K).

A5.3 Amine Temperature-Programmed Desorption

Reaction rates in catalysis are rigorously normalized by the number of active sites. For zeolite catalysts like SPP-HZSM-5, the active sites are Brønsted-acidic protons, which are enumerated by titrations with amines followed by temperature programmed desorption (TPD). Figure A5.3 shows the rate of amine desorption during TPD for (a) a small amine, NH_3, which titrates all acid sites, and (b) a bulky amine, 2,6-di-*tert-*

320

butylpyridine which is too large to enter the microporous zeolite channels and thus titrates only external acid sites.[2] The total number of acid sites as determined by NH_3 TPD is 141.2 μmol g^{-1}, in agreement with the expected number of acid sites for this material (Si/Al = 100) of 165 μmol g^{-1}, and the number of external acid sites is 56.6 μmol g^{-1}, corresponding to 40% of active sites on the external surface.
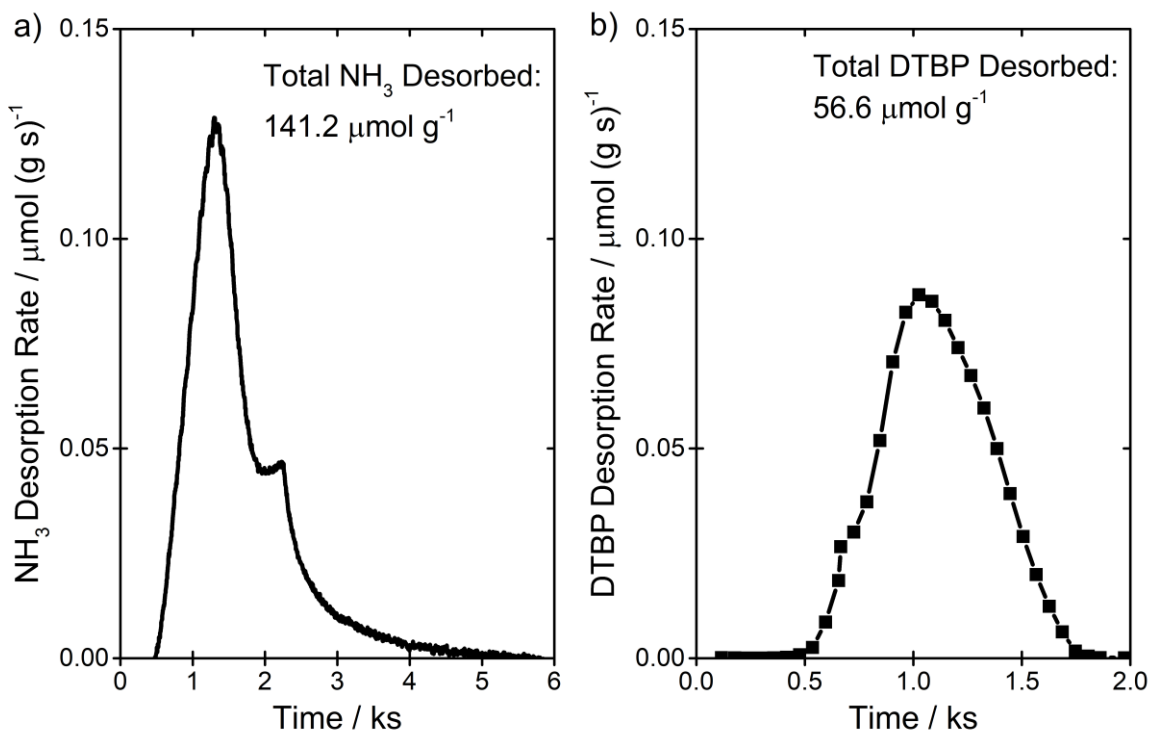
Figure A5.3: Desorption rate of amines during temperature ramp and hold on SPP-HZSM-5. a) NH_3 desorption starting at 423 K and ramping at 0.167 K s^{-1} and holding at 723 K. Data were collected at 4 s intervals using online MS. b) di-*tert*-butylpyridine (DTBP) desorption start at 353 K and ramping at 0.33 K s^{-1} until 873 K. Data were collected at one-minute intervals using GC-FID.

A5.4 Effect of pretreatment in 2,6-di-tert-butylpyridine on DPM rates

The SPP-HZSM-5 catalyst has a high fraction of acid sites on the external surface of the catalyst (40%) compared to typical nanoscale HZSM-5 catalysts. The location of the active sites may impact the intrinsic reaction rates for DPM formation. To test this, the

rate of DPM formation was measured with and without a pre-treatment in 2,6-di-*tert*-butylpyridine (DTBP), which titrates all external acid sites, leaving only the acid site in the microporous channels available for catalysis.[75] These DPM rates are reported in Figure A5.4 normalized by catalyst mass (a) and by active sites available for catalysis (b). The rate per available site was slightly higher without a DTBP pretreatment, suggesting that the external active sites are more active for DPM formation. The nature of the transient is the same with and without a DTBP pre-treatment, suggesting that the underlying mechanism for DPM^+ formation is not a function of acid site location.
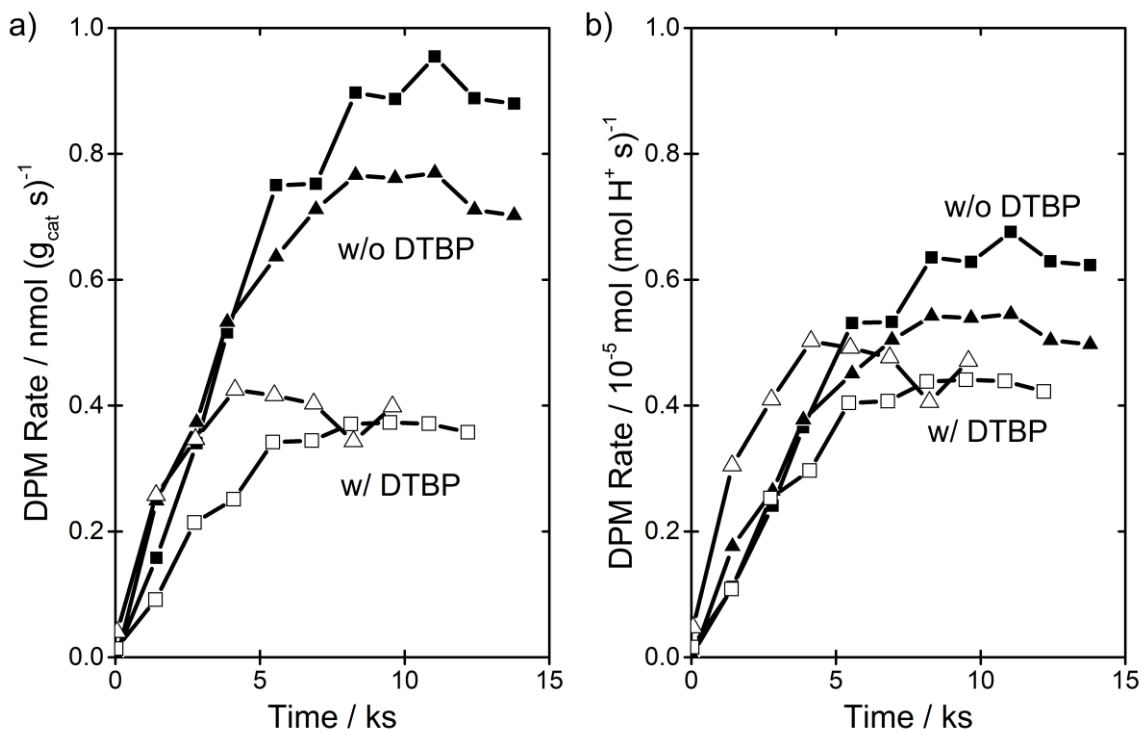
Figure A5.4: Rate of diphenylmethane formation on SPP-HZSM-5 with (open symbols) and without (filled symbols) a pretreatment in 2,6-di-*tert*-butylpyridine (DTBP) at 353 K, 0.031-0.033 kPa HCHO, 3.18-3.31 kPa H_2O, 7.44-7.72 kPa C_6H_6. Shapes indicate different experimental trials. a) Rate per mass catalyst b) rate normalized by non-titrated acid sites.

A5.5 Degree of rate control analysis

We demonstrated in Chapter 4 how to apply the degree of rate control concept to transient reaction rates using eq. (A5.4):

$$X_{RC,i}(t) = \left(\frac{\partial \ln r\,(t)}{\partial(-G^o_{TS,i}/RT)} \right)_{G^o_{j \neq TS,i},\tau_j} \tag{A5.4}$$

where $G^o_{TS,i}$ is the standard-state free energy of transition state i and τ_j are the time-constants for the transient rate. Here, we illustrate the calculation of the degrees of rate control for transient rates of DPM formation and demonstrate how degree of rate control is a useful concept for understanding transient kinetics. The transient rate of DPM formation is (eq. (A5.5)):

$$r_{DPM}(t) = \frac{f_1 f_2}{f_1 + f_2}$$

$$+ \left(f_2 \theta_{DPM^+,0} - \frac{f_1 f_2}{f_1 + f_2} \right) \exp(-(f_1 + f_2)(t - t_0)) \quad \forall\, t \in [t_0, t_1] \tag{A5.5}$$

where f_1 and f_2 are (eqs. (A5.6) and (A5.7)):

$$f_1 = \frac{\dfrac{k_1 K_{HCHO}}{K_{hyd} K_{H_2O}} P_{HCHO,0} P_{C_6 H_6}}{\dfrac{K_{C_6 H_6}}{K_{H_2O}} P_{C_6 H_6} P_{H_2O} + P^2_{H_2O}} \tag{A5.6}$$

$$f_2 = k_2 P_{C_6 H_6} \tag{A5.7}$$

The degrees of rate control formula for this rate function can be rewritten in terms of f_i as (eqs. (A5.8) and (A5.9)):

$$X_{RC,1}(t) = \left(\frac{\partial \ln r\,(t)}{\partial \left(-G_{TS,1}^o/RT\right)} \right)_{G_{j\neq TS,1}^o, \tau_j} = \frac{k_1}{r(t)} \left(\frac{\partial r(t)}{\partial k_1} \right)_{k_{j\neq i}, \tau_j}$$

$$= \frac{f_1}{r(t)} \left(\frac{\partial r(t)}{\partial f_1} \right)_{f_{j\neq i}, \tau_j} \tag{A5.8}$$

$$X_{RC,2}(t) = \left(\frac{\partial \ln r\,(t)}{\partial \left(-G_{TS,2}^o/RT\right)} \right)_{G_{j\neq TS,1}^o, \tau_j} = \frac{k_2}{r(t)} \left(\frac{\partial r(t)}{\partial k_2} \right)_{k_{j\neq i}, \tau_j}$$

$$= \frac{f_2}{r(t)} \left(\frac{\partial r(t)}{\partial f_2} \right)_{f_{j\neq i}, \tau_j} \tag{A5.9}$$

where the final two terms are equivalent because $f_i \propto k_i$. To calculate the degrees of rate control during the transient using eqs. (A5.8) and (A5.9), it is necessary to identify the time constants, τ_j, as the quantities that multiply time, t, in the analytical rate function in eq. (A5.5). The transient rate function can be re-written as eq. (A5.11):

$$r_{DPM}(t) = \frac{f_1 f_2}{f_1 + f_2} + \left(f_2 \theta_{DPM^+,0} - \frac{f_1 f_2}{f_1 + f_2} \right) \exp(-(t - t_0)/\tau) \quad \forall\, t \in [t_0, t_1] \tag{A5.11}$$

where the time constant $\tau = (f_1 + f_2)^{-1}$ in the exponential. Applying eq. A5.8 to eq. (A5.11), $X_{RC,1}$ is (eq. (A5.12)):

$$X_{RC,1}(t) = \frac{\dfrac{f_1 f_2^2}{(f_1 + f_2)^2} \left(1 - \exp\left(-\dfrac{(t - t_0)}{\tau} \right) \right)}{\dfrac{f_1 f_2}{f_1 + f_2} + \left(f_2 \theta_{DPM^+,0} - \dfrac{f_1 f_2}{f_1 + f_2} \right) \exp\left(-\dfrac{t - t_0}{\tau} \right)} \tag{A5.12}$$

and similarly $X_{RC,2}(t)$ is (eq. (A5.13)):

$$X_{RC,2}(t) = \frac{\dfrac{f_1^2 f_2}{(f_1 + f_2)^2} + \left(f_2 \theta_{DPM^+,0} - \dfrac{f_1^2 f_2}{(f_1 + f_2)^2}\right) \exp\left(-\dfrac{t - t_0}{\tau}\right)}{\dfrac{f_1 f_2}{f_1 + f_2} + \left(f_2 \theta_{DPM^+,0} - \dfrac{f_1 f_2}{f_1 + f_2}\right) \exp\left(-\dfrac{t - t_0}{\tau}\right)} \tag{A5.13}$$

The degrees of rate control during each of the step-change experiments (see Figure 5.1) is shown in Figure A5.5. During each experiment, at the time of the step-change, $X_{RC,1} = 0$ and $X_{RC,2} = 1$. The reaction orders at the time of the step-change are the same as the reaction orders for step 2, the consumption of DPM^+. Thus, at the time of the step-change, the rate is zero-order in HCHO and H_2O and first-order in C_6H_6. This is used to rationalize why at the time of the step-change in HCHO and H_2O pressure, the rate is unaffected, and therefore the rate through the step-change is continuous, while the rate is immediately perturbed and therefore discontinuous through the step-change in C_6H_6 pressure.
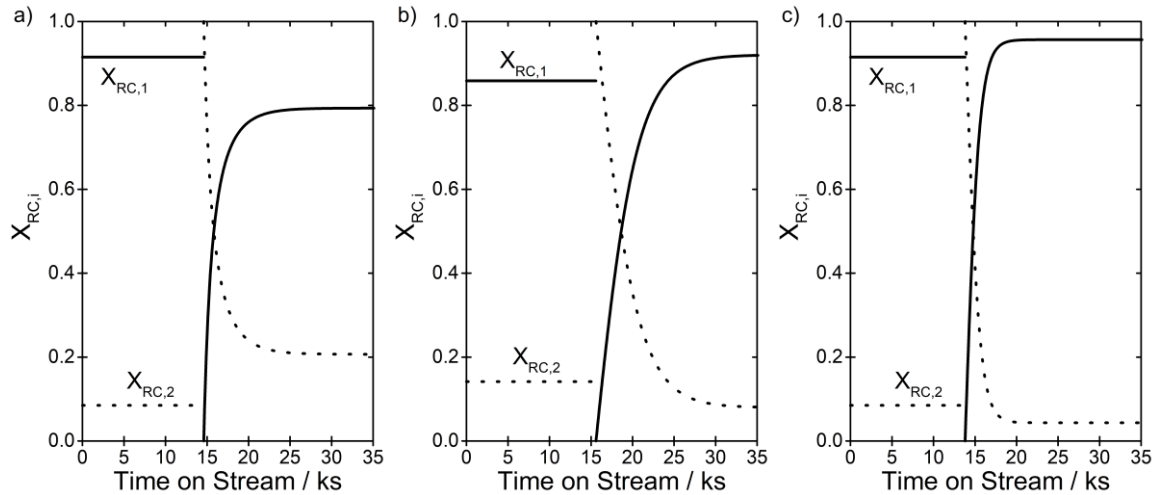
Figure A5.5: Transient degrees of rate control $X_{RC,1}$ (solid line) and $X_{RC,2}$ (dotted line) calculated by eqs. (A5.12) and (A5.13)**Error! Reference source not found.**, respectively or each of the transient rates in Figure 1. Each experiment begins with fresh catalyst (t = 0) and after reaching steady-state a reactant partial pressure is step-changed. a) Step-change in HCHO pressure from 0.010 to 0.028 kPa with T = 393 K, 0.41 kPa C_6H_6, 3.7 kPa H_2O, b) step-change in H_2O pressure from 3.8 to 5.8 kPa with T = 393 K, 0.41 kPa C_6H_6, 0.019 kPa HCHO, c) step-change in C_6H_6 pressure from 0.41 to 1.3 kPa with T = 393 K, 0.010 kPa HCHO, and 3.7 kPa H_2O.

A5.6 Summary of all reaction conditions

All 153 reaction conditions, rates, predicted rates with estimated parameters in Table 2, and the steady-state kinetic degrees of rate control are summarized in **Table A5.1**.

Table A5.1: All reaction conditions, measured rate, predicted rates, and degrees of rate control for DPM formation from HCHO and C_6H_6 on SPP-HZSM-5

T / K	HCHO Pressure / kPa	C_6H_6 Pressure / kPa	H_2O Pressure/ kPa	Measured Rate / 10^{-5} mol DPM $(mol\ s)^{-1}$	Predicted Rate / 10^{-5} mol DPM $(mol\ s)^{-1}$	$X_{RC,1}$	$X_{RC,2}$
393	0.028	0.41	3.65	9.67	7.16	0.79	0.21
393	0.019	0.41	3.69	5.97	5.21	0.85	0.15
393	0.009	0.41	3.83	3.01	2.61	0.92	0.08
393	0.029	0.41	3.94	8.07	6.66	0.81	0.19
393	0.019	0.40	3.88	4.72	4.76	0.86	0.14
393	0.017	0.42	3.91	5.93	4.42	0.87	0.13
393	0.005	0.42	3.76	1.32	1.46	0.96	0.04
393	0.036	0.42	4.01	9.63	7.84	0.78	0.22
393	0.018	0.40	3.93	5.82	4.50	0.87	0.13
393	0.005	0.39	3.75	1.55	1.42	0.96	0.04
393	0.037	0.40	4.10	9.11	7.63	0.77	0.23
393	0.019	0.41	3.86	4.87	4.80	0.86	0.14
393	0.187	0.37	4.27	23.05	18.40	0.41	0.59
393	0.134	0.48	4.93	14.12	17.17	0.58	0.42
393	0.173	0.45	4.13	19.32	21.39	0.44	0.56
393	0.204	0.47	2.18	33.26	31.42	0.21	0.79
393	0.092	0.41	4.20	13.20	14.13	0.59	0.41
393	0.194	0.47	4.09	17.97	23.18	0.41	0.59
393	0.019	0.87	3.98	8.04	6.95	0.90	0.10
393	0.019	0.37	3.83	5.90	4.54	0.85	0.15
393	0.018	0.37	3.79	5.82	4.46	0.86	0.14
393	0.019	0.56	3.89	6.70	5.69	0.88	0.12
393	0.020	0.44	3.93	5.97	5.16	0.86	0.14
393	0.177	0.34	7.61	10.89	9.87	0.65	0.35
393	0.352	0.35	8.01	14.75	14.34	0.51	0.49
393	0.090	0.42	1.84	29.11	24.30	0.31	0.69
393	0.183	0.78	3.92	31.46	34.04	0.48	0.52
393	0.187	0.25	3.94	11.13	13.49	0.34	0.66
393	0.012	1.48	2.35	11.44	9.66	0.92	0.08
393	0.011	1.45	1.05	21.80	20.80	0.83	0.17
393	0.011	1.44	5.90	2.34	2.89	0.98	0.02
393	0.010	1.39	3.34	6.22	5.35	0.95	0.05
393	0.014	0.44	0.28	23.91	28.01	0.24	0.76
393	0.016	0.44	0.33	29.93	27.76	0.24	0.76
393	0.018	0.42	1.08	14.29	16.84	0.52	0.48
393	0.019	0.44	1.74	12.43	12.11	0.67	0.33
393	0.020	0.44	1.91	13.72	11.45	0.69	0.31
393	0.019	0.43	1.92	11.81	11.22	0.69	0.31
393	0.022	0.43	1.98	10.75	11.75	0.67	0.33
393	0.018	0.41	3.84	6.32	4.74	0.86	0.14
393	0.018	0.43	3.88	4.89	4.78	0.87	0.13
393	0.019	0.40	5.75	3.07	2.64	0.92	0.08
393	0.016	0.41	7.17	1.37	1.70	0.95	0.05
393	0.016	0.40	9.02	0.73	1.13	0.97	0.03

T / K	HCHO Pressure / kPa	C_6H_6 Pressure / kPa	H_2O Pressure/ kPa	Measured Rate / 10^{-5} mol DPM $(mol\ s)^{-1}$	Predicted Rate / 10^{-5} mol DPM $(mol\ s)^{-1}$	$X_{RC,1}$	$X_{RC,2}$
393	0.014	0.40	9.43	1.03	0.91	0.97	0.03
393	0.019	0.38	12.47	0.47	0.73	0.98	0.02
393	0.021	0.40	1.99	10.55	11.13	0.67	0.33
393	0.019	0.39	7.30	2.53	1.82	0.94	0.06
393	0.010	0.53	2.02	5.93	7.22	0.84	0.16
393	0.011	1.45	2.03	8.97	10.38	0.91	0.09
393	0.011	0.15	3.81	1.47	1.48	0.88	0.12
393	0.010	0.29	3.85	2.20	2.16	0.91	0.09
393	0.013	0.32	3.86	2.80	2.91	0.89	0.11
393	0.014	1.14	3.92	4.83	5.89	0.94	0.06
393	0.011	4.14	3.96	4.66	5.96	0.98	0.02
393	0.011	1.45	3.99	4.81	4.91	0.96	0.04
393	0.015	0.63	4.00	3.90	4.64	0.91	0.09
393	0.011	0.45	4.02	3.33	3.09	0.92	0.08
393	0.012	0.27	4.05	2.32	2.26	0.90	0.10
393	0.013	0.29	4.06	2.86	2.66	0.89	0.11
393	0.012	0.44	4.08	3.31	3.13	0.91	0.09
393	0.012	1.35	4.11	4.90	5.16	0.95	0.05
393	0.012	0.89	4.20	4.15	4.25	0.94	0.06
393	0.012	0.43	4.21	3.52	2.97	0.92	0.08
393	0.015	0.36	6.54	0.93	1.59	0.95	0.05
393	0.009	0.30	6.66	0.73	0.85	0.97	0.03
393	0.012	0.48	6.91	1.16	1.46	0.96	0.04
393	0.012	0.31	7.10	0.56	1.03	0.96	0.04
393	0.012	0.27	7.32	0.56	0.89	0.96	0.04
393	0.013	0.36	7.38	0.85	1.18	0.96	0.04
393	0.012	0.50	7.39	1.01	1.36	0.97	0.03
393	0.014	1.03	7.41	1.61	2.39	0.97	0.03
393	0.012	0.20	7.46	0.38	0.65	0.96	0.04
393	0.031	1.30	7.50	3.23	5.69	0.95	0.05
393	0.012	1.42	7.59	1.91	2.32	0.98	0.02
393	0.012	0.14	7.61	0.39	0.46	0.96	0.04
393	0.013	0.67	7.73	1.26	1.69	0.97	0.03
393	0.030	0.59	7.75	2.17	3.35	0.93	0.07
393	0.011	0.95	7.85	1.52	1.62	0.98	0.02
393	0.012	0.51	7.88	1.34	1.25	0.97	0.03
393	0.027	0.80	8.26	2.87	3.34	0.95	0.05
393	0.024	0.53	8.30	2.32	2.30	0.95	0.05
393	0.007	4.11	8.78	1.55	1.66	1.00	0.00
363	0.018	0.74	0.14	17.39	16.53	0.42	0.58
363	0.012	1.40	1.30	2.07	2.11	0.96	0.04
363	0.012	1.40	2.27	0.96	1.00	0.98	0.02
363	0.013	1.46	0.11	17.54	23.15	0.59	0.41
363	0.012	1.50	0.15	14.47	18.07	0.69	0.31
363	0.018	1.54	0.19	20.51	20.19	0.66	0.34
363	0.011	1.74	1.94	1.34	1.24	0.98	0.02
363	0.011	1.03	0.92	2.84	2.71	0.93	0.07
363	0.010	1.64	0.92	3.56	2.89	0.95	0.05
363	0.011	0.89	0.93	2.79	2.49	0.93	0.07
363	0.011	0.32	0.93	1.15	1.51	0.88	0.12
363	0.011	1.02	0.93	2.49	2.61	0.93	0.07
363	0.012	0.45	0.98	2.47	1.77	0.90	0.10
363	0.012	1.49	1.07	2.21	2.68	0.95	0.05
363	0.011	1.74	1.94	1.19	1.24	0.98	0.02
363	0.011	0.44	1.98	0.52	0.59	0.97	0.03
363	0.010	3.17	2.00	1.00	1.31	0.99	0.01
363	0.011	1.26	2.06	0.85	1.00	0.98	0.02

327

T / K	HCHO Pressure / kPa	C_6H_6 Pressure / kPa	H_2O Pressure/ kPa	Measured Rate / 10^{-5} mol DPM $(mol\ s)^{-1}$	Predicted Rate / 10^{-5} mol DPM $(mol\ s)^{-1}$	$X_{RC,1}$	$X_{RC,2}$
363	0.011	0.98	2.10	0.87	0.85	0.98	0.02
363	0.011	0.44	2.11	0.61	0.55	0.97	0.03
363	0.011	1.63	2.15	1.13	1.06	0.98	0.02
363	0.012	0.27	2.19	0.40	0.37	0.96	0.04
363	0.011	1.40	4.08	0.27	0.38	0.99	0.01
363	0.101	0.28	2.16	2.98	2.65	0.76	0.24
363	0.213	0.24	2.17	4.06	3.75	0.59	0.41
363	0.021	0.77	2.07	1.33	1.46	0.95	0.05
363	0.031	0.87	2.27	2.07	1.96	0.94	0.06
363	0.061	0.89	2.09	4.10	4.19	0.88	0.12
363	0.109	0.90	2.19	5.42	6.44	0.82	0.18
363	0.210	0.77	2.25	9.22	9.26	0.69	0.31
363	0.197	0.97	3.09	4.48	7.05	0.81	0.19
363	0.045	0.90	0.90	7.78	8.67	0.75	0.25
363	0.073	0.96	0.75	14.28	14.59	0.61	0.39
363	0.204	1.00	4.09	2.96	5.06	0.87	0.13
363	0.209	0.44	2.16	6.91	6.27	0.63	0.37
363	0.032	3.59	5.15	0.54	1.26	0.99	0.01
363	0.017	0.38	0.83	3.53	2.72	0.82	0.18
363	0.058	0.73	2.10	4.16	3.54	0.87	0.13
363	0.019	0.79	2.11	1.33	1.34	0.96	0.04
363	0.010	0.95	0.94	2.20	2.28	0.94	0.06
363	0.059	0.74	2.09	4.21	3.62	0.87	0.13
363	0.088	0.67	1.97	5.61	5.09	0.80	0.20
363	0.090	0.43	1.91	5.59	4.02	0.76	0.24
378	0.011	0.63	0.95	8.00	6.46	0.82	0.18
378	0.011	1.65	1.08	9.94	7.91	0.92	0.08
378	0.011	0.39	1.70	2.78	2.67	0.88	0.12
378	0.010	0.85	1.94	3.92	3.09	0.94	0.06
378	0.010	0.83	1.97	3.82	2.93	0.94	0.06
378	0.011	0.68	1.99	3.39	2.81	0.93	0.07
378	0.010	0.71	2.06	3.28	2.66	0.94	0.06
378	0.011	1.73	2.12	4.35	3.80	0.96	0.04
378	0.010	1.65	4.17	1.65	1.49	0.98	0.02
378	0.010	1.28	4.33	1.35	1.20	0.98	0.02
378	0.011	0.16	4.39	0.24	0.30	0.97	0.03
378	0.010	0.38	4.18	0.91	0.65	0.97	0.03
378	0.011	0.44	0.91	7.72	5.78	0.77	0.23
378	0.011	0.47	2.06	2.95	2.23	0.92	0.08
378	0.011	0.74	4.21	1.50	1.02	0.98	0.02
378	0.011	0.75	4.19	1.48	1.04	0.98	0.02
378	0.010	0.84	1.96	3.94	2.99	0.94	0.06
378	0.011	0.88	0.92	8.21	7.84	0.85	0.15
378	0.039	0.37	2.18	9.36	5.44	0.75	0.25
378	0.202	0.42	2.05	19.38	15.51	0.36	0.64
378	0.104	0.49	2.10	11.41	12.83	0.55	0.45
378	0.203	1.00	2.20	26.36	29.04	0.50	0.50
378	0.059	0.98	2.03	14.45	14.14	0.75	0.25
378	0.089	0.41	4.30	5.46	4.61	0.81	0.19
378	0.010	0.28	0.89	4.75	4.32	0.73	0.27
378	0.009	0.21	1.99	2.01	1.21	0.90	0.10
378	0.184	0.41	3.98	10.07	8.62	0.64	0.36

A5.7 Derivation of DPM⁺ formation rate function (eq. (5.12))

The rate of DPM formation is given by eq. (A5.14):

$$\frac{r_{DPM}}{L} = k_2 P_{C_6H_6} \theta_{DPM^+} \tag{A5.14}$$

where k_2 is the elementary step rate constant for the deprotonation of DPM⁺ and θ_{DPM^+} is the fractional coverage of DPM⁺. The steady-state fractional coverage of DPM⁺ is determined by the eq. (A5.15):

$$\frac{d\theta_{DPM^+}}{dt} = 0 = \frac{r_1}{L} - \frac{r_2}{L} \tag{A5.15}$$

where r_1 and r_2 are the rate functions for the formation and consumption of DPM⁺, respectively. The rate of consumption of DPM⁺ is simply the rate of DPM formation ($r_2 = r_{DPM}$) from eq. (A5.14). The rate-determining step for DPM⁺ formation is the alkylation of benzene by adsorbed HCHO, the rate of which is given by (eq. (A5.16)):

$$\frac{r_1}{L} = k_1 \theta_{HCHO^*} P_{C_6H_6} \tag{A5.16}$$

The site balance for this reaction is eq. (A5.17):

$$\theta_* + \theta_{C_6H_6^*} + \theta_{HCHO^*} + \theta_{H_2O^*} + \theta_{DPM^+} = 1 \tag{A5.17}$$

The fractional coverage of each species is quasi-equilibrated except for DPM⁺ species, and are determined by eqs. (A5.18)-(A5.20):

$$K_{C_6H_6} = \frac{\theta_{C_6H_6^*}}{\theta_* P_{C_6H_6}} \tag{A5.18}$$

$$K_{HCHO} = \frac{\theta_{HCHO^*}}{\theta_* P_{HCHO}} \qquad \text{(A5.19)}$$

$$K_{H_2O} = \frac{\theta_{H_2O^*}}{\theta_* P_{H_2O}} \qquad \text{(A5.20)}$$

where the standard-state pressure $P^\ominus = 1 \text{ kPa}$ is incorporated into the equilibrium constants for convenience. Combining eqs. (A5.17)-(A5.20), the fractional coverage of HCHO can be found (eq. (A5.21)):

$$\theta_{HCHO^*} = \frac{K_{HCHO} P_{HCHO}}{1 + K_{HCHO} P_{HCHO} + K_{C_6H_6} P_{C_6H_6} + K_{H_2O} P_{H_2O}} (1 - \theta_{DPM^+}) \qquad \text{(A5.21)}$$

Recall that there is an additional equilibrium between HCHO, H_2O, and CH_4O_2 which, from eq. (5.9) is (eq. (A5.22)):

$$P_{HCHO} = \frac{P_{HCHO,0}}{1 + K_{hyd} P_{H_2O}} \qquad \text{(A5.22)}$$

where $P_{HCHO,0}$ is the HCHO pressure fed into the reaction. Combining eqs. (A5.15), (A5.16), (A5.21) and (A5.22) we have an equation that can be solved for the steady-state fractional coverage of DPM$^+$ (eq. (A5.23)):

$$\frac{r_1}{L} = \frac{k_1 \dfrac{K_{HCHO} P_{HCHO,0}}{1 + K_{hyd} P_{H_2O}} P_{C_6H_6}}{1 + \dfrac{K_{HCHO} P_{HCHO}}{1 + K_{hyd} P_{H_2O}} + K_{C_6H_6} P_{C_6H_6} + K_{H_2O} P_{H_2O}} \theta_{*'} \qquad \text{(A5.23)}$$

where $\theta_{*'}$ was defined as the sum of all surface species equilibrated with vacant sites, $\theta_{*'} = \theta_* + \theta_{C_6H_6} + \theta_{HCHO} + \theta_{H_2O} = 1 - \theta_{DPM^+}$. Equation (A5.23) is identical to eq.

(5.10). The steady-state rate is found by solving for the fractional coverage of I* in eq. (A5.24):

$$\frac{d\theta_{I^*}}{dt} = 0 = \frac{k_1 \frac{K_{HCHO} P_{HCHO,0}}{1 + K_{hyd} P_{H_2O}} P_{C_6H_6}}{1 + \frac{K_{HCHO} P_{HCHO}}{1 + K_{hyd} P_{H_2O}} + K_{C_6H_6} P_{C_6H_6} + K_{H_2O} P_{H_2O}} (1 - \theta_{I^*})$$

$$- k_2 P_{C_6H_6} \theta_{I^*} = f_1(1 - \theta_{I^*}) - f_2 \theta_{I^*} \tag{A5.24}$$

The solution to eq. (A5.24) is eq. (A5.25):

$$\theta_{I^*} = \frac{f_1}{f_1 + f_2} \tag{A5.25}$$

and because the steady-state rate is $r/L = f_2 \theta_{I^*}$, the steady-state rate is (eq. (A5.26)):

$$\frac{r}{L} = \frac{f_1 f_2}{f_1 + f_2}$$

$$= \frac{k_1 k_2 K_{HCHO} P_{HCHO,0} P_{C_6H_6}/(1 + K_{hyd} P_{H_2O})}{\frac{k_1 K_{HCHO} P_{HCHO,0}}{1 + K_{hyd} P_{H_2O}} + k_2 + \frac{k_2 K_{HCHO} P_{HCHO,0}}{1 + K_{hyd} P_{H_2O}} + k_2 K_{C_6H_6} P_{C_6H_6} + k_2 K_{H_2O} P_{H_2O}} \tag{A5.26}$$

which is identical to eq. 12.

A5.8 Transport effects on transient rate measurements

In a transient experiment, there is always going to be an effect of transport since the diffusion of reactant into a particle can never be instantaneous. However, we argue that the discontinuities we observe when step changing the partial pressure of benzene (see Figure 1c) or when we switch the feed composition from benzene to toluene (Figure 5b) that this is suggestive that the transport effects are negligible in these experiments. To

331

demonstrate this, we consider a simplified reaction-diffusion model where a surface species, A*, is formed irreversibly by a reaction that is first-order in species A and consumed by an irreversible reaction with A to form the final product B (Scheme A5.1). We then assume that the rate of diffusion into the catalyst, where the reaction occurs, is proportional to the difference in partial pressure of A between the external surface and the internal surface, described by eqs. (A5.27) and (A5.28):

$$\frac{d\theta_{A^*}}{dt} = k_1 A_z (1 - \theta_{A^*}) - k_2 A_z \theta_{A^*} \tag{A5.27}$$

$$\frac{dA_z}{dt} = D(A_g - A_z) \tag{A5.28}$$

where A_z is the concentration of A in the zeolite phase and A_g is the concentration of A in the gas-phase and D is an effective mass-transfer coefficient with units of inverse time. This parameter describes the rate of flux at the gas-zeolite boundary. This is intended to be a simplified example that does not rigorously consider the geometry or partition coefficients at the gas-zeolite boundary and assumes that the average concentration of A inside the zeolite phase is described by A_z. At large D, the concentration of A inside of the zeolite rapidly converges to the concentration of A in the gas phase, and thus we would expect at the limit that D approaches infinity that the transient rate of product formation during a step-change in A_g becomes negligibly impacted by diffusive transport limitations. For $k_1 = k_2 = 1$ au and a step-change in A_g from 1 au to 3 au while at steady-state at time t = 0 au, the rate during the transient at varying values for D are shown in Figure A5.6. In Figure A5.6, after the maximum is reached, the transient rate approaches that of the high D limit, and as D becomes small, a maxima is not observed

because the pseudo-steady-state approximation becomes valid on θ_{A^*} in eq. (A5.27) as the time-scale for changes in A_z become much larger than the time scale in the change for θ_{A^*}. In the DPM transient rate measurements, the time scale for the zeolite concentration to reflect the concentration of the gas-phase is small because the rate appears discontinuous and reaches a maximum when step-changing the pressure of C_6H_6 or when changing the composition of the feed, and more closely resembles the simulation results for $D = 10^1 - 10^2$ au than lower values for D in Figure A5.6. Thus we infer that diffusive transport limitations during these transient rate measurements are negligible.

Scheme A5.1. Reaction of zeolite-phase A to form B in a hypothetical reaction network.
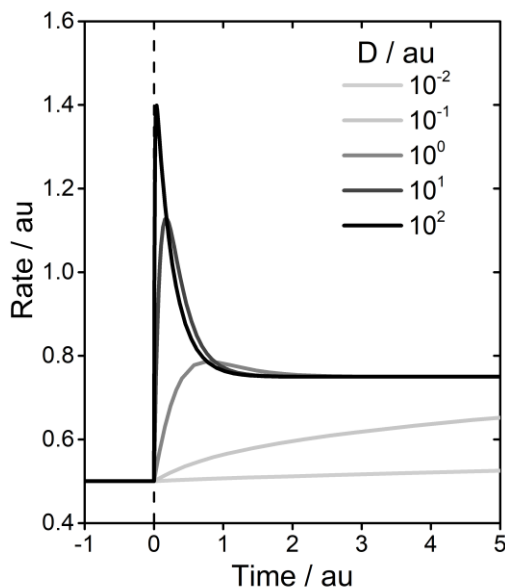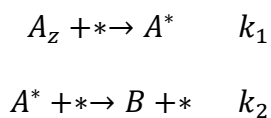
$$A_z + * \rightarrow A^* \qquad k_1$$

$$A^* + * \rightarrow B + * \qquad k_2$$

Figure A5.6: Transient rate for the reaction shown in Scheme 1 observed after a step-change in A_g from 1 to 3 au at time t = 0 (dashed line) at varying values for the pseudo-diffusion coefficient D. Higher values of D correspond to less diffusion limitations.

A5.9 Benzaldehyde formation rates

During HCHO reaction with C_6H_6, a benzaldehyde (C_6H_5CHO) byproduct was sometimes observed when operating at high HCHO feed pressures. Figure A5.7a shows the rate of DPM and benzaldehyde formation as a function of HCHO pressure. Figure A5.7b shows the benzaldehyde rate as a function of HCHO pressure while normalizing by the number of "bare" protons, i.e. sites that are not covered in DPM^+. These are the sites available for benzyl alcohol disproportionation. Assuming the pseudo-steady-state approximation is valid on benzyl alcohol ($C_6H_5CH_2OH$) for the simplified mechanism shown in Scheme A5.2, we can write eq. (A5.29):

$$\frac{dP_{C_6H_5CH_2OH}}{dt} = k_1 P_{C_6H_6} P_{HCHO} - 2k_2 P_{C_6H_5CH_2OH}^2 - k_3 P_{C_6H_5CH_2OH} P_{C_6H_6} \qquad \text{(A5.29)}$$

which when solved gives the pseudo-steady-state benzyl alcohol pressure (eq. (A5.30)):

$$P_{C_6H_5CH_2OH} = \frac{-k_3 P_{C_6H_6} + \sqrt{k_3^2 P_{C_6H_6}^2 + 8k_1 k_2 P_{C_6H_6} P_{HCHO}}}{4k_2} \qquad \text{(A5.30)}$$

When the rate of C_6H_5CHO formation is much smaller than the rate of DPM^+ formation, $2k_2 P_{C_6H_5CH_2OH}^2 \ll k_3 P_{C_6H_5CH_2OH} P_{C_6H_6}$, the pseudo-steady-state balance on benzyl alcohol is approximately (eq. (A5.31)):

$$\frac{dP_{C_6H_5CH_2OH}}{dt} = k_1 P_{C_6H_6} P_{HCHO} - k_3 P_{C_6H_5CH_2OH} P_{C_6H_6} \qquad \text{(A5.31)}$$

and the pseudo-steady-state partial pressure of $C_6H_6CH_2OH$ simplifies to eq. (A5.32):

$$P_{C_6H_5CH_2OH} \approx \frac{k_1 P_{HCHO}}{k_3} \qquad \text{(A5.32)}$$

The rate of benzyl alcohol formation is (eq. (A5.33)):

334

$$\frac{r}{L} = \frac{k_2 P_{C_6H_5CH_2OH}^2}{1 + K_{H_2O}P_{H_2O} + K_{C_6H_6}P_{C_6H_6}}(1 - \theta_{DPM^+}) \qquad \text{(A5.33)}$$

where the $(1 - \theta_{DPM^+})$ arises because only sites not covered in DPM$^+$ catalyze this reaction. From eqs. (A5.30) and (A5.32), the benzyl alcohol pressure can be at most first order in HCHO pressure. If the benzyl alcohol pressure is proportional to the HCHO pressure (eq. (A5.32)), then the benzaldehyde rate per non-DPM$^+$ covered site appears second order in HCHO (eq. (A5.33)), as observed in Figure A5.6b.

Benzaldehyde formation could impact the kinetics of DPM formation as it is a competitive route for the consumption of benzyl alcohol. To understand the effect this pathway may have on DPM kinetics, consider the two limiting scenarios: (i) formation of DPM$^+$ is rate controlling and (ii) consumption of DPM$^+$ is rate controlling. Benzaldehyde formation will decrease the rate per non-DPM$^+$ covered site (f_1) of forming DPM$^+$ because some benzyl alcohol is consumed via this parallel pathway, however the rate of consuming DPM$^+$ per DPM$^+$ covered site (f_2) is unaffected by benzaldehyde formation. The steady-state rate of DPM$^+$ formation at low HCHO pressures is $r/L = f_1 f_2/(f_1 + f_2) \approx f_1$ (see eq. (A5.26)) because forming DPM$^+$ is rate controlling ($f_1 \ll f_2$), and thus at this reaction condition benzaldehyde formation could reduce the rate because benzaldehyde formation reduces the value of f_1. At high HCHO pressures, where consuming DPM$^+$ is rate controlling ($f_1 \gg f_2$), the DPM rate is $r/L = f_1 f_2/(f_1 + f_2) \approx f_2$. At this condition, benzaldehyde formation will not affect the rate of DPM formation because this competitive pathway does not change f_2. In experiments, benzaldehyde is only observed at high HCHO pressures when the rate-limiting step is DPM$^+$ deprotonation where $r/L \approx f_2$, thus we conclude that the competitive pathway of

benzyl alcohol consumption to form benzaldehyde does not have an appreciable impact on the kinetic model described by eq. (5.12).
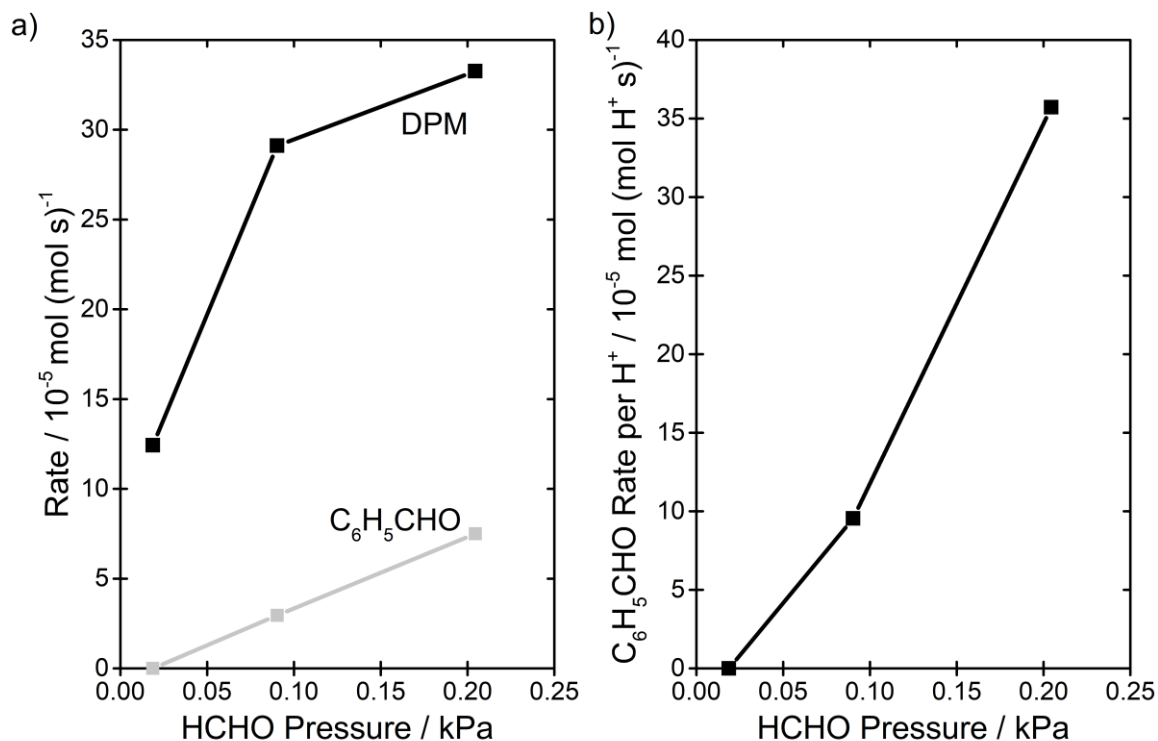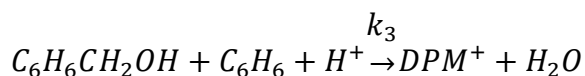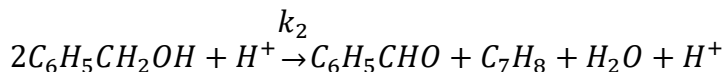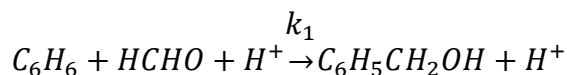

Figure A5.7: a) The rate of DPM and C_6H_5CHO formation as a function of $P_{HCHO,0}$ at 1.7-2.2 kPa H_2O, 0.42-0.47 kPa C_6H_6 and 393 K. b) The same C_6H_5CHO rates in a) except normalized by the number of non DPM^+ covered sites as predicted by the kinetic model.

Scheme A5.2: Simplified reaction mechanism for benzaldehyde formation as a parallel pathway to DPM^+ formation

$$C_6H_6 + HCHO + H^+ \xrightarrow{k_1} C_6H_5CH_2OH + H^+$$

$$2C_6H_5CH_2OH + H^+ \xrightarrow{k_2} C_6H_5CHO + C_7H_8 + H_2O + H^+$$

$$C_6H_6CH_2OH + C_6H_6 + H^+ \xrightarrow{k_3} DPM^+ + H_2O$$

A6 A method for assessing catalyst deactivation: A case study on methanol-to-hydrocarbons conversion

A6.1 Deactivation during MTH on HZSM-5 from 623 to 723 K with HCHO co-feeds

The conversion versus time-on-stream data on HZSM-5 with 12 kPa methanol and varying HCHO co-feed pressures at 673 K and 723 K are presented in Figure A6.1 and Figure A6.2, respectively. The slopes of linear fits of these data were used to estimate dX/dt at each reaction condition.
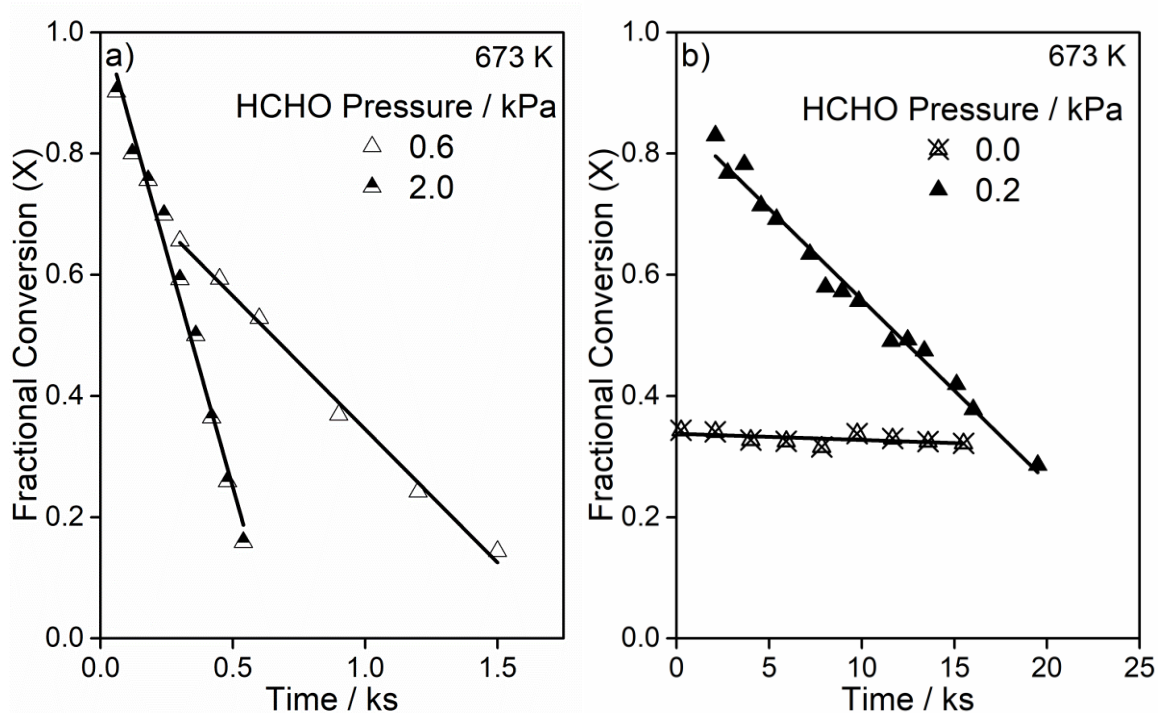

Figure A6.1: Conversion versus time at 673 K with 12 kPa methanol on HZSM-5 and a) 0.6-2.0 kPa HCHO co-feed and b) 0.0-0.2 kPa HCHO co-feed pressures. Solid lines are linear fits.
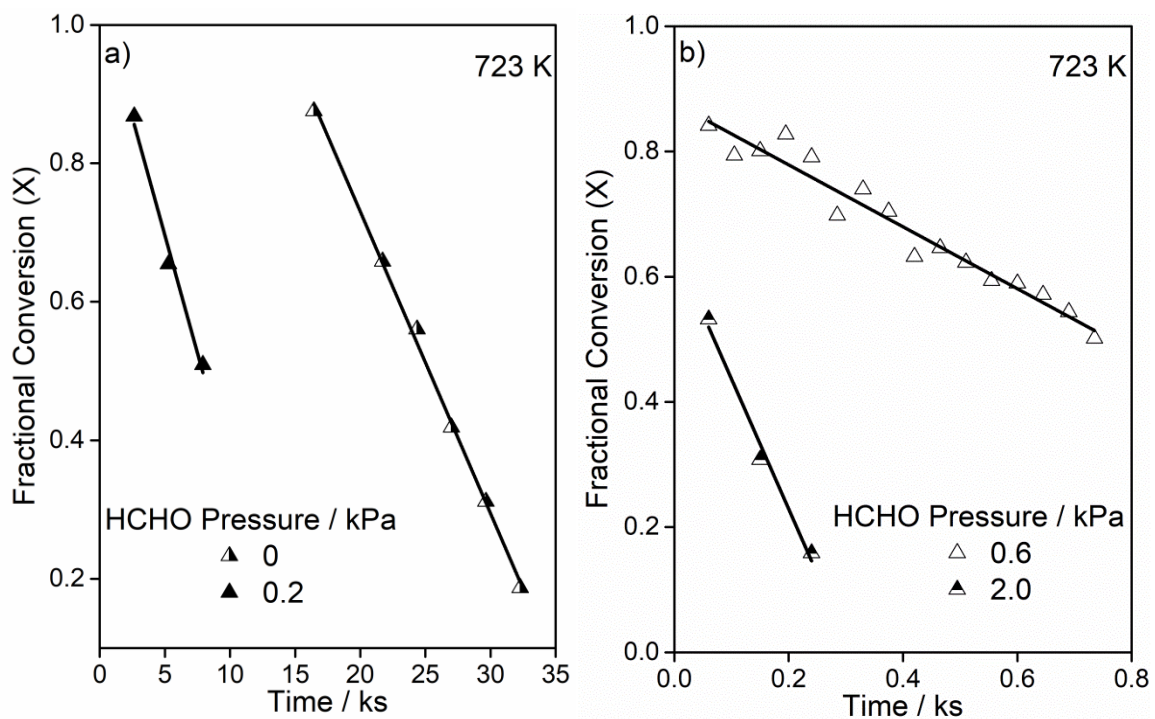
Figure A6.2: Conversion versus time at 723 K with 12 kPa methanol on HZSM-5 and a) 0-0.2 kPa HCHO co-feed and b) 0.6-2.0 kPa HCHO co-feed pressures. Solid lines are linear fits.

The site-loss yields versus methanol conversion on HZSM-5 with 12 kPa methanol and varying HCHO co-feed pressures at 673 K and 723 K are presented in Figure A6.3. The site-loss yields were calculated using Equation 2 and the data presented in Figure 4a and Figures A6.1 and A6.2.
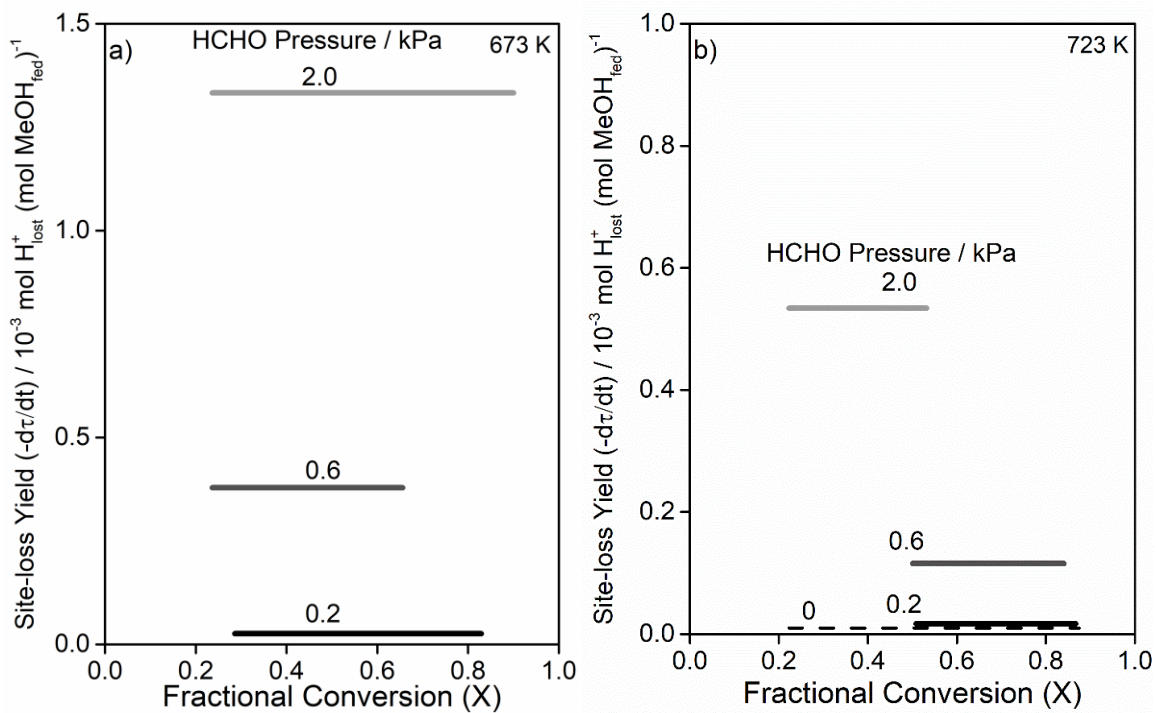
Figure A6.3: Site-loss yield as a function of conversion on HZSM-5 with 12 kPa methanol, 0–2.0 kPa HCHO at a) 673 K and b) 723 K.

The slopes of the linear fits of the data presented in Figure 4a and the conversion ranges of the data used for the linear fit are presented in Table A6.1. These slopes are used as estimates of $dX/d\tau$.

Table A6.1: Slope of Conversion versus Contact Time Curve Over Indicated Conversion Range from 623–723 K with 12 kPa methanol on HZSM-5

Temperature / K	dX/dτ / mol MeOH (mol H$^+$ s)$^{-1}$	Conversion Range
623	1.01	11.6-89.1%
673	1.16	23.6-91.8%
723	3.89	22.3-90.0%

The slopes of the linear fits of the conversion versus time-on-stream curves presented in Figures 6.4b, A6.1, and A6.2 and the conversion ranges of these data are presented in Table A6.2. These data are estimates of dX/dt. The site-loss yields, -dτ/dt, calculated using Equation 2 are presented in Table A6.2 with the corresponding conversion range over which the site-loss yield was calculated. The site-loss yield data are presented graphically in Figure 4d.

Table A6.2: Slope of Conversion versus Time Curve over Indicated Conversion Range and Calculated Site-loss Yield (-dτ/dt) from 623–723 K, 12 kPa methanol and varying HCHO Co-feed Pressure on HZSM-5.

Temperature / K	HCHO Pressure / kPa	dX/dt / ks^{-1}	Conversion Range	-dτ/dt / 10^{-3} mol H$^+$ (mol MeOH)$^{-1}$	Conversion Range
623	0.2	-0.059	24.8-97.6%	0.059	11.6-89.1%
623	0.6	-0.379	10.4-52.8%	0.377	11.6-52.8%
623	2.0	-1.170	30.0-82.7%	1.164	30.0-89.1%
673	0.2	-0.030	28.6-82.9%	0.026	28.6-82.9%
673	0.6	-0.440	14.3-65.6%	0.378	23.6-65.6%
673	2.0	-1.549	15.9-90.2%	1.332	23.6-90.0%
723	0.0	-0.040	18.7-87.5%	0.010	22.3-87.5%
723	0.2	-0.068	50.8-86.7%	0.017	50.8-86.7%
723	0.6	-0.450	50.1-84.1%	0.116	50.1-84.1%
723	2.0	-2.075	15.9-53.2%	0.534	22.3-53.2%

A6.2 Catalyst characterization

Ammonia temperature programmed-desorption was used to determine the acid site density of the HZSM-5 sample used in this study. The ammonia was adsorbed at 423 K and the sample was heated to 823 K at a ramp rate of 0.167 K s^{-1}. The ammonia desorbed as one peak as shown in Figure A6.4; the total amount of ammonia desorbed was 228 μmol g^{-1}. Ammonia was assumed to desorb with 1:1 stoichiometry with acid sites in the HZSM-5 sample.
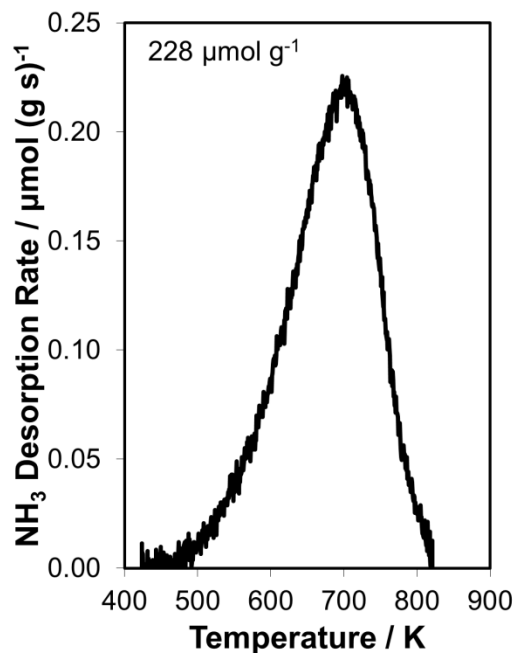

Figure A6.4: Ammonia temperature programmed desorption on the HZSM-5 sample (CBV8014).

The surface area and micropore volume of the HZSM-5 sample used in this work are presented in Table A6.3. These data are comparable to those reported by Ilias et al.[1]

Table A6.3: Catalyst characterization of the HZSM-5 sample used in this study by nitrogen adsorption.

Sample	BET Surface Area / m² g^{-1}	Micropore volume / cm^3 g^{-1}
HZSM-5	399.9	0.15

A6.3 Mathematical description for increased site-loss selectivity with increasing HCHO co-feed pressure

We discuss below a rationale for why the observation that site-loss selectivity of HCHO increases with increasing HCHO pressure discussed in Case 1 implies (i) multiple pathways of HCHO consumption, with a subset of these pathways consuming active sites and the remainder not consuming active sites; and (ii) HCHO reaction pathways that consume active sites are enhanced by increasing HCHO pressure more that pathways that do not consume active sites. Consider two types of reactions that consume HCHO, one that consumes an active site to form coke (eq. (A6.1)) and a second reaction that consumes HCHO to form a non-coke species without consuming an active site (eq. (A6.2)), where ν_i are stoichiometric coefficients, and A, B, C, and D, are reactant or product species

$$HCHO + \nu_A A + \nu_* * \rightarrow \nu_C C \tag{A6.1}$$

$$HCHO + \nu_B B \rightarrow \nu_D D \tag{A6.2}$$

Under conditions where HCHO is completely consumed, the site-loss yield of HCHO is given by eq. (A6.3) and A6.4:

$$\text{Site-loss selectivity} = \frac{-\nu_* \dot{\xi}_{S3.1}}{\dot{n}_{HCHO}} = \frac{-\nu_* \dot{\xi}_{S3.1}}{\dot{\xi}_{S3.1} + \dot{\xi}_{S3.2}} \tag{A6.3}$$

$$\dot{\xi}_i = \int_0^{n_*(t)} r_i \, dn_* \tag{A6.4}$$

where $\dot{\xi}_i$ are the moles of reaction i occurring per unit time in the entire reactor bed. The negative sign is introduced because ν_i values are negative for reactants and positive for products and site-loss selectivity is a positive number. The site-loss selectivity increases with increasing HCHO co-feed pressure, and thus is positive order in HCHO pressure (eq. (A6.5))

$$\frac{-\nu_* \dot{\xi}_{S3.1}}{\dot{\xi}_{S3.1} + \dot{\xi}_{S3.2}} \propto P_{HCHO}^a, a > 0 \tag{A6.5}$$

This positive order dependence on HCHO co-feed pressure requires that $\dot{\xi}_{S3.2}$ is on the order of or greater than $\dot{\xi}_{S3.1}$, and thus $\dot{\xi}_{S3.2} \neq 0$, and that the dependence of $\dot{\xi}_{S3.1}$ on HCHO pressure is higher order than the dependence of $\dot{\xi}_{S3.2}$ on HCHO pressure. Assuming that both reactions are first-order in HCHO and first-order in the other species reacting with HCHO the $\dot{\xi}_i$ values are given by eqs. A6.6 and A6.7:

$$\dot{\xi}_{S3.1} = \int_0^{n_*(t)} r_{S3.1} dn_* = \int_0^{n_*(t)} k_{S3.1} P_{HCHO} P_A dn_* \tag{A6.6}$$

$$\dot{\xi}_{S3.2} = \int_0^{n_*(t)} r_{S3.2} dn_* = \int_0^{n_*(t)} k_{S3.2} P_{HCHO} P_B dn_* \tag{A6.7}$$

where r_i are the per-site rates of reaction i, and k_i are second order rate constants of reaction.

The positive order dependence of site-loss selectivity on HCHO pressure implies that increasing HCHO pressure increases the average concentration of species A relative to species B along the region of the reactor bed that catalyzes HCHO conversion reactions. This could be, for example, because species A is itself HCHO and that deactivation reactions are second order in HCHO. Alternatively, species A could be a

product of HCHO reaction with species B. In this way, the concentration of species A is increased by increasing the HCHO pressure, enhancing the rate of site-loss reactions. Finally, the concentration of species B could simply be decreased by increasing HCHO pressure, thereby enhancing the rate of site-loss relative to the rate of other HCHO consuming reactions in the reactor bed.

A6.4 Calculation of cumulative site-loss yield for generic n^{th} order reaction system

We derive below Equation 12, the cumulative site-loss yield for a generic n^{th} order reaction in a plug-flow reactor (PFR). For a PFR, a mass balance can be represented by eq. (A6.8):

$$\frac{d\dot{n}_R}{dV_R} = -r\delta \tag{A6.8}$$

where $\dot{n}_R$ is the molar flow rate of reactant R, V_R is the volume of the reactor, r is the rate of consumption of R per active site, and δ is the moles of active sites per reactor volume. Consider the reaction rate of a simple n^{th} order reaction given in eq. (A6.9):

$$r = kP_R^n \tag{A6.9}$$

where P_R is the partial pressure of reactant R. For systems with constant density and volumetric flow rate, the pressure and molar flow rate of R are described by eqs. (A6.10) and (A6.11):

$$\dot{n}_R = \dot{n}_{R0}(1 - X) \tag{A6.10}$$

$$P_R = P_{R0}(1 - X) \tag{A6.11}$$

where $\dot{n}_{R0}$ is the inlet molar reactant flow rate, P_{R0} is the inlet reactant partial pressure, and X is the fractional conversion of reactant R. eqs. (A6.10) and (A6.11) can be substituted into eq. A6.8 to obtain eq. (A6.12):

$$\dot{n}_{R0}\frac{dX}{dV_R} = kP_{R0}^n(1-X)^n\delta \tag{A6.12}$$

Rearranging eq. (A6.12) gives eq. (A6.13):

$$\frac{dX}{d(\delta V_R/\dot{n}_{R0})} = kP_{R0}^n(1-X)^n \tag{A6.13}$$

Equation (A6.13) is simplified by noting the identities for total number of sites, n_*, and contact time, τ, given by eqs. (A6.14) and (A6.15) respectively:

$$\delta V_R = n_* \tag{A6.14}$$

and

$$\tau = n_*/\dot{n}_{R0} \tag{A6.15}$$

By substitution of eqs. (A6.14) and (A6.15) into eq. (A6.13), eq. (A6.16) is obtained:

$$\frac{dX}{d\tau} = kP_{R0}^n(1-X)^n \tag{A6.16}$$

Separating variables and integrating eq. (A6.16), noting that the upper bounds of the definite integrals are functions of time (eq. (A6.17)):

$$\int_0^{X(t)}\frac{dX}{(1-X)^n} = \int_0^{\tau(t)}kP_{R0}^n d\tau \tag{A6.17}$$

Equation (A6.18) is obtained:

$$\frac{\left(1-X(t)\right)^{1-n}-1}{n-1} = kP_{R0}^n\tau(t) \tag{A6.18}$$

Equation (A6.18) can be rearranged to give an equation for conversion as a function of contact time (eq. (A6.19))

$$X(t) = 1 - [(n-1)kP_{R0}^n \tau(t) + 1]^{\frac{1}{1-n}} \tag{A6.19}$$

If it is assumed site-loss yield is a constant, γ, then τ as a function of time is given by eq. (A6.20):

$$\tau(t) = \tau_0 - \gamma t \tag{A6.20}$$

Finally, substituting eq. (A6.20) and eq. (A6.19) into the definition of cumulative site-loss selectivity (eq. (A6.21)) and integrating from 0 to τ_0/γ, the time that $\tau = 0$, we arrive at an equation for cumulative site-loss selectivity (eq. (A6.22)) that is identical to Equation 6.12.

$$\text{Cumulative Site-loss Selectivity} = \frac{n_{*,0}}{\int_0^\infty X(t)\dot{n}_{R0}\,dt} \tag{A6.21}$$

$$= \tau_0 \left(\int_0^{\frac{\tau_0}{\gamma}} 1 - [(n-1)kP_{R0}^n(\tau_0 - \gamma t) + 1]^{\frac{1}{1-n}} dt \right)^{-1} \tag{A6.22}$$

A6.5 Impact of co-feeding HCHO on dX/dτ

Conversion versus contact time curves were measured with and without a 0.2 kPa HCHO co-feed at 673 K with 12 kPa methanol. The slopes of these curves ($dX/d\tau$) were identical when compared at the same fractional conversion of methanol, as shown in Figure A6.5a. The fractional conversion without a HCHO co-feed is measured at steady-state, but because of catalyst deactivation with HCHO co-feed (see Figure A6.5b), the initial fractional conversion (~ 5 minutes time on stream) is used. To avoid measuring a new contact time curve for each HCHO co-feed pressure, it is assumed that co-feeding HCHO has negligible impact on the slope of the conversion versus contact time curve at all reaction conditions.
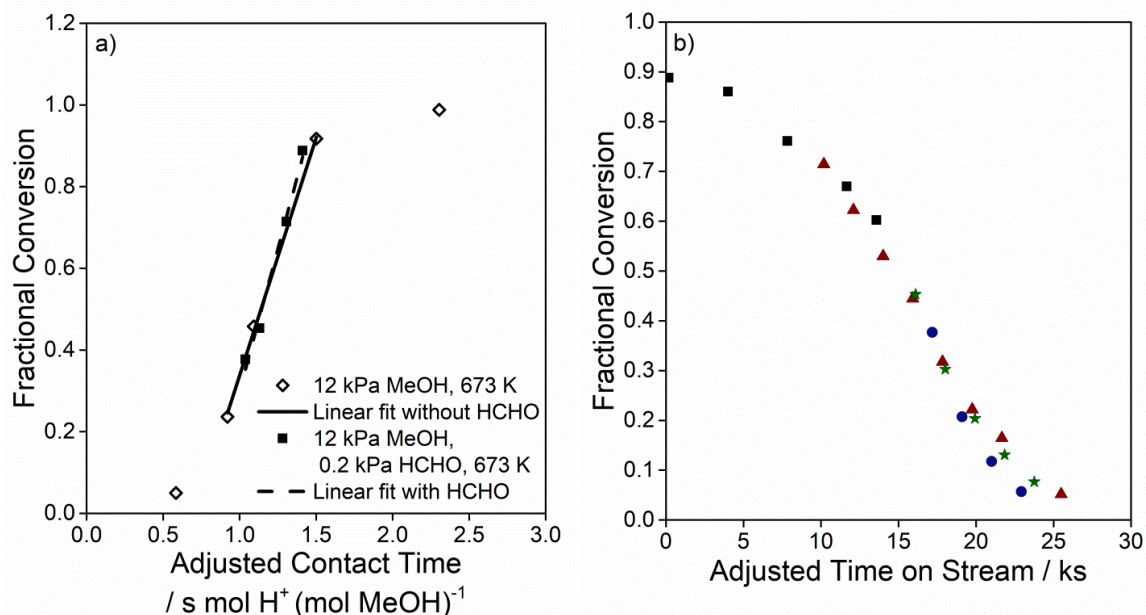
Figure A6.5: a) Conversion as a function of contact time (adjusted +/- a constant value so the curves overlay) with 12 kPa methanol at 673 K with and without a 0.2 kPa HCHO co-feed. b) Conversion versus time on stream (adjusted +/- a constant value so the curves overlay) with 12 kPa methanol and 0.2 kPa HCHO at 673 K. Each set of data points is a different initial contact time.

A6.6 Methods

A6.6.1 Methanol-to-hydrocarbons catalysis

Methanol (Chromosolv, ≥99% purity, Sigma-Aldrich) was fed by syringe pump (Cole Parmer 78-0100C) and vaporized into a heated stream of helium carrier gas (≥99.997%, Matheson). Helium flow rates were regulated by mass flow controllers (Brooks SLA5850). The methanol and helium flow rates were adjusted to achieve the desired contact time (0.19–12.4 s mol H$^+$ (mol MeOH)$^{-1}$) and methanol pressure (12 kPa) for each experiment. This reactant stream was fed to a quartz tube reactor (0.4–1 cm i.d.) containing HZSM-5 (Zeolyst, CBV8014, 0.0070–0.1121 g) zeolite catalysts (177–400 µm aggregates) diluted with quartz sand (0.1–0.25 g, washed with 2 M HNO$_3$, rinsed with deionized water, and thermally treated at 1273 K in flowing air for 12 h). The quartz

tube reactors were heated to reaction temperature (623–723 K) by a resistively heated furnace (National Element FA120) with a PID controller (Watlow 96). The reactor temperature was monitored by a K-type thermocouple (Omega) placed on the outside of the quartz tube at the axial center of the reactor bed. The reactor bed was thermally treated in air (Matheson, Ultra Zero Certified, 1.67 cm^3 s^{-1}) at 823 K for 6 h before each experiment. Fractional conversion of methanol is defined as the total carbon molar flow rate of non-reactant species (methanol and its dehydration product dimethyl ether (DME)) divided by the total carbon molar flow rate minus the molar flow rate of HCHO. This is shown mathematically in eq. (A6.23), where $n_{C,i}$ is the number of carbon atoms in species i and $\dot{n}_i$ are molar effluent flow rates of species i, where i is any reactant or product species observed in the effluent.

$$\text{Fractional Conversion} = \frac{\sum_i n_{C,i}\dot{n}_i - (2\dot{n}_{DME} + \dot{n}_{Methanol} + \dot{n}_{HCHO})}{\sum_i n_{C,i}\dot{n}_i - \dot{n}_{HCHO}} \qquad (A6.23)$$

Contact time versus conversion data were obtained by varying the liquid flow rate of methanol (0.1–1.6 cm^3 h^{-1}) and helium (0.154–3.42 cm^3 s^{-1}) while maintaining a constant methanol pressure (12 kPa) without regenerating the catalyst between changes in contact time. The first data point taken with time on stream was re-measured at the end of the experiment to verify that deactivation was negligible. Formaldehyde trimers (1,3,5-trioxane, ≥99%, Sigma-Aldrich) were dissolved in methanol as a formaldehyde source to study the effect of formaldehyde co-feed pressure on the rate of catalyst deactivation (60:1–6:1 methanol:formaldehyde) during MTH conversion. The composition of the reactor effluent was monitored by a gas chromatograph (Agilent 7890) equipped with an HP-Plot/Q column (30 m × 0.530 mm × 40 µm) connected in series with a CP-Molsieve

5Å column (25 m × 0.530 mm × 40 μm). The outlets of the columns were connected to a thermal conductivity detector followed by an oxidation-methanation reactor (Polyarc®, Activated Research Company) and a flame ionization detector. The effluent stream of the reactor was directly injected into the GC or stored in 250 μL stainless steel sample loops heated to 373 K and analyzed immediately after the reaction when fine temporal resolution was necessary.

A6.6.2 Ammonia temperature-programmed desorption measurement

Ammonia (NH_3) temperature-programmed desorption (TPD) experiments were used to enumerate acid site densities for each zeolite material following the methods presented by Bates et al.[78] Ammonia (Praxair, 1% in He, 0.14 cm^3 s^{-1}) was diluted in helium (0.64 cm^3 s^{-1}) and fed to a fixed bed of HZSM-5 zeolite catalysts (177–400 μm aggregates, 0.074 g) heated to 423 K. The concentration of NH_3 in the reactor effluent was monitored by an on-line mass spectrometer (m/z = 16). The reactor bed was bypassed before exposure to flowing NH_3 to obtain a baseline signal. Upon exposure to the reactor bed, for a period of time no NH_3 was observed in the effluent as it was consumed completely by adsorption reactions on the acid sites of the zeolite. Once the zeolite was saturated, NH_3 concentration in the effluent returned to baseline levels, at which point NH_3 flow to the reactor was suspended. The reactor was then flushed with helium (0.64 cm^3 s^{-1}) for eight hours before heating to 823 K at a ramp rate of 0.167 K s^{-1}. The total moles of NH_3 desorbed during the temperature ramp were assumed stoichiometric with the number of moles of acid sites in the reactor bed.

A6.6.3 Nitrogen adsorption measurements

A Micromeritics ASAP 2020 instrument was used to measure the external surface area and micropore volume of 0.0512 g of HZSM-5 catalyst used in this study. The sample was heated to 723 K for 4 h under vacuum (< 1 Pa) to degas the sample prior to nitrogen adsorption. Nitrogen was adsorbed at liquid nitrogen temperature and the external surface area and micropore volume were determined using the Brunauer–Emmett–Teller (BET) and the t-plot method, respectively.